Morphological responses in drainage basins affected by coseismic landslides triggered by the 2018 Eastern Iburi Earthquake, Hokkaido, Japan

（2018年北海道胆振東部地震による地震性斜面崩壊に影響された流域における地形的応答）

Graduate School of Environmental Science, Hokkaido University

LO Lap Wing

Contents

Chapter 4. Results

Chapter 5. Discussion

List of Figure

(c) April 23, 2020, (d) June 25, 2020, (e) September 14, 2020, (f) October 30, 2020, (g) April 13, 2021, (h) June 21, 2021, (i) August 27, 2021, (j) October 29, 2021.

Figure 4.3.1: Bar charts indicating the results of parameters of watershed geometry (Study sites A-D). (a) Basin length (L_b), (b) Basin area (A), (c) Basin perimeter (P), (d) Form factor (F_f), (e) Elongation ratio (R_e), (f) Circularity ratio (R_c), (g) Compactness coefficient (C_c).

Figure 4.3.2: Line graphs and bar chart indicating some results of parameters of drainage network (Study sites A-D). (a) Length of main stream channel , (b) Total length of tributaries, (c) Stream order (U), (d) Stream number (N_u), (e) Total stream length (L_u), (f) Mean stream length (L_m), (g) Gradient of mainstream.

Figure 4.3.3: Results of parameters of drainage texture (Study sites A-D). (a) Stream frequency (F_s), (b) Drainage texture (D_t), (c) Drainage density (Dd), (d) Drainage intensity (D_i), (e) Infiltration number (I_f), (f) Length of overland flow (L_o), (g) Constant of channel maintenance (C).

Figure 4.3.4:.Results of parameters of relief characteristics (Study sites A-D). (a) Relief ratio (R_h), (b) Ruggedness number (R_n), (c) Dissection Index (Dis).

Figure 4.3.5: Results of hydrological parameters (Study sites A-D). (a) Hydraulic radius (R), (b) Slope (10m from stream head) (S), (c) Shear stress ($\boldsymbol{\tau}$), (d) Critical shear stress ($\boldsymbol{\tau}_c$), (e) Velocity (v), (f) Peak specific discharge per unit rainfall intensity (k_p)

Figure 4.4.1: Landslide (Areas with elevation decrease) (m^2) and Sedimentation (Areas with elevation increase) (m^2) of Study site A – D: October 05, 2012 – September 11, 2018 (Period 1) and September 11, 2018 – October 29, 2021 (Period 2 – 9).

Figure 4.4.2: Landslide (Areas with elevation decrease) volume (m^3) and Sedimentation (Areas with elevation increase) volume (m^3) of Study site A – D: October 05, 2012 – September 11, 2018 (Period 1) and September 11, 2018 – October 29, 2021 (Period 2 – 9).

Figure 4.4.3: Stream length (m) in landslides areas (Areas with elevation decrease) and Sedimentation areas (Areas with elevation increase) (Study site A – D): October 05, 2012

List of Table

Table 5.1: Changes of geomorphometric and hydraulic parameters correspond with increase of rainfall intensity (1 mm/per hour, daily maximum) recorded by Atsuma Meteorological Station (Japan Meteorological Agency, 2023) during the investigation periods of this study.

Table 5.3.1: Quantitative analysis of Landslide (Elevation decreased area) mobility, Sediment connectivity and 4 geomorphometric parameters (Study sites A -D) with ranking from highest value (1^{st}) to lowest value (4^{th}): Analysis from the pre-seismic ALS DEM on October 05, 2012 and post-seismic ALS DEM on September 11, 2018 (Period 1).

Table 5.3.2: Quantitative analysis of Landslide (Elevation decreased area) mobility, Sediment connectivity and 4 geomorphometric parameters (Study sites A -D) with ranking from highest value (1^{st}) to lowest value (4^{th}): Analysis from the post-seismic ALS DEM on September 11, 2018 and UAV-Lidar DEM on October 29, 2021 (Period 2-9).

Table 5.4.1: NDVI (Average between Aug 29 ~ Sep 05, 2018: Sensor: SGLI (CGOMC)) and Jun 21, 2021) of several tributaries in site D.

Table 5.4.2: Soil temperature (°C), soil moisture (m^3/m^3) and PAR Photosynthetic Active Radiation (µmol m^{-2} s^{-1}) of 4 sets of Data micro station loggers in Study site B.

Abstract

Magnitude 6.7 earthquake happened in Eastern Iburi Prefecture, Hokkaido on 6th September, 2018 whose epicenter with focus depth of 37 km was located at 42.690°N and 142.007°E within the Ishikari Teichi Touen Fault Zone. Numerous coseismic landslides (n = 7837) covered over 700 km^2. Tarumae-d tephra layer with fine-grained texture and high-water infiltration capacity was considered as the inherent factor of the coseismic landslides. Gradual post-seismic changes in catchments, including geomorphology, development of fluvial channels, drainage pattern, and continuous slope processing are expected. This study aims to identify the morphological responses of drainage basins affected by coseismic landslide with drainage network development, elevation changes and sediment connectivity, which are assessed by mapping stream networks, quantifying drainage basin hydro-geomorphometric parameters and sediment mobility, following the 2018 Hokkaido Eastern Iburi Earthquake with exploration of fluvial and slope processes affecting those responses across 4 adjacent watersheds with varying shapes, which correspond with multi and inter-related aspects of rainfall intensity, characteristics of soil minerals, varying forms of drainage basins, lack of root reinforcement with limited vegetation recovery and freeze-thaw action on bare slopes.

The study sites are 4 catchments along the Atsuma River with less artificial modifications after the earthquake, which are located on the left side of Apporo Reservoir with coseismic landslides and sedimentation of collapsed materials caused by the earthquake. Digital Elevation Models by Airborne laser scanning of October 2012 and September 2018 from Hokkaido Prefecture, as well as those and orthorectified images by Unmanned Aerial Vehicle based Structure-from-Motion Multi-View Stereo photogrammetry in April 2020 to August 2021 and Light Detection and Ranging of October 2021 taken by field surveys were used. Visual inspections and Geographical Information System analysis were performed for analyzing drainage basin morphology, channel network extraction, stream profile analysis, and morphological change detection between multiple DEMs. Extraction of stream network and stream head location were conducted by using the threshold area assisted with threshold of flow accumulation and flow direction. By the observed continuous gully erosion channel development on slid slopes and results of quantitative analysis in the multi-temporal DEMs and orthophotos, progressive drainage network development and changes in drainage basin hydro-geomorphometric parameters have been confirmed

Potentially higher surface runoff with fluvial erosion and stream channel

development on bare slopes with further slope deformations were expected. This study will contribute to identify and develop an inventory about the effects of the 2018 Hokkaido Eastern Iburi Earthquake on the morphological responses of drainage basin . The results of progressive drainage network development and changes in drainage basin fluvial-geomorphological parameters by multi and inter-related aspects analysis, might be valuable for long-term effects investigation, continuous monitoring for landslide with risk reduction and comprehensive understanding on progressive fluvial landscape evolutionary studies, such as the role of landslides on slope-fluvial channel initiation and drainage headward erosion, which would be beneficial for the investigation of sediment connectivity in catchments affected by earthquake.

The scientific analysis, by using multi-perspectives and multi-functions orientated approach (Lo. et al., 2023) (Lo. T.L.W. 2025) of the present study, for identifying and developing an inventory of the various post-seismic morphological responses in 4 drainage basins affected by coseismic landslides including several perspectives such as Post-seismic: Elevation changes, Sediment connectivity and Drainage network developments supported by mapping of stream networks and quantitative analysis of 35 inter-related hydro-geomorphometric parameters, associated with the analysis of various corresponding factors, which are inter-active and inter-related, indicating those various co-existing post-seismic phenomenon have complicated and inter-reacted relationship with each other, which are relatively more reliable and convincible aspects and be able to eliminate the under-estimation on the influence of other correspondent factors. The present study highlights the importance of multi-aspects inter-related/functional analysis (which are always under-estimated in scientific study) in explanation of various co-existed natural phenomenon is one of the objectives and functions.

The analytical method in this study for extracting stream network and stream head location by using the threshold areas of watershed with flow accumulation and flow direction with field verification may be applicable on fluvial system analysis of large-scale watersheds.

Chapter 1. Introduction

In areas impacted by coseismic landslides, not only coseismic landform deformation directly associated with the earthquake, but also sustained changes in slope and channel morphology after the seismic event occur. These changes include further landslide occurrences, activated sediment supply, sediment delivery, and stream channel development (Li et al., 2015; Twidale, 2004). To better understand the morphological evolution of drainage basins following earthquakes, systematic geomorphometric analysis is essential (Zhang and Guilbert, 2012). Magnitude 6.7 earthquake happened in Eastern Iburi Prefecture, Hokkaido on 6th September, 2018 whose epicenter with focus depth of 37 km was located at 42.690°N and 142.007°E within the Ishikari Teichi Touen Fault Zone. Numerous coseismic landslides (n = 7837) covered over 700 km^2. Tarumae-d tephra layer with fine-grained texture and high-water infiltration capacity was considered as the inherent factor of the coseismic landslides. In the context of the 2018 Hokkaido Eastern Iburi Earthquake, previous studies have focused on analyzing coseismic landform changes directly induced by coseismic landslides in the region (Wang et al., 2019; Ishimaru et al., 2020). Gradual post-seismic changes in catchments, including development of fluvial channels, geomorphology, drainage pattern, and continuous slope processing are expected. However, long-term investigation of post-seismic morphological responses of drainage basin such as drainage network development, morphological changes and related hydro-geomorphometric parameters, with those correspondent environmental factors in multi and inter-related aspects remains not thoroughly investigated in these study areas.

This study aims to identify and develop an inventory of morphological responses on drainage basins affected by coseismic landslide with drainage network developments, elevation changes and sediment connectivity, which are assessed by mapping stream networks, quantifying drainage basin hydro-geomorphometric parameters and sediment connectivity, following the 2018 Hokkaido Eastern Iburi Earthquake with exploration of fluvial and slope processes across 4 adjacent watersheds with varying shapes, which correspond with variation of rainfall intensity, lack of vegetation cover on bare slopes, characteristics of soil minerals and freeze-thaw action on slid slopes. The study sites are 4 catchments with similar geological and climatic conditions, areas less than 1 km^2 along the Atsuma River and less artificial modifications after the earthquake, which are located on the left side of Apporo Reservoir with coseismic landslides and sedimentation of collapsed materials caused by the earthquake. These small catchments are suitable for high-resolution mapping, aerial photos and relatively detailed site-specific assessment and verification with field surveys, which are important for specific fluvial studies such as intensity of erosions, location of stream head, headward erosion, discharge, gully streams and sedimentation mechanism. Systematic analysis focuses on small-local scale catchments were limited.

Topographical data collected by Airborne laser scanning of October 2012 and September 2018 from Hokkaido Prefecture, as well as those and orthorectified images by Unmanned Aerial Vehicle based Structure-from-Motion Multi-View Stereo photogrammetry in April 2020 to August 2021 and Light Detection and Ranging of October 2021 taken by field surveys were used for producing dense point cloud, orthorectified images and Digital Elevation Models by Agisoft Metashape. Geographical Information System analysis (QGIS 3.22.7) were performed for analyzing drainage basin morphology with channel network extraction, longitudinal profile analysis, morphological change detection and quantitative analysis between multiple DEMs. For the extraction of stream channels, a threshold value of 100 m^2 was set as the channel heads. Due to the variability in penetration of detection between UAV-SfM and UAV-LiDAR, adjustment by the threshold value of flow accumulation in each set of DEMs was done, which were visually corresponds to the morphological features of channels heads and matches the locations in the field. 35 hydro-geomorphometric parameters were examined in this study. Those selected parameters are proposed to be used for inter-basin comparison and are able to indicate predominant processes within watershed relating to mass movement, surface water flow, and understanding of soil erosion, fluvial erosion and discharge characteristics of ungauged stream and hydrogeomorphic process such as sediment supply, transport processes and runoff components, which are related to the post-seismic changes of drainage basin morphology and development of stream network in the study sites.

By the observations during the field surveys and results of quantitative analysis of hydro-geomorphometric parameters in the multi-temporal DEMs and orthophotos, fluvial channels development, morphological changes, continuous fluvial erosion and stream heads migration on slid slopes were confirmed. More sediment were mobilized and delivered out of catchments with increasing parameters of drainage network, texture and relief characteristics during post-seismic period 5, 7 and 9, with high rate of erosion during post-seismic periods in all study sites were confirmed. Site B and D (circular form of catchment) have higher average value and intensity of changes in most of hydro-geomorphometric parameters and higher volume of erosion than site A and C. Site A and

C exhibited fluctuating temporal trends of geomorphometric parameters in certain post-seismic periods, likely due to its gentler slopes and elongated, narrow shape, which limits surface runoff and gully expansion in small tributaries. In contrast, steeper slopes and wider terrain in site B and D allow more surface runoff contributing tributary formation and gully expansion, making it more prone to erosion.

Changes on geomorphometric and hydraulic parameters with fluvial network development and morphology consist of gradual and periodical fluvial erosion, slope processes, gully and channel networks, were corresponding with rainfall intensity, soil minerals on slid slopes, variability on forms of drainage basins, lack of root reinforcement by vegetation recovery and freeze – thaw action, with interactions of higher surface runoff, fluvial erosion, stream channel development and further slope deformations.

The construction of an inventory describing post-earthquake geomorphic responses at the basin scale is one of the contribution of the present study. Besides, the present research identified and developed an inventory of the post-seismic morphological responses in drainage basins including inter-active and co-existed natural phenomenon (i.e. elevation changes, Sediment connectivity, drainage network developments with mapping of stream networks and quantitative hydro-geomorphometric parameters) among 4 adjacent watersheds affected by the 2018 Hokkaido Eastern Iburi Earthquake, by using Digital Elevation Models and Geographical Information System. The systematic data analysis of various hydro-geomorphological parameters, spatial distribution of areas with elevation changes and identification of drainage network development in landslide-affected drainage basin provide evidence and understanding on slope-fluvial processes and contribution to other scientific researches in drainage system. The comparison on small scale/sub-watershed affected by coseismic landslides with different shapes/forms of catchments play important role on conservation and management of watershed in the aspects of erosional and sedimentation rates in those slid slopes affected coseismic landslides which are very essential for tectonic active regions. The present research aroused the importance for concerning small-scale/sub-watersheds on fluvial-morphology which was under-estimated and relevant related researches were limited. Furthermore, the approach of multi-inter-related perspectives and multi-function analysis with combination of hydraulic and geomorphometric parameters provides more detail and comprehensive analysis and understanding in fluvial morphology at those catchment affected by coseismic landslides. Besides, the methodology of using threshold areas with value of flow accumulation, flow direction and site-verification for stream channels and stream heads extraction provides an alternative analytical method on stream network extraction and stream head location and makes the analysed result more accurate and reliable which may also be applied on case study of large scale watershed. Furthermore, systematic combined analysis with multi-perspectives and multi-function correspondent factors (rainfall intensity, variation in forms of watershed, property of soil minerals, level of root reinforcement and freeze and thaw action) on small scale sub-watershed with various co-existing natural phenomenon in the present study were very limited and rare. Using multi-perspectives and multi-functions orientated approach in the present study contribute to relatively more reliable and convincible scientific analysis and results, and also be able to eliminate the under-estimation on the influence of other correspondent factors for giving a relatively more comprehensive analysis and understanding from an unbiased aspects on the formation, process and results of those natural phenomenon. The above key findings in the present study may contribute to continuous and progressive scientific research on fluvial evolutionary study in catchments affected by coseismic landslides. The present study highlight the interactions between fluvial erosion and deposition in mountainous basins which enhances understanding of post-seismic hydro-geomorphometric evolution in landslide-affected slopes and the interrelationships between those corresponding factors in multi-aspects. The analyzed results of progressive drainage network development and changes in drainage basin fluvial-geomorphological parameters might be valuable for long-term effects investigation, continuous monitoring for landslide with risk reduction and long-term fluvial landscape evolutionary studies, such as the role of landslides on slope-fluvial channel initiation and drainage headward erosion, which would be beneficial for progressive fluvial-evolutionary study, watershed management and investigation of sediment connectivity in catchments affected by earthquake, such as necessity for effective soil protection measures on slopes affected by coseismic landslides based on the difference in form of catchments. Further assessments and monitoring on morphological changes and drainage network development, impact of other factors and detailed processes over years or decades are recommended.

1.1 The 2018 Hokkaido Eastern Iburi Earthquake

In accordance with the Japan Meteorological Agency (JMA), strong earthquake with Magnitude 6.7 happened in Iburi sub-prefecture of Southern Hokkaido at 03:07am on 6th September, 2018, which caused large scale of landslides in Eastern Iburi region (Figure 1.1).

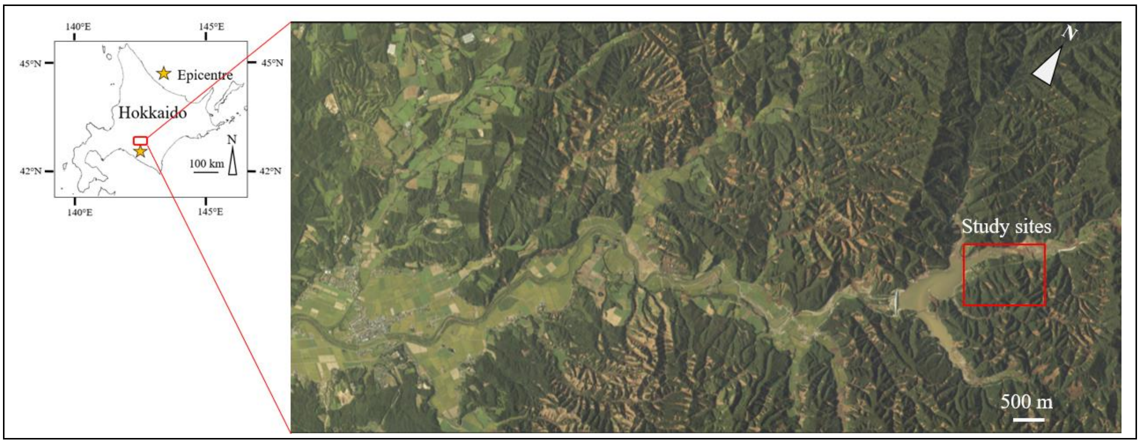

Figure 1.1: 2018 Hokkaido Eastern Iburi Earthquake (HEIE): An aerial photo taken on 6th September, 2018 indicating ground surface after 2018 Hokkaido Eastern Iburi earthquake in northern Atsuma Town. Source: Geospatial Information Authority of Japan

As reported by the Geospatial Information Authority of Japan (GSI) and Geological Survey of Japan (GSJ), the Epicenter with the focus depth of 37 km was located at 42.690°N and 142.007°E near Karumai Fault, Biratori Fault and Atsuma Fault within Ishikari Teichi Touen Fault Zone which has been shown in Figure . Apart from that, 230 aftershocks were recorded between 6th and 8th September, 2018. On average, 7cm uplift of land surface was recorded by Geospatial Information Authority of Japan (GSI). Moreover, based on the PlanetScope images, 7837 coseismic landslides were identified and the estimated landslide coverage area was about 700 km^2 (Wang et al., 2019). Most of the coseismic landsides were shallow soil slides which happened in the locations with average slope gradient of 19°. What is more, in general, 99% of the coseismic landslides were located in areas with less than 300 meters in elevation and within 100 meters distance from rivers (Wang et al., 2019). The fine-grained size of Ta-d tephra layers (0.008 mm-0.71 mm grain diameter) was sensitive to liquefaction and collapsed during earthquake (Kokusho and Fujita, 2001; Kasai and Yamada, 2019). Previous strong earthquake with magnitude 6.8 happened in Hokkaido on 20th February, 1913.

1.2 Literature review

Investigations have been carried out for the mechanisms of coseismic landslides in Eastern Iburi region (e.g., Ishimaru et al., 2020; Wang et al., 2019), for which the Tarumae-d tephra layer with fine-grained texture and high water infiltration capacity (Ishimaru et al., 2020) was considered as the inherent factor (Kasai and Yamada, 2019).

Earthquake with coseismic landslides could have effects on fluvial channel (Li et al., 2008). Tectonism such as earthquakes could change the fluvial and drainage patterns (Twidale, 2004). Slight inclination of slope may cause the change of drainage pattern from parallel or subparallel pattern (Twidale, 2004). Also, steeper the slope, more streams might be expected (Johnson, 1933; Dietrich et al., 1986). Changes of fluvial channel morphology (Li et al., 2015) such as slope of stream channel (Twidale, 2004) in areas with coseismic landslide are expected. A systematic geomorphometric analysis helps to understand linear, areal, and relief aspects of drainage basin (Zhang and Guilbert, 2012).

Continuous changes in fluvial channels, slopes and drainage patterns are expected during post-seismic periods. In addition, the inter-relationship between drainage density, channel slope, hillslope and channelization were estimated to be significant (Lin and Oguchi, 2004) and the analysis of longitudinal & transverse profiles of hilly and mountainous watersheds to a certain extent may indicate the changes on fluvial geomorphology in Japan (Lin and Oguchi, 2009). Quantitative analysis of geomorphometric parameters were necessary to indicate the form and predominant processes within watershed relating to mass movement, surface water and understanding of soil erosion and discharge characteristics of stream (Ayele Almaw Fenta, 2017; Prabhakaran and Jawahar Raj., 2018). The channel head location may be determined by a tradeoff between the frequency of shallow landsliding and the magnitude and frequency of bedload transport (Hattanji et al., 2006). Channel head advances upstream by shallow landsliding and migrates downstream as a result of sediment supply for side slopes during the landslide recurrence interval (Imaizumi et al., 2010). In mountains with frequent landslides, active sediment supply from lateral hillslopes buries channels and facilitates downstream migration of channel heads, (Imaizumi et at., 2010). Channel heads could advance upstream by shallow landsliding (Dietrich et al., 1987).

High-magnitude earthquakes and related coseismic landslides often generate large volumes of mobile sediment in catchments (Keefer, 1984; Keefer, 1994; Wang et al., 2015), which was expected as a key role in the long-term erosional budget (Keefer, 1994; Parker et al., 2011; Roback et al., 2018). Spatial distribution of coseismic landslides might be related to the distribution of landslide debris which was delivered directly to channel especially coarser ones, in connected channels (Li et al., 2015). Locations of sediment accumulations within channels depend on various factors in watersheds such as sediment supply, watershed areas and channel gradients (Dadson et al.,2004; Koi et al., 2008). In earthquakes, sediments produced by landslides are accumulated within channels and hillslopes more than rainfall-induced landslides (Dadson et al., 2004). 60-90% of sediment produced by 1993 Hokkaido Nansei-oki earthquake remained within watersheds (area: 3-16 km2) in Japan (Saito et al., 1995). Sediment deposits in the reservoir increased in the period of sediment supply by landslides in the Miyagawa Dam Watershed (Imaizumi and Sidle, 2007). The distribution of landslides induced by earthquake has been studied as their importance in sediment storage in watersheds (Korup, 2005) which affected discharge with the study of hydrology & hydro-geomorphology. Besides, correlation between landslide areal density (LAD), channel connected landslide areal density, landslide channel connectivity and suspended sediment yield were investigated (Li et al., 2008). The sediment connectivity for a long term should be related to the catchment-wide geomorphological dynamics including sediment cascades. Therefore, investigations on the sediment connectivity between landslides and channels is crucial for assessing the increase or decrease in the sediment yield in the catchments for decadal or century scales (Koi et al., 2008; Li et al., 2015) and alters spatial sediment dynamics in watersheds (Dadson et al.,2004; Koi et al., 2008). Those analysis are essential for designing disaster risk reduction (Arata et al., 2021) and the linkage and spatial variation can contribute for predicting long term sediment dynamics. However, those aspects were poorly understood at present (De Vente et al., 2013).

As an important indicator for landslide hazard and risk assessments, landslide mobility has attracted considerable attention in the literature, which has potential direct societal impacts because with increasing travel distance and height of landslide (Zhao et al 2021). Landslide mobility index is commonly known as the H/L ratio (Corominas, 1996). Landslide mobility induced by the 2018 Hokkaido Eastern Iburi earthquake is described by the relationship: H/L = 1.46–0.24 × log10 (landslide area), whereas 7058 landslides triggered by the 2018 Hokkaido Eastern Iburi earthquake exhibited an average landslide mobility of 0.33. (Zhao et al 2021).

Assessments of long-term, post-seismic morphological responses in drainage basin including fluvial processes and slope processing are relatively limited. Even gradual, such post-seismic changes may cause increases in sediment yield with different patterns (Li et al., 2015; Mizugaki et al., 2019), and it is necessary to continuously monitor the post-seismic morphological changes with fluvial characteristics such as drainage network development and hydro-geomorphometric parameters in the Iburi region.

A preliminary study conducted by Lo et al. (2023) and Lo (2025) revealed coseismic and post-seismic changes in morphometric parameters within two drainage areas, linked to stream network developments. By combining those concepts, further explores on the temporal changes in hydro-geomorphometric parameters, elevation across watersheds, drainage network with developing a robust inventory for continued monitoring of slope and fluvial processes, enhancing our understanding of interactions between fluvial erosion and deposition in mountainous basins, sediment dynamics in earthquake-affected drainage basins with diverse catchment forms, long-term assessment of drainage network development with changes in different hydro-geomorphometric parameters, sediment connectivity and mobility with slope processing and morphological changes caused by coseismic landslides following the 2018 Hokkaido Eastern Iburi Earthquake.

Global Navigation Satellite System (GNSS) have been considered as effective tools and key technique for acquisition of topographic information with high resolution and accuracy in field survey (Hayakawa and Oguchi, 2014). Application of Structure-from-Motion and laser scanning technology have been considered as effective tools and key technique for acquisition of topographic information with high resolution and accuracy in field survey (Ajioka and Hori, 2014; Hayakawa, 2016). Apart from that, stream profile morphology could be analyzed efficiently and precisely by using Digital Elevation Models (DEMs) and Geographical Information System (GIS) (Hayakawa and Oguchi, 2006). Using unmanned Aerial Vehicle (UAV) have been considered as one of widely recognized methods for mapping and monitoring different active deformation at the earth's surface (Fonstad et al., 2013; Piras et al., 2017; Feurer et al., 2018; Hayakawa et al., 2017) such as river morphodynamics (Gomez and Purdie, 2016; Aicardi et al., 2017; Bolognesi et al., 2016; Benassai et al., 2017). The improvement of UAV technology could provide more accurate investigation and analyses for the changes of drainage geomorphology. SfM can be applied on fluvial study for geomorphological mapping and to detect changes in landforms measurements. By taking photos, operating alignment and meshing, topographic data such as DEMs and 2.5D data with z values based on x y plane coordinates can be generated for extracting contours, profile, slope gradient, etc. Consequently, by comparison the DEM of Difference (DoD) in different periods, the changes in landform and geomorphology could be shown (Lane et al., 2003). The mapping of landslides displacement could be achieved (Lucieer et al., 2013). The UAV-based SfM-MVS photogrammetry (acquisition of aerial photos by UAV) was suitable for investigation of larger coverage area with more than 100 photos per each flight for making high resolution 3 dimensional images for analysis. In advance, due to relatively simple equipment with low-cost and shorter investigation time (Nyimbili et al., 2016), Structure from Motion (SfM) have become one of the most essential techniques in remote sensing for creating 3D models from multi images with high accuracy (Ajioka and Hori, 2014). To a large extent, Structure from Motion techniques could also be applied in varies sciences such as geomorphology, geology, mountain hydrology (Scaioni et al, 2018) by providing millimeter-scale measurements with high accuracy and resolution Digital Elevation Models (DEMs), orthorectified, contour and hillshade images. In accordance with Nyimbili et al., 2016, wide range of applications have included geomorphology in monitoring river ($A = \pi r^2$) bed topography and planform, river bank and gully erosion (e.g. Frankl et al., 2013). UAVs and SfM-MVS-photogrammetry were regarded as potential applications on investigation landslides triggered by earthquake. By using the sequential Digital Surface Models (DSMs), the difference of DSMs based on cell-by-cell subtraction could be produced which might be relevant to geomorphic studies of the topographic and volumetric changes though time.

1.3 Objective

The objectives of this research are to identify the post-seismic morphological responses in drainage basins including among 4 adjacent watersheds with different plan forms with similar geology, climate, and vegetation covers affected by the 2018 Hokkaido Eastern Iburi Earthquake (HEIE), and to an inventory of those responses including comparative analysis on elevation changes, drainage network developments, quantitative analysis of inter-related hydro-geomorphometric parameters and sediment connectivity which correspond with multi aspects analysis of rainfall intensity, soil minerals on slid slopes, variability on forms of drainage basins, lack of root reinforcement by vegetation recovery and freeze – thaw action, on bare slopes during coseismic (5th October, 2012 - 11th September, 2018) and post-seismic periods (11th September, 2018 - 29th October, 2021) by using UAV-based multi-temporal topographic data (DEMs) and Geographical Information System (GIS) with the threshold area of sub-watersheds assisted by threshold of flow accumulation and flow direction and field verification. The findings in the present research can contribute to long-term assessment of drainage network development with changes in different hydraulic and geomorphometric parameters, sediment connectivity and mobility with morphological changes in drainage basins caused by coseismic landslides following the 2018 Hokkaido Eastern Iburi Earthquake, which will be useful for monitoring of slope processing, fluvial landscape evolution, watershed conservation with management and enhancing our understanding of sediment dynamics in earthquake-affected drainage basins with diverse catchment forms with evaluating the rate of fluvial erosion and sedimentation in the earthquake-affected drainage basins with different forms of catchment.

Chapter 2. Study sites

2.1 Location

The study sites are 4 small catchments on the left of Atsuma River (Figure 2.1). The target catchments A, B C, and D are located approximately 10 km horizontal distance from the epicentre (42.690ºN and 142.007ºE) (Japan Meteorological Agency 2019) with an area of 70315.02 m^2 (0.070 km^2), 104006.01 m^2 (0.104 km^2), 81639.45 m^2 (0.082 km^2) and 191068.22 m^2 (0.191 km^2) for locations A to D respectively (Figure 2.1.b, c, d and e). The basin of site A and C showed a relatively narrow shape (ca. 130 m in width and 670 m in length; 158 m in width and 637 m in length respectively) with less tributaries, which can be regarded as the "elongated" form, while site B and D showed a relatively wide shape (ca. 250 m in width and 650 m in length; 374 m in width and 710 m in length respectively) with more tributaries, which is closer to the "circular" form (Horton, 1932; Prabhakaran and Jawahar, 2018), Coseismic landslides and sedimentation of collapsed debris could be identified within the study sites (Figure 2.1 e). The estimated areas affected by coseismic landslide were about 10718.80 m^2 (0.011 km^2), 20832.97 m^2 (0.021 km^2), 7100.51 m^2 (0.007 km^2) and 76839.04 m^2 (0.07684904 km^2) for location A to D respectively. Approximately 15.24%, 20.03%, 8.70% and 40.22% of area in the catchment A to D respectively were affected by the coseismic landslides. Relatively less impacts by artificial modification than the other slopes in the area after earthquake and preserved natural conditions are expected. The target watersheds are appropriate for UAV mapping for comparisons. Small check dams have been constructed at the outlet of the tributaries draining into the downstream Apporo Reservoir. Watersheds of study sites A – D are less than 1 km^2 (small scale) which are considered as sub-/mini-/micro-watershed They are suitable for detailed site-specific study and assessment such as intensity of erosions, impacts of spring, location of stream heads, discharge, gully stream and sedimentation mechanism with field surveys verification and assessment features with high-resolution maps and aerial photos, which play important role on conservation and management of watersheds. However, analysis on sub-watershed was relatively limited (Amiri et al., 2019). Morphometric variations in drainage basins during post-seismic periods due to the variability on forms of catchments were expected in 4 studied catchments, which can be divided into circular shaped and elongated shape. Analysis on those corresponding effects was limited.

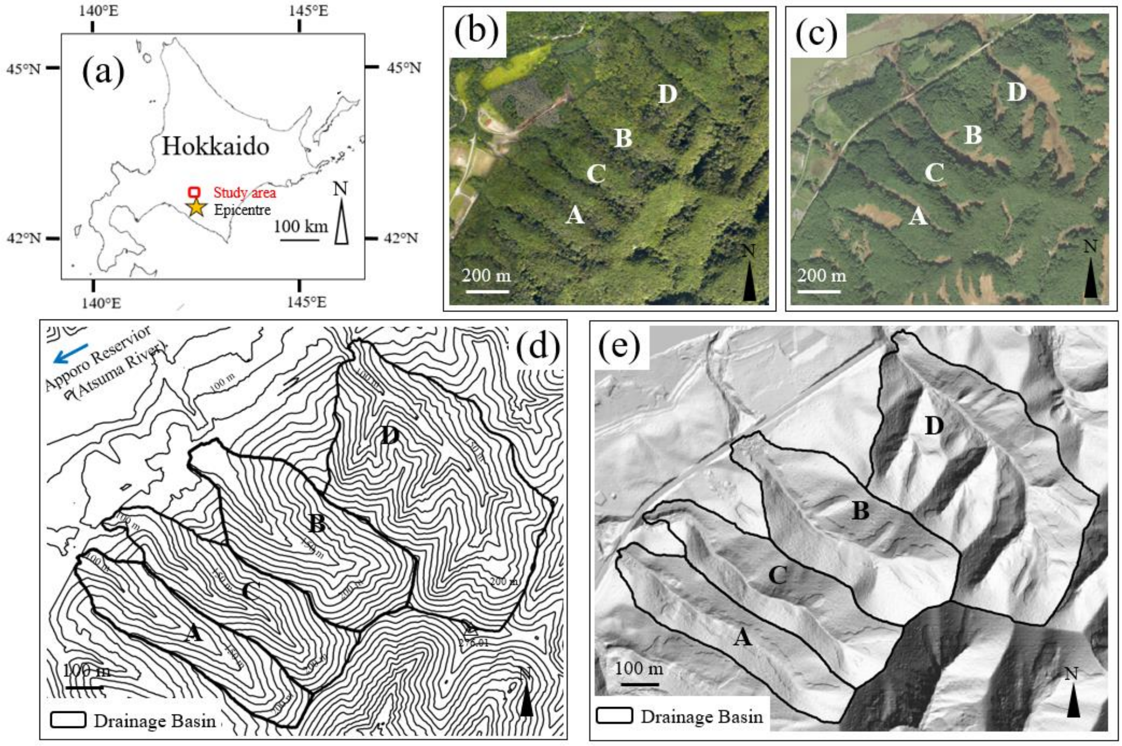

Figure 2.1: Study area. (a) Location of the study area in Hokkaido, Japan (GSI). (b) Aerial photos of Study site A−D on October 5, 2012 (GSI). (c) Aerial photos of Study site A−D on September 11, 2018 (GSI). (d) Contour map around the study area (delineated from post-seismic ALS DEM: September 11, 2018) (e) Hillshade images of Study site A−D (September 11, 2018) (Hokkaido Prefecture, 2020).

2.2 Geological structure

Eastern Iburi region is an area with folding and faulting (Ayalew et al., 2011). The parent rock in Eastern Iburi region was classified as Neogene Sedimentary rocks (23 Ma-2.6Ma) (Matsuno and Ishida, 1960, Takahashi and Wada, 1984) (Figure 2.2.1)

Source: Geological Survey of Japan, Active Fault Database of Japan

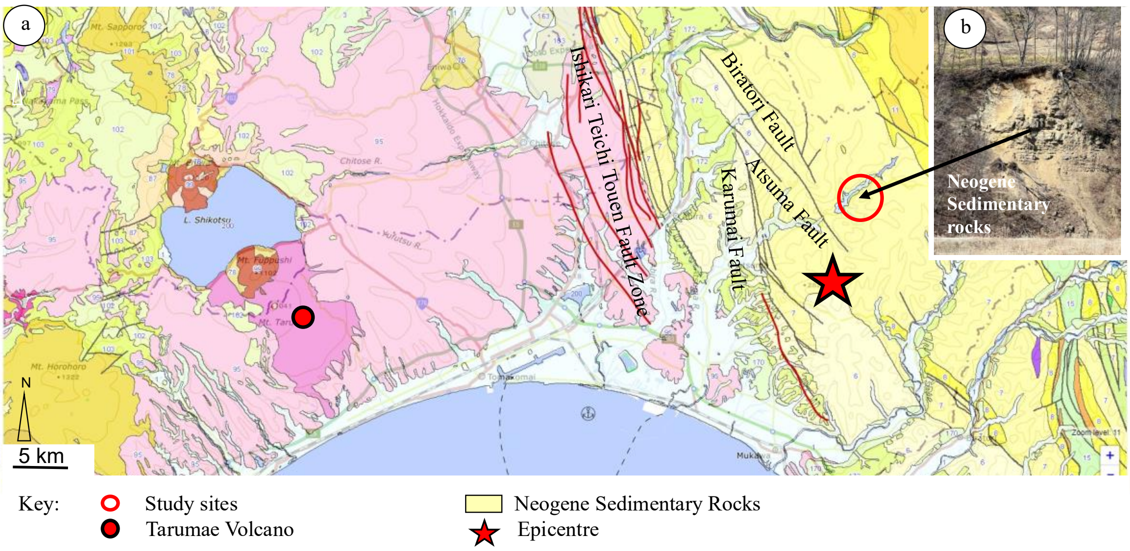

Figure 2.2.1: (a) Geological map of Eastern Iburi Region (Geological Survey of Japan, Active Fault Database of Japan) https://gbank.gsj.jp/activefault/search. (b) Neogene Sedimentary rocks (photo: April 23, 2020)

Substrate rocks of the 4 study sites are shale and mudstone of Karumai formation of Late Miocene (Ito et al, 2020) formed 11.6 million to 5.3 million years ago (Matsuno and Ishida, 1960; Takahashi and Wada, 1984). Volcanic ash from Tarumae volcanic eruption (~9000 years ago) formed thick tephra layers (1-3 m) and covered the bedrocks (Uda et al., 1979; Hirose et al., 2018; Yamagishi and Yamazaki., 2018). Three major types of the tephra layers were identified, namely Spfa-l (42 ka) by Shikotsu caldera eruption (Machida and Arai, 2003), En-a pumice (20 ka) by Eniwa volcano eruption (Machida and Arai, 2003), and Ta-d pumice (9 ka) by Tarumae volcano eruption (Hirose et al., 2018) with more than 50 cm thickness (Ishimaru et al., 2020). In the northern part of the study area, the En-a layer is thick, at > ca. 100 cm, while in the southern part, the Ta-d layer is thick, at > ca. 50 cm (Ishimaru et al., 2020). According to the grain size distribution analysis of Ta-d tephra layers, the main components of soil in the tephra layer were sand, silt and clay with grain size diameter between 0.008 mm and 0.71 mm (Kasai and Yamada, 2019) (Figure 2.2.2), which was sensitive to liquefaction and collapsed during earthquake (Kasai and Yamada, 2019). The tephra layers were the main constituents of the landslides caused by this earthquake (Ishimaru et al., 2020).

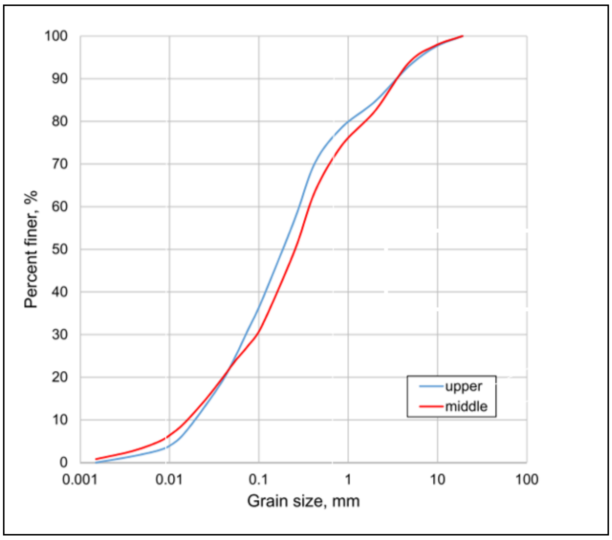

Figure 2.2.2: Grain size distribution of Ta-d soil samples. Upper: sample collected from the upper part of the layer; Middle sample collected from the middle part of the layer. (Kasai and Yamada, 2019)

2.3 Climate

2.3.1 Rainfall

According to Atsuma Meteorological Station (42°43.8'N, 141°53.3'E, ca. 11 km west away from the study sites), the annual total rainfall in Iburi Prefecture varied between 802 mm and 1594 mm (1923-2021), while the total annual rainfall in Atsuma region was 1136.5 mm in 2018, 849.0 mm in 2019, 797.5 mm in 2020 and 1077 mm in 2021 (Japan Meteorological Agency (2023)). The total monthly rainfall was 155 mm on October 2018, while it was higher than 100 mm on June, August and October, 2019, and March and August, 2020, and April, June, August, October and November, 2021. Typhoon No. 21 reached Hokkaido on September 5, 2018 with the maximum daily rainfall intensity of 9 mm/hr (Investigation Period 1). Typhoon No. 24 reached Hokkaido on October 1, 2018 with maximum daily rainfall intensity of 9.5 mm/hr and 13.5 mm/hr on October 1 and 2, 2018 respectively The maximum daily rainfall intensity increased gradually from April 15, 2019 (5 mm/hr) to Oct 4, 2019 with 19.5 mm/hr in October due to the intensive rainfall by Typhoon No. 18 which approached Hokkaido on October 4, 2019 (Investigation Period 2). In 2020, the maximum daily rainfall intensity increased gradually from April 29 (5 mm/hr) to September 5 with16.5 mm/hr (Investigation Period 3 and 4). In 2021, the maximum rainfall intensity increased gradually from April 18 (7 mm/hr) to August 10 with 22.5 mm/hr, which decreased to 13.5 mm/hr on 11th October (Investigation Period 7 to 9). The maximum daily rainfall increased from April, 2021 (49 mm/hr) to August, 2021 (77.5 mm/hr) (Figure 2). The total monthly rainfall increased from May, 2018 (67.5 mm) to August, 2018 (217.5 mm) (Investigation Period 1); from April, 2019 (41 mm) to August, 2019 (170.5 mm) (Investigation Period 2); from May, 2020 (54.5 mm) to August, 2020 (118.5 mm) (Investigation Period 3); and from May, 2021 (90.5 mm) to October, 2021 (151.5 mm) (Investigation Period 7 to 9) (Japan Meteorological Agency (2023)) (Figure 2.3.1).

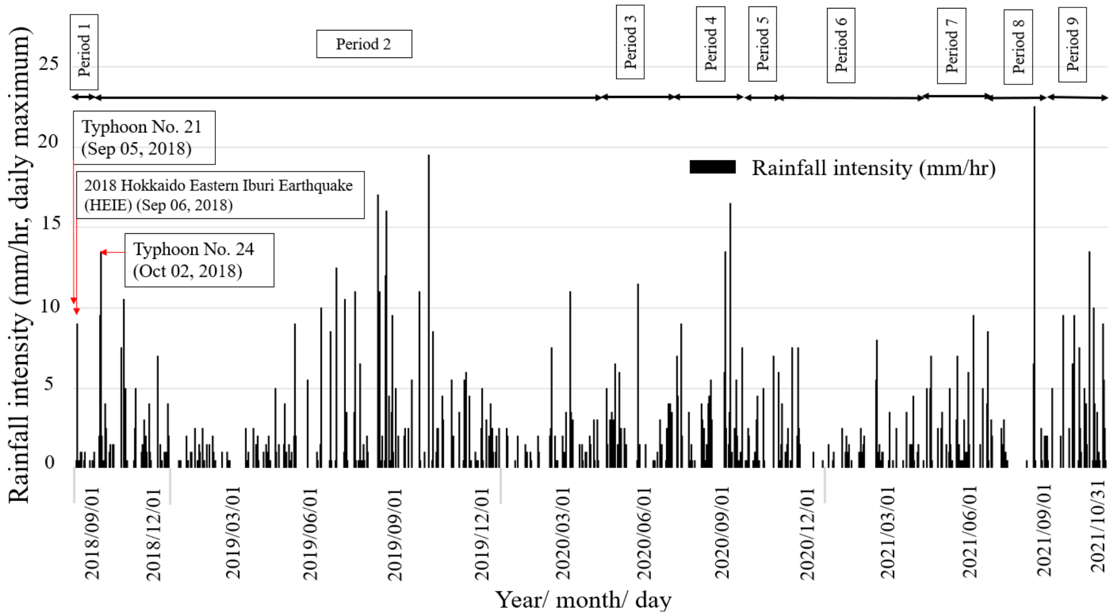

Figure 2.3.1. Rainfall intensity (mm/hr, daily maximum) and from September 2018 to October 2021 recorded by Atsuma Meteorological Station (Japan Meteorological Agency, 2023)

2.3.2 Temperature

According to Atsuma Meteorological Station (42°43.8’N, 141°53.3’E, ca. 11 km west away from the study sites), the annual mean temperatures were 7.3°C, 7.5°C, 7.9°C and 8.0°C for 2018, 2019, 2020 and 2021 respectively, while the annual mean temperature of years from 1984 to 2021 was and 6.88°C. The annual maximum and minimum temperatures were 30.9°C and -24.1°C (2018), 32.2°C and -22.9°C (2019), 32.9°C and -23.6°C (2020) and 34.1°C and -23.7°C (2021) Winter season is between November to March (1991-2021) with average maximum daily temperature of 5.5℃ (November 2021) and minimum of -9.8 ℃ (January 1998) (Japan Meteorological Agency, 2023). According to the nearby meteorological station at Abira (42º48.8´N, 141º44.7´E, ca. 15 km away), maximum snow depth in the region is 69 cm in average (1991-2021) peaking in February. Maximum snow depth was 69 cm, 65 cm, 52cm and 63 cm from 2018 to 2021 during the investigation periods (Japan Meteorological Agency, 2023).

Number of days with daily maximum and minimum temperature above 0℃ (above freezing point) and below 0℃(below freezing point) in each month from September 2018 to October 2021 recorded at Atsuma Meteorological Station were indicated in Fig.2.3.2 (Japan Meteorological Agency, 2023).Within those, totally 16 months between September 2018 and October 2021 had 10 or more than 10 days with maximum daily temperature above 0ºC and minimum daily temperature below 0ºC. Between October 2020 (Autumn) and April 2021 (Spring) (Investigation Period 6), 5 months had 10 or more than 10 days with maximum daily temperature above 0℃ (freezing point) and minimum daily temperature below 0℃ (freezing point). Also, November 2020 (Autumn) and April 2021(Spring) (within Investigation Period 6) had 19 days per month with maximum daily temperature above 0℃ (freezing point) and minimum daily temperature below 0℃ (freezing point) (Figure 2.3.2).

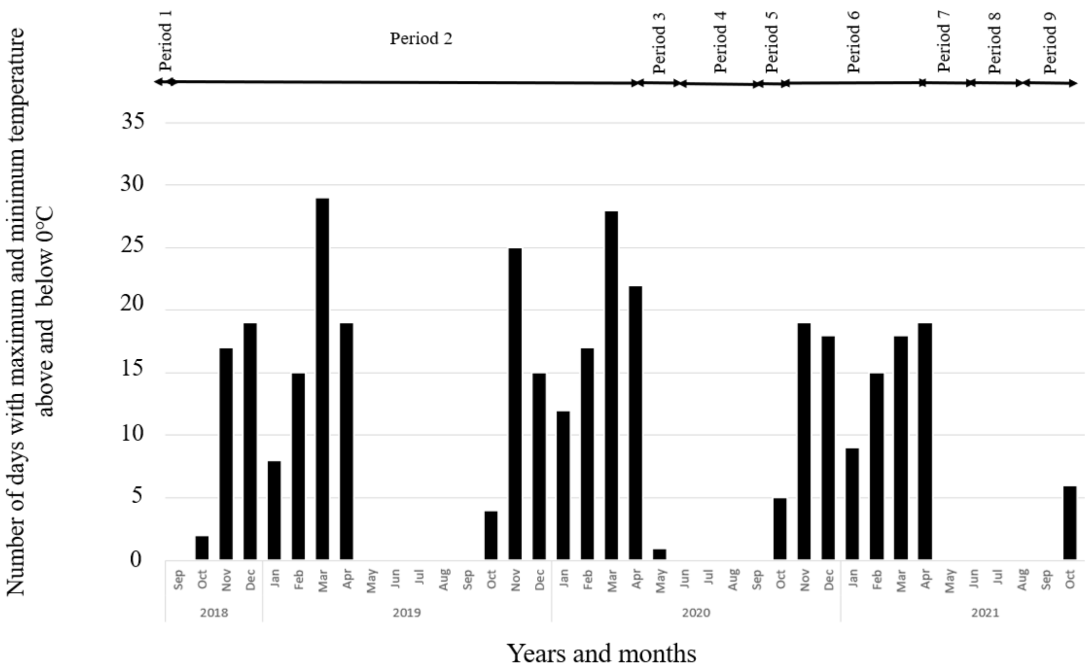

Figure 2.3.2. Number of days with maximum and minimum temperature above 0℃ and below 0℃ in each month from September 2018 to October 2021 at Atsuma Meteorological Station (Japan Meteorological Agency, 2023)

Chapter 3. Methodology

Continuous investigations were conducted for collection of high resolution images and relatively precise topographic data with geo-reference. The post-seismic morphological responses of drainage basin in the study catchments were examined by comparing the post-seismic Digital elevation models (DEMs), aerial photos and orthorectified images generated from topographic data, which were collected by application of unmanned aerial vehicle (UAV) during the field surveys.

3.1. Data collection

3.1.1 Field surveys with Unmanned Aerial Vehicle (UAV)

For data and information collection, 8 field surveys were conducted from April 2020 to October 2021 (Period 2 to 9) which were indicated in Table 1. Weather condition was considered to ensure stable and safe autonomous UAV flight. A UAV of DJI Phantom 4 RTK, equipped with an RGB camera (20 M sensor and pre-calibrated lens) (Figure 3.1.1 b), and Matrice 300 RTK with Lidar sensor (Figure 3.1.1 c) were used with the terrain following mode to keep the relative flight height of approximately 100 m from the ground. A base station of global navigation satellite system (GNSS) receiver (DJI D-RTK2) (Figure 3.1.1 a) was used to perform the real-time kinematic (RTK) correction of the GNSS-derived aircraft positions during the flight, providing the geographic coordinates of each camera image at a centimeter-level accuracy. Aerial photos taken by the UAV were used for processing dense point clouds, DEMs and high resolution orthorectified images (Figure 3.1.2 a-c). We also performed field observations of the study sites by walking along the drainage valleys on study site B and D (Figure 3.1.1 d-j) until the upslope of drainage basin to identify morphological changes such as stream-bed deposition, gully erosion and stream network development (Figure 3.1.1 d-j).

3.1.2 Digital Elevation Modes (DEMs) by Airborne Laser Scanning models (ALS) and UAV-based SfM photogrammetry and UAV- Light Detection and Ranging (LiDAR)

Computer software such as Agisoft was applied to make the Digital Elevation Models (DEMs) and orthorectified images with high accuracy of geo-reference (Figure 3.1.2.1 a-c). Digital elevation models (DEMs) with a 0.5-m resolution, generated from airborne laser scanning (ALS) data of October 5 in 2012 and September 11 in 2018 (Hokkaido Prefecture, 2020a, b), were used to represent topography of pre- and post-earthquake. Acquisition of aerial photos by unmanned aerial vehicle (UAV) DJI Phantom 4 RTK and Matrice 300 RTK (Figure 3.1.1 b and c) were conducted during the field surveys (Figure 3.1.1 a-j) 4 times in 2020 (April 23, June 25, September 14, and October 30) and 3 times in 2021 (April 13, June 21, August 27 and October 29). DEM by UAV-Lidar was conducted on October 29, 2021. Based on the UAV-based aerial images, Structure-from-Motion Multi-View Stereo (SfM-MVS) photogrammetry was then performed using Agisoft Metashape software to generate point cloud (Figure 3.1.2.1 a), DEMs (Figure 3.1.2.1 b) and orthorectified mosaic images (Figure 3.1.2.1 c). The resolution of DEMs and orthorectified images were set at the finest capability (several to ten centimeters) of the point cloud density by SfM-MVS photogrammetry for each data set and the average camera location errors: X, Y and Z altitude (cm) of UAV-SfM DEMs from April 23, 2020 to August 27, 2021 are indicated in Table 3.1.1. A threshold value of 100 m^2 was used and converted to pixel counts depending on grid size. These values were empirically calibrated rather than uniformly standardized, so direct numerical comparisons across time periods are not the focus due to resolution differences. This study emphasizes structural and spatial characteristics. Different values of flow accumulation were applied to extract the stream channels and stream heads in each set of DEMs (Figure 3.1.2.1 (d), Figure 3.1.2.2, Figure 3.1.2.3, Figure 3.1.2.4 and Table 3.1.3) which were visually correspondent with the geomorphological features of stream channels and stream heads in the field and orthorectified images (Figure 3.1.2.1 (d)). Flow direction is used as additional supportive analysis to show the possible convergence of water flows at the stream head (Figure 3.1.2.1 (d)). The purpose for indicating stream head locations is providing supportive materials for the analysis of hydraulic parameters (i.e. the calculation of hydraulic radius, shear stress, critical shear stress and velocity and specific discharge) to identify and confirm the initiation of fluvial erosion at the stream head location, which is essential for confirming the correspondent stream network development and drainage pattern in the study sites.

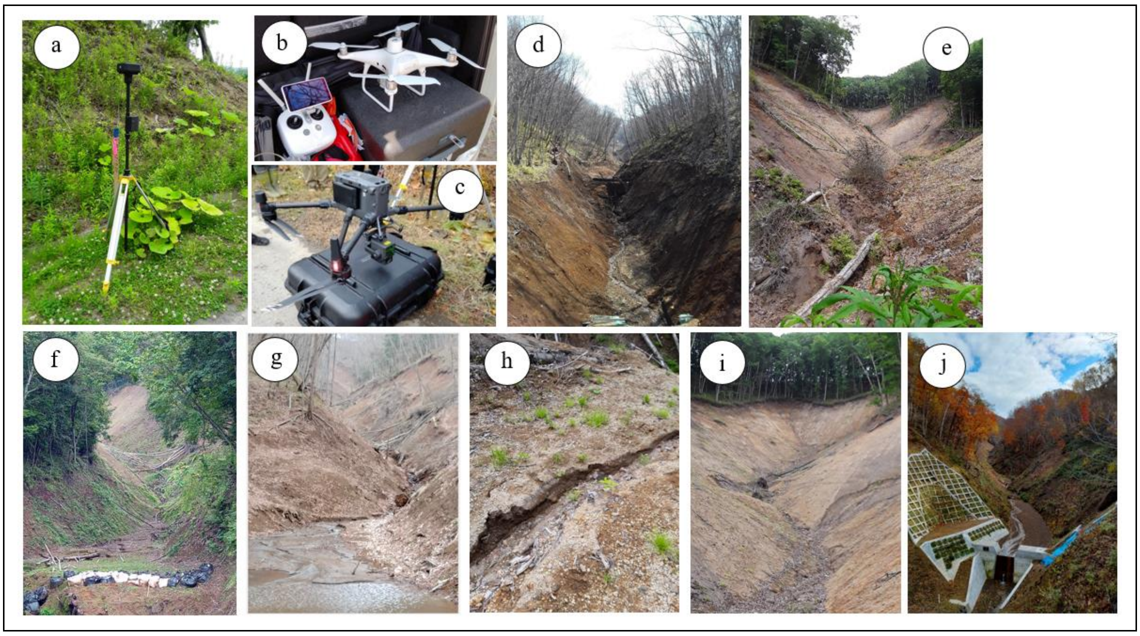

Figure 3.1.1: Field surveys: (a) A base station of global navigation satellite system (GNSS) receiver (DJI D-RTK2), (b) UAV of DJI Phantom 4 RTK, (c) Matrice 300 RTK with Lidar sensor, (d) Field survey April 23, 2020, (e) Field survey June 25, 2020, (f) Field survey September 14, 2020 (g) Field survey April 13, 2021, (h) Field survey June 21, 2021, (i) Field survey August 27, 2021, (j) Field survey October 29, 2021

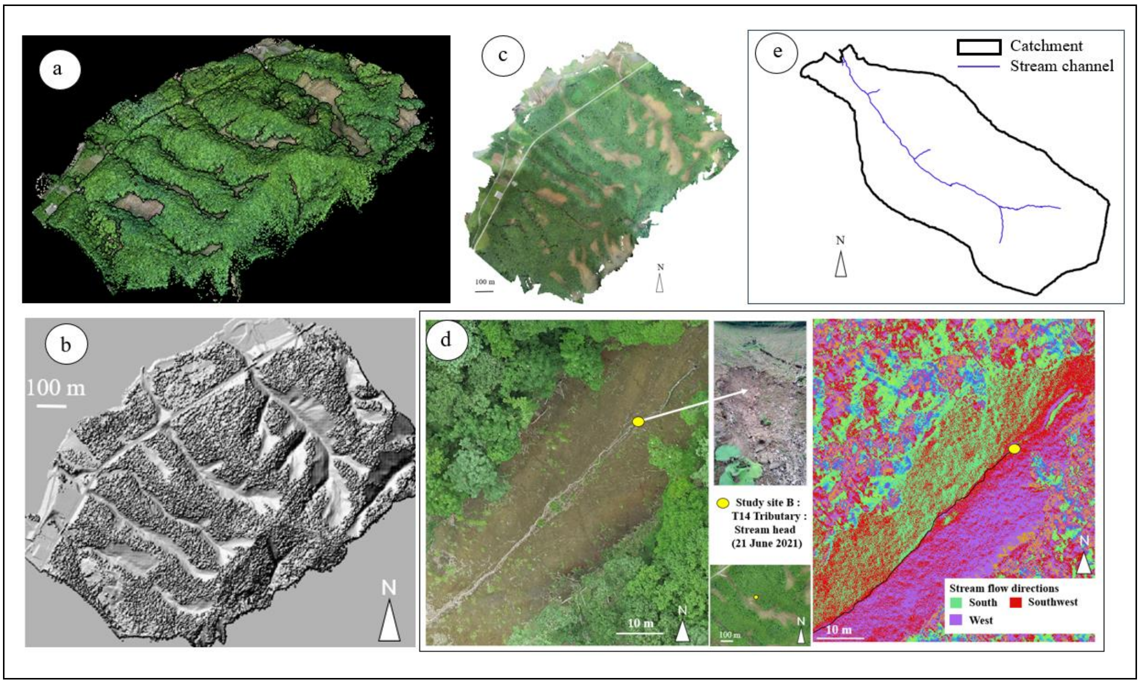

Figure 3.1.2.1: Data analysis (a) point cloud, (b) Digital Elevation Models DEMs, (c) Orthorectified mosaic image. (d) An example of a stream head with threshold value of 100 m^2 and adjustment of the threshold value of flow accumulation in DEM (June 21, 2021). (e) An example of delineation of catchment and stream channels in study site B by ALS DEM (2012).

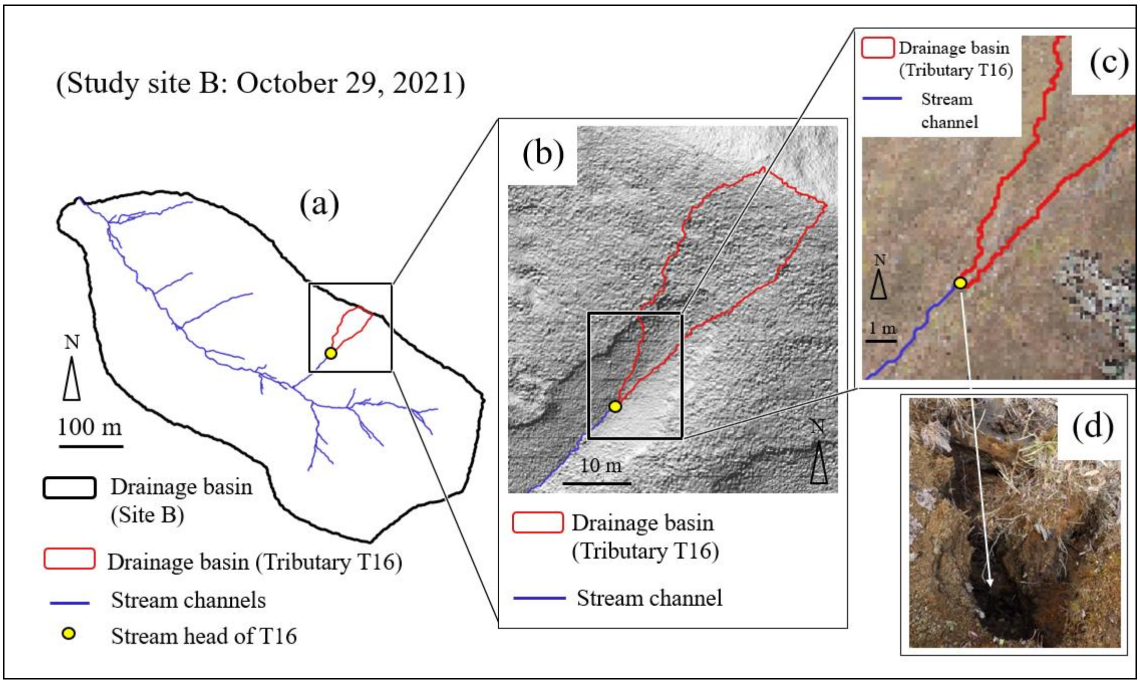

Figure 3.1.2.2: An example of the identified stream head location and it's catchment (Period 9) in site B derived from: (a) and (b) UAV-lidar DTM, (c) Orthorectified image, (d) Field photo (Lo, 2025).

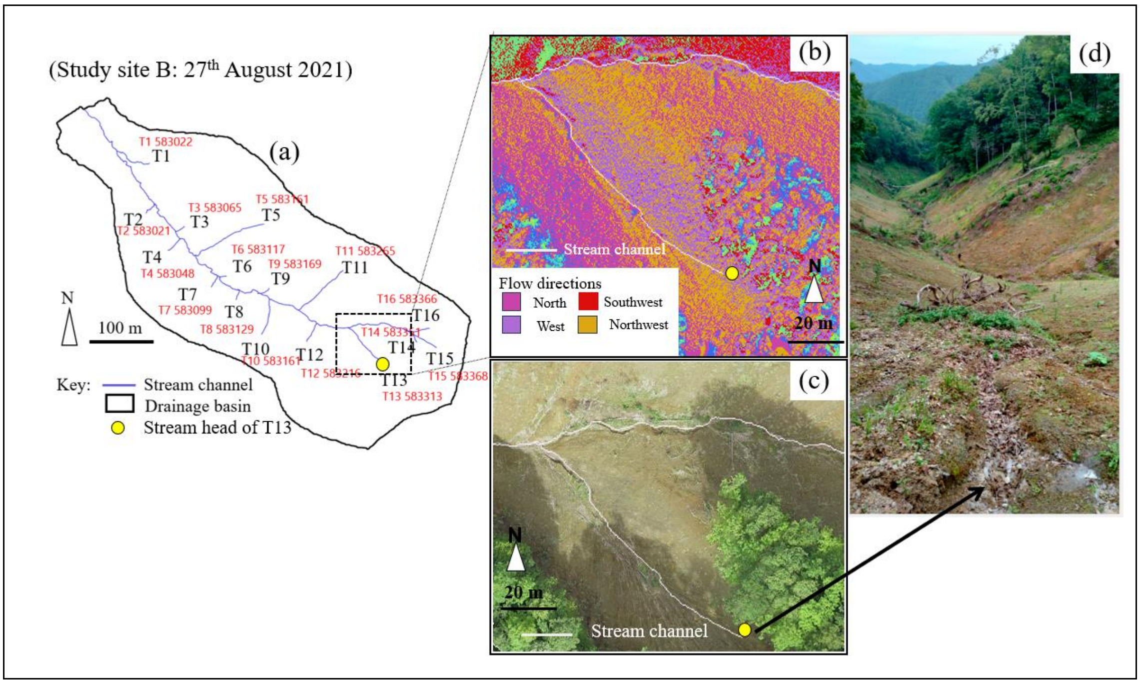

Figure 3.1.2.3: An example of the identified stream head location and it's flow accumulation (Period 8) in site B derived from: (a) and (b) UAV-SfM DSM, (c) Orthorectified image, (d) Field photo. (*Red number in (a): Value of flow accumulation of tributaries:)

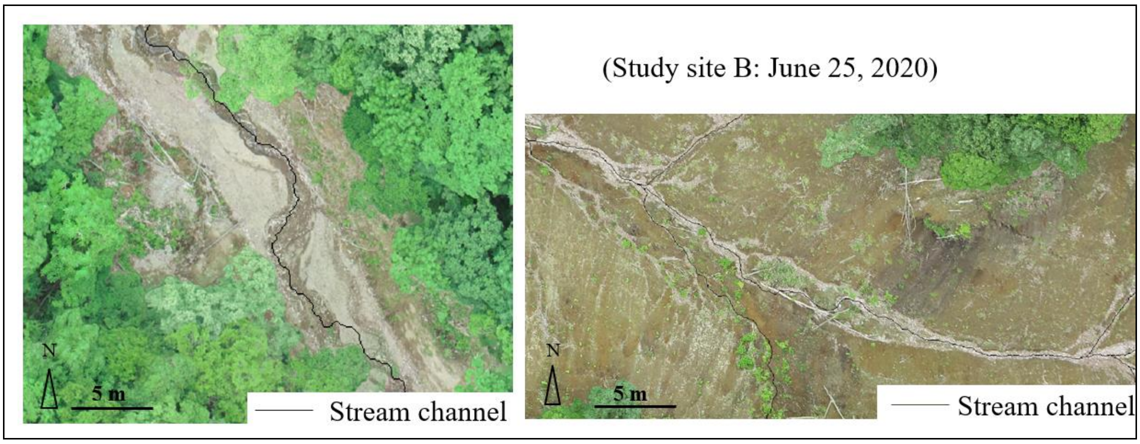

Figure 3.1.2.4: Examples of identified stream channels correspondent with orthorectified images (Period 2) in site B.

3.1.3 Periods of detection

The periods of changes in detection (Table 3.1.3) were divided into 9 sections as follows. Period 1: from October 5, 2012 to September 11, 2018 (6 years including the earthquake event), for which ALS DEMs are available; Period 2: September 11, 2018 to April 23, 2020 (approximately 1.5 years); Period 3: April 23, 2020 to June 25, 2020 (2 months), Period 4: June 25, 2020 to September 14, 2020 (2.5 months); Period 5: September 14, 2020 to October 30, 2020 (1.5 month); Period 6: October 30, 2020 to April 13 in 2021 (5.5 months); Period 7: April 13, 2021 to June 21, 2021 (2.5 months); Period 8: June 21, 2021 to August 27, 2021 (2 months); Period 9: August 27, 2021 to October 29, 2021 (2 months) for which UAV-SfM derived DEMs are applied for Period 2 to 8 and UAV-Lidar derived DEMs are applied for Period 9 (Table 3.1.3).

Period		Period 1	Period 2	Period 3	Period 4	Period 5	Period 6	Period 7	Period 8	Period 9
Duration (months)		72	20	2	3	2	5	2	2	2
Date	Oct 05, 2012	Sep 11, 2018	Apr 23, 2020	Jun 25, 2020	Sep 14, 2020	Oct 30, 2020	Apri 13, 2021	Jun 21, 2021	Aug 27, 2021	Oct 29, 2021
Type of acquisition	ALS	ALS	UAV-SfM	UAV-SfM	UAV-SfM	UAV-SfM	UAV-SfM	UAV-SfM	UAV-SfM	UAV-Lidar
Resolution of DEM (m)	0.5	0.5	0.115	0.112	0.062	0.073	0.092	0.079	0.249	0.02
Average camera location error										
X- Altitude (cm)	-	-	1.79	0.54	9.84	6.29	0.36	1.19	2.21	-
Y- Altitude (cm)	-	-	1.66	0.39	20.92	17.1	0.50	1.46	2.22	-
Z- Altitude (cm)	-	-	4.4	1.06	14.96	20.02	1.40	2.95	3.49	-
Threshold (flow accumulation	10278	11081	117484	227905	133874	158256	306852	157317	404280	18972

Table 3.1.3: Properties of topographic data and threshold value of flow accumulation for channel head identification.

3.1.4 Data of Soil moisture, Soil temperature, Photosynthetic active radiation (PAR) and Rainfall intensity (mm/hr)

On March 15, 2023, four sets (Set A, B, D and E) of USB Data micro station loggers (HOBO H21-USB), 5cm fork-shaped soil moisture sensors (S-SMC-M005), Soil temperature sensors (S-TMB-M002) and Photosynthetic active radiation (PAR) sensors (SLIA-M003) (Figure 3.1.4.1) were set on 4 target slide slopes caused by coseismic landslides after the 2018 Hokkaido Eastern Iburi Earthquake (two sets near stream outlet and two sets at middle course of stream in Study site B with north-facing and south-facing aspects (Figure 3.1.4.2) to measure the daily and seasonal variations on top soil moisture (m^3/m^3), soil temperature (°C) and Photosynthetic active radiation (PAR) (µmol m^{-2} s^{-1}).

Set B and E of Data multi station loggers were set on north-east facing slopes in middle course of main stream channel and lower course of main stream channel (near stream outlet) respectively (Figure3.1.4.2), while Set A and D of Data multi station loggers were set on south-west facing slopes in middle course of main stream channel and lower course of main stream channel (near stream outlet) respectively.

Also, on March 15, 2023, one set (Set C) of USB Data micro station loggers (HOBO H21-USB), 5cm fork-shaped soil moisture sensors (S-SMC-M005), Soil temperature sensors (S-TMB-M002), Photosynthetic active radiation (PAR) sensors (SLIA-M003) and Rain gauge (Davis) for micro-station logger (Figure 3.1.4.1 and 3.1.4.3) was set in set at upper course of stream in Study site D with north-facing aspect (Figure 3.1.4.3) D to measure the daily and seasonal variations on top soil moisture (m^3/m^3), soil temperature (°C) and Photosynthetic active radiation (PAR) (µmol m^{-2} s^{-1}) and Rainfall intensity (mm/hr). Rain gauge (Davis)(for micro-station logger) of Set C was set at the upper course of study site D (Figure 3.1.4.3) (42°46’ 44“N, 142°1’ 18“E) with the elevation 140 m for recording the data of rainfall intensity (mm/hr).

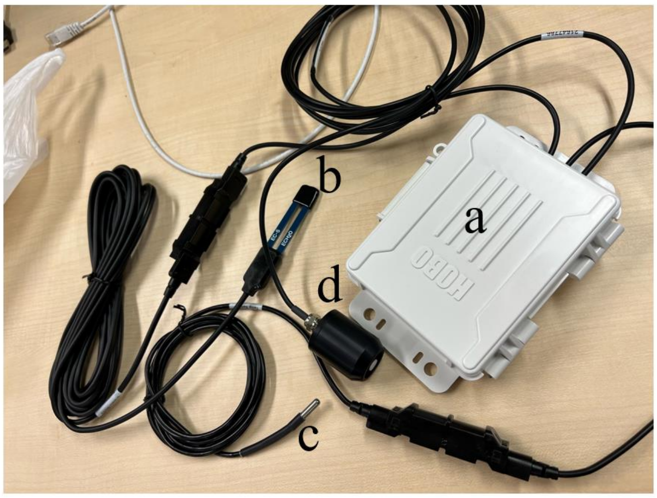

Figure 3.1.4.1: Equipment: (a) Data micro station loggers (HOBO H21-USB), (b)5cm fork-shaped soil moisture sensors (S-SMC-M005), (c) Soil temperature sensors (S-TMB-M002) and (d) Photosynthetic active radiation (PAR) sensors (SLIA-M003).

The coordinates of Set A was 42.7781°N, 142.0158°E. The coordinates of Set B was 42.7778°N, 142.0161°E. The coordinates of Set D was 42.7792°N, 142.0144°E. The coordinates of Set E was 42.7790°N, 142.0143°E. The coordinates of Set C was 42.7789°N, 142.0217°E.

The measurement are continued automatically for recording the daily data on top soil temperature, moisture and solar insolation on the target slid slopes on study site B and D, caused by coseismic landslides after the 2018 Hokkaido Eastern Iburi Earthquake.

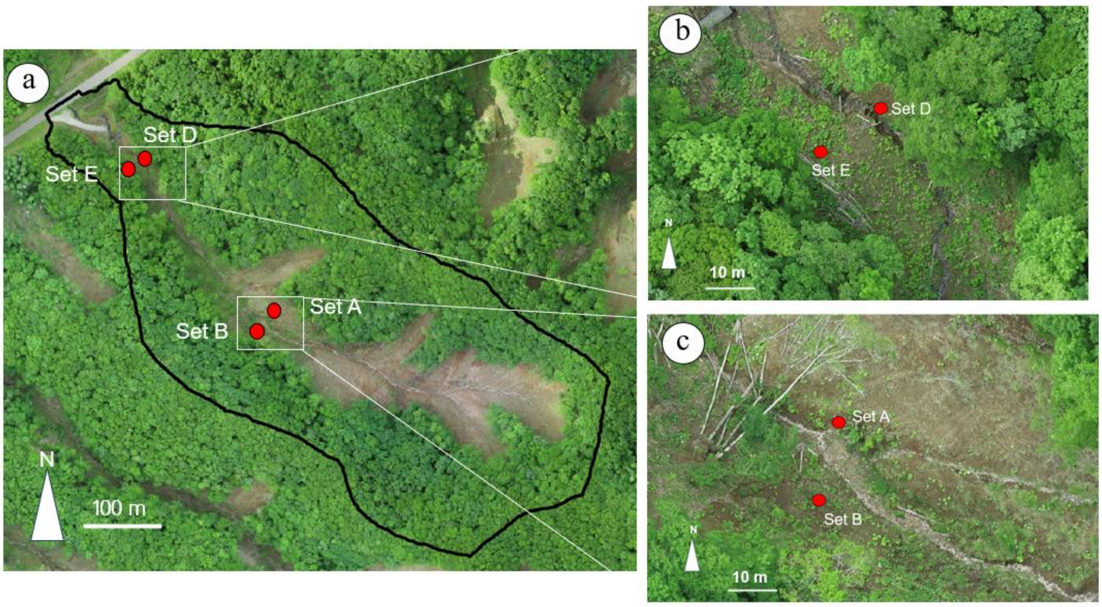

Figure 3.1.4.2: Locations of equipment (Set A, B, D and E) for measuring soil moisture (m^3/m^3), soil temperature (°C) and Photosynthetic Active Radiation (PAR) ($\mu mol\ m^{-2}\ s^{-1}$) in Study site B: (a) Overview of locations, (b) Location of Set D and E near outlet of stream, (c) Location of Set A and B in the middle course of stream.

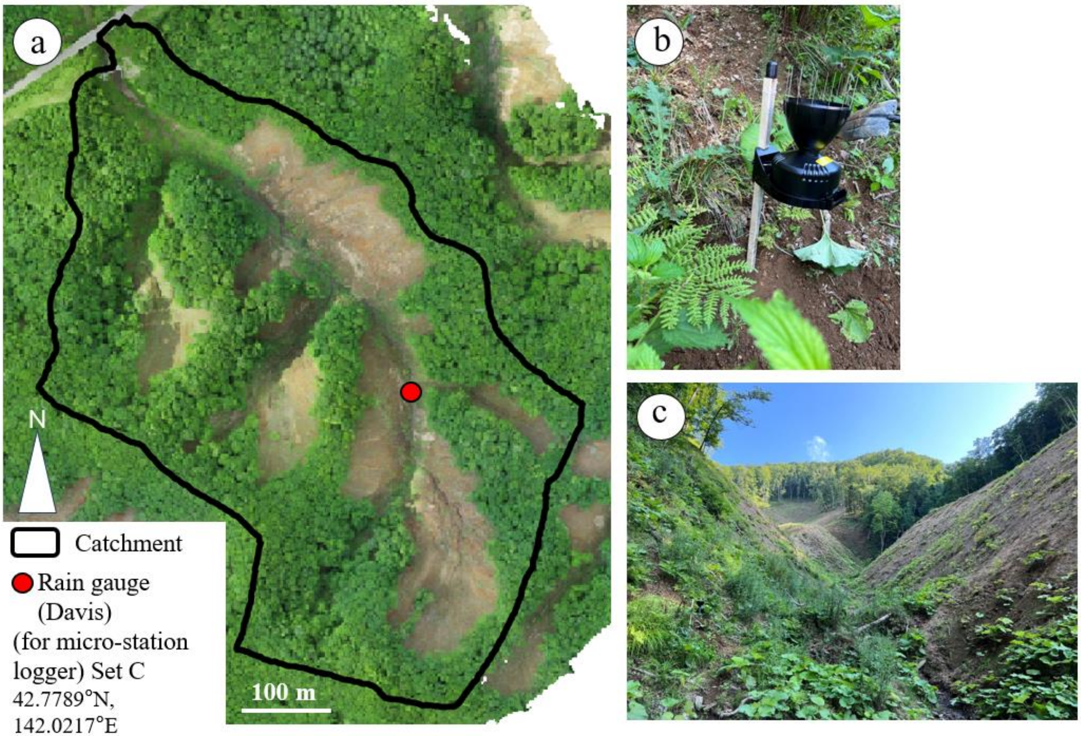

Figure 3.1.4.3: Locations of equipment (Set C) for measuring soil moisture (m^3/m^3), soil temperature (°C) and Photosynthetic Active Radiation (PAR) ($\mu mol\ m^{-2}\ s^{-1}$) and rainfall intensity in Study site D: (a) Overview of location, (b) Rain gauge (Davis) for micro-station logger, (c) Situation around Set C.

3.1.5 Data of Frost heave

Field surveys were conducted on November 8 and 30, 2022, April 2, 10 and 18, 2023, November 30, 2023. The temperature of frost heave was measured by Flir Infra-red camera attached with the i-Phone13 Pro Max. (Figure 3.1.5)

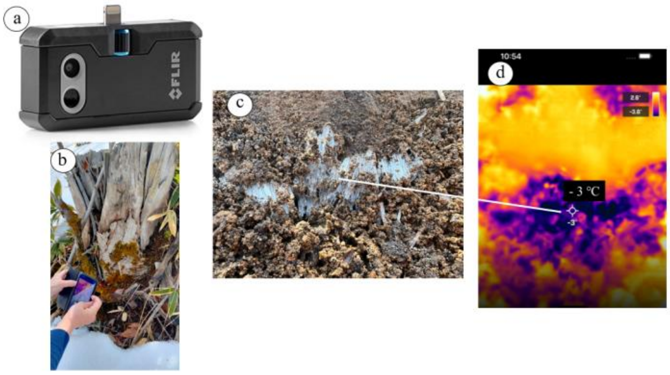

Figure 3.1.5: Measurement of temperature of frost heave: (a) Flir Infra-red camera, (b) Flir Infra-red camera attached with i-Phone 13 Pro Max for measurement, (c) Frost heave observed in Study site B during field survey on April 2, 2023, (d) Temperature of the frost heave (- 3 °C) .

3.2. Data Analysis

3.2.1 Geospatial Information System (GIS) Analysis

Geospatial Information System (GIS) software QGIS 3.22.7 was used for geospatial analysis of topographic data and mapping of stream channels, which performed to characterize the drainage network development. Morphological changes were also examined by subtracting the DEMs with different time of acquisitions.

For the extraction of stream channels, the results from theoretical estimation of stream head location by using Digital elevation Model (DEMs) varied significantly with the field observed situations and did not match with the field observed situation, which suggested that a visual comparison is necessary between the network image with both the field observed and cartographic channel network patterns are necessary (Gandolfi and Bischetti ,1997) (Bischetti et al.,1998) (Alsaihani and Alharbi, 2024). However, those researches did not mention how to match DEMs analysis with the field observations. So, this research is trying to fill this gap by using "different value of flow accumulation" to fit the theoretical results with real observations in the field and orthorectified images, together with other supporting analysis (e.g. flow direction, hydraulic radius, critical shear stress, shear stress, slope of 10 m from stream heads and elevation differences (m).

We set a threshold value of 100 m^2 and using different value of flow accumulation to extract the channel heads in each set of DEMs (Figure 3.1.2 b and Table 3.1.3), which were visually corresponds to the morphological features of channels heads and matches the locations (depressions) in the field and orthorectified images (Figure 3.1.2 d).

Flow direction is used as additional supportive analysis to show the possible convergence of water flows at the (depressions in field) stream head (Figure 3.1.2.d). Some fine rills convergence at the stream head was identified in the field and orthorectified images, which may indicate the starting of fluvial erosion at that location (stream head) and formation of that small depression. Hydraulic radius, critical shear stress, shear stress, slope of 10 m from stream heads and elevation differences (m) at that depression (stream head) might also be the additional supportive analysis for the possible accumulation of water flows which originated the erosion at the locations/depressions (stream heads). The flow direction indicated the geomorphic conditions of the valley (Al Sawaf et al., 2023), and the pattern of flow direction was used for matching with the pattern of stream channels extracted in the DEMs (Figure 3.1.2.d).

For the delineation of drainage basins (catchments) and stream channels (Figure 3.1.2 e), ALS DEMs and UAV-Lidar DEM were used for representing relatively smooth surface without vegetation cover. The catchment delineated from ALS DEM Sep 11, 2018 was applied on the analysis during Period 2 to 8 (Figure 3.1.2 e).

3.2.2 Quantitative analysis of geomorphometric and hydraulic parameters

For quantitative analysis of post-seismic drainage basin characteristics, 35 parameters indicating geomorphometric and hydraulic characteristics were examined (Table 3.2.1). 35 inter-reacted hydro-geometric parameters which are multi-perspectives/multi-functions orientated approach to explain the occurrence of various inter-related post-seismic phenomenon in this study on a relatively comprehensive, logical and rational aspects. This kind of approach are always un-estimated and rare in scientific researches of Post-seismic fluvial-geomorphology.

The analysis of the 29 geomorphometric parameters was divided into to two sections for comparison, that is pre- and post-earthquake (Period 1) and post-earthquake periods (Period 2 – 9), while the analysis of 6 hydraulic parameters was examined during the post-earthquake periods (Period 2 – 4 and Period 6 – 8). All results were derived from the DEMs and stream network data for analyzing temporal changes morphological responses in drainage basin , including elevation change, locations and extensions of stream channels and stream heads. Those selected parameters are proposed to be used for inter-basin comparison and are able to indicate predominant processes within watershed relating to mass movement, surface water flow and understanding of soil erosion, fluvial erosion and discharge characteristics of ungauged stream (Prabhakaran et al., 2018) and hydrogeomorphic process such as sediment supply/transport processes and runoff components (Montgomery and Dietrich, 1992) (Imaizumi et al., 2010), which are related to the post-seismic changes of drainage basin morphology and development of stream network in the study sites.

Within them, 29 parameters were identified as geomorphometric parameters which were categorized into four categories: watershed geometry, drainage network, drainage texture, and relief characteristics (Table 3.2.1). For watershed geometry, basin length, basin area, basin perimeter, form factor, elongation ration, circularity ratio and compactness coefficient were analyzed. For drainage network, length of main stream channel, total length of tributaries, stream order, stream number, total stream length, mean of total stream length, stream length ratio, bifurcation ratio and gradient of main stream were analyzed. For drainage texture, stream frequency, drainage texture, drainage density, drainage intensity, infiltration number, length of overland flow and constant of channel maintenance were calculated. For relief characteristics, height of basin outlet, maximum height of basin, total basin relief, relief ratio, ruggedness number and dissection index were analyzed. The analysis indicates the changes during the whole Investigation Period 1 to 9 (from Oct 05, 2012 to Oct 29, 2021) in this study.

6 other parameters were identified as hydraulic parameters (Table 3.2.1) including hydraulic radius, slope (10 m from stream head), shear stress, critical shear stress, velocity and peak specific discharge per unit rainfall intensity, which contribute for fluvial landscape evolutionary studies such as channel initiation and headward extension. All results were derived from the UAV-SfM DEMS with different time of acquisitions for analyzing temporal changes in drainage basin characteristics, which contribute for fluvial landscape evolutionary studies such as channel initiation and headward extension. The analysis indicates the changes during Investigation Period 2 to 8 (from Apr 23, 2020 to Aug 27, 2021) in this study due to the availability of orthorectified mosaic images of study site for confirming the location of stream channels and channel heads.

Those selected parameters are proposed to be used for inter-basin comparison and are able to indicate predominant processes within watershed relating to mass movement, surface water flow and understanding of soil erosion, fluvial erosion and discharge characteristics of ungauged stream (Prabhakaran et al., 2018) and hydrogeomorphic process such as sediment supply/transport processes and runoff components (Montgomery and Dietrich, 1992) (Imaizumi et al., 2010), which are related to the post-seismic changes of drainage basin morphology and development of stream network in the study sites with temporal changes in drainage basin characteristics, including elevation change, locations and extensions of stream channels and stream heads. For Hydrological characteristics, Hydraulic radius, Shear stress, Critical shear stress, Velocity and Peak specific discharge were integrated as Hydraulic parameters. which contribute for fluvial landscape evolutionary studies such as channel initiation and headward extension.

3.2.2.1 Geomorphometric parameters

3.2.2.1.1 Watershed geometry

Basin length (L_b) is defined as the longest dimension of the basin parallel to the principal drainage line (Schumm, 1956), which is measured in the unit of meters. Basin area (A) is another important parameter like the length of the stream, which is defined as the area of the catchment (Schumm, 1956) and indicates the relationship between the total catchment areas and the total stream lengths supported by the contributing areas. Basin Perimeter (P) is the outer boundary of the catchment that enclosed its area (Schumm, 1956). It is measured along the divides between catchment and may be used as an indicator of catchment size and shape.

Form factor (F_f) is the ratio of the basin area and square root of the basin length (Horton 1932). The form factor (F_f) indicates a perfect circular catchment with value of 0.754. Smaller form factors (F_f) indicate long-narrow basins. Short-wide basins have larger form factors (F_f). Catchment with higher form factor (F_f) indicates high peak flows of shorter duration. Elongation ratio (R_e) is the ratio of diameter of a circle having the same area as of the basin and maximum basin length (Schumm 1956). Drainage basins with very low relief and circular shape have values close to 1.0 where concentration of runoff discharge is more efficient than elongated basins.

Circularity ratio (R_e) (Miller 1953) (Strahler 1964) is a dimensionless quantitative method for the out-line form of watershed. It is defined as the ratio of catchment area to the area of a circle having the same perimeter as the catchment. Compactness coefficient (C_c) is the ratio of perimeter of watershed to circumference of circular area, which equals the area of the catchment (Gravelius,1914), which is independent of size of catchment and dependent only on the slope.

3.2.2.1.2 Drainage network

Length of main stream channel is the length in meters along the longest watercourse from the outflow point of designated sub-catchment to the upper limit to the catchment boundary. Total length of tributaries is the total length of all tributaries in meters (1^{st} order stream) within the catchment.

Stream order (*U*) is the notion of stream orders (Horton, 1945). First-order streams are those with no tributaries, second-order streams are those which receive as tributaries only streams of the first order. One of the lower-order streams is renumbered every time two channels of equal order join one another. The main stream is denoted by the same order number all the way to its headwaters, and hence one of the first-order streams (normally either the longest or the one which seems the most direct upstream continuation of the main stream) has to be renumbered as second order. The renumbering procedure is repeated with higher-order streams and the N^{th} order stream extends headward to the beginning of the longest tributary for making a stream-order map. Stream order (*U*) is also the position of a stream in the hierarchy of tributaries (Stralhler 1964). Trunk stream has the highest stream order. The numbers of each stream order (*U*) form an inverse geometric sequence with order number, by which the number of stream decreases with increasing stream order (*U*).

Stream number (N_u) is the number of stream segments within watershed, which from an inverse geometric sequence with order number (Horton 1945). Total stream length (L_u) is the total horizontal distance of channel from the stream head to the stream outlet (Horton 1945; Strahler 1964) which is positively correlated with mean annual runoff. (Morisawa 1962). Mean of stream length (L_m) is a dimensional property revealing the characteristic size of components of a drainage network and its contributing watershed surfaces (Strahler, 1964). It is obtained by dividing the total length of stream of an order by total number of segments in the order.

Stream length ratio (R_L) is the length ratio of the mean (L_u) length of an segments of a order of stream to the mean length of segments of the next lower order (L_{u-1}) (Horton 1945; Strahler 1964), which tends to be constant throughout the successive orders of a basin. His law of stream lengths refers that the mean stream lengths of stream segments of each of the successive orders of a watershed tend to approximate a direct geometric sequence in which the first term (stream length) is the average length of segments of the first order. Changes of stream length ratio from one order to another order indicating their late youth stage of geomorphic development (Singh and Singh, 1997).

Bifurcation ratio (R_b) is measuring the ratio of number of streams of a given stream order (N_u) to the number of streams of next higher order (N_{u+1}), which is not same from one order to its next order and these irregularities are dependent upon the geological and lithological development of drainage basin (Horton 1945; Strahler 1964). Gradient of mainstream (m/m) is the ratio of difference in maximum and minimum elevation of mainstream to the horizontal distance of stream channel between stream head and stream outlet. Slope analysis is important for indicating specific feature of the earth's surface form. Maximum slope line is well marked in the direction of a channel reaching downwards on the ground surface (Pareta and Pareta, 2011).

3.2.2.1.3 Drainage texture

Stream frequency (F_s) is the number of stream segments per unit area (Horton 1932). It represents a ratio between total number of stream to area of watershed. Stream frequency (F_s) varies inversely with the mean annual rainfall (Morisasa 1962). Drainage texture (D_t) is one of the important concept of geomorphology which means that the relative spacing of drainage lines. Drainage texture is on the underlying lithology, infiltration capacity and relief aspect of the terrain. It is total number of stream segments of all orders per perimeter of that area (Horton,1945). (Smith, 1950) has classified drainage texture into five different textures i.e., very coarse (<2), coarse (2 to 4), moderate (4 to 6), fine (6 to 8) and very fine (>8).

Drainage density (D_d) refers to the total length of streams within a watershed per unit area (Horton 1932) which is one of the most sensitive and variable morphometric parameters with direct relationship with rainfall intensity (D_i) (Chorley and Morgan 1962) and mean annual run off (Morisawa 1962). Drainage intensity (D_i) was defined as the ratio of the stream frequency to the drainage density (Faniran 1968). The higher the value of drainage intensity (D_i) may indicate higher rate of gully erosion, risk of landslides and highly susceptible to flooding.

Infiltration number (I_f) reflects the infiltration potential of a watershed (Faniran 1968). The infiltration number (I_f) is also defined as the product highly related to stream frequency and drainage density which indicated the infiltration characteristics of the watershed. Length of overland flow (L_o) describes the length of flow of water over the ground surface before it becomes concentrated in definite stream channels (Horton 1945). Furthermore, river basins with lower overland flow (L_o) values also designate that in such basins less rainfall is adequate to pay a substantial volume of surface run off to stream discharge (Muthukrishnan et al., 2013). Constant of channel maintenance (*C*) was suggested by Schumm (1956) to indicate the number of km^2 of basin surface required to develop and sustain a channel 1 km long. It also shows inverse of the value of drainage density (Schumm, 1956).

3.2.2.1.4 Relief characterisitics

Height of basin outlet (Z_{min}) is the elevation of stream outlet of the catchment (m) derived from GIS analysis of Digital Elevation Models (DEMs). Maximum height of basin (Z_{max}) is the highest elevation of the catchment (m) derived from the GIS analysis of DEMs. Total basin relief (H) is the difference in the elevation between the highest point of a watershed and the lowest point on the valley floor, which can also be defined as the difference between Maximum height of basin (Z_{max}) and Height of basin outlet (Z_{min}) (Strahler 1964).

Relief ratio (R_h) is defined as the ratio between the total relief of a basin and the longest dimension of the basin parallel to the main drainage line (Schumm, 1956). The possibility of a close correlation between relief ratio and hydrologic characteristics of a basin suggested by Schumm who found that sediments loose per unit area is closely correlated with relief ratios.

Ruggedness number (R_n) is an index suggested by Strahler (1964) which can reflect the situation of slope steepness and length in a watershed. High values of the ruggedness number (R_n) indicated that slopes are steep and long (Chow 1964). Dissection index (D_{is}) (Gravelius 1914) is a parameter measuring the degree of dissection or vertical erosion and is able to explain the stages of terrain or landscape development in any given watershed (Singh and Dubey 1994).

	Geomorphometric parameters	Unit	References	Equations
Watershed geometry	Basin length (L_b)	m	(Schumm 1956)	GIS Software Analysis
	Basin area (A)	m^2	(Schumm 1956)	GIS Software Analysis
	Basin Perimeter (P)	m	(Schumm 1956)	GIS Software Analysis
	Form factor (F_f)	–	(Horton 1932)	$F_f = A/L_b^2$
	Elongation ratio (R_e)	–	(Schumm 1956)	$R_e = (2/L_b) \text{ x } (A/\pi)^{0.5}$
	Circularity ratio (R_c)	–	(Miller 1953)	$R_c = 4\pi A/P^2$
	Compactness coefficient (C_c)	–	(Gravelius 1914)	$C_c = P/2\ (\pi A)^{0.5}$
Drainage network	Length of mainstream channel	m	–	GIS Software Analysis
	Total length of tributaries (1st order	m	–	GIS Software Analysis
	Stream order (U)	–	(Horton 1945);(Stralhler 1964)	Hierarchical Rank
	Stream number (N_u)	–	(Horton 1945)	$N_u = N_1 + N_2 + ...N_n$
	Total stream length (L_u)	m	(Horton 1945; Strahler 1964)	$L_u = L_1 + L_2 + ...L_n$
	Mean stream length (L_m)	m	(Strahler 1964)	$L_m = L_u/N_u$
	Stream length ratio (R_L)		(Horton 1945; Strahler 1964)	$R1 = L_{mu}/L_{mu-1}$
	Bifurcation ratio (R_b)	–	(Horton 1945; Strahler 1964)	$R_b = N_u/N_{u+1}$
	Gradient of mainstream	m/m		$(E_{max}* - E_{min}*) / L_m*$
Drainage texture	Stream frequency (F_s)	$1/km^2$	(Horton 1932)	$F_s = N_u/A$
	Drainage texture (D_t)	1/km	(Horton 1945)	$D_t = N_u/P$
	Drainage density (D_d)	km/km^2	(Horton 1932)	$D_d = L_u/A*$
	Drainage intensity (D_i)	1/km	(Faniran 1968)	$D_i = F_s*/D_d$
	Infiltration number (I_f)	$1/10^6 \cdot m^3$	(Faniran 1968)	$I_f = F_s* \text{ x } D_d$
	Length of overland flow (L_o)	km	(Horton 1945)	$L_o = 1/(2D_d)$
	Constant of channel maintenance (C)	km^2/km	(Schumm 1956)	$C = 1/D_d$
Relief characteristics	Height of basin outlet (Z_{min})	m	–	GIS Software Analysis
	Maximum height of basin (Z_{max})	m	–	GIS Software Analysis
	Total basin relief (H)	m	(Strahler 1964)	$H = Z_{max} - Z_{min}$
	Relief ratio (R_h)	–	(Schumm 1965)	$R_h = H/L_b$
	Ruggedness number (R_n)	km/km^2	(Strahler 1964)	$R_n = H \text{ x } D_d$
	Dissection index (D_{is})		(Gravelius 1914); (Singh & Dubey 1994)	$D_{is} = H/Z_{max}$
	Hydraulic Parameters			
	Hydraulic radius (R)	m	(Ellenberger, 2014)	$R = B_1 h$
	Slope (10 m from stream head) (S)	tanø	(Imaizumi et al., 2010)	tanø
	Shear stress (τ)	Nm^{-2}	(Parchure and Mehta, 1985)	$\tau = pgRS$
	Critical shear stress (τ_c)	Nm^{-2}	(Azmayeen and Mohammed., 2021)	$\tau_c = \tau[(\sigma - p)gd]^{-1}$
	Velocity (v)	$m\ s^{-1}$	(Bhaskar et al 1997)	$v = (n^{-1} * R^{2/3} * S^{1/2})$
	Peak specific discharge per unit rainfall intensity (k_p)	mm	(Hattanji et al., 2006)	$k_p = Q_p/I_R$

Table 3.2.1. Hydraulic and geomorphometric parameters of drainage basin characteristics examined in this study

3.2.2.2 Hydraulic parameters

3.2.2.2.1 Hydraulic radius (*R*)

Hydraulic radius (R) is the ratio of the flow area to the wetted perimeter of the conduit in which it is flowing (Ellenberger, 2014). It is used for measuring channel flow efficiency, which is one of the main properties that control the amount of fluid discharge of a channel and its ability to move sediments (Wei et al., 2023). A high hydraulic radius value indicates that the channel contains a lower volume of contact fluid and a greater cross-sectional area. These conditions result in increased flow velocity and capacity, as well as improved channel efficiency (Wei et al., 2023). Hydraulic radius, in original or modified formulations, has successfully addressed issues like flow resistance, sediment transport rate, and local scour, attributable to its basis in characterizing large-scale flow structures. new possibilities for using hydraulic radius, as a physically justifiable length scale, to link turbulent flow structure, geometrical boundary condition and sediment transport for better understanding flow dynamics across subfields of hydrology and environmental fluid mechanics (Wei et al., 2023). (B_1 is the coefficients given by the given by the cross-sectional gradient of the channel bed. h is the water depth).

3.2.2.2.2 Slope (10 m from stream head) (*S*)

Slope gradients affect hydro-erosional parameter and runoff and erosion peaks usually increased with increasing gradient (Zhang et al., 2017). Slope affects rate of infiltration (Morbidelli et al., 2018). Slope Analysis is the most important and specific feature of the earth's surface form. Maximum slope line is well marked in the direction of a channel reaching downwards on the ground surface (Pareta and Pareta, 2011). Gradient of slid slope 10 meters from stream head (*S*) (tanø) (Table 2) were calculated (Imaizumi et al., 2010) by dividing elevation difference between stream head and stream channel 10 meters downward from stream head with the horizontal distance of 10 m. Those analyzed values (*S*) were applied on other equations of other hydrological parameters in this study.

3.2.2.2.3 Shear stress (τ)

A log-linear relationship between erosion rate and shear stress in excess of bed shear strength was observed (Parchure and Mehta, 1985), which was focused on erosion rate models for kaolinite. A relationship between critical shear stress and "linear slope" of erosion rate versus shear stress for soils with 50–80% silt size materials was developed (Hanson and Simon, 2001). A model for estimating the critical shear stress based on the percent silt and clay content in the material was suggested (Julian and Torres, 2006). p is the mass density of water (~$1.0\times10^3 kgm^{-3}$) and g is the acceleration of gravity ($9.8\ ms^{-2}$), τ is the shear stress (Nm^{-2}), R is the hydraulic radius (m), S is Slope (10 m from stream head) (m/m).

3.2.2.2.4 Critical shear stress (τ_c)

Critical shear stress (τ_c) is the parameter indicating the relationship between erodibility to geotechnical properties (Azmayeen and Mohammed., 2021). A relation between critical shear stress with soil plasticity index, the dispersion ratio and clay percentage was developed (Smerdon and Beasley 1961). It is used to compare with shear stress. The entrainment of sediment occurs when the critical shear stress is smaller than shear stress. σ is the mass density of the sediment (~2.65 kgm^{-3}), p is the mass density of water (~$1.0\times10^3 kgm^{-3}$), d is grain size of sediment (m) and τ_c is the critical shear stress (Nm^{-2}).

3.2.2.2.5 Velocity (*v*)

The relationship between velocity and effective rainfall intensity have been observed (Bhaskar et al 1997). The internal numerical relationship between the characteristic flow velocity and the terrain and geomorphologic features of a watershed was confirmed by using the multivariate regression method in the study of total 120 sub-basins in the Yangtze River Basin (Chen et al., 2019). Flow velocities were correlated with the discharge and hydraulic radius. (Li et al., 2020). Velocity is an important parameter related to slope gradient, flow discharge, topography, and surface conditions (Zhang et al., 2010, Lei et al., 2005). Flow velocity is also an essential flow hydraulic characteristic to calculate soil detachment, transport and flow resistance variables (Huang et al., 2018). n is Manning's roughness coefficient, R is hydraulic radius (m) and S is the slope (10 m from stream head) (m/m).

3.2.2.2.6 Peak specific discharge per unit rainfall intensity (k_p)

The pattern of relationships between catchment area and specific discharge can be used to assess the storage and discharge properties of catchments, associated with the effects of precipitation and evapotranspiration (Asano et al., 2020). The increase in specific discharge with increasing catchment size was observed (Egusa et al., 2016; Shaman et al., 2004), which was related to spatial variation in precipitation. Decreases in peak event flow-specific discharge with catchment area have also been demonstrated (Furey & Gupta, 2005; Ogden & Dawdy, 2003). Also, the relationship between specific discharge and catchment area with the participating of precipitation into the flood quick flow were examined (Asano et al., 2020). Q_p is the peak discharge (m^3s^{-1}), I_R is rainfall intensity (mm/hr).

3.2.3 Quantitative analysis of Landslide (Areas with elevation decrease) mobility and sediment (Areas with elevation increase) connectivity

For Post-seismic Period 1, Landslide area (x) (m^2) is defined as the areas with elevation decrease in Study site A, B, C and D delineated by subtracting Post-seismic ALS DEM in September 11, 2018 with Pre-seismic ALS DEM in October 05, 2012, whereas those locations are defined as areas with coseismic landslides induced by the 2018 Hokkaido Eastern Iburi earthquake happed on September 06, 2018 within the study sites A, B, C and D,

Sedimentation area (m^2) is defined as the areas with elevation increase in Study site A, B, C and D delineated by subtracting Post-seismic ALS DEM in September 11, 2018 with Pre-seismic ALS DEM in October 05, 2012, whereas those locations are defined as areas with sedimentation induced by the 2018 Hokkaido Eastern Iburi earthquake happed on September 06, 2018 within the study sites A, B, C and D,

Volume (m^3) of landslide (elevation decrease) was calculated by multiplying the Landslide area (x) (m^2) with the vertical elevation decrease (m), delineated by subtracting Post-seismic ALS DEM in September 11, 2018 with Pre-seismic ALS DEM in October 05, 2012,

Volume (m^3) of sedimentation (elevation increase) was calculated by multiplying the areas with elevation increase with the vertical elevation decrease, delineated by subtracting Post-seismic ALS DEM in September 11, 2018 with Pre-seismic ALS DEM in October 05, 2012,

During the post-seismic Period 2–9, areas (m^2) with elevation decrease were considered as locations with fluvial erosion delineated by subtracting the Light Detection and Ranging (Lidar) DEMs in October 2021 with the Post-seismic ALS DEM in September 2018. Volume (m^3) of those material in areas with elevation decrease was calculated by multiplying the area (m^2) of elevation decrease with the vertical elevation decrease (m), delineated by subtracting the Light Detection and Ranging (Lidar) DEMs in October 2021 with the Post-seismic ALS DEM in September 2018.

Areas (m^2) with elevation increase were considered as locations with fluvial sedimentation delineated by subtracting the Light Detection and Ranging (Lidar) DEMs in October 2021 with the Post-seismic ALS DEM in September 2018. Volume (m^3) of those material in areas with elevation increase was calculated by multiplying the area (m^2) of elevation increase with the vertical elevation increase (m), delineated by subtracting the Light Detection and Ranging (Lidar) DEMs in October 2021 with the Post-seismic ALS DEM in September 2018.

3.2.3.1 Landslide (Areas with elevation decrease) mobility

As an important indicator for landslide hazard and risk assessments, landslide (area with elevation decrease) mobility has attracted considerable attention in the literature, which has potential direct societal impacts because with increasing travel distance and height of landslide (Zhao et al 2021). Landslide (areas with elevation decrease) mobility index is commonly known as the H/L ratio (Corominas, 1996). Landslide mobility induced by the 2018 Hokkaido Eastern Iburi earthquake is described by the relationship: $H/L = 1.46–0.24 \times \log_{10}$ (landslide area), whereas 7058 landslides triggered by the 2018 Hokkaido Eastern Iburi earthquake exhibited an average landslide mobility of 0.33. (Zhao et al 2021).

In this study, Landslide area (x) (m^2) is defined as the areas with elevation decrease in Study site A, B, C and D delineated by subtracting Post-seismic ALS DEM in September 11, 2018 with Pre-seismic ALS DEM in October 05, 2012, whereas those locations are defined as areas with coseismic landslides induced by the 2018 Hokkaido Eastern Iburi earthquake happed on 6^{th} September 2018 within the study sites A, B, C and D,

Landslide (area with elevation decrease) mobility index with height, travel distance and area of landslide (elevation decrease) were used to indicate the characteristics of coseismic landslides, by which the spatial variability and linkage of coseismic landslides and sediment accumulation could be examined (Zhao et al, 2021).

The Landslide (area of elevation decrease) mobility index is calculated by the same equation: y (H/L) = 1.46 - 0.24 x log10 (x), whereas x is the landslide area (m^2) and y is the landslide mobility (H/L value). High H/L value indicates low mobility, whereas low H/L value indicates high mobility. Decrease of H/L value indicates increase in mobility, while increase of H/L value indicates decrease in mobility (Zhao et al, 2021).

Travel distance (m) of landslides (areas with elevation decrease) induced by the 2018 Hokkaido Eastern Iburi earthquake is described by the relationship: y = (log(x) – 1.0) 4.7 + 18 (y is travel distance , x is landslide area) (Zhao et al, 2021)

Landslide (area of elevation decrease) height (m) is described by the relationship: y = (log(x) - 0.6)3.4 -6 , whereas y is the landslide height and x is the landslide (elevation decrease) area. (Zhao et al, 2021)

3.2.3.2 Sediment connectivity

Sediment connectivity indicated the spatial variability and linkage of coseismic landslides and the sediment accumulations in stream channel (Arata, et al 2021). Landslide area density (LAD) was used to examine spatial variability of landslide occurrences in watersheds. Deposit length ratio (DLR)was used to examine in-channel sediment accumulations within watersheds.

Landslide area density (LAD) was calculated by dividing Landslide area (x) (m^2) by drainage basin area (m^2) of Study site A, B, C and D. Landslide area density (LAD) was used to examine spatial variability of landslide occurrences in watersheds.

Deposit length ratio (DLR) was calculated by dividing Total length of stream channel impacted by sediment deposit with the total stream length within the drainage basin of Study site A, B, C and D. Deposit length ratio (DLR)was used to examine in-channel sediment accumulations within watersheds.

Increase of Landslide area density (LAD) with increasing Deposit length ratio (DLR) (positively correlated) was observed in small watershed with drainage basin area less than 0.5 km^2, whereas smaller sub-watershed had higher Landslide area density (LAD) (Arata 2021).

Quantitative analysis		Unit	References	Equation
Landslide mobility	Landslide mobility index (y (H/L))	-	Zhao et al, 2021	y (H/L) = 1.46 - 0.24 x log10 (x)
	Travel distance (y)	m	Zhao et al, 2021	y = (log(x) – 1.0) 4.7 + 18
	Landslide height (y)	m	Zhao et al, 2021	y = (log(x) - 0.6)3.4 -6
Sediment connectivity	Landslide area density (LAD)	m^2/m^2	Arata 2021	x/B
	Deposit length ratio (DLR)	-	Arata 2021	LS/LD

* x is the landslide area (m^2), B is drainage basin area (m^2)
* LS is total stream length impacted by sediment deposit (m)
* LD is total stream length within the drainage basin (m)

Table 3.2.3: Quantitative analysis: Landslide (Areas with elevation decrease) mobility and Sediment connectivity.

Those hydro-geomorphometric and sediment connectivity parameters (indicators)) were the dimensional quantitative method and fundamental model to indicate the different predominant fluvial processes in drainage system study which will contribute to indicate the post-seismic morphological responses on elevation changes and drainage network development in fluvial evolutionary process as the evidence for those co-occurrence of natural post-seismic phenomenon in the study sites even without continuous measurement of hydrological elements, such as stream discharge and stream flow velocity at every locations. The coherent explanatory framework of the present study based on the detail individual data analysis of hydro-geomorphometric parameters will finally illustrate the linkage of various drainage basin characteristics with differences and sediment connectivity.

3.2.4 X-ray diffraction (XRD) Analysis (Identification of Paleosol) of soil samples on the slid slopes in Study site B.

The presence of paleosol, which exposed on sliding surface (Wang and Nam., 2023) caused by coseismic landslides in the study sites, was examined by analysing the mineral composition of the 2 soil samples collected on the slid slopes in study site B (Figure 5.2.2 and 5.2.3) with the X-ray diffusion (XRD) method. Mineral composition was analyzed for both silt (>4 μm) and clay (<4 μm) fractions, as well as potential source materials by using a powder XRD method. A powder sample mounted on a glass holder was scanned from 2° to 40° 2θ by 1° 2θ/min at 40 kV and 20 mA using CuKα radiation, where the diffraction intensity (counts per second: cps) was recorded with a 0.02° 2θ step (Lee et al, 2022). Identification of major and clay minerals was performed according to the position of diagnostic peaks of these minerals on the XRD diffractograms.

The results were compared with the analysis by Wang and Nam (2023) (Figure 5.2.1) to confirm the presence of paleosol on the exposed slide slope for examining the correspondence of the soil characteristics with the sediment mobility and connectivity, which facilitated the changes of morphology in drainage basin and development of drainage network in the study site during post-seismic periods.

Chapter 4. Results

4.1 Post-seismic morphological changes identified by ALS and UAV-LiDAR DEMs in Study sites A – D: Investigation Period 1: October 05, 2012 – September 11, 2018 and Period 2 – 9: April 23, 2020 – October 29, 2021)

Digital elevation model (DEM) with a 0.5-m resolution, generated from airborne laser scanning (ALS) data of October 05 in 2012 (Hokkaido Prefecture, 2020a) (Figure 4.1.1 a) represented the situation before the 2018 Hokkaido Eastern Iburi Earthquake. Digital elevation model (DEM) with a 0.5-m resolution, generated from airborne laser scanning (ALS) data of September 11, 2018 (Hokkaido Prefecture, 2020b) represented the situation after the earthquake (Figure 4.1.1 b).

In study site A, elongated areas of coseismic landslides could be identified along the upper part of the drainage area. Another small rectangular shaped coseismic landslides area was located at the north facing slope in the lower part of drainage area. The areas with coseismic landslide occupied 18.01 % of the total area of drainage basin. Linear sediment deposition area could be identified along the lower course of stream which extended gradually to the outlet of stream in Study site A, which occupied 3.33 % of the total area of drainage basin (Figure 4.1.1 a and b). In study site B, a large area of coseismic landslides could be identified at the sub-catchments from middle to upper part of the drainage basin. Few small elongated shaped areas of coseismic landslides were located and extended from main valley to south facing sub-catchment where new tributaries may be expected. The areas with coseismic landslide occupied 21.84 % of the total area of drainage basin. Linear sediment deposition area could be identified obviously along the lower course of stream which extended gradually to the outlet of stream in Study site B, which occupied 3.13 % of the total area of drainage basin (Figure 4.1.1. a and b). In study site C, elongated areas of coseismic landslides could be identified along the upper part and valley-side slopes of the drainage area. Another small circular-shaped coseismic landslides area was located at the south facing slope in the upper part of drainage area. The areas with coseismic landslide occupied 11.06 % of the total area of drainage basin. Linear sediment deposition area could be identified along the lower course of stream which extended gradually to the outlet of stream in Study site C, which occupied 2.68 % of the total area of drainage basin (Figure 4.1.1 a and b). In study site D, large areas of coseismic landslides could be identified at the sub-catchments from lower to middle and upper part of the drainage basin, where new tributaries with stream network development may be expected. Extensive south-facing slopes with coseismic landslides were located at the valley side of middle course of drainage basin where rills and gully erosion may be expected. The areas with coseismic landslide occupied 31.89 % of the total area of drainage basin. Linear sediment deposition area could be identified obviously along the main stream channel and the intersection with sub-catchments from upper to lower course, which extended gradually to the outlet of stream in Location D, which occupied 1.36 % of the total area of drainage basin (Figure 4.1.1 a and b).

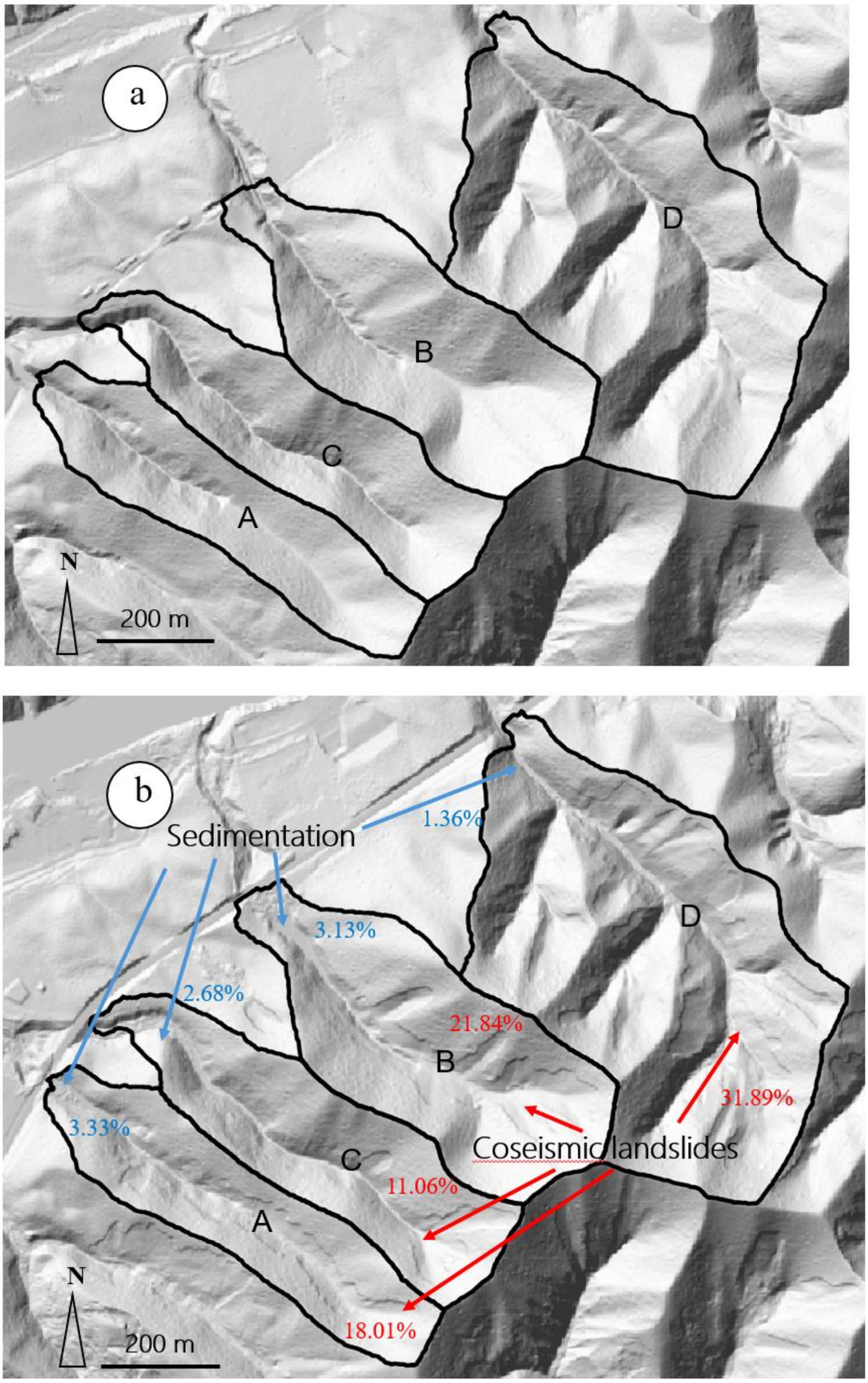

Figure 4.1.1: Post-seismic changes identified by ALS DEM in Study sites A – D: (Investigation Period 1: 05 October 2012 – 11 September, 2018): (a) Hillshade image of ALS DEM in October 2012. (b) Hillshade image of ALS DEM in September 2018 after the earthquake (Hokkaido Prefecture, 2020a, b).

Figure 4.1.1 a shows the Post seismic morphological changes in elevation identified by ALS DEMs (Investigation Period 1: 05 October 2012 – 11 September, 2018), while Figure 4.1.2 shows those changes identified by ALS DEMs and Light Detection and Ranging (Lidar) DEMs (Investigation Period 2 – 9: 11 September, 2018 – 29 October, 2021) in Study site A – D.

In study site A, after the earthquake, the catchment basin area, basin length, basin perimeter and basin slope were of study site A were 70315 m^2 (0.07 km^2), 616.26 m (0.62 km), 1944.71 m (1.91 km) and 0.22 (12.65^o) respectively. These indicated decrease in basin area (-322 m^2) and basin slope (-0.02 m/m (-0.85^o)) with increase in basin length (+1.19m) and basin perimeter (+30.99m). In Figure 4.1.2 a, the areas with elevation decrease from - 0.2 m to - 10 m at the upper part of valley were identified as coseismic landslides. The total area and volume of coseismic landslide were about 12721 m^2 and 62334 m^3 respectively. In that location, elongated extension of mainstream and tributaries with total length of 266.59 m (31.23 m + 13.32 m + 222.05 m) was identified. Volume (with elevation decrease) per unit area of catchment (m^3/m^2) was 0.88 (m^3/m^2). The areas with elevation increase from + 0.2 m to +20 m at the lower part of valley and near the outlet of stream were identified as sedimentation areas. The total area and volume of sedimentation were about 2351 m^2 and 23278 m^3 respectively. The length of stream flow across the sedimentation areas were 93.34 m, 30.42 m, 21.72 m, 41.86 m, 67.73 m and 16.95 m, which contributed a total of 272.02 m. Volume (with elevation increase) per unit area of catchment (m^3/m^2) was 0.331 (m^3/m^2). In Figure 4. b, elevation decreased area at the stream mouth was mainly due to artificial modification. The other elevation decreased areas mainly located at middle course of stream from - 0.2 m to - 2 m in linear shape which might imply fluvial erosion along gully stream channel. The total area and volume of elevation decrease were about 1829 m^2 and 1646 m^3 respectively. In that location, elongated extension of mainstream and tributaries with 35.99 m, 7.77 m, 85.52 m, 53.41 m and 11.16 m, which contributed a total length of 193.85 m was identified. Volume (with elevation decrease) per unit area of catchment (m^3/m^2) was 0.024 (m^3/m^2).
Some small individual elevation increased areas at the middle course of stream from + 0.2 m to +2 m might imply the accumulation of collapsed vegetation and sediment from slip slope by small scale landslides during the post-seismic periods . The total area and volume of elevation increase were about 240 m^2 and 250 m^3 respectively. The total length of stream flow across the sedimentation areas was 15.79 m. Volume (with elevation increase) per unit area of catchment (m^3/m^2) was 0.004 (m^3/m^2).

In study site B, for study site B, the catchment basin area, basin length, basin perimeter and basin slope were 104006 m^2 (0.104 km^2), 576.73 m (0.58 km), 1433.99 m (1.43 km) and 0.31 (17.48) respectively after the earthquake. These indicated increase in basin area (+64 m^2), basin length (+12.6 m), basin perimeter (+40.09 m) and basin slope (+ 0.01(0.78º)). In Figure 4.1.2 a, the areas with elevation decrease from – 0.2 m to - 10 m at the valley-side slopes of upper part of valley were identified as coseismic landslides. The total area and volume of coseismic landslide were about 22706 m^2 and 111259 m^3 respectively. In that location, an elongated extension of mainstream and development of tributaries were identified. The length of stream flow across the coseismic landslide areas were 36.82 m, 32.98 m, 116.88 m, 32.47 m, 13.00 m, 70.22 m, 36.02 m, 16.27 m, 24.86 m which contributed a total of 379.53 m. Volume (with elevation decrease) per unit area of catchment (m^3/m^2) was 1.070 (m^3/m^2). The areas with elevation increase from + 0.2 m to + 20 m at the lower part of valley and near the outlet of stream were identified as sedimentation areas. The total area and volume of sedimentation were about 3250 m^2 and 32175 m^3 respectively. The length of stream flow across the sedimentation areas were 51.09 m, 132.12 m and 50.61 m, which contributed to a total of 233.81 m. Volume (with elevation increase) per unit area of catchment (m^3/m^2) was 0.309 (m^3/m^2). In Figure 4.1.2 b, elevation decreased area at the stream mouth was mainly due to artificial modification. The other elevation decreased areas mainly located at middle course of stream from - 0.2 m to - 2 m in obvious linear shape which might imply fluvial erosion along gully stream channel. The total area and volume of elevation decrease were about 5164 m^2 and 4647 m^3 respectively. In that location, elongated extension of mainstream and tributaries with 10.13 m, 39.65 m, 9.18 m, 22.21 m and 122.45 m, which contributed to total length of 203.61 m was identified. Volume (with elevation decrease) per unit area of catchment (m^3/m^2) was 0.045 (m^3/m^2). Linear shape of elevation increased areas from + 0.2 m to + 2 m might imply the sediment deposition along the lower course of stream. Some small individual elevation increased areas from + 0.2 m to + 2 m might imply the accumulation of collapsed vegetation and sediment from slip slope by small scale landslides during the post-seismic periods. The total area and volume of elevation increase were about 373 m^2 and 149 m^3 respectively. The length of stream flow across the sedimentation areas were 35.79 m and 25.74 m, which contributed a total of 61.52 m. Volume (with elevation increase) per unit area of catchment (m^3/m^2) was 0.001 (m^3/m^2).

In study site C, after the earthquake, the catchment basin area, basin length, basin perimeter and basin slope were of study site C were 81639.454 m^2 (0.08 km^2), 616.87 m (0.62 km), 2011.55 m (2.01 km) and 0.27 (15.11º) respectively. These indicated decrease in basin area (-7350 m^2) and increase in basin slope (+0.01 m/m (+0.57º)) with decrease in basin length (-24.36m) and basin perimeter (-143.98m). In Figure 4.1.2 a, the areas with elevation decrease from - 0.2 m to - 10 m at the upper part of valley were identified as coseismic landslides. The total area and volume of coseismic landslide were about 9027 m^2 and 44231 m^3 respectively. In that location, an extension of main stream and tributaries with28.91 m, 33.67 m, 18.84 m, 24.69 m, 14.11 m and 11.49 m, which contributed to total length of 131.71 m was identified. Volume (with elevation decrease) per unit area of catchment (m^3/m^2) was 0.542 (m^3/m^2). The areas with elevation increase from + 0.2 m to +20 m at the lower part of valley and near the outlet of stream were identified as sedimentation areas. The total area and volume of sedimentation were about 2188 m^2 and 21664 m^3 respectively. The length of stream flow across the sedimentation areas were 45.28 m, 94.92 m, 49.47 m and 37.03 m, which contributed a total of 226.70 m. Volume (with elevation increase) per unit area of catchment (m^3/m^2) was 0.265 (m^3/m^2). In Figure 4.1.2 b, elevation decreased area at the stream mouth was mainly due to artificial modification. The other elevation decreased areas mainly located at middle course of stream from - 0.2 m to - 2 m in linear shape which might imply fluvial erosion along gully stream channel. The total area and volume of elevation decrease were about 3167 m^2 and 1267 m^3 respectively. In that location, elongated extension of mainstream and tributaries with 9.98 m, 20.03 m, 45.07 m, 11.48 m, 24.98 m, 19.48 m, 27.66 m, 15.10 m and 23.33 m, which contributed to total length of 197.11 m was identified. Volume (with elevation decrease) per unit area of catchment (m^3/m^2) was 0.015 (m^3/m^2). Some small individual elevation increased areas at the middle course of stream from + 0.2 m to +2 m might imply the accumulation of collapsed vegetation and sediment from slip slope by small scale landslides during the post-seismic periods . The total area and volume of elevation increase were about 224 m^2 and 202 m^3 respectively. The length of stream flow across the sedimentation areas were 13.23 m and 12.56 m, which contributed a total of 25.79 m. Volume (with elevation increase) per unit area of catchment (m^3/m^2) was 0.002(m^3/m^2).

In study site D, for study site D, the catchment basin area, basin length, basin perimeter and basin slope were 191068.22 m2 (0.19 km2), 683.01 m (0.68 km), 2571.44 m (2.57 km) and 0.27 (15.11º) respectively after the earthquake. These indicated decrease in basin area (-1411.64 m2), basin length (-1.29 m), basin perimeter (-5.00 m) and basin slope (-0.01(-0.57º)). In Figure 4.1.2. a, the areas with elevation decrease from -0.2 m to -10 m at the valley-side slopes of sub-catchments of lower, middle and upper part of valley were identified as coseismic landslides. The total area and volume of coseismic landslide were about 60934 m^2 and 298577 m^3 respectively. In that location, an elongated extension of mainstream and development of tributaries were identified. The length of stream flow across the coseismic landslide areas were 68.34 m, 34.96 m, 33.00 m, 33.04 m, 15.40 m, 32.76 m, 30.95 m, 25.53 m and 5.28 m, which contributed a total of 292.60 m. Volume (with elevation decrease) per unit area of catchment (m^3/m^2) was 1.563 (m^3/m^2). The areas with elevation increase from + 0.2 m to + 20 m at the lower part of valley and near the outlet of stream were identified as sedimentation areas. The total area and volume of sedimentation were about 2590 m^2 and 25640 m^3 respectively. The length of stream flow across the sedimentation areas were 34.72 m, 20.89 m, 32.34 m, 12.75 m, 23.81 m, 16.77 m, 19.83 m, 46.77 m, 39.02 m, 22.93 m, 35.52 m, 39.75 m, 38.71 m, 16.65 m, 10.99 m, 6.48 m, 87.51 m and 22.67 m, which contribute a total about 528.08 m. Volume (with elevation increase) per unit area of catchment (m^3/m^2) was 0.134 (m^3/m^2). In Figure 4.1.2 b, elevation decreased area at the stream mouth was mainly due to artificial modification. The other elevation decreased areas mainly located at middle course of stream from - 0.2 m to - 2 m in obvious linear shape which might imply fluvial erosion along main stream and gully stream channels (tributaries). The total area and volume of elevation decrease were about 15373 m^2 and 13836 m^3 respectively. In that location, elongated extension of mainstream and tributaries were 50.19 m, 28.40 m, 35.97 m, 41.45 m, 81.52 m and 16.52 m, which contributed to total length of 254.05 m was identified. Volume (with elevation decrease) per unit area of catchment (m^3/m^2) was 0.075 (m^3/m^2). Linear shape of elevation increased areas from + 0.2 m to + 2 m might imply the sediment deposition along the lower course of stream. Some small individual elevation increased areas from + 0.2 m to + 2 m might imply the accumulation of collapsed vegetation and sediment from slip slope in sub-catchments by small scale landslides during the post-seismic periods. The total area and volume of elevation increase were about 1065 m^2 and 958 m^3 respectively. The length of stream flow across the sedimentation areas were 32.57 m, 34.60 m, 17.85 m and 25.32 m, which contributed to total of 110.34 m. Volume (with elevation increase) per unit area of catchment (m^3/m^2) was 0.005 (m^3/m^2).

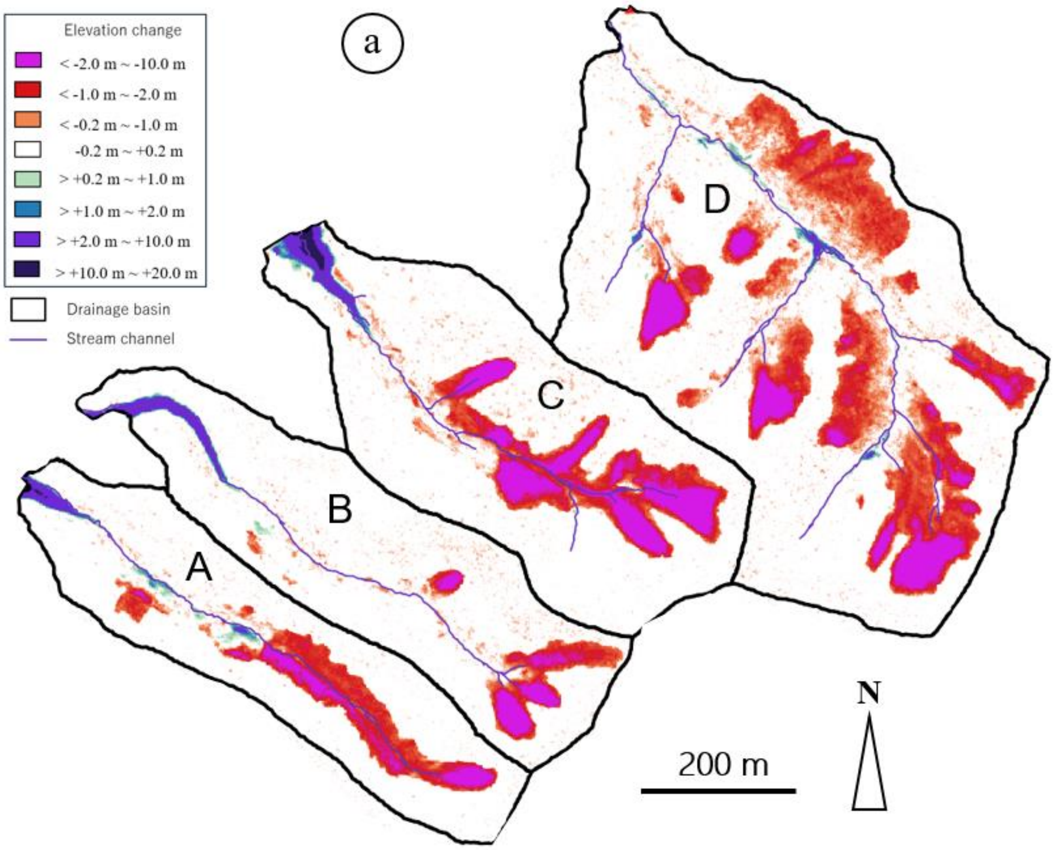

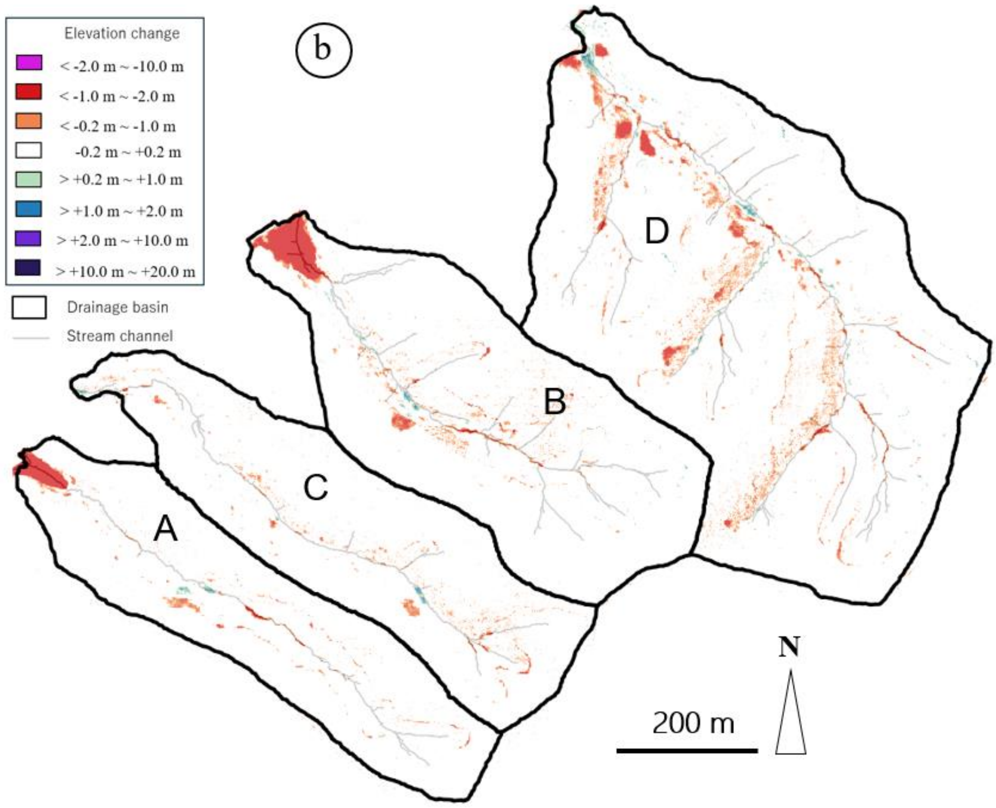

Figure 4.1.2: Post seismic morphological changes in elevation in Study site A – D: (a)

(Investigation Period 1: 05 October 2012 – 11 September, 2018), (b) Investigation Period 2 – 9: 11 September, 2018 – 29 October, 2021.

4.2 Post-seismic drainage network development

The Stream length (m) of all tributaries (1st order streams), Stream length (m) of 2nd to 4th order streams, Elevation of stream heads and outlets (m) and Gradient (m/m) of all tributaries (1st order streams) in Study site A - D during the investigation periods of this study are indicated in Table 4.2.1, 4.2.2, 4.2.3 and 4.2.4 respectively.

4.2.1 Study site A

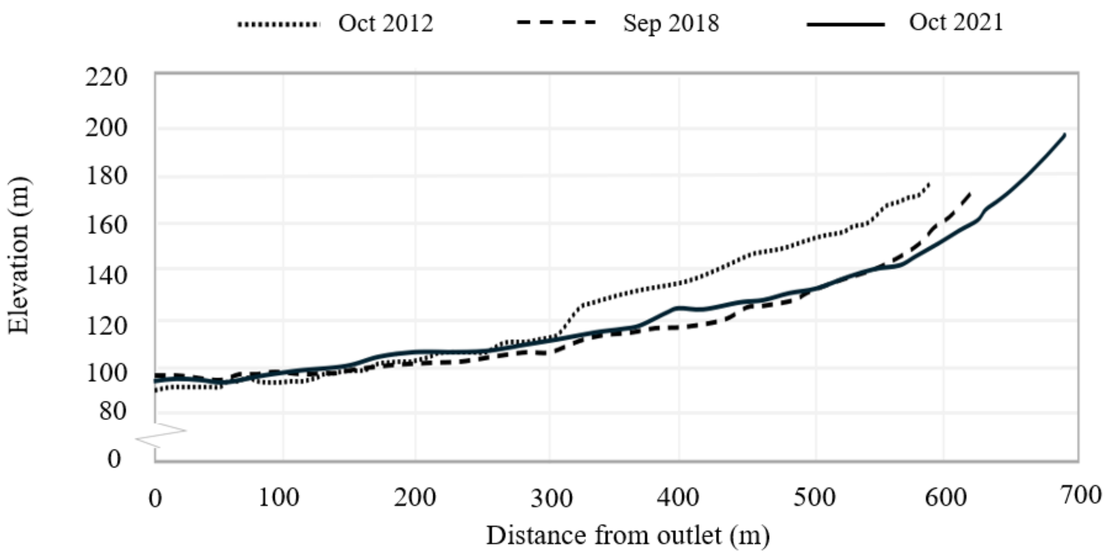

Figure 4.2.1.1: Pre- and post-seismic longitudinal profile of the mainstream in site A: October 05, 2012, September 11, 2018, and October 29, 2021.

Longitudinal profiles of mainstream based on Oct 2012 ALS DEM, Sep 2018 ALS DEM and Oct 2021 UAV-Lidar DEM in Study site A was plotted in Figure 4.2.1.1. The analyzed results of Drainage network, Stream length (m) of all tributaries (1st, 2nd , 3rd, and 4th order streams), Elevation of stream head and stream outlet (m) of all tributaries (1st order stream), Gradient of all tributaries (1st order streams), Stream number (N_u), Stream order (U) and Length of main stream channel (m), during the investigation periods of this study were indicated in Figure 4.2.1.2, Table 4.2.1, Table 4.2.2, Table 4.2.3, Table 4.2.4 and Table 4.3.1 The extension of main stream heads, contributing longer mainstream channels were confirmed. Also, steeper slopes near stream heads were observed based.

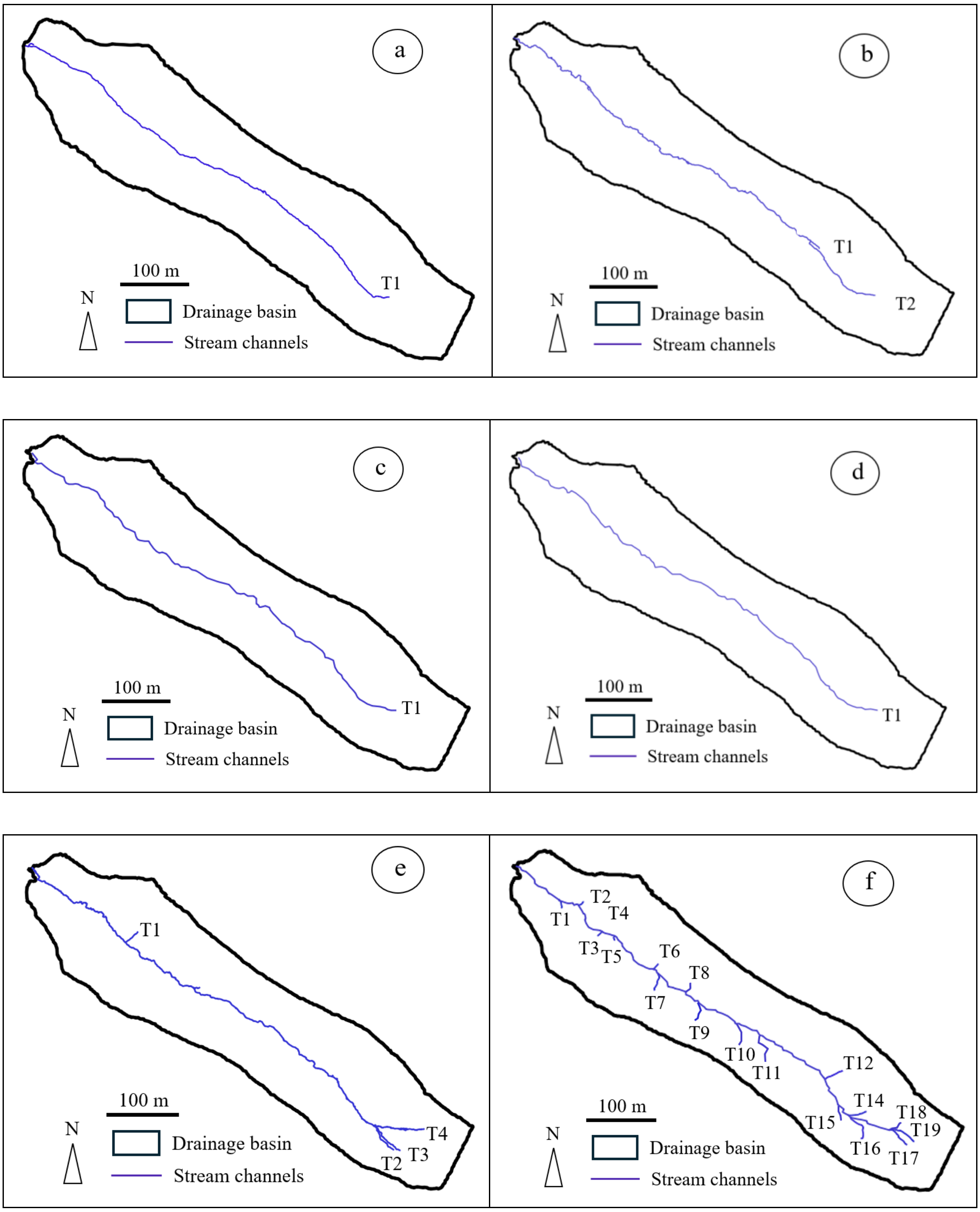
a
T1
100 m
N
Drainage basin
Stream channels
b
T1
T2
100 m
N
Drainage basin
Stream channels
c
T1
100 m
N
Drainage basin
Stream channels
d
T1
100 m
N
Drainage basin
Stream channels
e
T1
T2
T3
T4
100 m
N
Drainage basin
Stream channels
f
T1
T2
T3
T4
T5
T6
T7
T8
T9
T10
T11
T12
T14
T15
T16
T17
T18
T19
100 m
N
Drainage basin
Stream channels

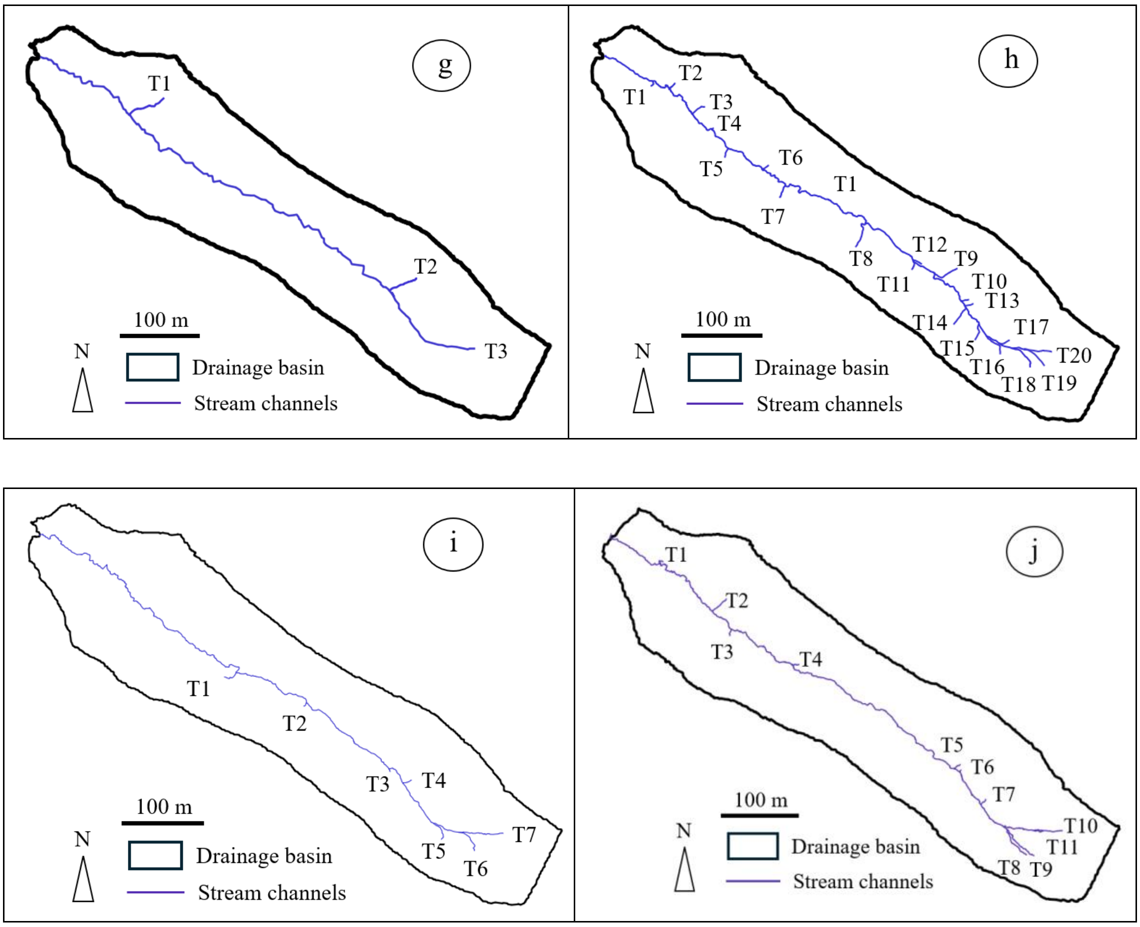

Figure 4.1.1.2: Pre and Post-seismic drainage network development in study site A. Hillshade image and stream network for (a) October 05, 2012, (b) September 11, 2018, (c) April 23, 2020, (d) June 25, 2020, (e) September 14, 2020, (f) October 30, 2020, (g) April 13, 2021, (h) June 21, 2021, (i) August 27, 2021, (j) October 29, 2021.

4.2.2 Study site B

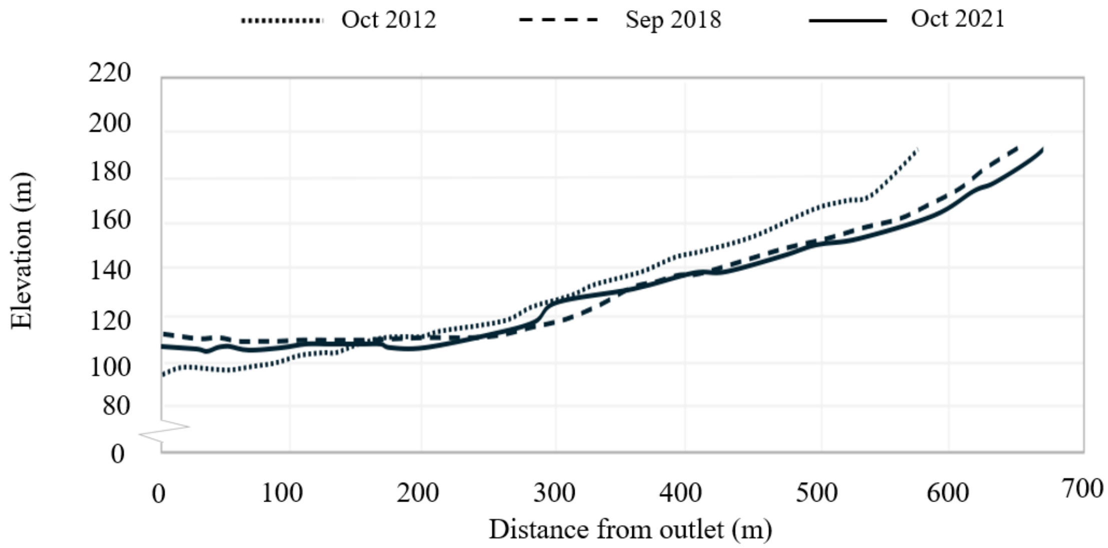

Figure 4.2.2.1 Pre- and post-seismic longitudinal profile of the mainstream in site B: October 05, 2012, September 11, 2018, and October 29, 2021.

Longitudinal profiles of mainstream based on Oct 2012 ALS DEM, Sep 2018 ALS DEM and Oct 2021 UAV-Lidar DEM in Study site A was plotted in Figure 4.2.1.2.The analyzed results of Drainage network, Stream length (m) of all tributaries (1st, 2nd , 3rd, and 4th order streams), Elevation of stream head and stream outlet (m) of all tributaries (1st order stream), Gradient of all tributaries (1st order streams), Stream number (N_u), Stream order (U) and Length of main stream channel (m), during the investigation periods of this study were indicated in Figure 4.2.2.2, Table 4.2.1, Table 4.2.2, Table 4.2.3, Table 4.2.4 and Table 4.3.2. The extension of channel near stream heads, contribution longer mainstream channels were confirmed. Also, steeper slopes near stream head were observed based on Oct 2012 ALS DEM , Sep 2018 ALS DEM and Oct 2021 UAV-Lidar DEM.

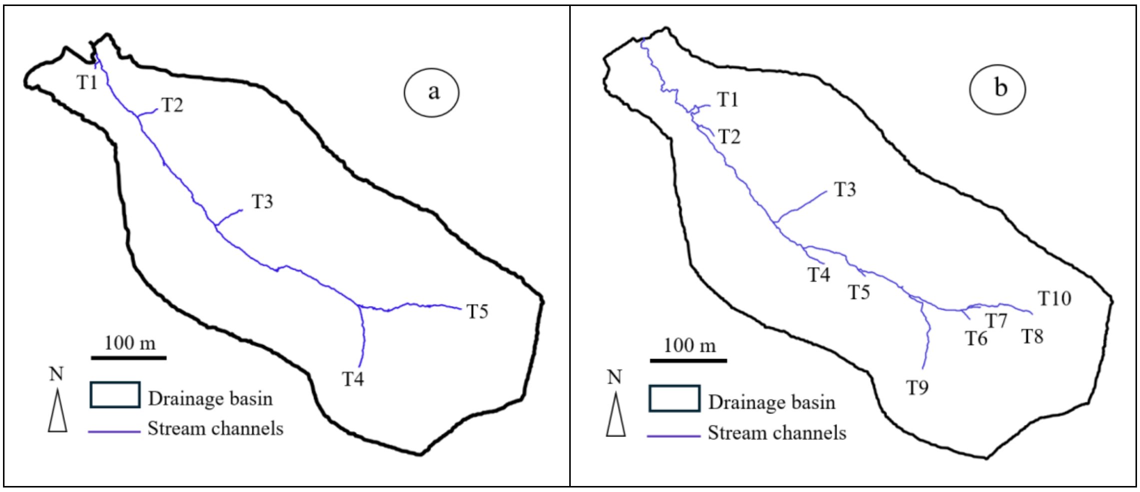

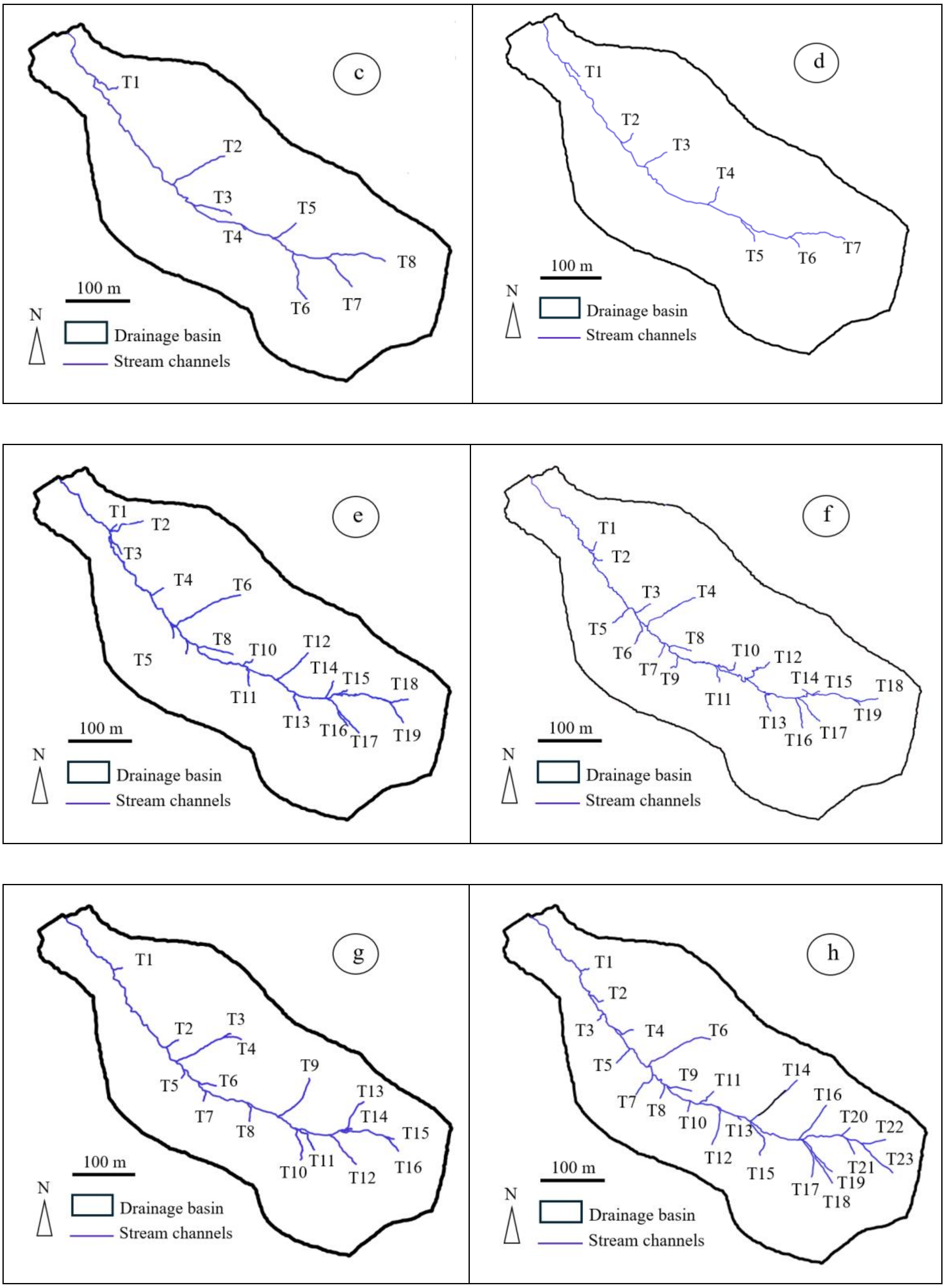
c
T1
T2
T3
T4
T5
T6
T7
T8
100 m
N
Drainage basin
Stream channels
d
T1
T2
T3
T4
T5
T6
T7
100 m
N
Drainage basin
Stream channels
e
T1
T2
T3
T4
T5
T6
T8
T10
T11
T12
T13
T14
T15
T16
T17
T18
T19
100 m
N
Drainage basin
Stream channels
f
T1
T2
T3
T4
T5
T6
T7
T8
T9
T10
T11
T12
T13
T14
T15
T16
T17
T18
T19
100 m
N
Drainage basin
Stream channels
g
T1
T2
T3
T4
T5
T6
T7
T8
T9
T10
T11
T12
T13
T14
T15
T16
100 m
N
Drainage basin
Stream channels
h
T1
T2
T3
T4
T5
T6
T7
T8
T9
T10
T11
T12
T13
T14
T15
T16
T17
T18
T19
T20
T21
T22
T23
100 m
N
Drainage basin
Stream channels

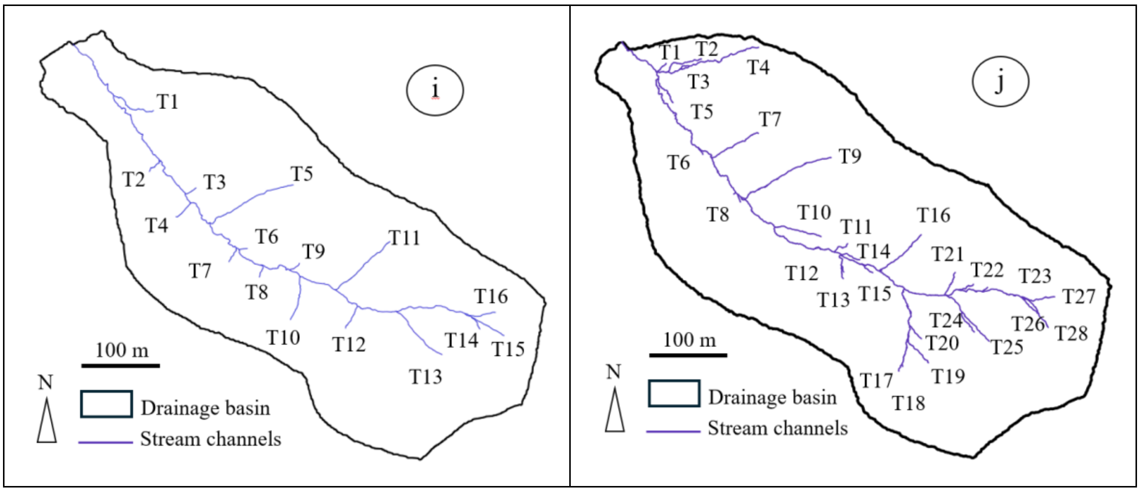

Figure 4.2.2.2: Pre and Post-seismic drainage network development in study site B. Hillshade image and stream network for (a) October 05, 2012, (b) September 11, 2018, (c) April 23, 2020, (d) June 25, 2020, (e) September 14, 2020, (f) October 30, 2020, (g) April 13, 2021, (h) June 21, 2021, (i) August 27, 2021, (j) October 29, 2021.

4.2.3 Study site C

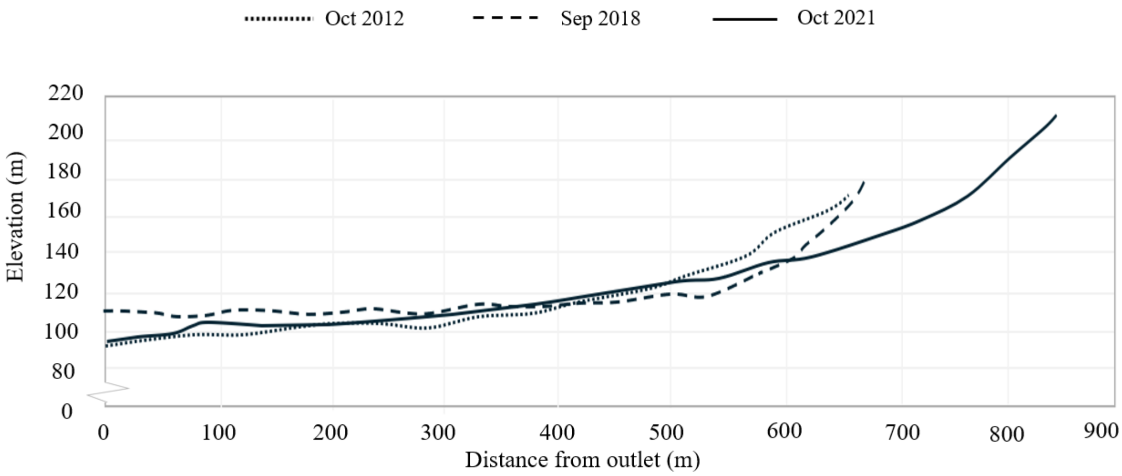

Pre- and post-seismic longitudinal profile of the mainstream in site C: October 05, 2012, September 11, 2018, and October 29, 2021.

Figure 4.2.3.1: Pre- and post-seismic longitudinal profile of the mainstream in site C: October 05, 2012, September 11, 2018, and October 29, 2021.

Longitudinal profiles of mainstream based on Oct 2012 ALS DEM, Sep 2018 ALS DEM and Oct 2021 UAV-Lidar DEM in Study site A was plotted in Figure 4.2.3.2. The analyzed results of Drainage network, Stream length (m) of all tributaries (1st, 2nd , 3rd, and 4th order streams), Elevation of stream head and stream outlet (m) of all tributaries (1st order stream), Gradient of all tributaries (1st order streams), Stream number (N_u), Stream order (U) and Length of main stream channel (m), during the investigation periods of this study were indicated in Figure 4.2.3.2, Table 4.2.1, Table 4.2.2, Table 4.2.3, Table 4.2.4 and Table 4.3.3. The extension of main stream heads, contributing longer mainstream channels were confirmed. Especially, the extension of stream channel near the steam head during Period 2 – 9 was obvious Also, steeper slopes near stream heads were observed based on Oct 2012 ALS DEM, Sep 2018 ALS DEM and Oct 2021 UAV-Lidar DEM.

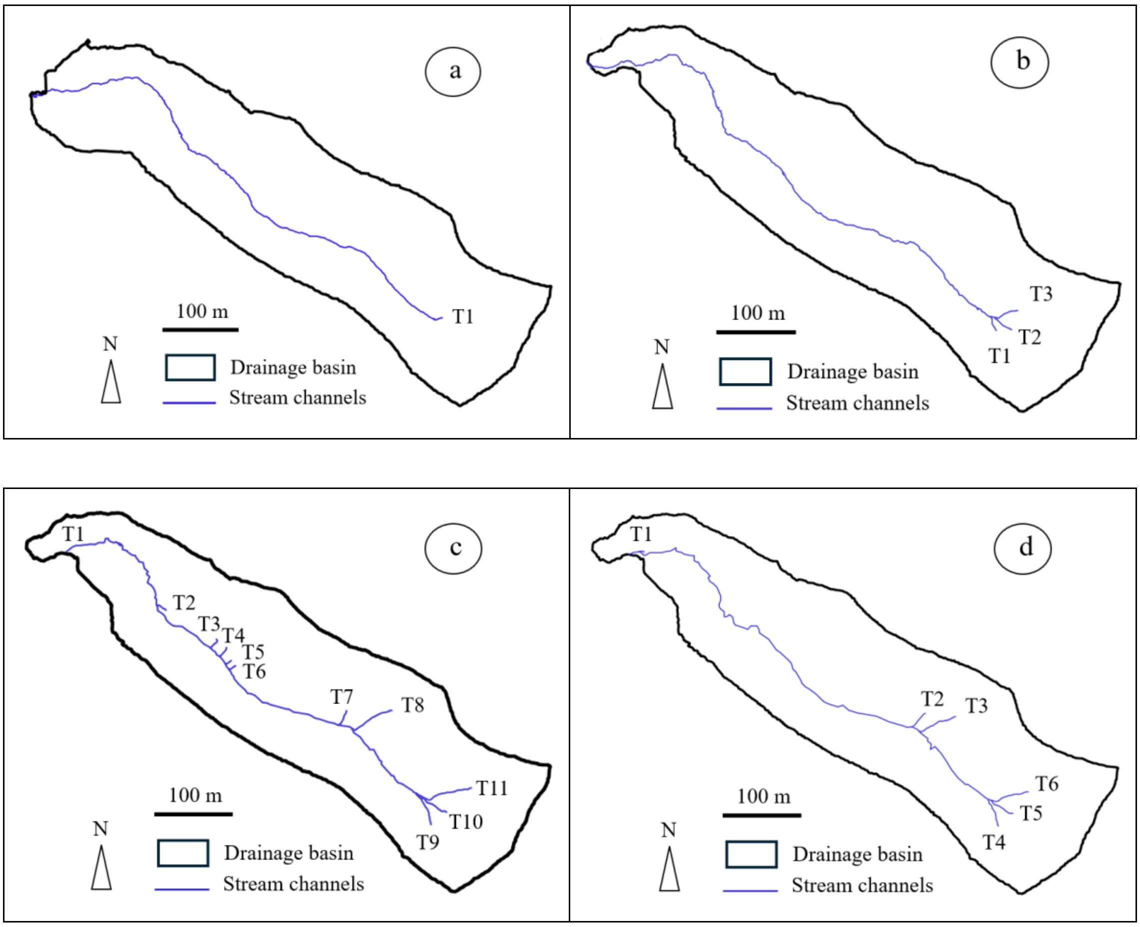

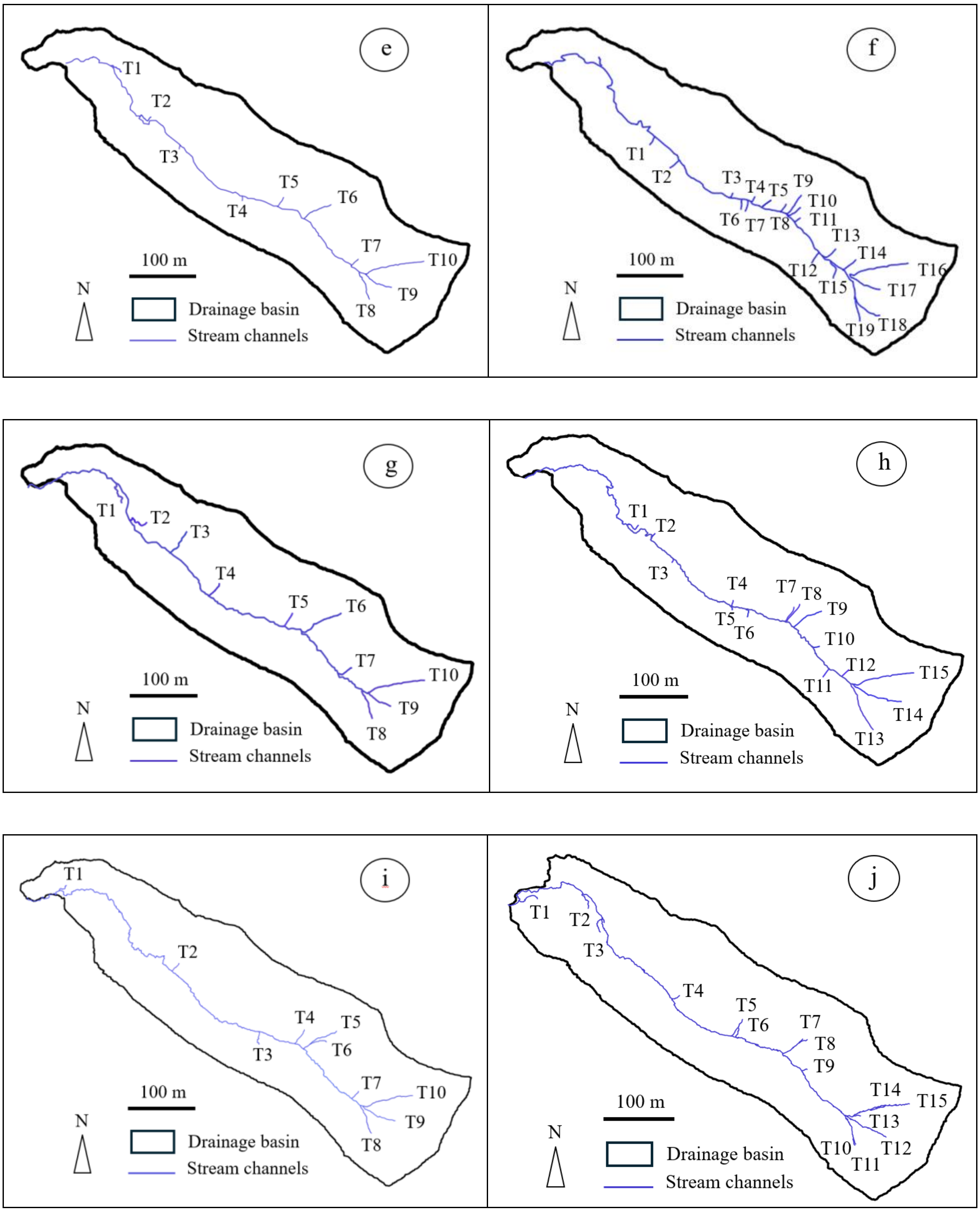

Figure 4.2.3.2: Pre and Post-seismic drainage network development in study site C. Hillshade image and stream network for (a) October 05, 2012, (b) September 11, 2018, (c) April 23, 2020, (d) June 25, 2020, (e) September 14, 2020, (f) October 30, 2020, (g) April 13, 2021, (h) June 21, 2021, (i) August 27, 2021, (j) October 29, 2021.

4.2.4 Study site D

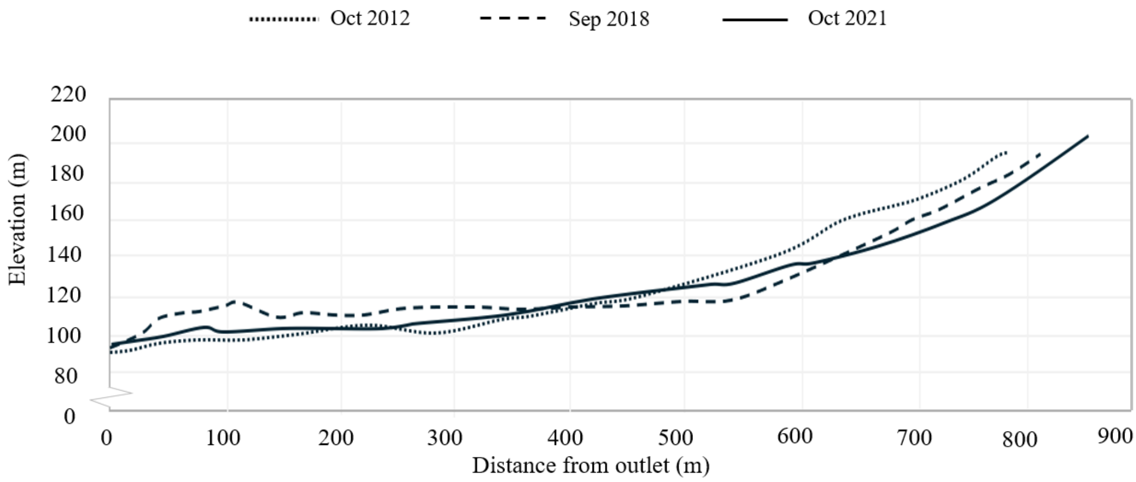

Pre- and post-seismic longitudinal profile of the mainstream in site D: October 05, 2012, September 11, 2018, and October 29, 2021.

Figure 4.2.4.1: Pre- and post-seismic longitudinal profile of the mainstream in site D: October 05, 2012, September 11, 2018, and October 29, 2021.

Longitudinal profiles of mainstream based on Oct 2012 ALS DEM, Sep 2018 ALS DEM and Oct 2021 UAV-Lidar DEM in Study site A was plotted in Figure 4.2.4.1. The analyzed results of Drainage network, Stream length (m) of all tributaries (1^{st}, 2^{nd} , 3^{rd}, and 4^{th} order streams), Elevation of stream head and stream outlet (m) of all tributaries (1^{st} order stream), Gradient of all tributaries (1^{st} order streams), Stream number (N_u), Stream order (U) and Length of main stream channel (m), during the investigation periods of this study were indicated in Figure 4.2.4.2, Table 4.2.1, Table 4.2.2, Table 4.2.3, Table 4.2.4 and Table 4.3.4 The extension of stream channel near stream heads, contributing longer mainstream channels were confirmed. Especially, the extension of stream channel near the steam head during Period 2 – 9 was obvious Also, steeper slopes near stream heads were observed based on Oct 2012 ALS DEM, Sep 2018 ALS DEM and Oct 2021 UAV-Lidar DEM.

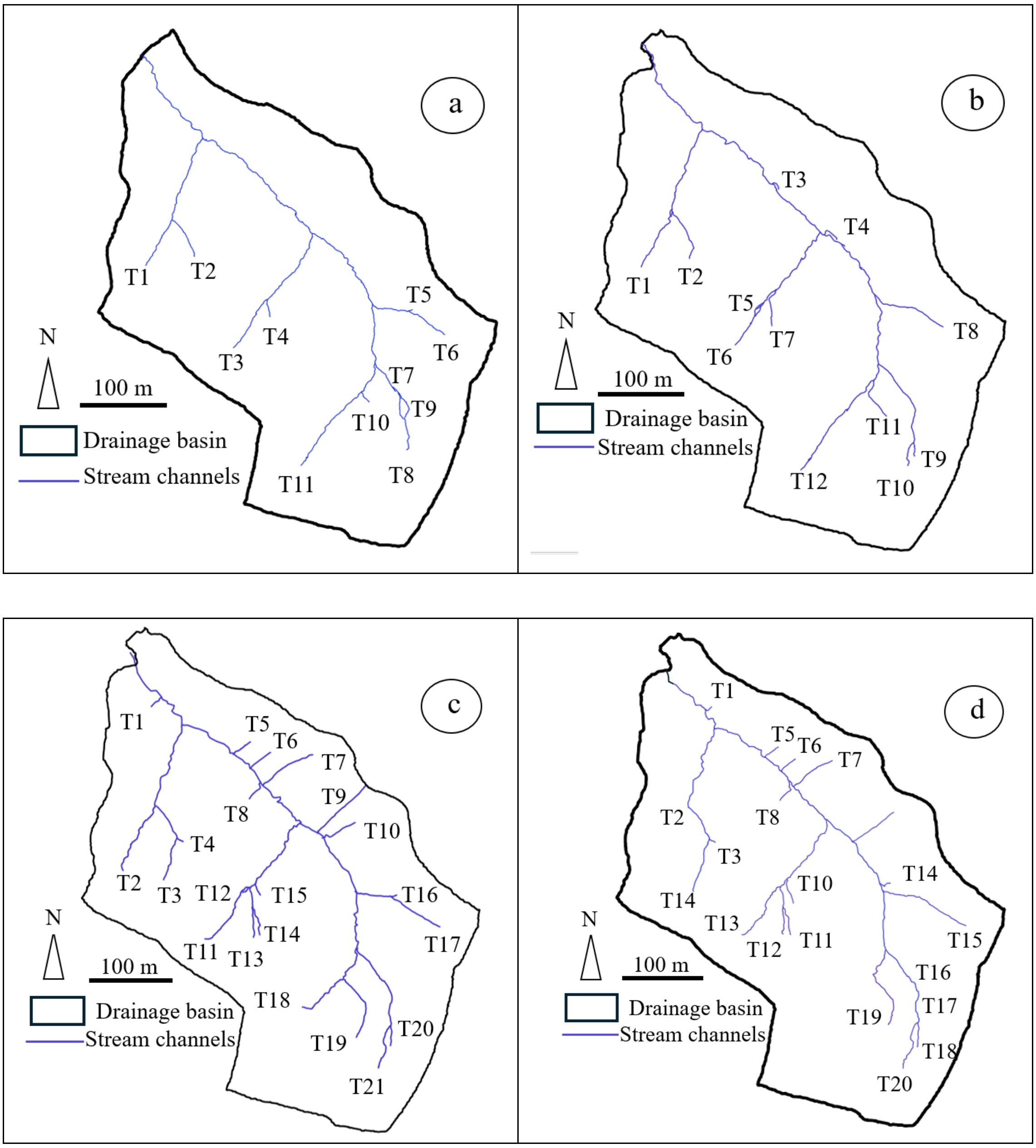
a
T1
T2
T3
T4
T5
T6
T7
T8
T9
T10
T11
N
100 m
Drainage basin
Stream channels
b
T1
T2
T3
T4
T5
T6
T7
T8
T9
T10
T11
T12
N
100 m
Drainage basin
Stream channels
c
T1
T2
T3
T4
T5
T6
T7
T8
T9
T10
T11
T12
T13
T14
T15
T16
T17
T18
T19
T20
T21
N
100 m
Drainage basin
Stream channels
d
T1
T2
T3
T5
T6
T7
T8
T10
T11
T12
T13
T14
T14
T15
T16
T17
T18
T19
T20
N
100 m
Drainage basin
Stream channels

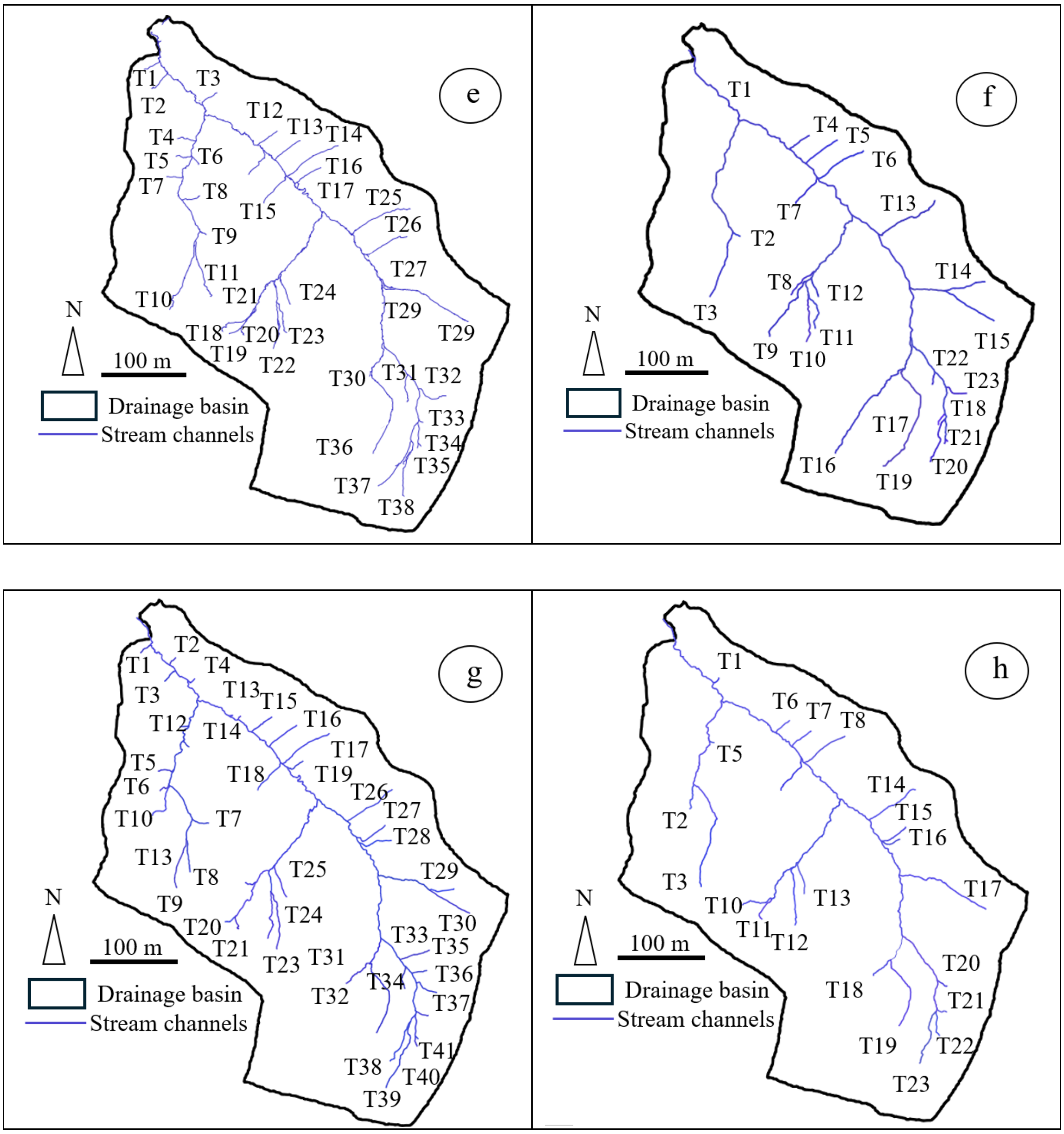

e
T1
T2
T3
T4
T5
T6
T7
T8
T9
T10
T11
T12
T13
T14
T15
T16
T17
T18
T19
T20
T21
T22
T23
T24
T25
T26
T27
T29
T29
T30
T31
T32
T33
T34
T35
T36
T37
T38
N
100 m
Drainage basin
Stream channels
f
T1
T2
T3
T4
T5
T6
T7
T8
T9
T10
T11
T12
T13
T14
T15
T16
T17
T18
T19
T20
T21
T22
T23
N
100 m
Drainage basin
Stream channels
g
T1
T2
T3
T4
T5
T6
T7
T8
T9
T10
T12
T13
T13
T14
T15
T16
T17
T18
T19
T20
T21
T23
T24
T25
T26
T27
T28
T29
T30
T31
T32
T33
T34
T35
T36
T37
T38
T39
T40
T41
N
100 m
Drainage basin
Stream channels
h
T1
T2
T3
T5
T6
T7
T8
T10
T11
T12
T13
T14
T15
T16
T17
T18
T19
T20
T21
T22
T23
N
100 m
Drainage basin
Stream channels

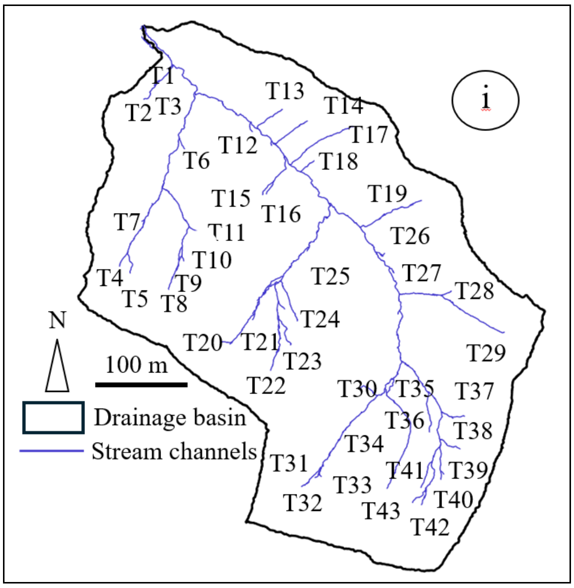

Figure 4.2.4.2: Pre and Post-seismic drainage network development in study site D. Hillshade image and stream network for (a) October 05, 2012, (b) September 11, 2018, (c) April 23, 2020, (d) September 14, 2020, (e) October 30, 2020, (f) April 13, 2021, (g) June 21, 2021, (h) August 27, 2021, (i) October 29, 2021.

Date	Oct 05, 2012				Sep 11, 2018				Apr 23, 2020			
	Stream length of tributaries (1st order stream) (m)				Stream length of tributaries (1st order stream) (m)				Stream length of tributaries (1st order stream) (m)			
Study sites	A	B	C	D	A	B	C	D	A	B	C	D
Tributary												
1	586.42	10.86	659.35	73.36	14.40	13.66	17.69	94.76	238.12	45.94	44.96	44.39
2		24.84		61.09	63.9	24.05	23.97	73.33		32.32	13.58	86.16
3		36.95		83.96		68.12	28.43	14.07		2.52	15.06	65.20
4		71.06		24.69		32.88		26.09		33.29	12.34	10.18
5		126.2		5.12		10.28		22.34		3.51	14.11	31.34
6				62.00		12.81		69.60		60.49	7.79	36.30
7				6.24		13.83		52.00		20.15	19.35	83.84
8				86.22		9.66		104.05		72.69	54.69	32.11
9				43.48		93.82		19.48			42.90	108.89
10				17.52		40.70		35.58			34.28	57.46
11				135.88				57.38			61.79	111.60
12								158.72				14.42
13												44.32
14												44.04
15												18.60
16												8.15
17												81.37
18												180.34
19												98.65
20												28.23
21												68.52
22												
23												
24												
25												
26												
27												
28												
29												
30												
31												
32												
33												
34												
35												
36												
37												
38												
39												
40												
41												
42												
43												

Date	Jun 25, 2020				Sep 14, 2020				Oct 30, 2020			
	Stream length of tributaries (1st order stream) (m)				Stream length of tributaries (1st order stream) (m)				Stream length of tributaries (1st order stream) (m)			
Study sites	A	B	C	D	A	B	C	D	A	B	C	D
Tributary												
1	496.53	38.89	10.11	No data	12.10	21.19	20.32	11.27	12.64	12.89	13.59	28.38
2		13.80	19.58		26.23	14.27	23.85	16.96	8.83	10.92	11.98	33.29
3		56.98	42.57		23.80	17.67	5.62	9.21	6.97	27.23	28.31	29.98
4		11.64	32.34		36.68	18.46	5.64	75.35	5.54	67.58	67.58	32.06
5		17.90	33.98			22.18	6.72	25.01	5.82	27.69	27.69	25.46
6		56.84	67.84			94.65	10.60	25.30	8.52	35.12	31.16	15.68
7		149.67				23.42	12.81	65.10	21.97	19.85	20.87	25.58
8						10.90	38.90	33.66	10.63	37.99	38.95	31.33
9						19.01	41.07	68.46	46.02	24.23	25.99	10.23
10						24.40	79.05	35.56	42.41	38.12	39.37	69.72
11						26.42		42.23	50.00	21.01	20.06	115.50
12						30.38		39.68	23.23	59.66	57.09	36.02
13						58.65		93.43	33.35	29.89	30.23	45.99
14						68.31		18.91	21.89	9.96	10.36	87.00
15						17.19		126.06	35.75	12.03	12.92	51.06
16						36.75		14.22	2.25	36.01	36.32	40.95
17						47.44		6.21	29.64	49.01	48.04	10.57
18						23.73		33.56	7.00	9.02	8.51	20.63
19						57.89		121.51	27.10	13.99	14.15	7.01
20								70.58				9.31
21												23.44
22												70.97
23												50.80
24												47.31
25												96.25
26												74.89
27												15.67
28												20.65
29												137.68
30												194.75
31												42.00
32												79.66
33												6.55
34												5.31
35												6.41
36												106.23
37												22.05
38												84.31
39												
40												
41												
42												
43												

Date	Apr 13, 2021				Jun 21, 2021				Aug 27, 2021				Oct 29, 2021			
	Stream length of tributaries (1st order stream) (m)				Stream length of tributaries (1st order stream) (m)				Stream length of tributaries (1st order stream) (m)				Stream length of tributaries (1st order stream) (m)			
Study sites	A	B	C	D	A	B	C	D	A	B	C	D	A	B	C	D
Tributary																
1	44.71	12.03	37.68	19.66	6.05	11.48	24.89	16.62	16.97	50.78	15.32	9.63	11.20	13.10	37.30	6.97
2	32.39	18.24	35.63	11.00	9.95	24.52	6.77	13.24	3.53	17.55	14.53	7.40	21.52	44.50	30.43	8.79
3	124.63	10.63	38.76	92.32	16.67	13.91	5.09	20.55	2.88	13.58	20.48	94.40	7.97	10.94	26.50	34.54
4		22.66	21.71	32.50	1.33	28.49	8.54	10.82	9.79	21.23	22.79	34.73	9.62	96.68	12.09	19.14
5		12.12	21.74	52.70	10.06	24.05	5.72	21.48	22.59	97.18	39.89	7.51	8.79	38.42	27.88	26.87
6		24.69	58.91	74.19	7.83	88.82	12.75	16.50	28.89	8.90	23.43	23.09	2.75	8.34	14.53	13.29
7		13.79	20.77	43.98	14.56	35.09	21.80	22.26	47.40	17.63	13.03	33.15	8.51	58.20	7.29	18.73
8		25.74	39.52	47.23	31.76	18.78	28.90	41.92		14.32	40.69	64.01	40.27	8.16	13.33	59.72
9		64.66	35.48	96.13	27.35	31.54	42.29	64.07		12.73	48.68	54.71	47.34	109.87	8.14	7.06
10		48.47	74.84	65.43	7.76	13.85	10.49	52.98		47.65	67.95	42.46	11.15	53.85	10.67	8.34
11		34.89		52.58	7.73	26.26	12.84	12.73		77.71		33.77	36.69	20.51	8.74	13.45
12		51.38		26.34	9.48	49.17	12.22	11.09		26.51		80.07		14.65	65.05	15.15
13		50.62		96.67	8.78	5.95	67.44	4.25		67.43		42.27		7.77	10.22	43.43
14		13.44		56.45	21.19	77.26	70.78	5.47		15.40		74.33		23.17	22.66	54.60
15		10.98		76.70	17.68	52.53	80.82	33.16		37.54		38.03		17.28	28.92	22.24
16		24.29		153.98	25.40	54.74		44.00		32.00		25.88		59.77		17.73
17				159.31	11.55	48.62		72.31				132.52		8.91		97.93
18				17.87	29.71	10.04		46.33				34.14		2.61		23.50
19				64.56	26.81	29.40		25.36				98.22		30.04		91.46
20				5.69	28.42	14.88		16.89				15.50		18.21		62.42
21				3.46		22.36		21.71				15.04		28.23		7.04
22				16.48		30.68		16.04				33.21		19.78		79.62
23				31.13		54.02		65.24				77.22		7.06		48.56
24								78.66						28.17		12.60
25								43.47						41.96		57.65
26								70.54						23.77		13.89
27								45.66						38.64		9.87
28								44.61						43.41		14.30
29								31.58								96.13
30								57.76								26.92
31								47.15								34.89
32								102.48								9.59
33								39.58								5.28
34								29.76								153.00
35								19.60								22.90
36								31.40								55.50
37								16.93								34.39
38								60.35								32.96
39								94.41								5.16
40								13.12								10.82
41								4.32								37.18
42																22.96
43																28.08

Table 4.2.1: Stream length (m) of all tributaries (1st order streams) (Study site A - D) during the investigation periods of this study

	Date	Oct 05, 2012				Sep 11, 2018			
		Stream length of 2nd order stream (m)				Stream length of 2nd order stream (m)			
	Study sites	A	B	C	D	A	B	C	D
1			451.36		127.53	574.64	613.12	637.84	119.70
2					48.36				133.12
3					54.76				24.52
4					53.91				124.72
5									
6									
7									
8									
9									
10									
	Total		451.36		284.56		613.12	637.84	402.06
	average		451.36		71.14		613.12	637.84	100.52
		Stream length of 3rd order stream (m)				Stream length of 3rd order stream (m)			
	Study sites	A	B	C	D	A	B	C	D
1					604.38				629.03
2									
3									
	Total				604.38				629.03
	average				604.38				629.03
		Stream length of 4th order stream (m)				Stream length of 4th order stream (m)			
	Study sites	A	B	C	D	A	B	C	D
1									
	Total								
	average								

	Date	Apr 23, 2020				Jun 25, 2020			
		Stream length of 2nd order stream (m)				Stream length of 2nd order stream (m)			
	Study sites	A	B	C	D	A	B	C	D
1			443.34	706.03	195.10		348.86	567.23	No data
2					166.24				
3					53.24				
4					57.48				
5					131.15				
6									
7									
8									
9									
10									
	Total		443.34	706.03	603.21		348.86	567.23	No data
	average		443.34	706.03	120.64		348.86	567.23	No data
		Stream length of 3rd order stream (m)				Stream length of 3rd order stream (m)			
	Study sites	A	B	C	D	A	B	C	D
1					657.05				No data
2									
3									
	Total				657.05				No data
	average				657.05				No data
		Stream length of 4th order stream (m)				Stream length of 4th order stream (m)			
	Study sites	A	B	C	D	A	B	C	D
1									
	Total								
	average								

	Date	Sep 14, 2020				Oct 30, 2020			
		Stream length of 2nd order stream (m)				Stream length of 2nd order stream (m)			
	Study sites	A	B	C	D	A	B	C	D
1		574.64	24.83	546.23	177.77	3.82	639.99	643.94	208.78
2			78.44		147.30	12.45			92.24
3					325.79				30.74
4									46.05
5									29.91
6									
7									
8									
9									
10									
	Total	574.64	103.27	546.23	650.86	16.27	639.99	643.94	407.72
	average	574.64	51.64	546.23	162.72	8.14	639.99	643.94	81.54
		Stream length of 3rd order stream (m)				Stream length of 3rd order stream (m)			
	Study sites	A	B	C	D	A	B	C	D
1			434.04		309.77	659.60			130.84
2									406.75
3									
	Total		434.04		309.77	659.60			537.59
	average		434.04		309.77	659.60			537.59
		Stream length of 4th order stream (m)				Stream length of 4th order stream (m)			
	Study sites	A	B	C	D	A	B	C	D
1									411.43
	Total								411.43
	average								411.43

	Date	Apr 13, 2021				Jun 21, 2021			
		Stream length of 2nd order stream (m)				Stream length of 2nd order stream (m)			
	Study sites	A	B	C	D	A	B	C	D
1		440.44	68.90	614.79	156.14	590.52	79.09	734.73	27.71
2			305.61		50.32		27.50		11.59
3					47.10				38.41
4					138.91				77.93
5					171.02				222.25
6									26.94
7									82.37
8									
9									
10									
	Total		374.51	614.79	563.49	590.52	106.59	734.73	487.20
	average		374.51	614.79	112.70	590.52	53.30	734.73	69.60
		Stream length of 3rd order stream (m)				Stream length of 3rd order stream (m)			
	Study sites	A	B	C	D	A	B	C	D
1			226.79		543.63		485.41		134.66
2									381.66
3									
	Total		226.79		543.63		485.41		516.32
	average		226.79		543.63		485.41		258.16
		Stream length of 4th order stream (m)				Stream length of 4th order stream (m)			
	Study sites	A	B	C	D	A	B	C	D
1									381.66
	Total								381.66
	average								381.66

	Date	Aug 27, 2021				Oct 29, 2021			
		Stream length of 2nd order stream (m)				Stream length of 2nd order stream (m)			
	Study sites	A	B	C	D	A	B	C	D
1		560.91	574.65	123.55	121.66	5.64	92.58	27.00	20.47
2				10.80	37.73	40.12	24.82	44.71	36.61
3					180.66		92.10	42.25	36.59
4					195.76		15.67		20.99
5							12.37		15.90
6									22.84
7									17.71
8									43.47
9									17.45
10									8.75
	Total	560.91	574.65	134.35	535.81	45.76	237.54	113.96	240.78
	average	560.91	574.65	67.175	133.95	22.88	47.51	37.99	24.08
		Stream length of 3rd order stream (m)				Stream length of 3rd order stream (m)			
	Study sites	A	B	C	D	A	B	C	D
1				562.26	623.21	611.41	549.73	769.98	148.74
2									156.77
3									404.48
	Total			562.26	623.21	611.41	549.73	769.98	709.99
	average			562.26	623.21	611.41	549.73	769.98	236.66
		Stream length of 4th order stream (m)				Stream length of 4th order stream (m)			
	Study sites	A	B	C	D	A	B	C	D
1									404.44
	Total								404.44
	average								404.44

Table 4.2.2: Stream length (m) of all $2^{nd,}$ 3^{rd} and 4^{th} order streams (Study site A - D) during the investigation periods of this study

Tributary	Date	Oct 05, 2012				Sep 11, 2018				Apr 23, 2020				Jun 25, 2020				Sep 14, 2020			
		Elevation of stream heads and outlets of tributaries (1st order stream) (m)				Elevation of stream heads and outlets of tributaries (1st order stream) (m)				Elevation of stream heads and outlets of tributaries (1st order stream) (m)				Elevation of stream heads and outlets of tributaries (1st order stream) (m)				Elevation of stream heads and outlets of tributaries (1st order stream) (m)			
	Study sites	A	B	C	D	A	B	C	D	A	B	C	D	A	B	C	D	A	B	C	D
1	Stream head	175.70	99.85	171.13	146.97	150.17	117.70	171.12	152.41	175.67	98.06	100.53	127.42	171.39	115.97	96.14	No data	171.11	113.02	105.05	105.33
	Stream outlet	88.03	97.53	88.34	120.98	148.08	110.16	162.27	119.60	102.41	84.80	96.30	94.89	97.17	108.86	95.4		165.21	109.84	104.38	96.71
2	Stream head		121.02		145.46	175.48	110.97	177.33	149.18		115.41	106.77	147.01		126.91	155.14		187.00	111.16	114.06	127.73
	Stream outlet		104.63		120.98	148.08	110.35	164.25	119.60		98.80	106.24	121.34		115.93	136.21		170.27	110.31	106.65	121.40
3	Stream head		143.09		176.38		153.48	182.97	111.82		108.47	121.88	171.34		151.58	169.92		122.49	139.69	115.19	147.54
	Stream outlet		122.05		140.84		121.28	164.25	111.00		108.16	110.60	142.77		123.51	138.3		106.87	112.59	110.55	142.80
4	Stream head		182.02		155.16		138.19		124.18		143.82	123.06	147.60		149.29	177.91		188.51	122.01	127.84	183.75
	Stream outlet		160.4		140.84		132.24		122.69		132.32	111.64	142.77		144.75	161.74		170.27	113.74	123.88	142.80
5	Stream head		192.88		156.75		146.79		150.46		133.42	122.60	118.36		159.62	179.44			135.45	145.06	115.77
	Stream outlet		160.40		154.66		145.40		143.97		132.41	112.72	108.33		151.85	161.72			117.18	131.85	108.43
6	Stream head				185.93		171.00		174.53		161.59	118.24	133.72		176.67	199.70			176.33	169.97	128.94
	Stream outlet				154.66		164.83		143.97		135.87	113.52	110.05		152.18	158.27			123.43	138.74	109.98
7	Stream head				167.93		171.91		164.19		149.11	150.14	156.58		192.08				140.79	168.92	150.65
	Stream outlet				165.86		167.59		138.22		140.68	135.01	112.46		152.18				126.35	157.43	112.61
8	Stream head				190.22		179.79		177.28		161.70	177.82	130.74						133.35	181.01	130.32
	Stream outlet				169.10		177.08		133.92		140.68	137.57	111.62						131.61	161.27	111.06
9	Stream head				180.31		182.12		189.31			178.10	182.72						145.04	189.39	169.42
	Stream outlet				169.10		154.33		184.30			158.42	124.54						131.51	165.27	125.69
10	Stream head				161.96		191.10		194.12			179.75	157.70						156.70	216.67	159.25
	Stream outlet				153.34		177.08		184.30			162.83	125.24						138.41	165.27	138.23
11	Stream head				193.33				177.12			198.65	191.26						150.62		173.52
	Stream outlet				153.34				151.20			162.83	142.55						140.33		158.15
12	Stream head								197.10				145.32						158.01		174.32
	Stream outlet								151.20				142.70						145.07		158.15
13	Stream head												174.44						184.12		183.76
	Stream outlet												158.26						151.74		142.76
14	Stream head												172.69						173.35		142.95
	Stream outlet												158.26						152.04		133.54
15	Stream head												151.84						172.32		189.38
	Stream outlet												139.23						164.29		136.17
16	Stream head												157.11						198.01		178.45
	Stream outlet												153.89						175.38		173.79
17	Stream head												189.08						206.77		184.73
	Stream outlet												153.89						175.38		183.00
18	Stream head												180.34						201.64		194.48
	Stream outlet												154.17						189.74		183.51
19	Stream head												197.63						227.23		190.28
	Stream outlet												154.17						189.74		146.90
20	Stream head												191.86								208.13
	Stream outlet												183.46								183.51
21	Stream head												204.31								
	Stream outlet												183.46								
22	Stream head																				
	Stream outlet																				
23	Stream head																				
	Stream outlet																				
24	Stream head																				
	Stream outlet																				
25	Stream head																				
	Stream outlet																				
26	Stream head																				
	Stream outlet																				
27	Stream head																				
	Stream outlet																				
28	Stream head																				
	Stream outlet																				
29	Stream head																				
	Stream outlet																				
30	Stream head																				
	Stream outlet																				
31	Stream head																				
	Stream outlet																				
32	Stream head																				
	Stream outlet																				
33	Stream head																				
	Stream outlet																				
34	Stream head																				
	Stream outlet																				
35	Stream head																				
	Stream outlet																				
36	Stream head																				
	Stream outlet																				
37	Stream head																				
	Stream outlet																				
38	Stream head																				
	Stream outlet																				
39	Stream head																				
	Stream outlet																				
40	Stream head																				
	Stream outlet																				
41	Stream head																				
	Stream outlet																				
42	Stream head																				
	Stream outlet																				
43	Stream head																				
	Stream outlet																				

Tributary	Date	Oct 30, 2020				Apr 13, 2021				Jun 21, 2021				Aug 27, 2021				Oct 29, 2021			
		Elevation of stream heads and outlets of tributaries (1st order stream) (m)				Elevation of stream heads and outlets of tributaries (1st order stream) (m)				Elevation of stream heads and outlets of tributaries (1st order stream) (m)				Elevation of stream heads and outlets of tributaries (1st order stream) (m)				Elevation of stream heads and outlets of tributaries (1st order stream) (m)			
	Study sites	A	B	C	D	A	B	C	D	A	B	C	D	A	B	C	D	A	B	C	D
1	Stream head	123.35	111.78	111.78	108.10	125.53	117.15	105.37	112.17	98.27	117.20	113.80	106.43	117.47	146.34	96.72	121.54	98.25	119.30	99.55	100.05
	Stream outlet	97.17	109.99	109.99	90.44	99.44	109.93	105.10	92.98	98.03	109.86	106.64	93.78	109.89	102.46	95.13	92.47	98.17	109.34	97.09	95.35
2	Stream head	103.94	116.21	116.21	113.95	168.19	136.67	115.87	148.24	128.95	117.85	115.71	126.76	127.11	137.47	117.81	142.48	114.84	133.90	105.15	122.93
	Stream outlet	98.68	110.70	110.70	91.60	149.52	117.88	106.27	142.53	98.19	111.05	110.01	94.29	126.51	107.84	106.05	139.01	101.44	116.67	103.99	115.82
3	Stream head	107.32	137.57	137.57	120.12	184.18	163.07	141.21	196.95	106.92	117.54	113.25	109.77	144.42	12.34	166.72	202.96	110.94	127.80	106.00	134.01
	Stream outlet	100.30	117.46	117.46	97.18	149.52	157.19	108.88	142.56	99.04	112.23	111.40	94.84	143.87	111.94	122.57	139.01	106.28	123.00	105.48	115.82
4	Stream head	107.89	159.01	159.01	137.52		175.15	139.23	121.74	106.53	138.73	130.63	104.12	151.26	153.26	151.09	134.36	113.40	159.47	121.64	169.90
	Stream outlet	105.84	122.65	122.65	104.79		157.19	117.84	108.37	105.24	113.70	124.06	96.80	147.31	113.18	132.19	117.02	112.61	123.00	113.22	156.48
5	Stream head	110.34	137.83	137.83	122.19		131.55	152.05	141.75	112.62	144.78	126.52	144.70	185.11	198.82	190.90	128.89	151.12	111.30	147.37	178.88
	Stream outlet	107.09	116.44	116.44	109.24		125.97	133.29	110.11	106.42	117.29	124.09	116.90	159.37	118.42	143.26	105.42	147.81	110.02	125.26	156.48
6	Stream head	115.07	136.83	136.83	121.44		139.43	179.54	153.80	112.09	171.84	134.74	129.62	184.75	133.12	168.23	112.15	150.00	114.09	136.01	118.06
	Stream outlet	108.97	119.73	119.73	109.53		131.83	137.40	111.88	108.73	123.70	126.22	121.10	168.69	128.36	143.26	104.23	149.34	113.50	126.05	109.76
7	Stream head	124.11	144.56	144.56	133.64		144.91	167.17	141.22	121.90	150.68	155.00	154.76	191.46	140.21	188.81	128.58	159.05	151.39	158.79	160.17
	Stream outlet	109.28	130.43	130.43	114.94		133.75	153.02	112.02	113.63	126.29	136.13	142.71	168.69	127.83	153.49	105.87	157.02	114.74	154.93	152.23
8	Stream head	146.67	140.55	140.55	153.17		154.64	181.35	149.53	152.97	144.25	159.61	182.52		143.61	178.62	146.30	186.37	122.29	161.97	183.05
	Stream outlet	115.43	131.31	131.31	123.04		145.08	161.28	137.35	130.82	131.42	136.23	153.51		133.46	157.76	108.01	167.45	120.18	154.93	152.23
9	Stream head	165.85	148.83	148.83	147.06		191.13	185.88	188.54	156.21	141.08	170.02	197.46		145.68	188.24	138.27	190.05	173.57	148.71	160.56
	Stream outlet	114.57	133.65	133.65	141.96		151.77	165.24	142.54	143.92	131.87	138.70	153.51		140.44	159.53	107.00	167.45	121.42	143.05	157.67
10	Stream head	147.49	153.61	153.61	199.80		171.24	214.62	182.53	154.14	148.11	153.73	133.89		195.94	203.41	212.63	183.30	143.69	182.07	150.85
	Stream outlet	131.43	144.40	144.40	147.69		156.43	165.24	153.15	151.01	137.53	144.51	121.31		142.37	159.53	156.79	178.51	132.15	177.38	148.26
11	Stream head	147.48	170.05	170.05	211.76		173.48		172.65	144.40	149.78	166.77	116.13		194.42		205.12	194.24	150.34	181.40	149.15
	Stream outlet	136.05	143.85	143.85	147.69		157.80		153.15	139.82	140.51	153.78	109.32		148.12		156.79	178.51	144.41	177.38	142.47
12	Stream head	164.49	172.24	172.24	120.18		190.93		158.17	141.17	171.98	168.09	113.70		166.98		174.12		154.74	196.13	108.68
	Stream outlet	153.31	150.81	150.81	106.89		164.91		139.59	139.51	145.07	157.18	105.65		153.61		137.96		148.83	162.23	106.32
13	Stream head	164.6	167.75	167.75	136.09		199.54		178.12	155.94	151.10	200.93	104.58		198.79		160.40		151.30	173.46	125.64
	Stream outlet	153.31	157.46	157.46	109.05		169.65		125.54	152.16	149.60	161.55	104.16		161.25		135.01		148.83	166.53	108.74
14	Stream head	171.27	170.70	170.70	155.90		174.82		191.67	163.87	198.25	206.92	107.74		198.01		170.09		148.72	195.35	138.25
	Stream outlet	160.51	168.01	168.01	111.16		170.83		153.51	152.74	151.92	162.88	105.59		190.35		121.66		145.24	183.20	109.93
15	Stream head	175.29	177.32	177.32	141.28		194.54		189.08	164.44	172.01	214.60	121.50		217.12		152.06		151.62	213.69	141.70
	Stream outlet	161.37	170.28	170.28	111.10		189.74		153.51	157.24	152.05	162.87	108.35		190.35		126.15		149.01	183.20	131.72
16	Stream head	180.95	189.25	189.25	141.61		202.42		204.40	169.91	194.26		138.12		204.95		141.52		180.90		140.67
	Stream outlet	179.81	163.34	163.34	114.32		189.74		154.11	160.88	164.26		110.09		186.73		126.21		151.61		131.72
17	Stream head	199.09	185.91	185.91	116.68				235.7	170.08	195.69		153.18				185.85		187.30		159.41
	Stream outlet	179.81	164.07	164.07	113.40				154.11	165.42	165.97		112.58				132.98		183.79		112.42
18	Stream head	186.71	205.94	205.94	189.60				187.10	187.63	203.00		141.92				155.81		184.67		129.62
	Stream outlet	183.61	189.22	189.22	173.97				181.97	170.26	177.63		112.02				150.78		183.79		114.13
19	Stream head	199.68	206.59	206.59	179.76				205.13	191.55	194.68		129.41				196.58		190.36		171.71
	Stream outlet	183.61	189.22	189.22	173.97				183.33	175.59	177.63		113.56				150.78		174.52		125.01
20	Stream head				161.40				194.17	189.07	189.69		185.91				177.06		178.19		191.73
	Stream outlet				157.54				192.22	175.59	180.44		172.50				170.92		169.83		156.24
21	Stream head				166.22				192.78		196.93		211.35				184.04		175.64		159.81
	Stream outlet				155.73				192.22		182.49		172.5				176.61		164.13		156.24
22	Stream head				187.70				173.13		208.95		172.06				190.37		174.01		195.62
	Stream outlet				157.54				165.23		191.54		148.40				180.30		168.63		163.18
23	Stream head				173.78				188.55		226.61		187.30				208.42		177.46		174.86
	Stream outlet				157.54				173.45		191.54		158.11				180.30		175.46		163.18
24	Stream head				162.42								215.01						187.25		161.25
	Stream outlet				137.60								158.11						174.57		153.53
25	Stream head				168.78								165.15						197.22		167.89
	Stream outlet				124.94								139.10						174.57		139.28
26	Stream head				166.19								172.66						199.53		131.76
	Stream outlet				128.70								125.56						189.30		129.18
27	Stream head				136.56								159.13						206.91		132.94
	Stream outlet				133.01								128.72						188.82		132.14
28	Stream head				140.22								157.87						211.04		160.00
	Stream outlet				135.29								129.80						189.30		154.28
29	Stream head				188.35								185.62								192.78
	Stream outlet				135.88								166.17								154.28
30	Stream head				211.63								191.08								173.74
	Stream outlet				145.10								166.17								156.09
31	Stream head				177.86								160.73								206.36
	Stream outlet				164.47								154.25								187.67
32	Stream head				195.34								201.43								194.50
	Stream outlet				172.27								154.25								190.40
33	Stream head				183.75								186.99								193.77
	Stream outlet				181.77								162.96								190.40
34	Stream head				192.40								176.88								215.79
	Stream outlet				191.37								165.79								153.73
35	Stream head				193.51								182.57								154.55
	Stream outlet				191.37								169.22								150.70
36	Stream head				238.19								187.73								180.48
	Stream outlet				190.69								173.67								165.35
37	Stream head				203.27								188.79								188.48
	Stream outlet				196.11								182.49								165.35
38	Stream head				233.00								209.94								188.07
	Stream outlet				196.11								187.02								173.86
39	Stream head												233.52								191.34
	Stream outlet												187.02								181.51
40	Stream head												196.42								193.15
	Stream outlet												192.20								192.10
41	Stream head												192.96								201.73
	Stream outlet												192.20								189.06
42	Stream head																				210.21
	Stream outlet																				200.75
43	Stream head																				211.35
	Stream outlet																				200.75

Table 4.2.3: Elevation of stream heads and outlets of all tributaries (1st order streams) (Study site A - D) during the investigation periods of this study

Date	Oct 05, 2012				Sep 11, 2018				Apr 23, 2020				Jun 25, 2020				Sep 14, 2020			
	Gradient of tributaries (m/m)				Gradient of tributaries (m/m)				Gradient of tributaries (m/m)				Gradient of tributaries (m/m)				Gradient of tributaries (m/m)			
Study sites	A	B	C	D	A	B	C	D	A	B	C	D	A	B	C	D	A	B	C	D
Tributary																				
1	0.13	0.21	0.13	0.35	0.09	0.55	0.50	0.35	0.14	0.29	0.09	0.73	0.15	0.18	0.07	No data	0.49	0.15	0.03	0.76
2		0.66		0.40	0.14	0.03	0.56	0.40		0.48	0.04	0.30		0.80	0.96		0.67	0.05	0.31	0.37
3		0.57		0.42		0.47	0.69	0.06		0.13	0.75	0.44		0.49	0.74		0.66	1.53	0.83	0.51
4		0.30		0.58		0.18		0.06		0.35	0.92	0.47		0.43	0.50		0.69	0.45	0.70	0.54
5		0.28		0.41		0.47		0.29		0.29	0.70	0.32		0.43	0.52			0.82	0.89	0.29
6				0.50		0.48		0.44		0.43	0.61	0.65		0.43	0.61			0.56	0.77	0.75
7				0.33		0.31		0.50		0.42	0.78	0.53		0.26				0.62	0.90	0.58
8				0.24		0.28		0.42		0.29	0.74	0.60						0.16	0.51	0.57
9				0.26		0.29		0.26			0.46	0.53						0.71	0.59	0.64
10				0.49		0.34		0.28			0.49	0.56						0.75	0.65	0.59
11				0.29				0.45			0.58	0.44						0.39		0.36
12								0.29				0.18						0.43		0.41
13												0.38						0.55		0.44
14												0.33						0.32		0.50
15												0.68						0.47		0.42
16												0.40						0.62		0.33
17												0.43						0.66		0.28
18												0.31						0.50		0.33
19												0.44						0.65		0.36
20												0.30								0.35
21												0.30								
22																				
23																				
24																				
25																				
26																				
27																				
28																				
29																				
30																				
31																				
32																				
33																				
34																				
35																				
36																				
37																				
38																				
39																				
40																				
41																				
42																				
43																				

Date	Oct 30, 2020				Apr 13, 2021				Jun 21, 2021				Aug 27, 2021				Oct 29, 2021			
	Gradient of tributaries (m/m)				Gradient of tributaries (m/m)				Gradient of tributaries (m/m)				Gradient of tributaries (m/m)				Gradient of tributaries (m/m)			
Study sites	A	B	C	D	A	B	C	D	A	B	C	D	A	B	C	D	A	B	C	D
Tributary																				
1	2.07	0.24	0.13	0.62	0.58	0.60	0.01	0.98	0.04	0.64	0.29	0.76	0.45	0.86	0.10	0.32	0.01	0.76	0.07	0.67
2	0.60	0.21	0.46	0.67	0.58	1.03	0.27	0.52	3.09	0.28	0.84	2.45	0.17	1.69	0.81	0.47	0.62	0.39	0.04	0.81
3	1.01	0.54	0.71	0.77	0.28	0.55	0.83	0.59	0.47	0.38	0.36	0.73	0.19	0.85	2.16	0.68	0.58	0.44	0.02	0.53
4	0.37	2.42	0.54	1.02		0.79	0.99	0.41	1.00	0.88	0.77	0.68	0.40	1.89	0.83	0.50	0.08	0.38	0.70	0.70
5	0.56	0.52	0.77	0.51		0.46	0.86	0.60	0.62	1.14	0.42	1.29	1.14	0.83	1.19	3.13	0.38	0.03	0.79	0.83
6	0.72	0.70	0.49	0.76		0.31	0.72	0.57	0.43	0.54	0.67	0.52	0.56	0.53	1.07	0.34	0.24	0.07	0.69	0.62
7	0.68	0.38	0.68	0.73		0.81	0.68	0.66	0.57	0.70	0.87	0.54	0.48	0.70	2.71	0.69	0.24	0.63	0.53	0.42
8	2.94	0.81	0.24	0.96		0.37	0.51	0.26	0.70	0.68	0.81	0.69		0.71	0.51	0.60	0.47	0.26	0.53	0.52
9	1.11	0.49	0.58	0.50		0.61	0.58	0.48	0.45	0.29	0.74	0.69		0.41	0.59	0.57	0.48	0.47	0.70	0.41
10	0.38	0.82	0.23	0.75		0.31	0.66	0.45	0.40	0.76	0.88	0.24		1.12	0.65	1.32	0.43	0.21	0.44	0.31
11	0.23	0.37	1.31	0.55		0.45		0.37	0.59	0.35	1.01	0.53		0.60		1.43	0.43	0.29	0.46	0.50
12	0.61	1.55	0.38	0.37		0.51		0.71	0.18	0.55	0.89	0.73		0.50		0.45		0.40	0.52	0.16
13	0.34	0.58	0.34	0.59		0.59		0.54	0.43	0.25	0.58	0.10		0.56		0.60		0.32	0.68	0.39
14	0.49	0.18	0.26	0.51		0.30		0.68	0.53	0.60	0.62	0.39		0.50		0.65		0.15	0.54	0.52
15	0.39	0.23	0.54	0.59		0.44		0.46	0.41	0.38	0.64	0.40		0.71		0.68		0.15	1.05	0.45
16	0.45	0.74	0.71	0.67		0.52		0.33	0.34	0.55		0.64		0.57		0.59		0.49		0.50
17	0.65	1.11	0.45	0.31				0.51	0.40	0.61		0.57				0.40		0.39		0.48
18	0.44	0.15	1.96	0.76				0.29	0.58	0.64		0.65				0.15		0.34		0.66
19	0.59	0.25	1.23	0.83				0.34	0.60	0.58		0.63				0.47		0.53		0.51
20				0.41				0.34	0.47	0.62		0.79				0.40		0.50		0.57
21				0.45				0.16		0.65		1.79				0.29		0.41		0.51
22				0.42				0.48		0.57		1.48				0.30		0.27		0.41
23				0.32				0.49		0.65		0.45				0.36		0.28		0.24
24				0.52								0.72						0.45		0.61
25				0.46								0.60						0.54		0.50
26				0.50								0.67						0.43		0.19
27				0.27								0.67						0.47		0.08
28				0.24								0.63						0.50		0.40
29				0.38								0.62								0.40
30				0.34								0.43								0.66
31				0.32								0.14								0.54
32				0.29								0.46								0.43
33				0.30								0.61								0.64
34				0.19								0.37								0.41
35				0.33								0.68								0.17
36				0.45								0.45								0.27
37				0.32								0.37								0.41
38				0.44								0.38								0.20
39												0.49								0.20
40												0.32								0.30
41												0.18								0.34
42																				0.41
43																				0.38

Table 4.2.4.: Graident (m/m) of all tributaries (1^{st} order streams) (Study site A - D) during the investigation periods of this study

4.3. Quantitative analysis of post-seismic morphological responses in drainage basin by geomorphometric and hydraulic parameters.

4.3.1 Study site A

4.3.1.1. Watershed geometry

The results of quantitative analysis on watershed geometry in Study site A were indicated in Table 4.3.1 and Table 4.3.5-

4.3.1.1.1. Basin length (L_b) (m)

The Basin length (L_b) increased from 615.07 m to 616.26 m during Period 1 and then decreased to 608.57 m during Period 2 – 9. It indicates a fluctuating trend in Basin length (L_b) (m).

4.3.1.1.2. Basin area (A) (m^2)

Basin area (A) (m^2) decreased from 70637 m^2 to 70315 m^2 during Period 1and then further decreased to 69015 m^2 during Period 2 – 9. It indicated a decreasing trend in Basin area (A) (m^2).

4.3.1.1.3. Basin Perimeter (P) (m)

Basin Perimeter (P) (m) increased from 1913.58 m to 1944.57 m during Period 1and then increased to 2186.40 m during Period 2 – 9. It indicates an increasing trend in Basin Perimeter (P) (m).

4.3.1.1.4. Form factor (F_f)

Form factor (F_f) remained with the value of 0.19 during Period 1 and Period 2 – 9. It indicates a steady trend in Form factor (F_f).

4.3.1.1.5. Elongation ratio (R_e)

Elongation ratio (R_e) remained with the value of 0.49 during Period 1 and Period 2 – 9. It indicates a steady trend in Elongation ratio (R_e).

4.3.1.1.6. Circularity ratio (R_c)

Circularity ratio (R_c) decreased from 0.24 to 0.22 during Period 1 and then further decreased to 0.21 during Period 2 – 9. It indicates a decreasing trend in Circularity ratio (R_c).

4.3.1.1.7. Compactness coefficient (C_c)

Compactness coefficient (C_c) increased from 2.03 to 2.07 during Period 1 and then further increased to 2.15 during Period 2 – 9. It indicates an increasing trend in Compactness coefficient (C_c).

4.3.1.2 Drainage network

The results of quantitative analysis on drainage network in Study site A were indicated in Table 4.3.1and Table 4.3.6.

4.3.1.2.1. Length of mainstream channel (m)

Length of mainstream channel (m) increased from 586.42 m to 638.30 m during Period 1; decreased to 586.73 m during Period 2; decreased to 552.82 m during Period 3; increased to 574.64 m during Period 4: June 25, 2020 to September 14, 2020; increased to 616.26 m during Period 5; increased to 618.64 m during Period 6; increased to 618.94 during Period 7; decreased to 608.31 m during Period 8; and increased to 688.22 m during Period 9 (2 months). It indicates a general increasing trending in Length of mainstream channel (m).

4.3.1.2.2. Total length of tributaries (1st order stream) (m)

Total length of tributaries (1st order stream) (m) increased from 586.42 m to 14.40 m during Period 1; increased to 586.73 m during Period 2; decreased to 552.82 m during Period 3; decreased to 62.12 m during Period 4; increased to 820.37 m during Period 5); decreased to 320.07 m during Period 6; decreased to 132.05 m during Period 7; decreased to 692.96 m during Period 8; and increased to 205.81 m during Period 9. It indicates a general decreasing trend in Total length of tributaries (1st order stream) (m).

4.3.1.2.3. Stream order (U)

Stream order (U) increased from 1 to 2 during Period 1; decreased to 1 during Period 2; remained as 1 during Period 3; remained as 1 during Period 4; increased to 3 during Period 5 (1.5 months); decreased as 2 during Period 6; remained as 2 during Period 7; remained as 2 during Period 8; and increased to 3 during Period 9. It indicates a general increasing trend in Stream order (U).

4.3.1.2.4. Stream number (N_u)

Stream number (N_u) increased from 1 to 3 during Period 1; decreased to 1 during Period 2; remained as 1 during Period 3: April 23, 2020 to June 25, 2020 (2 months);

increased to 5 during Period 4; increased to 22 during Period 5; decreased to 4 during Period 6; increased to 21 during Period 7; decreased to 8 during Period 8; and increased to 14 during Period 9. It indicates a general increasing trend in Stream number (N_u).

4.3.1.2.5. Total stream length (L_u) (m)

Total stream length (L_u) (m) increased from 586.42 m to 638.30 m during Period 1; decreased to 586.73 m during Period 2; decreased to 552.82 m during Period 3; increased to 636.76 m during Period 4; increased to 1075.70 m during Period 5; increased to 1260.81 m during Period 6; decreased to 910.59 during Period 7; decreased to 692.96 m during Period 8; and increased to 865.98 m during Period 9. It indicates a general increasing trend in Total stream length (L_u) (m).

4.3.1.2.6. Mean stream length (L_m) (m)

Mean stream length (L_m) (m) increased from 586.42 m to 638.30 m during Period 1; decreased to 586.73 m during Period 2; decreased to 552.82 m during Period 3; decreased to 127.35 m during Period 4; increased to 358.57 m during Period 5; decreased to 315.20 m during Period 6; decreased to 43.36 during Period 7; increased to 86.62 m during Period 8; and decreased to 64.86 m during Period 9. It indicates a general decreasing trend in Mean stream length (L_m) (m).

4.3.1.2.7 Stream length ratio (R_L)

Stream length ratio (R_L) was 0.83 in Period 1; 9.5 and 81.08 in Period 5; 16.61 in Period 6; 39.90 in Period 7; 29.73 in Period 8; and 1.30 and 25.08 in Period 9. It indicates a general increasing trend in Stream length ratio (R_L).

4.3.1.2.8 Bifurcation ratio (R_b)

Bifurcation ratio (R_b) was 2 in Period 1; 4 in Period 4; 9.5 and 2 in Period 5; 3 in Period 6; 20 in Period 7; 7 in Period 8; and 5.5 and 2 in Period 9. It indicates a general increasing trend in Bifurcation ratio (R_b).

4.3.1.2.9 Gradient of mainstream (m/m)

Gradient of mainstream (m/m) decreased from 0.15 to 0.12 during Period 1; increased to 0.14 during Period 2; increased to 0.15 during Period 3; increased to 0.17 during Period 4; decreased to 0.15 during Period 5; decreased to 0.14 during Period 6; increased to 0.15 during Period 7; increased to 0.16 during Period 8; and decreased to 0.15 during Period 9. It indicates a general steady trend in Gradient of mainstream (m/m).

4.3.1.3 Drainage texture

The results of quantitative analysis on drainage texture in Study site A were indicated in Table 4.3.1and Table 4.3.7.

4.3.1.3.1 Stream frequency (F_s) (1/km^2)

Stream frequency (F_s) (1/km^2) increased from 14.16 to 42.67 during Period 1; decreased to 14.22 during Period 2; remained as 14.22 during Period 3; increased to 71.11 during Period 4; increased to 312.88 during Period 5; decreased to 56.89 during Period 6; increased to 298.66 during Period 7; decreased to 113.77 during Period 8; and increased to 202.85 during Period 9. It indicates a general increasing trend in Stream frequency (F_s) (1/km^2).

4.3.1.3.2 Drainage texture (D_t) (1/km)

Drainage texture (D_t) (1/km) increased from 0.52 to 1.54 during Period 1; decreased to 0.51 during Period 2; remained as 0.51 during Period 3; increased to 2.57 during Period 4); increased to11.31 during Period 5; decreased to 2.06 during Period 6; increased to 10.8 during Period 7; decreased to 4.11 during Period 8; and increased to 6.40 during Period 9. It indicates a general increasing trend in Drainage texture (D_t) (1/km)

4.3.1.3.3 Drainage density (D_d) (km/km^2)

Drainage density (D_d) (km/km^2) increased from 5.17 to 9.28 during Period 1; decreased to 8.34 during Period 2; decreased to 7.86 during Period 3; increased to 9.06 during Period 4; increased to 15.30 during Period 5; increased to 17.93 during Period 6; decreased to 12.95 during Period 7; decreased to 9.86 during Period 8; and increased to 12.55 during Period 9. It indicates a general increasing trend in Drainage density (D_d) (km/km^2)

4.3.1.3.4 Drainage intensity (D_i) (1/km)

Drainage intensity (D_i) (1/km) increased from 2.74 to 4.60 during Period 1; decreased to 1.71 during Period 2; increased to 1.81 during Period 3; increased to 7.85 during Period 4; increased to 20.45 during Period 5; decreased to 3.17 during Period 6; increased to 23.06 during Period 7; decreased to 11.54 during Period 8; and increased to 16.17 during Period 9. It indicates a general increasing trend in Drainage intensity (D_i) (1/km).

4.3.1.3.5 Infiltration number (I_f) ($1/10^6 \cdot m^3$)

Infiltration number (I_f) ($1/10^6 \cdot m^3$) increased from 73.21 to 396.00 during Period 1; increased to 118.59 during Period 2; decreased to 111.77 during Period 3; increased to 644.26 during Period 4; increased to 4786.50 during Period 5; decreased to 1020.03 during Period 6; increased to 3867.64 during Period 7; increased to 1121.25 during Period 8; and increased to 2545.32 during Period 9. It indicates a general increasing trend in Infiltration number (I_f) ($1/10^6 \cdot m^3$)

4.3.1.3.6 Length of overland flow (L_o) (m)

Length of overland flow (L_o) (m) decreased from 0.10 to 0.05 during Period 1; increased to 0.06 during Period 2; remained as 0.06 during Period 3: April 23, 2020 to June 25, 2020 (2 months); remained as 0.06 during Period 4; decreased to 0.03 during Period 5; remained as 0.03 during Period 6; increased to 0.04 during Period 7; increased to 0.05 during Period 8; and decreased to 0.04 during Period 9. It indicates a general decreasing trend in Length of overland flow (L_o) (m).

4.3.1.3.7 Constant of channel maintenance (C) (km^2/km)

Constant of channel maintenance (C) (km^2/km) decreased from 0.19 to 0.11 during Period 1; increased to 0.12 during Period 2; increased to 0.13 during Period 3; decreased to 0.11 during Period 4; decreased to 0.07 during Period 5; decreased to 0.06 during Period 6; increased to 0.08 during Period 7; increased to 0.10 during Period 8; and decreased to 0.08 during Period 9. It indicates a general decreasing trend in Constant of channel maintenance (C) (km^2/km).

4.3.1.4 Relief characteristics

The results of quantitative analysis on relief characteristics in Study site A were indicated in Table 4.3.1 and Table 4.3.8.

4.6.1.4.1 Height of basin outlet (Z_{min}) (m)

Height of basin outlet (Z_{min}) (m) increased from 88.03 m to 96.95 m during Period 1; increased to 102.41 m during Period 2; decreased to 97.17 m during Period 3; increased to 97.44 m during Period 4; increased to 97.49 m during Period 5; increased to 98.28 m during Period 6; decreased to 98.24 m during Period 7; decreased to 93.58 m during Period 8; and decreased to 90.40 m during Period 9. It indicates a general increasing trend in Height of basin outlet (Z_{min}) (m).

4.3.1.4.2 Maximum height of basin (Z_{max}) (m)

Maximum height of basin (Z_{max}) (m) decreased from 235.66 m to 235.26 m during Period 1; remained as 235.26 m during Period 2, Period 3, Period 4, Period 5, Period 6, Period 7, Period 8; and decreased to 235.12 m during Period 9. It indicates a general steady trend in Maximum height of basin (Z_{max}) (m).

4.3.1.4.3 Total basin relief (H) (m)

Total basin relief (H) (m) decreased from 147.63 m to 138.31 m during Period 1; decreased to 132.85 m during Period 2; increased to 138.09 m during Period 3; decreased to 137.32 m during Period 4; increased to 137.77 m during Period 5; decreased to 136.98 m during Period 6; increased to 137.02 m during Period 7; increased to 141.68 m during Period 8; and increased to 144.72 m during Period 9. It indicates a general decreasing trend in Total basin relief (H) (m).

4.3.1.4.4 Relief ratio (R_h)

Relief ratio (R_h) decreased from 0.24 to 0.22 during Period 1; remained as 0.22 during Period 2, Period 3: April 23, 2020 to June 25, 2020 (2 months), Period 4, Period 5, Period 6, Period 7, and increased to 0.23 during Period 8; and increased to 0.24 during Period 9. It indicates a general steady trend in Relief ratio (R_h).

4.3.1.4.5 Ruggedness number (R_n) (km/km^2)

Ruggedness number (R_n) (km/km^2) increased from 0.76 to 1.28 during Period 1; decreased to 1.11 during Period 2; increased to 1.28 during Period 3; decreased to 1.24 during Period 4; increased to 2.11 during Period 5; increased to 2.46 during Period 6; decreased to 1.77 during Period 7; decreased to 1.39 during Period 8; and increased to 1.82 during Period 9. It indicates a general increasing trend in Ruggedness number (R_n) (km/km^2).

4.3.1.4.6 Dissection index (D_{is})

Dissection index (D_{is}) decreased from 0.63 to 0.59 during Period 1; decreased to 0.56 during Period 2; increased to 0.59 during Period 3: April 23, 2020 to June 25, 2020 (2 months); decreased to 0.58 during Period 4; increased to 0.59 during Period 5; decreased to 0.58 during Period 6; remained as 0.58 during Period 7; increased to 0.60 during Period 8; and increased to 0.62 during Period 9. It indicates a general decreasing trend in Dissection index (D_{is}).

4.3.1.5 Hydraulic Parameters

The results of quantitative analysis on hydraulic parameters in Study site A were indicated in Table 4.3.1 and Table 4.3.9.

4.3.1.5.1 Hydraulic radius (*R*) (m)

Hydraulic radius (*R*) (m) remained as 0.05 m during Period 2 and Period 3; increased to 0.12 m during Period 4; decreased to 0.04 m during Period 6; increased to 0.05 m during Period 7; and decreased to 0.04 m during Period 8. It indicates a general decreasing trend in Hydraulic radius (*R*) (m).

4.3.1.5.2 Slope (10 m from stream head) (*S*) (tanø)

Slope (10 m from stream head) (*S*) (tanø) decreased from 0.48 (tanø) (Period 2); to 0.37 (tanø) (Period 3); increased to 0.45 (tanø) during Period 4; decreased to 0.43 (tanø) during Period 6); increased to 0.54 (tanø) during Period 7; and increased to 0.64 (tanø) during Period 8. It indicates a general increasing trend in Slope (10 m from stream head) (*S*) (tanø).

4.6.1.5.3 Shear stress (τ) (Nm^{-2})

Shear stress (τ) (Nm^{-2}) decreased from 243.06 (Nm^{-2}) (Period 2); to 184.16 (Nm^{-2}) (Period 3); increased to 544.28 (Nm^{-2}) during Period 4; decreased to 173.72 (Nm^{-2}) during Period 6; increased to 254.12 (Nm^{-2}) during Period 7; and decreased to 219.10 (Nm^{-2}) during Period 8. It indicates a general decreasing trend in Shear stress (τ) (Nm^{-2}).

4.3.1.5.4 Critical shear stress (τ_c) (Nm^{-2})

Critical shear stress (τ_c) (Nm^{-2}) decreased from 0.069 (Nm^{-2}) (Period 2); to 0.052 (Nm^{-2}) (Period 3); increased to 0.155 (Nm^{-2}) during Period 4; decreased to 0.050 (Nm^{-2}) during Period 6; increased to 0.072 (Nm^{-2}) during Period 7; and decreased to 0.062 (Nm^{-2}) during Period 8. It indicates a general decreasing trend in Critical shear stress (τ_c) (Nm^{-2}).

4.3.1.5.5 Velocity (v) (ms^{-1})

Velocity (v) (ms^{-1}) decreased from 0.011 (ms^{-1}) (Period 2; to 0.008 (ms^{-1}) (Period 3); increased to 0.057 (ms^{-1}) during Period 4; decreased to 0.006 (ms^{-1}) during Period 6; increased to 0.010 (ms^{-1}) during Period 7; and decreased to 0.007 (ms^{-1}) during Period 8. It indicates a general decreasing trend in Velocity (v) (ms^{-1}).

4.3.1.5.6 Peak specific discharge per unit rainfall intensity (k_p) (mm)

Peak specific discharge per unit rainfall intensity (k_p) (mm) increased from 1.39 mm (Period 2); to 1.87 mm (Period 3)); decreased to 1.76 mm (ms^{-1}) during Period 4; decreased to 0.50 mm during Period 6; increased to 0.59 mm during Period 7; and decreased to 0.06 mm during Period 8. It indicates a general decreasing trend in Peak specific discharge per unit rainfall intensity (k_p) (mm).

Study site A	Date	Oct 05, 2012	Sep 11, 2018	Apr 23, 2020	Jun 25, 2020	Sep 14, 2020	Oct 30, 2020	Apr 13, 2021	Jun 21, 2021	Aug 27, 2021	Oct 29, 2021
Geomorphometric parameters	Unit										
Watershed geometry											
Basin length (L_b)	m	615.07	616.26	–	–	–	–	–	–	–	608.57
Basin area (A)	m^2	70637	70315	–	–	–	–	–	–	–	69015
Basin Perimeter (P)	m	1913.58	1944.57	–	–	–	–	–	–	–	2186.4
Form factor (F_f)	–	0.19	0.19	–	–	–	–	–	–	–	0.19
Elongation ratio (R_e)	–	0.49	0.49	–	–	–	–	–	–	–	0.49
Circularity ratio (R_c)	–	0.24	0.22	–	–	–	–	–	–	–	0.21
Compactness coefficient (C_c)	–	2.03	2.07	–	–	–	–	–	–	–	2.15
Drainage network											
Length of mainstream channel	m	586.42	638.30	586.73	552.82	574.64	616.26	618.64	618.94	608.31	688.22
Total length of tributaries (1st order stream)	m	586.42	14.4	586.73	552.82	62.12	399.83	820.37	320.07	132.05	205.81
Stream order (U)	–	1	2	1	1	1	3	2	2	2	3
Stream number (N_u)	–	1	3	1	1	5	22	4	21	8	14
Total stream length (L_u)	m	586.42	638.30	586.73	552.82	636.76	1075.70	1260.81	910.59	692.96	865.98
Mean stream length (L_m)	m	586.42	638.30	586.73	552.82	127.35	358.57	315.20	43.36	86.62	61.86
Stream length ratio (R_L)	–	–	8.03	–	–	–	9.5, 81.08	1.61	36.90	29.73	1.30, 25.08
Bifurcation ratio (R_b)	–	–	2	–	–	4	9.5, 2	3	20	7	5.5, 2
Gradient of mainstream	m/m	0.15	0.12	0.14	0.15	0.17	0.15	0.14	0.15	0.16	0.15
Drainage texture											
Stream frequency (F_s)	$1/km^2$	14.16	42.67	14.22	14.22	71.11	312.88	56.89	298.66	113.77	202.85
Drainage texture (D_t)	1/km	0.52	1.54	0.51	0.51	2.57	11.31	2.06	10.80	4.11	6.40
Drainage density (D_d)	km/km^2	5.17	9.28	8.34	7.86	9.06	15.30	17.93	12.95	9.86	12.55
Drainage intensity (D_i)	1/km	2.74	4.60	1.71	1.81	7.85	20.45	3.17	23.06	11.54	16.17
Infiltration number (I_f)	–	73.21	396.00	118.59	111.77	644.26	4786.50	1020.03	3867.64	1121.25	2545.32
Length of overland flow (L_o)	km	0.10	0.05	0.06	0.06	0.06	0.03	0.03	0.04	0.05	0.04
Constant of channel maintenance (C)	km^2/km	0.19	0.11	0.12	0.13	0.11	0.07	0.06	0.08	0.10	0.08
Relief characteristics											
Height of basin outlet (Z_{min})	m	88.03	96.95	102.41	97.17	97.44	97.49	98.28	98.24	93.58	90.40
Maximum height of basin (Z_{max})	m	235.66	235.26	235.26	235.26	235.26	235.26	235.26	235.26	235.26	235.12
Total basin relief (H)	m	147.63	138.31	132.85	138.09	137.32	137.77	136.98	137.02	141.68	144.72
Relief ratio (R_h)	–	0.24	0.22	0.22	0.22	0.22	0.22	0.22	0.22	0.23	0.24
Ruggedness number (R_n)	km/km^2	0.76	1.28	1.11	1.28	1.24	2.11	2.46	1.77	1.39	1.82
Dissection index (D_{is})		0.63	0.59	0.56	0.59	0.58	0.59	0.58	0.58	0.60	0.62
Hydraulic Parameters											
Hydraulic radius (R)	m	–	–	0.05	0.05	0.12	–	0.04	0.05	0.04	–
Slope (10 m from stream head) (S)	tanø	–	–	0.48	0.37	0.45	–	0.43	0.54	0.64	–
Shear stress (τ)	Nm^{-2}	–	–	243.06	184.16	544.28	–	173.72	254.12	219.1	–
Critical shear stress (τ_c)	Nm^{-2}	–	–	0.069	0.052	0.155	–	0.050	0.072	0.062	–
Velocity (v)	$m\,s^{-1}$	–	–	0.011	0.008	0.057	–	0.006	0.010	0.007	–
Peak specific discharge per unit rainfall intensity (k_p)	mm	–	–	1.39	1.87	1.76	–	0.50	0.59	0.06	–

Table 4.3.1: Study site A: Results of quantitative analysis of post-seismic drainage basin characteristics by geomorphometric and hydraulic parameters during investigation periods.

4.3.2 Study site B

4.3.2.1 Watershed geometry

The results of quantitative analysis on watershed geometry in Study site B were indicated in Table 4.3.2 and Table 4.3.5.

4.3.2.1.1 Basin length (*L_b*) (m)

The Basin length (L_b) increased from 564.13 m to 576.73 m during Period 1 and then decreased to 578.64 m during Period 2 – 9. It indicates a general increasing trend in Basin length (L_b) (m).

4.3.2.1.2 Basin area (*A*) (m^2)

Basin area (A) (m^2) decreased from 103942 m^2 to 104006 m^2 during Period 1 and then further decreased to 103968 m^2 during Period 2 – 9. It indicates a general increasing trend in Basin area (A) (m^2)

4.3.2.1.3 Basin Perimeter (*P*) (m)

Basin Perimeter (P) (m) increased from 1393.90 m to 1433.99 m during Period 1 and then increased to 1413.23 m during Period 2 – 9. It indicates a general increasing trend in Basin Perimeter (P) (m).

4.3.2.1.4 Form factor (*F_f*)

Form factor (F_f) decreased from 0.33 to 0.31 during Period 1 and remained as 0.31 during Period 2 – 9. It indicates a general decreasing trend in Form factor (F_f).

4.3.2.1.5 Elongation ratio (*R_e*)

Elongation ratio (R_e) decreased from 0.65 to 0.63 during Period 1 and remained as 0.63 during Period 2 – 9. It indicates a general decreasing trend in Elongation ratio (R_e).

4.3.2.1.6 Circularity ratio (*R_c*)

Circularity ratio (R_c) decreased from 0.67 to 0.64 during Period 1 and then remained as 0.64 during Period 2 – 9. It indicates a general decreasing trend in Circularity ratio (R_c).

4.3.2.1.7 Compactness coefficient (*C_c*)

Compactness coefficient (C_c) increased from 1.22 to 1.25 during Period 1 and then remained as 1.25 during Period 2 – 9. It indicates a general increasing trend in Compactness coefficient (C_c).

4.3.2.2 Drainage network

The results of quantitative analysis on drainage network in Study site B were indicated in Table 4.3.2 and Table 4.3.6.

4.3.2.2.1 Length of mainstream channel (m)

Length of mainstream channel (m) increased from 577.56 m to 653.85 m during Period 1; decreased to 516.02 m during Period 2; decreased to 498.21 m during Period 3; increased to 564.86 m during Period 4; increased to 594.99 m during Period 5; decreased to 566.69 m during Period 6; increased to 618.52 during Period 7; decreased to 612.19 m during Period 8; and increased to 685.72 m during Period 9. It indicates a general increasing trend in Length of mainstream channel (m).

4.3.2.2.2 Total length of tributaries (1st order stream) (m)

Total length of tributaries (1st order stream) (m) increased from 269.91 m to 319.81 m during Period 1; decreased to 310.52 m during Period 2; decreased to 149.35 m during Period 3; increased to 632.91 m during Period 4; decreased to 547.15 m during Period 5; decreased to 438.63 m during Period 6; increased to 766.4 m during Period 7; decreased to 558.14 m during Period 8; and increased to 876.00 m during Period 9. It indicates a general increasing trend in Total length of tributaries (1st order stream) (m).

4.3.2.2.3 Stream order (U)

Stream order (U) was 2 during Period 1; remained as 2 during Period 2 and Period 3; increased to 3 during Period 4; decreased to 2 during Period 5; increased to 3 during Period 6; remained as 3 during Period 7; decreased to 2 during Period 8; and increased to 3 during Period 9. It indicates a general increasing trend in Stream order (U).

4.3.2.2.4 Stream number (N_u)

Stream number (N_u) increased from 6 to 11 during Period 1; decreased to 9 during Period 2; decreased to 8 during Period 3; increased to 22 during Period 4; decreased to 20 during Period 5; decreased to 19 during Period 6; increased to 26 during Period 7; decreased to 17 during Period 8; and increased to 34 during Period 9. It indicates a general increasing trend in Stream number (N_u).

4.3.2.2.5 Total stream length (L_u) (m)

Total stream length (L_u) (m) increased from 721.28 m to 923.93 m during Period 1; decreased to 753.85 m during Period 2; decreased to 694.26 m during Period 3; increased to 1121.88 m during Period 4; decreased to 1199.59 m during Period 5; decreased to 1039.93 m during Period 6; increased to 1358.44 m during Period 7; decreased to 1132.79 m during Period 8; and increased to 1663.27 m during Period 9. It indicates a general increasing trend in Total stream length (L_u) (m).

4.3.2.2.6 Mean stream length (**L_m**) (m)

Mean stream length (L_m) (m) decreased from 120.21 m to 84.81 m during Period 1; decreased to 83.76 m during Period 2 increased to 86.78 m during Period 3; decreased to 50.99 m during Period 4; increased to 59.98 m during Period 5; decreased to 54.73 m during Period 6; decreased to 52.25 during Period 7; increased to 66.63 m during Period 8; and decreased to 48.92 m during Period 9. It indicates a general decreasing trend in Mean stream length (L_m) (m).

4.3.2.2.7 Stream length ratio (**R_L**)

Stream length ratio (R_L) increased from 8.36 to 19.17 in Period 1; 11.42 during Period 2; 7.70 during Period 3; 1.55 and 8.41 during Period 4; 22.36 during Period 5; 6.83 and 1.21 in Period 6; 1.60 and 9.11 during Period 7; 16.47 during Period 8; and 1.52 and 11.57 during Period 9. It indicates a general increasing trend in Stream length ratio (R_L).

4.3.2.2.8 Bifurcation ratio (**R_b**)

Bifurcation ratio (R_b) increased from 5 to 10 in Period 1; 8 during Period 2; 7 during Period 3: April 23, 2020 to June 25, 2020 (2 months); 9.5 and 2 during Period 4; 19 during Period 5; 8 and 2 in Period 6; 11.5 and 2 during Period 7; 16 during Period 8; and 5.6 and 5 during Period 9. It indicates a general increasing trend in Bifurcation ratio (R_b).

4.3.2.2.9 Gradient of mainstream (m/m)

Gradient of mainstream (m/m) decreased from 0.17 to 0.12 during Period 1; increased to 0.15 during Period 2; increased to 0.17 during Period 3; increased to 0.21 during Period 4; decreased to 0.14 during Period 5; increased to 0.18 during Period 6; increased to 0.20 during Period 7; decreased to 0.19 during Period 8; and decreased to 0.12 during Period 9. It indicates a general decreasing trend in Gradient of mainstream (m/m).

4.3.2.3 Drainage texture

The results of quantitative analysis on drainage texture in Study site B were indicated in Table 4.3.2 and Table 4.3.7.

4.3.2.3.1 Stream frequency (**F_s**) (1/km^2)

Stream frequency (F_s) (1/km^2) increased from 57.72 to 105.76 during Period 1; decreased to 86.53 during Period 2: September 11, 2018 to April 23, 2020 (approximately 1.5 years); decreased to 76.92 during Period 3; increased to 211.53 during Period 4;

decreased to 192.30 during Period 5; decreased to 182.68 during Period 6; increased to 249.99 during Period 7; decreased to 163.45 during Period 8; and increased to 327.02 during Period 9. It indicates a general increasing trend in Stream frequency (F_s) (1/km^2).

4.3.2.3.2 Drainage texture (D_t) (1/km)

Drainage texture (D_t) (1/km) increased from 4.30 to 7.67 during Period 1; decreased to 6.28 during Period 2; decreased to 5.58 during Period 3; increased to 15.34 during Period 4; decreased to13.95 during Period 5; decreased to 13.25 during Period 6; increased to 18.13 during Period 7; decreased to 11.86 during Period 8; and increased to 23.75 during Period 9. It indicates a general increasing trend in Drainage texture (D_t) (1/km).

4.3.2.3.3 Drainage density (D_d) (km/km^2)

Drainage density (D_d) (km/km^2) increased from 6.94 to 8.97 during Period 1; decreased to 7.25 during Period 2; decreased to 6.68 during Period 3; increased to 10.79 during Period 4; increased to 11.53 during Period 5; decreased to 10.00 during Period 6; increased to 13.06 during Period 7; decreased to 10.89 during Period 8; and increased to 16.00 during Period 9. It indicates a general increasing trend in Drainage density (D_d) (km/km^2).

4.3.2.3.4 Drainage intensity (D_i) (1/km)

Drainage intensity (D_i) (1/km) increased from 8.32 to 11.79 during Period 1; increased to 11.94 during Period 2; decreased to 11.52 during Period 3; increased to 19.61 during Period 4; decreased to 16.67 during Period 5; increased to 18.27 during Period 6; increased to 19.14 during Period 7; decreased to 15.01 during Period 8; and increased to 20.44 during Period 9. It indicates a general increasing trend in Drainage intensity (D_i) (1/km).

4.3.2.3.5 Infiltration number (I_f) (1/10^6·m^3)

Infiltration number (I_f) (1/10^6·m^3) increased from 400.57 to 948.69 during Period 1; decreased to 627.21 during Period 2; decreased to 513.46 during Period 3; increased to 2281.67 during Period 4; decreased to 2217.92during Period 5; decreased to 1826.59 during Period 6; increased to 3265.10 during Period 7; decreased to 1780.25 during Period 8; and increased to 5231.69 during Period 9. It indicates a general increasing trend in Infiltration number (I_f) (1/10^6·m^3).

4.3.2.3.6 Length of overland flow (L_o) (m)

Length of overland flow (L_o) (m) decreased from 0.07 to 0.06 during Period 1; remained as 0.07 during Period 2; remained as 0.07 during Period 3; decreased to 0.05 during Period 4; decreased to 0.04 during Period 5; increased to 0.05 during Period 6; decreased to 0.04 during Period 7; increased to 0.05 during Period 8; and decreased to 0.03 during Period 9. It indicates a general decreasing trend in Length of overland flow (L_o) (m).

4.3.2.3.7 Constant of channel maintenance (*C*) (km^2/km)

Constant of channel maintenance (*C*) (km^2/km) decreased from 0.14 to 0.11 during Period 1; increased to 0.14 during Period 2; increased to 0.15 during Period 3; decreased to 0.09 during Period 4; remained as 0.09 during Period 5; increased to 0.10 during Period 6; decreased to 0.08 during Period 7; increased to 0.09 during Period 8; and decreased to 0.06 during Period 9. It indicates a general decreasing trend in Constant of channel maintenance (*C*) (km^2/km).

4.3.2.4 Relief characteristics

The results of quantitative analysis on relief characteristicss in Study site B were indicated in Table 4.6.2 and Table 4.3.8.

4.3.2.4.1 Height of basin outlet (Z_{min}) (m)

Height of basin outlet (Z_{min}) (m) decreased from 97.75 m to 85.70 m during Period 1; increased to 108.86 m during Period 2; increased to 111.62 m during Period 3; decreased to 108.77 m during Period 4; increased to 110.07 m during Period 5; decreased to 104.51 m during Period 6; increased to 104.74 m during Period 7; decreased to 102.48 m during Period 8; and increased to 104.26 m during Period 9. It indicates a general increasing trend in Height of basin outlet (Z_{min}) (m).

4.3.2.4.2 Maximum height of basin (Z_{max}) (m)

Maximum height of basin (Z_{max}) (m) decreased from 267.53 m to 267.34 m during Period 1; remained as 267.34 m during Period 2, Period 3, Period 4, Period 5, Period 6, Period 7, Period 8; and decreased to 266.79 m during Period 9. It indicates a general steady trend in Maximum height of basin (Z_{max}) (m).

4.3.2.4.3 Total basin relief (*H*) (m)

Total basin relief (*H*) (m) increased from 169.78m to 181.64 m during Period 1; decreased to 158.48 m during Period 2; decreased to 158.19 m during Period 3; increased to 158.57 m during Period 4; decreased to 157.27 m during Period 5; increased to 162.83 m during Period 6; decreased to 162.60 m during Period 7; increased to 164.84 m during Period 8; and decreased to 162.53 m during Period 9. It indicates a general decreasing trend in Total basin relief (*H*) (m).

4.3.2.4.4 Relief ratio (R_h)

Relief ratio (R_h) increased from 0.30 to 0.31 during Period 1; decreased to 0.27 during Period 2, and remained as 0.27 Period 3, Period 4, Period 5; increased to 0.28 during Period 6 and Period 7), and increased to 0.29 during Period 8; and decreased to 0.28 during Period 9. It indicates a general decreasing trend in Relief ratio (R_h).

4.3.2.4.5 Ruggedness number (R_n) (km/km^2)

Ruggedness number (R_n) (km/km^2) increased from 1.18 to 1.63 during Period 1; decreased to 1.15 during Period 2; decreased to 1.06 during Period 3; increased to 1.71 during Period 4; increased to 1.81 during Period 5; decreased to 1.63 during Period 6; increased to 2.21 during Period 7; decreased to 1.80 during Period 8; and increased to 2.60 during Period 9. It indicates a general increasing trend in Ruggedness number (R_n) (km/km^2).

4.3.2.4.6 Dissection index (D_{is})

Dissection index (D_{is}) increased from 0.63 to 0.68 during Period 1; decreased to 0.59 during Period 2; Period 3; Period 4; Period 5; increased to 0.61 during Period 6; remained as 0.61 during Period 7; increased to 0.62 during Period 8; and decreased to 0.61 during Period 9. It indicates a general decreasing trend in Dissection index (D_{is}).

4.3.2.5 Hydraulic Parameters

The results of quantitative analysis on hydraulic parameters in Study site B were indicated in Table 4.3.2 and Table 4.3.9.

4.3.2.5.1 Hydraulic radius (*R*) (m)

Hydraulic radius (*R*) (m) increased from 0.05 m during Period 2 to 0.08 during Period 3; increased to 0.10 m during Period 4; decreased to 0.06 m during Period 6; increased to 0.12 m during Period 7; and decreased to 0.03 m during Period 8. It indicates a general decreasing trend in Hydraulic radius (*R*) (m).

4.3.2.5.2 Slope (10 m from stream head) (*S*) (tanø)

Slope (10 m from stream head) (*S*) (tanø) increased from 0.63 (tanø) (Period 2; to 0.77 (tanø) (Period 3); remained as 0.77 (tanø) during Period 4; decreased to 0.61 (tanø) during Period 6; increased to 0.76 (tanø) during Period 7; and increased to 0.82 (tanø) during Period 8. It indicates a general increasing trend in Slope (10 m from stream head) (*S*) (tanø).

4.3.2.5.3 Shear stress (τ) (Nm^{-2})

Shear stress (τ) (Nm^{-2}) increased from 296.47 (Nm^{-2}) (Period 2; to 616.08 (Nm^{-2}) (Period 3); increased to 771.49 (Nm^{-2}) during Period 4; decreased to 331.43 (Nm^{-2}) during Period 6; increased to 908.66 (Nm^{-2}) during Period 7; and decreased to 249.85 (Nm^{-2}) during Period 8. It indicates a general decreasing trend in Shear stress (τ) (Nm^{-2}).

4.3.2.5.4 Critical shear stress (τ_c) (Nm^{-2})

Critical shear stress (τ_c) (Nm^{-2}) increased from 0.084 (Nm^{-2}) (Period 2); to 0.176 (Nm^{-2}) (Period 3); increased to 0.220 (Nm^{-2}) during Period 4; decreased to 0.094 (Nm^{-2}) during Period 6; increased to 0.259 (Nm^{-2}) during Period 7; and decreased to 0.071 (Nm^{-2}) during Period 8. It indicates a general decreasing trend in Critical shear stress (τ_c) (Nm^{-2}).

4.3.2.5.5 Velocity (v) (ms^{-1})

Velocity (v) (ms^{-1}) increased from 0.012 (ms^{-1}) (Period 2); to 0.042 (ms^{-1}) (Period 3); increased to 0.067 (ms^{-1}) during Period 4; decreased to 0.016 (ms^{-1}) during Period 6; increased to 0.095 (ms^{-1}) during Period 7; and decreased to 0.007 (ms^{-1}) during Period 8. It indicates a general decreasing trend in Velocity (v) (ms^{-1}).

4.3.2.5.6 Peak specific discharge per unit rainfall intensity (k_p) (mm)

Peak specific discharge per unit rainfall intensity (k_p) (mm) increased from 5.45 mm (Period 2); to 11.71 mm (Period 3); decreased to 1.86 mm (ms^{-1}) during Period 4; decreased to 0.94 mm during Period 6; increased to 4.53 mm during Period 7; and decreased to 0.01 mm during Period 8. It indicates a general decreasing trend in Peak specific discharge per unit rainfall intensity (k_p) (mm).

Study site B	Date	Oct 05, 2012	Sep 11, 2018	Apr 23, 2020	Jun 25, 2020	Sep 14, 2020	Oct 30, 2020	Apr 13, 2021	Jun 21, 2021	Aug 27, 2021	Oct 29, 2021
Geomorphometric parameters	Unit										
Watershed geometry											
Basin length (L_b)	m	564.13	576.73	–	–	–	–	–	–	–	578.64
Basin area (A)	m^2	103942	104006	–	–	–	–	–	–	–	103968
Basin Perimeter (P)	m	1393.90	1433.99	–	–	–	–	–	–	–	1415.23
Form factor (F_f)	–	0.33	0.31	–	–	–	–	–	–	–	0.31
Elongation ratio (R_e)	–	0.65	0.63	–	–	–	–	–	–	–	0.63
Circularity ratio (R_c)	–	0.67	0.64	–	–	–	–	–	–	–	0.64
Compactness coefficient (C_c)	–	1.22	1.25	–	–	–	–	–	–	–	1.25
Drainage network											
Length of mainstream channel	m	577.56	653.85	516.02	498.21	564.86	594.99	556.69	618.52	612.19	685.72
Total length of tributaries (1st order stream)	m	269.91	319.81	310.52	149.35	632.91	547.15	438.63	766.44	558.14	876.00
Stream order (U)	–	2	2	2	2	3	2	3	3	2	3
Stream number (N_u)	–	6	11	9	8	22	20	19	26	17	34
Total stream length (L_u)	m	721.28	923.93	753.85	694.26	1121.88	1199.59	1039.93	1358.44	1132.79	1663.27
Mean stream length (L_m)	m	120.21	84.81	83.76	86.78	50.99	59.98	54.73	52.25	66.63	48.92
Stream length ratio (R_L)	–	8.36	19.17	11.42	7.70	1.55, 8.41	22.36	6.83, 1.21	1.60, 9.11	16.47	1.52, 11.57
Bifurcation ratio (R_b)	–	5	10	8	7	9.5, 2	19	8, 2	11.5, 2	16	5.6, 5
Gradient of mainstream	m/m	0.17	0.12	0.15	0.17	0.21	0.14	0.18	0.20	0.19	0.12
Drainage texture											
Stream frequency (F_s)	$1/km^2$	57.72	105.76	86.53	76.92	211.53	192.30	182.68	249.99	163.45	327.02
Drainage texture (D_t)	1/km	4.30	7.67	6.28	5.58	15.34	13.95	13.25	18.13	11.86	23.75
Drainage density (D_d)	km/km^2	6.94	8.97	7.25	6.68	10.79	11.53	10.00	13.06	10.89	16.00
Drainage intensity (D_i)	1/km	8.32	11.79	11.94	11.52	19.61	16.67	18.27	19.14	15.01	20.44
Infiltration number (I_f)	–	400.57	948.69	627.21	513.46	2281.67	2217.92	1826.59	3265.10	1780.25	5231.69
Length of overland flow (L_o)	km	0.07	0.06	0.07	0.07	0.05	0.04	0.05	0.04	0.05	0.03
Constant of channel maintenance (C)	km^2/km	0.14	0.11	0.14	0.15	0.09	0.09	0.10	0.08	0.09	0.06
Relief characteristics											
Height of basin outlet (Z_{min})	m	97.75	85.70	108.86	111.62	108.77	110.07	104.51	104.74	102.48	104.26
Maximum height of basin (Z_{max})	m	267.53	267.34	267.34	267.34	267.34	267.34	267.34	267.34	267.34	266.79
Total basin relief (H)	m	169.78	181.64	158.48	158.19	158.57	157.27	162.83	162.60	164.86	162.53
Relief ratio (R_h)	–	0.30	0.31	0.27	0.27	0.27	0.27	0.28	0.28	0.29	0.28
Ruggedness number (R_n)	km/km^2	1.18	1.63	1.15	1.06	1.71	1.81	1.63	2.12	1.80	2.60
Dissection index (D_{is})		0.63	0.68	0.59	0.59	0.59	0.59	0.61	0.61	0.62	0.61
Hydraulic Parameters											
Hydraulic radius (R)	m	–	–	0.05	0.08	0.10	–	0.06	0.12	0.03	–
Slope (10 m from stream head) (S)	tanø	–	–	0.63	0.77	0.77	–	0.61	0.76	0.82	–
Shear stress (τ)	Nm^{-2}	–	–	296.47	616.08	771.49	–	331.43	908.66	249.85	–
Critical shear stress (τ_c)	Nm^{-2}	–	–	0.084	0.176	0.220	–	0.094	0.259	0.071	–
Velocity (v)	$m\,s^{-1}$	–	–	0.012	0.042	0.067	–	0.016	0.095	0.007	–
Peak specific discharge			–								
per unit rainfall intensity (k_p)	mm	–	–	5.45	11.71	1.86	–	0.94	4.53	0.01	–

Table 4.3.2: Study site B: Results of quantitative analysis of post-seismic drainage basin characteristics by 35 geomorphometric and hydraulic parameters during investigation periods.

4.3.3 Study site C

The results of quantitative analysis on watershed geometry in Study site C were indicated in Table 4.3.3 and Table 4.3.5. .

4.3.3.1 Watershed geometry

4.3.3.1.1 Basin length (L_b) (m)

The Basin length (L_b) decreased from 614.24 m to 616.87 m during Period and then decreased to 605.28 m during Period 2 – 9. It indicates a general decreasing trend in The Basin length (L_b).

4.3.3.1.2 Basin area (A) (m^2)

Basin area (A) (m^2) decreased from 88989 m^2 to 87639 m^2 during Period 1 and then further decreased to 82264 m^2 during Period 2 – 9. It indicates a general decreasing trend in Basin area (A) (m^2).

4.3.3.1.3 Basin Perimeter (*P*) (m)

Basin Perimeter (P) (m) decreased from 2011.55 m to 1433.99 m during Period 1 and then increased to 2298.40 m during Period 2 – 9. It indicates a general increasing trend in Basin Perimeter (P) (m).

4.3.3.1.4 Form factor (F_f)

Form factor (F_f) decreased from 0.22 to 0.21 during Period 1 and increased to 0.22 during Period 2 – 9. It indicates a general steady trend in Form factor (F_f).

4.3.3.1.5 Elongation ratio (R_e)

Elongation ratio (R_e) remained as 0.52 during Period 1 and increased to 0.53 during Period 2 – 9. It indicates a general increasing trend in Elongation ratio (R_e).

4.3.3.1.6 Circularity ratio (R_c)

Circularity ratio (R_c) increased from 0.24 to 0.25 during Period 1 and then decreased to 0.20 during Period 2 – 9. It indicates a general decreasing trend in Circularity ratio (R_c).

4.3.3.1.7 Compactness coefficient (C_c)

Compactness coefficient (C_c) decreased from 2.04 to 1.99 during Period 1 and then increased to 2.26 during Period 2 – 9. It indicates a general increasing trend in Compactness coefficient (C_c).

4.3.3.2 Drainage network

The results of quantitative analysis on drainage network in Study site C were indicated in Table 4.3.3 and Table 4.3.6. .

4.3.3.2.1 Length of mainstream channel (m)

Length of mainstream channel (m) increased from 659.35 m to 666.27 m during Period 1; increased to 767.82 m during Period 2; decreased to 626.07 m during Period 3; decreased to 625.30 m during Period 4; decreased to 594.99 m during Period 5; increased to 689.63 m during Period 6; increased to 815.55 during Period 7; decreased to 753.76 m during Period 8; and increased to 841.15 m during Period 9. It indicates a general increasing trend in Length of mainstream channel (m).

4.3.3.2.2 Total length of tributaries (1st order stream) (m)

Total length of tributaries (1st order stream) (m) decreased from 659.35 m to 70.09 m during Period 1; increased to 320.84 m during Period 2; decreased to 206.60 m during Period 3; increased to 223.58 m during Period 4; increased to 547.15 m during Period 5; decreased to 385.04 m during Period 6; increased to 411.34 m during Period 7; decreased to 30.68 m during Period 8; and increased to 323.75 m during Period 9. It indicates a general decreasing trend in Total length of tributaries (1st order stream) (m).

4.3.3.2.3 Stream order (U)

Stream order (U) increased from 1 to 2 during Period 1; remained as 2 during Period 2; Period 3; Period 4; Period 5; Period 6; Period 7; increased to 3 during Period 8; and Period 9. It indicates a general increasing trend in Stream order (U).

4.3.3.2.4 Stream number (N_u)

Stream number (N_u) increased from 1 to 4 during Period 1 increased to 12 during Period 2; decreased to 7 during Period 3; increased to 11 during Period 4; increased to 20 during Period 5; decreased to 11 during Period 6; increased to 16 during Period 7; decreased to 11 during Period 8; and increased to 19 during Period 9. It indicates a general increasing trend in Stream number (N_u).

4.3.3.2.5 Total stream length (L_u) (m)

Total stream length (L_u) (m) increased from 659.35 m to 707.93 m during Period 1; increased to 767.82 m during Period 2; decreased to 764.83 m during Period 3; increased to 769.81 m during Period 4; increased to 1199.59 m during Period 5; decreased to 999.83 m during Period 6; increased to 1146.07 m during Period 7; decreased to 1003.40 m during Period 8; and increased to 1207.69 m during Period 9. It indicates a general increasing trend in Total stream length (L_u) (m).

4.3.3.2.6 Mean stream length (L_m) (m)

Mean stream length (L_m) (m) decreased from 659.35 m to 176.98 m during Period 1; decreased to 63.99 m during Period 2; increased to 109.26 m during Period 3; decreased to 69.98 m during Period 4; decreased to 59.98 m during Period 5; increased to 90.89 m during Period 6; decreased to 71.63 during Period 7; increased to 91.22 m during Period 8; and decreased to 63.56 m during Period 9. It indicates a general decreasing trend in Mean stream length (L_m) (m).

4.3.3.2.7 Stream length ratio (R_L)

Stream length ratio (R_L) was 27.30 in Period 1; 24.21 during Period 2; 16.21 during Period 3; 24.43 during Period 4; 22.36 during Period 5; 15.97 in Period 6; 26.79 during Period 7; 67.18 and 8.37 during Period 8; and 37.99 and 20.27 during Period 9. It indicates a general increasing trend in Stream length ratio (R_L).

4.3.3.2.8 Bifurcation ratio (R_b)

Bifurcation ratio (R_b) was 3 in Period 1; 11 during Period 2; 6 during Period 3; 10 during Period 4; 19 during Period 5; 10 in Period 6; 15 during Period 7; 5 and 2 during Period 8; and 5 and 3 during Period 9. It indicates a general increasing trend in Bifurcation ratio (R_b).

4.3.3.2.9 Gradient of mainstream (m/m)

Gradient of mainstream (m/m) decreased from 0.13 during Period 1; remained as 0.13 during Period 2; increased to 0.17 during Period 3; increased to 0.19 during Period 4; decreased to 0.14 during Period 5; increased to 0.17 during Period 6; decreased to 0.15 during Period 7; remained as 0.15 during Period 8; and decreased to 0.14 during Period 9. It indicates a general decreasing trend in Gradient of mainstream (m/m).

4.3.3.3 Drainage texture

The results of quantitative analysis on drainage texture in Study site C were indicated in Table 4.3.3 and Table 4.3.7.

4.3.3.3.1 Stream frequency (F_s) (1/km^2)

Stream frequency (F_s) (1/km^2) increased from 11.24 to 49.00 during Period 1; increased to 146.99 during Period 2; decreased to 85.74 during Period 3; decreased to 13.47 during Period 4; increased to 24.50 during Period 5; increased to 134.74 during Period 6; increased to 195.98 during Period 7; decreased to 134.74 during Period 8; and increased to 230.96 during Period 9. It indicates a general increasing in Stream frequency (F_s) (1/km^2).

4.3.3.3.2 Drainage texture (D_t) (1/km)

Drainage texture (D_t) (1/km) increased from 0.46 to 1.99 during Period 1; increased to 5.96 during Period 2; decreased to 3.48 during Period 3; increased to 24.68 during Period 4; decreased to 19.43 during Period 5; decreased to 5.47 during Period 6; increased to 7.95 during Period 7; decreased to 5.47 during Period 8; and increased to 8.27 during Period 9. It indicates a general increasing trend in Drainage texture (D_t) (1/km).

4.3.3.3.3 Drainage density (D_d) (km/km^2)

Drainage density (D_d) (km/km^2) increased from 7.41 to 8.67 during Period 1; increased to 9.41 during Period 2; decreased to 9.37 during Period 3; decreased to 0.94 during Period 4; increased to 1.47 during Period 5; increased to 12.25 during Period 6; increased to 14.04 during Period 7; decreased to 12.29 during Period 8; and increased to 14.68 during Period 9. It indicates a general increasing trend in Drainage density (D_d) (km/km^2).

4.3.3.3.4 Drainage intensity (D_i) (1/km)

Drainage intensity (D_i) (1/km) increased from 1.52 to 5.65 during Period 1; increased to 15.63 during Period 2; decreased to 9.15 during Period 3; increased to 14.29 during Period 4; increased to 16.67 during Period 5; decreased to 11.00 during Period 6; increased to 13.96 during Period 7); decreased to 10.96 during Period 8; and increased to 15.73 during Period 9. It indicates a general increasing trend in Drainage intensity (D_i) (1/km).

4.3.3.3.5 Infiltration number (I_f) ($1/10^6 \cdot m^3$)

Infiltration number (I_f) ($1/10^6 \cdot m^3$) increased from 83.26 to 424.87 during Period 1; increased to 1382.44 during Period 2; decreased to 803.28 during Period 3; increased to 2273.23 during Period 4; increased to 23574.14 during Period 5; decreased to 1650.15 during Period 6; increased to 2751.29 during Period 7; decreased to 1656.04 during Period 8); and increased to 3390.63 during Period 9. It indicates a general increasing trend in Infiltration number (I_f) ($1/10^6 \cdot m^3$).

4.3.3.3.6 Length of overland flow (L_o) (m)

Length of overland flow (L_o) (m) decreased from 0.07 to 0.06 during Period 1; decreased to 0.05 during Period 2; remained as 0.05 during Period 3; increased to 0.09 during Period 4; decreased to 0.08 during Period 5; decreased to 0.04 during Period 6; remained as 0.04 during Period 7 and Period 8; and decreased to 0.03 during Period 9. It indicates a general decreasing trend in Length of overland flow (L_o) (m).

4.3.3.3.7 Constant of channel maintenance (C) (km^2/km)

Constant of channel maintenance (C) (km^2/km) decreased from 0.13 to 0.12 during

Period 1; decreased to 0.11 during Period 2 and Period 3; increased to 0.18 during Period 4; decreased to 0.12 during Period 5; decreased to 0.08 during Period 6; decreased to 0.07 during Period 7; increased to 0.08 during Period 8; and decreased to 0.07 during Period 9. It indicates a general decreasing trend in Constant of channel maintenance (*C*) (km^2/km).

4.3.3.4 Relief characteristics

The results of quantitative analysis on relief characterisitcs in Study site C were indicated in Table 4.3.3 and Table 4.3.8.

4.3.3.4.1 Height of basin outlet (Z_{min}) (m)

Height of basin outlet (Z_{min}) (m) increased from 88.34 m to 93.74 m during Period 1; increased to 108.86 m during Period 2; decreased to 98.87 m during Period 3; increased to 100.33 m during Period 4; increased to 110.07 m during Period 5; decreased to 94.67 m during Period 6; increased to 95.05 m during Period 7; decreased to 91.49 m during Period 8; and increased to 94.78 m during Period 9. It indicates a general increasing trend in Height of basin outlet (Z_{min}) (m)

4.3.3.4.2 Maximum height of basin (Z_{max}) (m)

Maximum height of basin (Z_{max}) (m) decreased from 258.71 m to 258.46 m during Period 1; remained as 258.46 m during Period 2, Period 3, Period 4, Period 5, Period 6, Period 7, Period 8; and decreased to 258.06 m during Period 9. It indicates a general steady trend in Maximum height of basin (Z_{max}) (m).

4.3.3.4.3 Total basin relief (*H*) (m)

Total basin relief (*H*) (m) decreased from 170.37 m to 164.72 m during Period 1; decreased to 149.60 m during Period 2 increased to 159.59 m during Period 3; decreased to 158.13 m during Period 4; decreased to 148.39 m during Period 5; increased to 163.79 m during Period 6; decreased to 163.41 m during Period 7; increased to 166.97 m during Period 8; and decreased to 163.28 m during Period 9. It indicates a general decreasing trend in Total basin relief (*H*) (m).

4.3.3.4.4 Relief ratio (R_h)

Relief ratio (R_h) remained as 0.27 during Period 1; decreased to 0.24 during Period 2, increased to 0.26 Period 3, increased to 0.27 during Period 4, remained as 0.27 in Period 5; and Period 6; decreased to 0.26 during Period 7, and increased to 0.27 during Period

8; and remained as 0.27 during Period 9. It indicates a general steady trend in Relief ratio (R_h).

4.3.3.4.5 Ruggedness number (R_n) (km/km^2)

Ruggedness number (R_n) (km/km^2) increased from 1.26 to 1.43 during Period 1; decreased to 1.41 during Period 2; increased to 1.50 during Period 3; decreased to 0.15 during Period 4; increased to 1.81 during Period 5; increased to 2.01 during Period 6; increased to 2.29 during Period 7; decreased to 2.05 during Period 8; and increased to 2.40 during Period 9. It indicates a general increasing trend in Ruggedness number (R_n) (km/km^2).

4.3.3.4.6 Dissection index (D_{is})

Dissection index (D_{is}) decreased from 0.66 to 0.64 during Period 1; decreased to 0.58 during Period 2; increased to 0.62 during Period 3; decreased to 0.61during Period 4; decreased to 0.57 during Period 5; increased to 0.63 during Period 6; remained as 0.63 during Period 7; increased to 0.65 during Period 8; and decreased to 0.63 during Period 9. It indicates a general decreasing trend in Dissection index (D_{is}).

4.3.3.5 Hydraulic Parameters

The results of quantitative analysis on hydraulic parameters in Study site C were indicated in Table 4.3.3 and Table 4.3.9.

4.3.3.5.1 Hydraulic radius (*R*) (m)

Hydraulic radius (*R*) (m) was 0.01 m during Period 2 and remained as 0.01 during Period 3; increased to 0.03m during Period 4; increased to 0.05 m during Period 6; increased to 0.09 m during Period 7; and decreased to 0.02 m during Period 8. It indicates a general decreasing trend in Hydraulic radius (*R*) (m).

4.3.3.5.2 Slope (10 m from stream head) (*S*) (tanø)

Slope (10 m from stream head) (*S*) (tanø) increased from 0.58 (tanø) (Period 2; to 0.72 (tanø) (Period 3); increased to 0.73 (tanø) during Period 4; decreased to 0.68 (tanø) during Period 6; increased to 0.84 (tanø) during Period 7; and decreased to 0.65 (tanø) during Period 8. It indicates a general increasing trend in Slope (10 m from stream head) (*S*) (tanø).

4.3.3.5.3 Shear stress (τ) (Nm^{-2})

Shear stress (τ) (Nm^{-2}) decreased from 81.94 (Nm^{-2}) (Period 2); to 65.68 (Nm^{-2}) (Period 3); decreased to 22.47 (Nm^{-2}) during Period 4; increased to 342.90 (Nm^{-2}) during Period 6; increased to 725.74 (Nm^{-2}) during Period 7; and decreased to 107.46 (Nm^{-2}) during Period 8. It indicates a general increasing trend in Shear stress (τ) (Nm^{-2}).

4.3.3.5.4 Critical shear stress (τ_c) (Nm^{-2})

Critical shear stress (τ_c) (Nm^{-2}) decreased from 0.023 (Nm^{-2}) (Period 2; to 0.019 (Nm^{-2}) (Period 3); decreased to 0.006 (Nm^{-2}) during Period 4; increased to 0.098 (Nm^{-2}) during Period 6; increased to 0.207 (Nm^{-2}) during Period 7; and decreased to 0.031 (Nm^{-2}) during Period 8. It indicates a general increasing trend in Critical shear stress (τ_c) (Nm^{-2}).

4..3.5.5 Velocity (v) (ms^{-1})

Velocity (v) (ms^{-1}) was 0.001 (ms^{-1}) in Period 2, Period 3 and during Period 4:; increased to 0.015 (ms^{-1}) during Period 6; increased to 0.055 (ms^{-1}) during Period 7; and decreased to 0.002 (ms^{-1}) during Period 8. It indicates a general increasing trend in Velocity (v) (ms^{-1}).

4.3.3.5.6 Peak specific discharge per unit rainfall intensity (k_p) (mm)

Peak specific discharge per unit rainfall intensity (k_p) (mm) decreased from 0.060 mm (Period 2); to 0.010 mm (Period 3); decreased to 0.001 mm (ms^{-1}) during Period 4; increased to 0.350 mm during Period 6; increased to 4.40 mm during Period 7; and decreased to 0.010 mm during Period 8. It indicates a general decreasing trend in Peak specific discharge per unit rainfall intensity (k_p) (mm).

Study site C	Date	Oct 05, 2012	Sep 11, 2018	Apr 23, 2020	Jun 25, 2020	Sep 14, 2020	Oct 30, 2020	Apr 13, 2021	Jun 21, 2021	Aug 27, 2021	Oct 29, 2021
Geomorphometric parameters	Unit										
Watershed geometry											
Basin length (L_b)	m	641.24	616.87	–	–	–	–	–	–	–	605.28
Basin area (A)	m^2	88989	87639	–	–	–	–	–	–	–	82264
Basin Perimeter (P)	m	2155.53	2011.55	–	–	–	–	–	–	–	2298.40
Form factor (F_f)	–	0.22	0.21	–	–	–	–	–	–	–	0.22
Elongation ratio (R_e)	–	0.52	0.52	–	–	–	–	–	–	–	0.53
Circularity ratio (R_c)	–	0.24	0.25	–	–	–	–	–	–	–	0.20
Compactness coefficient (C_c)	–	2.04	1.99	–	–	–	–	–	–	–	2.26
Drainage network											
Length of mainstream channel	m	659.35	666.27	767.82	626.07	625.30	594.99	689.63	815.55	753.76	841.15
Total length of tributaries (1st order stream)	m	659.35	70.09	320.84	206.60	223.58	547.15	385.04	411.34	30.68	323.75
Stream order (U)	–	1	2	2	2	2	2	2	2	3	3
Stream number (N_u)	–	1	4	12	7	11	20	11	16	11	19
Total stream length (L_u)	m	659.35	707.93	767.82	764.83	769.81	1199.59	999.83	1146.07	1003.40	1207.69
Mean stream length (L_m)	m	659.35	176.98	63.99	109.26	69.98	59.98	90.89	71.63	91.22	63.56
Stream length ratio (R_L)	–	–	27.30	24.21	16.21	24.43	22.36	15.97	26.79	67.18, 8.37	37.99, 20.27
Bifurcation ratio (R_b)	–	–	3	11	6	10	19	10	15	5, 2	5, 3
Gradient of mainstream	m/m	0.13	0.13	0.13	0.17	0.19	0.14	0.17	0.15	0.15	0.14
Drainage texture											
Stream frequency (F_s)	1/km^2	11.24	49.00	146.99	85.74	13.47	24.5	134.74	195.98	134.74	230.96
Drainage texture (D_t)	1/km	0.46	1.99	5.96	3.48	24.68	19.43	5.47	7.95	5.47	8.27
Drainage density (D_d)	km/km^2	7.41	8.67	9.41	9.37	0.94	1.47	12.25	14.04	12.29	14.68
Drainage intensity (D_i)	1/km	1.52	5.65	15.63	9.15	14.29	16.67	11.00	13.96	10.96	15.73
Infiltration number (I_f)	–	83.26	424.87	1382.44	803.28	2273.23	3574.14	1650.15	2751.29	1656.04	3390.63
Length of overland flow (L_o)	km	0.07	0.06	0.05	0.05	0.09	0.08	0.04	0.04	0.04	0.03
Constant of channel maintenance (C)	km^2/km	0.13	0.12	0.11	0.11	0.18	0.12	0.08	0.07	0.08	0.07
Relief characteristics											
Height of basin outlet (Z_{min})	m	88.34	93.74	108.86	98.87	100.33	110.07	94.67	95.05	91.49	94.78
Maximum height of basin (Z_{max})	m	258.71	258.46	258.46	258.46	258.46	258.46	258.46	258.46	258.46	258.06
Total basin relief (H)	m	170.37	164.72	149.6	159.59	158.13	148.39	163.79	163.41	166.97	163.28
Relief ratio (R_h)	–	0.27	0.27	0.24	0.26	0.27	0.27	0.27	0.26	0.27	0.27
Ruggedness number (R_n)	km/km^2	1.26	1.43	1.41	1.50	0.15	1.81	2.01	2.29	2.05	2.40
Dissection index (D_{is})		0.66	0.64	0.58	0.62	0.61	0.57	0.63	0.63	0.65	0.63
Hydraulic Parameters											
Hydraulic radius (R)	m	–	–	0.01	0.01	0.03	–	0.05	0.09	0.02	–
Slope (10 m from stream head) (S)	tanø	–	–	0.58	0.72	0.73	–	0.68	0.84	0.65	–
Shear stress (τ)	Nm^{-2}	–	–	81.94	65.68	22.47	–	342.9	725.74	107.46	–
Critical shear stress (τ_c)	Nm^{-2}	–	–	0.023	0.019	0.006	–	0.098	0.207	0.031	–
Velocity (v)	$m\ s^{-1}$	–	–	0.001	0.001	0.001	–	0.015	0.055	0.002	–
Peak specific discharge per unit rainfall intensity (k_p)	mm	–	–	0.06	0.01	0.00	–	0.35	4.40	0.01	–

Table 4.3.3: Study site C: Results of quantitative analysis of post-seismic drainage basin characteristics by 35 geomorphometric and hydraulic parameters during investigation periods.

4.3.4 Study site D

4.6.4.1 Watershed geometry

The results of quantitative analysis on watershed geometry in Study site D were indicated in Table 4.3.4 and Table 4.3.5.

4.3.4.1.1 Basin length (L_b) (m)

The Basin length (L_b) decreased from 684.30 m to 683.01 m during Period 1 and then decreased to 657.23 m during Period 2 – 9. It indicates a general decreasing trend in Basin length (L_b) (m).

4.3.4.1.2 Basin area (A) (m^2)

Basin area (A) (m^2) decreased from 192479 m^2 to 191068 m^2 during Period 1 and then further decreased to 185247 m^2 during Period 2 – 9. It indicates a general decreasing trend in Basin area (A) (m^2).

4.3.4.1.3 Basin Perimeter (*P*) (m)

Basin Perimeter (P) (m) decreased from 25.7644 m to 2571.44 m during Period 1 and then increased to 2941.60 m during Period 2 – 9. It indicates a general increasing trend in Basin Perimeter (P) (m).

4.3.4.1.4 Form factor (F_f)

Form factor (F_f) remained as 0.41 during Period 1 and increased to 0.43 during Period 2 – 9. It indicates a general increasing trend in Form factor (F_f).

4.3.4.1.5 Elongation ratio (R_e)

Elongation ratio (R_e) remained as 0.72 during Period 1 and increased to 0.74 during Period 2 – 9. It indicates a general increasing trend in Elongation ratio (R_e).

4.3.4.1.6 Circularity ratio (R_c)

Circularity ratio (R_c) remained as 0.36 during Period 1 and then decreased to 0.30 during Period 2 – 9. It indicates a general decreasing trend in Circularity ratio (R_c).

4.3.4.1.7 Compactness coefficient (C_c)

Compactness coefficient (C_c) decreased from 1.67 to 1.66 during Period 1 and then increased to 1.93 during Period 2 – 9. It indicates a general increasing trend in Compactness coefficient (C_c).

4.3.4.2 Drainage network

The results of quantitative analysis on drainage network in Study site D were indicated in Table 4.6.4 and Table 4.3.6.

4.3.4.2.1 Length of mainstream channel (m)

Length of mainstream channel (m) increased from 788.62 m to 812.27 m during Period 1; increased to 856.72 m during Period 2; decreased to 706.14 m during Period 3 and Period 4; increased to 953.41 m during Period 5; decreased to 753.26 m during Period 6; increased to 839.17 during Period 7; decreased to 822.08 m during Period 8; and increased to 899.58 m during Period 9. It indicates a general increasing trend in Length of mainstream channel (m).

4.3.4.2.2 Total length of tributaries (1st order stream) (m)

Total length of tributaries (1st order stream) (m) increased from 599.56 m to 727.40 m during Period 1; increased to 1254.17 m during Period 2; decreased to 932.27 m during Period 3 and Period 4; decreased to 1810.68 m during Period 5; decreased to 1296.36 m during Period 6; increased to 1486.40 m during Period 7; decreased to 1071.29 m during Period 8; and increased to 1464.65 m during Period 9. It indicates a general increasing trend in Total length of tributaries (1st order stream) (m).

4.3.4.2.3 Stream order (U)

Stream order (U) was 3 during Period 1; remained as 3 during Period 2 and during Period 3 and Period 4; increased to 4 during Period 5; decreased to 3 during Period 6; increased to 4 during Period 7; decreased to 3 during Period 8; and increased to 4 during Period 9. It indicates a general increasing trend in Stream order (U).

4.3.4.2.4 Stream number (N_u)

Stream number (N_u) increased from 16 to 17 during Period 1; increased to 27 during Period 2; decreased to 24 during Period 3 and Period 4; increased to 46 during Period 5; decreased to 29 during Period 6; increased to 51 during Period 7; decreased to 28 during Period 8; and increased to 57 during Period 9. It indicates a general increasing trend in Stream number (N_u).

4.3.4.2.5 Total stream length (L_u) (m)

Total stream length (L_u) (m) increased from 1488.50 m to 1758.49 m during Period 1; increased to 2514.43 m during Period 2; decreased to 1892.90 m during Period 3 and Period 4; increased to 2898.63 m during Period 5; decreased to 2247.34 m during Period 6; increased to 2841.43 m during Period 7; decreased to 2230.30 m during Period 8; and increased to 3320.03 m during Period 9. It indicates a general increasing trend in Total stream length (L_u) (m).

4.3.4.2.6 Mean stream length (L_m) (m)

Mean stream length (L_m) (m) increased from 99.23 m to 103.44 m during Period 1; decreased to 93.13 m during Period 2; decreased to 78.87 m during Period 3 and Period 4; decreased to 63.01 m during Period 5; decreased to 56.36 m during Period 6; decreased to 55.71 m during Period 7; increased to 79.65 m during Period 8; and decreased to 58.25

m during Period 9. It indicates a general decreasing trend in Mean stream length (L_m) (m).

4.3.4.2.7 Stream length ratio (R_L)

Stream length ratio (R_L) was 1.31 and 8.50 and 1.66 and 6.26 respectively in Period 1; 2.02 and 5.45 during Period 2; 4.65 and 1.43 during Period 3 and Period 4; 1.71, 3.29 and 1.53 during Period 5; 1.45 and 6.67 in Period 6; 1.92 and 3.49 during Period 7; 2.88 and 4.65 during Period 8; and 2.18, 3.19 and 1.71 during Period 9. It indicates a general increasing trend in Stream length ratio (R_L).

4.3.4.2.8 Bifurcation ratio (R_b)

Bifurcation ratio (R_b) was 2.75 and 3, and 3 and 4 respectively in Period 1; 4.20 and 5 during Period 2; 6.67 and 3 during Period 3and Period 4; 7.6, 3.8 and 2 during Period 5; 4.6 and 5 in Period 6; 5.86 and 3.5 during Period 7 5.75 and 4 during Period 8; and 4.3, 3.3 and 3 during Period 9. It indicates a general increasing trend in Bifurcation ratio (R_b).

4.3.4.2.9 Gradient of mainstream (m/m)

Gradient of mainstream (m/m) was 0.13 during Period 1 and Period 2; increased to 0.16 during Period 3 and Period 4; remained as 0.16 during Period 5; increased to 0.19 during Period 6; decreased to 0.17 during Period 7; decreased to 0.15 during Period 8; and decreased to 0.13 during Period 9. It indicates a general steady trend in Gradient of mainstream (m/m).

4.3.4.3 Drainage texture

The results of quantitative analysis on drainage texture in Study site D were indicated in Table 4.3.4 and Table 4.3.7.

4.3.4.3.1 Stream frequency (F_s) (1/km^2)

Stream frequency (F_s) (1/km^2) increased from 77.93 to 88.97 during Period 1; increased to 414.31 during Period 2; decreased to 125.61 during Period 3 and Period 4 ; increased to 240.75 during Period 5; decreased to 151.78 during Period 6; increased to 266.92 during Period 7; decreased to 146.54 during Period 8; and increased to 307.70 during Period 9. It indicates a general increasing trend in Stream frequency (F_s) (1/km^2).

4.3.4.3.2 Drainage texture (D_t) (1/km)

Drainage texture (D_t) (1/km) increased from 5.82 to 6.61 during Period 1; increased to 10.50 during Period 2; decreased to 9.33 during Period 3 and Period 4; increased to

17.89 during Period 5; decreased to 11.28 during Period 6; increased to 19.38 during Period 7; decreased to 10.89 during Period 8; and increased to 19.38 during Period 9. It indicates a general increasing trend in Drainage texture (D_t) (1/km).

4.3.4.3.3 Drainage density (D_d) (km/km^2)

Drainage density (D_d) (km/km^2) increased from 7.73 to 9.20 during Period 1; increased to 13.16 during Period 2; decreased to 9.91 during Period 3 and Period 4; increased to 15.17 during Period 5; decreased to 11.76 during Period 6; increased to 14.87 during Period 7; decreased to 11.67 during Period 8; and increased to 17.92 during Period 9. It indicates a general increasing trend in Drainage density (D_d) (km/km^2).

4.3.4.3.4 Drainage intensity (D_i) (1/km)

Drainage intensity (D_i) (1/km) decreased from 10.08 to 9.67 during Period 1; increased to 10.74 during Period 2; increased to 12.68 during Period 3 and Period 4:; increased to 15.87 during Period 5; decreased to 12.90 during Period 6; increased to 17.95 during Period 7; decreased to 12.55 during Period 8; and increased to 17.17 during Period 9.

4.3.4.3.5 Infiltration number (I_f) (1/10^6·m^3)

Infiltration number (I_f) (1/10^6·m^3) increased from 602.66 to 818.87 during Period 1:; increased to 1859.63 during Period 2; decreased to 1244.41 during Period 3 and Period 4; increased to 3652.36 during Period 5; decreased to 1785.22 during Period 6; increased to 3969.49 during Period 7; decreased to 1710.59 during Period 8; and increased to 5514.56 during Period 9. It indicates a general increasing trend in Infiltration number (I_f) (1/10^6·m^3).

4.3.4.3.6 Length of overland flow (L_o) (m)

Length of overland flow (L_o) (m) decreased from 0.06 to 0.05 during Period 1; decreased to 0.04 during Period 2; increased to 0.05 during Period 3 and Period 4; decreased to 0.03 during Period 5; increased to 0.04 during Period 6; decreased to 0.03 during Period 7; increased to 0.04 during Period 8; and decreased to 0.03 during Period 9. It indicates a general decreasing trend in Length of overland flow (L_o) (m).

4.3.4.3.7 Constant of channel maintenance (C) (km^2/km)

Constant of channel maintenance (C) (km^2/km) was 0.68 during Period 1; decreased to 0.67 during Period 2; decreased to 0.66 during Period 3 and during Period 4; increased to 0.68 during Period 5; decreased to 0.67 during Period 6; decreased to 0.66 during Period 7; increased to 0.68 during Period 8; and decreased to 0.67 during Period 9. It indicates a general decreasing trend in Constant of channel maintenance (C) (km^2/km).

4.3.4.4 Relief characteristics

The results of quantitative analysis on relief characteristicss in Study site D were indicated in Table 4.6.4 and Table 4.3.8.

4.3.4.4.1 Height of basin outlet (Z_{min}) (m)

Height of basin outlet (Z_{min}) (m) increased from 88.04 m to 89.15 m during Period 1; increased to 89.60 m during Period 2; increased to 92.50 m during Period 3 and Period 4; decreased to 88.60 m during Period 5; increased to 91.50 m during Period 6; increased to 93.99 m during Period 7; decreased to 89.21 m during Period 8; and increased to 90.30 m during Period 9. It indicates a general increasing trend in Height of basin outlet (Z_{min}) (m).

4.3.4.4.2 Maximum height of basin (Z_{max}) (m)

Maximum height of basin (Z_{max}) (m) decreased from 275.96 m to 275.35 m during Period 1; remained as 275.35 m during Period 2, Period 3, Period 4, Period 5, Period 6, Period 7, Period 8; and decreased to 275.23 m during Period 9. It indicates a general steady trend in Maximum height of basin (Z_{max}) (m).

4.3.4.4.3 Total basin relief (H) (m)

Total basin relief (H) (m) decreased from 187.92 m to 186.20 m during Period 1; decreased to 185.75 m during Period 2; decreased to 182.85 m during Period 3 and Period 4; increased to 186.75 m during Period 5; decreased to 183.85 m during Period 6; decreased to 181.36 m during Period 7; increased to 186.14 m during Period 8; and decreased to 184.39 m during Period 9. It indicates a general decreasing trend in Total basin relief (H) (m).

4.3.4.4.4 Relief ratio (R_h)

Relief ratio (R_h) was 0.27 during Period 1; remained as 0.27 during Period 2, Period 3, Period 4, Period 5; increased to 0.28 during Period 6 and Period 7, and increased to 0.29 during Period 8; and increased to 0.28 during Period 9. It indicates a general increasing trend in Relief ratio (R_h).

4.3.4.4.5 Ruggedness number (R_n) (km/km^2)

Ruggedness number (R_n) (km/km^2) increased from 1.45 to 1.71 during Period 1; increased to 2.44 during Period 2; decreased to 1.81 during Period 3 and Period 4; increased to 2.83 during Period 5; decreased to 2.16 during Period 6; increased to 2.70

during Period 7 decreased to 2.17 during Period 8; and increased to 3.31 during Period 9. It indicates a general increasing trend in Ruggedness number (R_n) (km/km^2).

4.3.4.4.6 Dissection index (D_{is})

Dissection index (D_{is}) was 0.68 during Period 1; decreased to 0.67 during Period 2; decreased to 0.66 during Period 3 and Period 4; increased to 0.68 during Period 5; decreased to 0.67 during Period 6; decreased to 0.66 during Period 7; increased to 0.68 during Period 8; and decreased to 0.67 during Period 9. It indicates a general decreasing trend in Dissection index (D_{is}).

4.3.4.5 Hydraulic Parameters

The results of quantitative analysis on hydraulic parameters in Study site D were indicated in Table 4.3.4 and Table 4.3.9.

4.6.4.5.1 Hydraulic radius (*R*) (m)

Hydraulic radius (*R*) (m) increased from 0.05 m during Period 2 to 0.11 during Period 3 and Period 4; decreased to 0.04 m during Period 6; increased to 0.05 m during Period 7; and decreased to 0.04 m during Period 8. It indicates a general decreasing trend in Hydraulic radius (*R*) (m).

4.3.4.5.2 Slope (10 m from stream head) (*S*) (tanø)

Slope (10 m from stream head) (*S*) (tanø) was 0.19 (tanø) (Period 2); increased to 0.42 (tanø) during Period 4; increased to 0.43 (tanø) during Period 6; increased to 0.54 (tanø) during Period 7; and increased to 0.64 (tanø) during Period 8. It indicates a general increasing trend in Slope (10 m from stream head) (*S*) (tanø).

4.3.4.5.3 Shear stress (τ) (Nm^{-2})

Shear stress (τ) (Nm^{-2}) was 100.73 (Nm^{-2}) (Period 2); increased to 462.57 (Nm^{-2}) during Period 4; decreased to 182.68 (Nm^{-2}) during Period 6; increased to 310.65 (Nm^{-2}) during Period 7; and decreased to 175.69 (Nm^{-2}) during Period 8. It indicates a general increasing trend in Shear stress (τ) (Nm^{-2}).

4.3.4.5.4 Critical shear stress (τ_c) (Nm^{-2})

Critical shear stress (τ_c) (Nm^{-2}) was 0.029 (Nm^{-2}) in Period 2; increased to 0.132 (Nm^{-2}) during Period 4; decreased to 0.052 (Nm^{-2}) during Period 6; increased to 0.089 (Nm^{-2}) during Period 7; and decreased to 0.001 (Nm^{-2}) during Period 8. It indicates a general decreasing trend in Critical shear stress (τ_c) (Nm^{-2}).

4.3.4.5.5 Velocity (v) (ms^{-1})

Velocity (v) (ms^{-1}) was 0.005 (ms^{-1}) in Period 2; increased to 0.044 (ms^{-1}) during Period 4; remained as 0.044 (ms^{-1}) during Period 6; increased to 0.010 (ms^{-1}) during Period 7; and decreased to 0.001 (ms^{-1}) during Period 8. It indicates a general decreasing trend in Velocity (v) (ms^{-1}).

4.3.4.5.6 Peak specific discharge per unit rainfall intensity (k_p) (mm)

Peak specific discharge per unit rainfall intensity (k_p) (mm) was 1.680 mm (Period 2); increased to 1.850 mm during Period 4; decreased to 0.080 mm during Period 6; increased to 0.110 mm during Period 7; and decreased to 0.010 mm during Period 8. It indicates a general decreasing trend in Peak specific discharge per unit rainfall intensity (k_p) (mm).

Study site D	Date	Oct 05, 2012	Sep 11, 2018	Apr 23, 2020	Jun 25, 2020	Sep 14, 2020	Oct 30, 2020	Apr 13, 2021	Jun 21, 2021	Aug 27, 2021	Oct 29, 2021
Geomorphometric parameters	Unit										
Watershed geometry											
Basin length (L_b)	m	684.30	683.01	–	–	–	–	–	–	–	657.23
Basin area (A)	m^2	192479	191068	–	–	–	–	–	–	–	185247
Basin Perimeter (P)	m	2576.44	2571.44	–	–	–	–	–	–	–	2941.60
Form factor (F_f)	–	0.41	0.41	–	–	–	–	–	–	–	0.43
Elongation ratio (R_e)	–	0.72	0.72	–	–	–	–	–	–	–	0.74
Circularity ratio (R_c)	–	0.36	0.36	–	–	–	–	–	–	–	0.30
Compactness coefficient (C_c)	–	1.67	1.66	–	–	–	–	–	–	–	1.93
Drainage network											
Length of mainstream channel	m	788.62	812.27	856.72	–	706.14	953.41	753.26	839.17	822.08	899.58
Total length of tributaries (1st order stream)	m	599.56	727.40	1254.17	–	932.27	1810.68	1296.36	1486.40	1071.29	1464.65
Stream order (U)	–	3	3	3	–	3	4	3	4	3	4
Stream number (N_u)	–	16	17	27	–	24	46	29	51	28	57
Total stream length (L_u)	m	1488.50	1758.49	2514.43	–	1892.90	2898.63	2247.34	2841.43	2230.30	3320.03
Mean stream length (L_m)	m	99.23	103.44	93.13	–	78.87	63.01	56.36	55.71	79.65	58.25
Stream length ratio (R_L)	–	1.31, 8.50	1.66, 6.26	2.02, 5.45	–	4.65. 1.43	1.71, 3.29, 1.53	1.45, 6.67	1.92, 3.49	2.88, 4.65	2.18, 3.19, 1.71
Bifurcation ratio (R_b)	–	2.75, 3	3, 4	4.2, 5	–	6.67, 3	7.6, 3.8, 2	4.6, 5	5.86, 3.5	5.75, 4	4.3, 3.3, 3
Gradient of mainstream	m/m	0.13	0.13	0.13	–	0.16	0.16	0.19	0.17	0.15	0.13
Drainage texture											
Stream frequency (F_s)	$1/km^2$	77.93	88.97	414.31	–	125.61	240.75	151.78	266.92	146.54	307.70
Drainage texture (D_t)	1/km	5.82	6.61	10.50	–	9.33	17.89	11.28	19.83	10.89	19.38
Drainage density (D_d)	km/km^2	7.73	9.20	13.16	–	9.91	15.17	11.76	14.87	11.67	17.92
Drainage intensity (D_i)	1/km	10.08	9.67	10.74	–	12.68	15.87	12.90	17.95	12.55	17.17
Infiltration number (I_f)	–	602.66	818.87	1859.63	–	1244.41	3652.36	1785.22	3969.46	1710.59	5514.56
Length of overland flow (L_o)	km	0.06	0.05	0.04	–	0.05	0.03	0.04	0.03	0.04	0.03
Constant of channel maintenance (C)	km^2/km	0.13	0.11	0.08	–	0.10	0.07	0.09	0.07	0.09	0.06
Relief characteristics											
Height of basin outlet (Z_{min})	m	88.04	89.15	89.60	–	92.50	88.60	91.50	93.99	89.21	90.30
Maximum height of basin (Z_{max})	m	275.96	275.35	275.35	–	275.35	275.35	275.35	275.35	275.35	275.23
Total basin relief (H)	m	187.92	186.20	185.75	–	182.85	186.75	183.85	181.36	186.14	184.93
Relief ratio (R_h)	–	0.27	0.27	0.27	–	0.27	0.27	0.27	0.27	0.27	0.28
Ruggedness number (R_n)	km/km^2	1.45	1.71	2.44	–	1.81	2.83	2.16	2.70	2.17	3.31
Dissection index (D_{is})		0.68	0.68	0.67	–	0.66	0.68	0.67	0.66	0.68	0.67
Hydraulic Parameters											
Hydraulic radius (R)	m	–	–	0.05	–	0.11	–	0.04	0.05	0.04	–
Slope (10 m from stream head) (S)	tanø	–	–	0.19	–	0.42	–	0.43	0.54	0.64	–
Shear stress (τ)	Nm^{-2}	–	–	100.73	–	462.57	–	182.68	310.65	175.69	–
Critical shear stress (τ_c)	Nm^{-2}	–	–	0.029	–	0.132	–	0.052	0.089	0.001	–
Velocity (v)	$m\ s^{-1}$	–	–	0.005	–	0.044	–	0.004	0.010	0.001	–
Peak specific discharge per unit rainfall intensity (k_p)	mm	–	–	1.680	–	1.850	–	0.080	0.110	0.010	–

Table 4.3.4: Study site D: Results of quantitative analysis of post-seismic drainage basin characteristics by 35 geomorphometric and hydraulic parameters during investigation periods.

Geomorphometric parameters					
Watershed geometry	Unit	Study sites	Oct 05, 2012	Sep 11, 2018	Oct 29, 2021
Basin length (L_b)	m	A	615.07	616.26	608.57
		B	564.13	576.73	578.64
		C	641.24	616.87	605.28
		D	684.3	683.01	657.23
Basin area (A)	m^2	A	70637	70315	69015
		B	103942	104006	103968
		C	88989	81639	82264
		D	192479	191068	185247
Basin Perimeter (P)		A	1913.58	1944.57	2186.4
	m	B	1393.90	1433.99	1415.23
		C	2155.53	2011.55	2298.4
		D	2576.44	2571.44	2941.6
Form factor (F_f)	–	A	0.19	0.19	0.19
		B	0.33	0.31	0.31
		C	0.22	0.21	0.22
		D	0.41	0.41	0.43
Elongation ratio (R_e)	–	A	0.49	0.49	0.49
		B	0.65	0.63	0.63
		C	0.52	0.52	0.53
		D	0.72	0.72	0.74
Circularity ratio (R_c)	–	A	0.24	0.22	0.21
		B	0.67	0.64	0.64
		C	0.24	0.25	0.2
		D	0.36	0.36	0.30
Compactness coefficient (C_c)	–	A	2.03	2.07	2.15
		B	1.22	1.25	1.25
		C	2.04	1.99	2.26
		D	1.67	1.66	1.93

Table 4.3.5: Results of parameters of watershed geometry of all study sites (A-D)

Geomorphometric												
Drainage network	Unit	Study sites	Oct 05, 2012	Sep 11, 2018	Apr 23, 2020	Jun 25, 2020	Sep 14, 2020	Oct 30, 2020	Apr 13, 2021	Jun 21, 2021	Aug 27, 2021	Oct 29, 2021
Length of mainstream	m	A	586.42	638.30	586.73	552.82	574.64	616.26	618.64	618.94	608.31	688.22
		B	577.56	653.85	516.02	498.21	564.86	594.99	556.69	618.52	612.19	685.72
		C	659.35	666.27	767.82	626.07	625.3	594.99	689.63	815.55	753.76	841.15
		D	788.62	812.27	856.72	–	706.14	953.41	753.26	839.17	822.08	899.58
Total length of tributaries (1st order stream)	m	A	586.42	14.4	586.73	552.82	62.12	399.83	820.37	320.07	132.05	205.81
		B	269.91	319.81	310.52	149.35	632.91	547.15	438.63	766.44	558.14	876.00
		C	659.35	70.09	320.84	206.60	223.58	547.15	385.04	411.34	30.68	323.75
		D	599.56	727.40	1254.17	–	932.27	1810.68	1296.36	1486.40	1071.29	1464.65
Stream order (U)	–	A	1	2	1	1	1	3	2	2	2	3
		B	2	2	2	2	3	2	3	3	2	3
		C	1	2	2	2	2	2	2	2	3	3
		D	3	3	3	–	3	4	3	4	3	4
Stream number (N_u)	–	A	1	3	1	1	5	22	4	21	8	14
		B	6	11	9	8	22	20	19	26	17	34
		C	1	4	12	7	11	20	11	16	11	19
		D	15	17	27	–	24	46	29	51	28	57
Total stream length (L_u)	m	A	586.42	638.30	586.73	552.82	636.76	1075.70	1260.81	910.59	692.96	865.98
		B	721.28	923.93	753.85	694.26	1121.88	1199.59	1039.93	1358.44	1132.79	1663.27
		C	659.35	707.93	767.82	764.83	769.81	1199.59	999.83	1146.07	1003.40	1207.69
		D	1488.50	1758.49	2514.43	–	1892.90	2898.63	2247.34	2841.43	2230.30	3320.03
Mean stream length (L_m)	m	A	586.42	638.30	586.73	552.82	127.35	358.57	315.20	43.36	86.62	61.86
		B	120.21	84.81	83.76	86.78	50.99	59.98	54.73	52.25	66.63	48.92
		C	659.35	176.98	63.99	109.26	69.98	59.98	90.89	71.63	91.22	63.56
		D	99.23	103.44	93.13	–	78.87	63.01	56.36	55.71	79.65	58.25
Stream length ratio (R_L)	–	A	–	8.03	–	–	–	9.5, 81.08	1.61	36.90	29.73	1.30, 25.08
		B	8.36	19.17	11.42	7.70	1.55, 8.41	22.36	6.83, 1.21	1.60, 9.11	16.47	1.52, 11.57
		C	–	27.30	24.21	16.21	24.43	22.36	15.97	26.79	67.18, 8.37	37.99, 20.27
		D	1.31, 8.50	1.66, 6.26	2.02, 5.45	–	4.65. 1.43	1.71, 3.29, 1.53	1.45, 6.67	1.92, 3.49	2.88, 4.65	18, 3.19, 1.71
Bifurcation ratio (R_b)	–	A	–	2	–	–	4	9.5, 2	3	20	7	5.5, 2
		B	5	10	8	7	9.5, 2	19	8, 2	11.5, 2	16	5.6, 5
		C	–	3	11	6	10	19	10	15	5, 2	5, 3
		D	2.75, 3	3, 4	4.2, 5	–	6.67, 3	7.6, 3.8, 2	4.6, 5	5.86, 3.5	5.75, 4	4.3, 3.3, 3
Gradient of mainstream	m/m	A	0.15	0.12	0.14	0.15	0.17	0.15	0.14	0.15	0.16	0.15
		B	0.17	0.12	0.15	0.17	0.21	0.14	0.18	0.20	0.19	0.12
		C	0.13	0.13	0.13	0.17	0.19	0.14	0.17	0.15	0.15	0.14
		D	0.13	0.13	0.13	–	0.16	0.16	0.19	0.17	0.15	0.13

Table 4.3.6: Results of parameters of drainage network of all study sites (A-D)

Geomorphometric parameters												
Drainage texture	Unit	Study site	Oct 05, 2012	Sep 11, 2018	Apr 23, 2020	Jun 25, 2020	Sep 14, 2020	Oct 30, 2020	Apr 13, 2021	Jun 21, 2021	Aug 27, 2021	Oct 29, 2021
Stream frequency (F_s)	1/km^2	A	14.16	42.67	14.22	14.22	71.11	312.88	56.89	298.66	113.77	202.85
		B	57.72	105.76	86.53	76.92	211.53	192.30	182.68	249.99	163.45	327.02
		C	11.24	49.00	146.99	85.74	13.47	24.5	134.74	195.98	134.74	230.96
		D	77.93	88.97	414.31	–	125.61	240.75	151.78	266.92	146.54	307.70
Drainage texture (D_t)	1/km	A	0.52	1.54	0.51	0.51	2.57	11.31	2.06	10.8	4.11	6.4
		B	4.30	7.67	6.28	5.58	15.34	13.95	13.25	18.13	11.86	23.75
		C	0.46	1.99	5.96	3.48	24.68	19.43	5.47	7.95	5.47	8.27
		D	5.82	6.61	10.50	–	9.33	17.89	11.28	19.83	10.89	19.38
Drainage density (D_d)	km/km^2	A	5.17	9.28	8.34	7.86	9.06	15.3	17.93	12.95	9.86	12.55
		B	6.94	8.97	7.25	6.68	10.79	11.53	10.00	13.06	10.89	16.00
		C	7.41	8.67	9.41	9.37	0.94	1.47	12.25	14.04	12.29	14.68
		D	7.73	9.20	13.16	–	9.91	15.17	11.76	14.87	11.67	17.92
Drainage intensity (D_i)	1/km	A	2.74	4.6	1.71	1.81	7.85	20.45	3.17	23.06	11.54	16.17
		B	8.32	11.79	11.94	11.52	19.61	16.67	18.27	19.14	15.01	20.44
		C	1.52	5.65	15.63	9.15	14.29	16.67	11.00	13.96	10.96	15.73
		D	10.08	9.67	10.74	–	12.68	15.87	12.90	17.95	12.55	17.17
Infiltration number (I_f)	–	A	73.21	396	118.59	111.77	644.26	4786.5	1020.03	3867.64	1121.25	2545.32
		B	400.57	948.69	627.21	513.46	2281.67	2217.92	1826.59	3265.10	1780.25	5231.69
		C	83.26	424.87	1382.44	803.28	2273.23	3574.14	1650.15	2751.29	1656.04	3390.63
		D	602.66	818.87	1859.63	–	1244.41	3652.36	1785.22	3969.46	1710.59	5514.56
Length of overland flow (L_o)	km	A	0.1	0.05	0.06	0.06	0.06	0.03	0.03	0.04	0.05	0.04
		B	0.07	0.06	0.07	0.07	0.05	0.04	0.05	0.04	0.05	0.03
		C	0.07	0.06	0.05	0.05	0.09	0.08	0.04	0.04	0.04	0.03
		D	0.06	0.05	0.04	–	0.05	0.03	0.04	0.03	0.04	0.03
Constant of channel maintenance (C)	km^2/km	A	0.19	0.11	0.12	0.13	0.11	0.07	0.06	0.08	0.10	0.08
		B	0.14	0.11	0.14	0.15	0.09	0.09	0.10	0.08	0.09	0.06
		C	0.13	0.12	0.11	0.11	0.18	0.12	0.08	0.07	0.08	0.07
		D	0.13	0.11	0.08	–	0.10	0.07	0.09	0.07	0.09	0.06

Table 4.3.7: Results of parameters of drainage texture of all study sites(A-D)

Geomorphometric parameters												
Relief characteristics	Unit	Study sites	Oct 05, 2012	Sep 11, 2018	Apr 23, 2020	Jun 25, 2020	Sep 14, 2020	Oct 30, 2020	Apr 13, 2021	Jun 21, 2021	Aug 27, 2021	Oct 29, 2021
Height of basin outlet (Z_{min})	m	A	880.3	96.95	102.41	97.17	97.44	97.49	98.28	98.24	93.58	90.4
		B	97.75	85.70	108.86	111.62	108.77	110.07	104.51	104.74	102.48	104.26
		C	88.34	93.74	108.86	98.87	100.33	110.07	94.67	95.05	91.49	94.78
		D	88.04	89.15	89.60	–	92.50	88.60	91.50	93.99	89.21	90.30
Maximum height of basin (Z_{max})	m	A	235.66	235.26	235.26	235.26	235.26	235.26	235.26	235.26	235.26	235.12
		B	267.53	267.34	267.34	267.34	267.34	267.34	267.34	267.34	267.34	266.79
		C	258.71	258.46	258.46	258.46	258.46	258.46	258.46	258.46	258.46	258.06
		D	275.96	275.35	275.35	–	275.35	275.35	275.35	275.35	275.35	275.23
Total basin relief (H)	m	A	147.63	138.31	132.85	138.09	137.32	137.77	136.98	137.02	141.68	144.72
		B	169.78	181.64	158.48	158.19	158.57	157.27	162.83	162.60	164.86	162.53
		C	170.37	164.72	149.6	159.59	158.13	148.39	163.79	163.41	166.97	163.28
		D	187.92	186.20	185.75	–	182.85	186.75	183.85	181.36	186.14	184.93
Relief ratio (R_h)	–	A	0.24	0.22	0.22	0.22	0.22	0.22	0.22	0.22	0.23	0.24
		B	0.30	0.31	0.27	0.27	0.27	0.27	0.28	0.28	0.29	0.28
		C	0.27	0.27	0.24	0.26	0.27	0.27	0.27	0.26	0.27	0.27
		D	0.27	0.27	0.27	–	0.27	0.27	0.27	0.27	0.27	0.28
Ruggedness number (R_n)	km/km^2	A	0.76	1.28	1.11	1.28	1.24	2.11	2.46	1.77	1.39	1.82
		B	1.18	1.63	1.15	1.06	1.71	1.81	1.63	2.12	1.80	2.60
		C	1.26	1.43	1.41	1.50	0.15	1.81	2.01	2.29	2.05	2.40
		D	1.45	1.71	2.44	–	1.81	2.83	2.16	2.70	2.17	3.31
Dissection index (D_{is})	–	A	0.63	0.59	0.56	0.59	0.58	0.59	0.58	0.58	0.6	0.62
		B	0.63	0.68	0.59	0.59	0.59	0.59	0.61	0.61	0.62	0.61
		C	0.66	0.64	0.58	0.62	0.61	0.57	0.63	0.63	0.65	0.63
		D	0.68	0.68	0.67	–	0.66	0.68	0.67	0.66	0.68	0.67

Table 4.3.8: Results of parameters of relief characteristics of all study sites(A-D)

Hydraulic Parameters												
	Unit	Study sites	Oct 05, 2012	Sep 11, 2018	Apr 23, 2020	Jun 25, 2020	Sep 14, 2020	Oct 30, 2020	Apr 13, 2021	Jun 21, 2021	Aug 27, 2021	Oct 29, 2021
Hydraulic radius (R)	m	A	–	–	0.05	0.05	0.12	–	0.04	0.05	0.04	–
		B	–	–	0.05	0.08	0.10	–	0.06	0.12	0.03	–
		C	–	–	0.01	0.01	0.003	–	0.05	0.09	0.02	–
		D	–	–	0.05	–	0.11	–	0.04	0.05	0.04	–
Slope (10 m from stream head) (S)	tanø	A	–	–	0.48	0.37	0.45	–	0.43	0.54	0.64	–
		B	–	–	0.63	0.77	0.77	–	0.61	0.76	0.82	–
		C	–	–	0.58	0.72	0.73		0.68	0.84	0.65	
		D	–	–	0.19	–	0.42	–	0.43	0.54	0.64	–
Shear stress (τ)	Nm^{-2}	A	–	–	243.06	184.16	544.28	–	173.72	254.12	219.1	–
		B	–	–	296.47	616.08	771.49	–	331.43	908.66	249.85	–
		C	–	–	81.94	65.68	22.47	–	342.9	725.74	107.46	–
		D	–	–	100.73	–	462.57	–	182.68	310.65	175.69	–
Critical shear stress (τ_c)	Nm^{-2}	A	–	–	0.069	0.052	0.155	–	0.050	0.072	0.062	–
		B	–	–	0.084	0.176	0.220	–	0.094	0.259	0.071	–
		C	–	–	0.023	0.019	0.006	–	0.098	0.207	0.031	–
		D	–	–	0.029	–	0.132	–	0.052	0.089	0.001	–
Velocity (v)	m s^{-1}	A	–	–	0.011	0.008	0.057	–	0.006	0.010	0.007	–
		B	–	–	0.012	0.042	0.067	–	0.016	0.095	0.007	–
		C	–	–	0.001	0.001	0.001	–	0.015	0.055	0.002	–
		D	–	–	0.005	–	0.044	–	0.004	0.010	0.001	–
Peak specific discharge								–				
per unit rainfall intensity (k_p)	mm	A	–	–	1.390	1.870	1.760	–	0.500	0.590	0.060	–
		B	–	–	5.450	11.710	1.860	–	0.940	4.530	0.014	–
		C	–	–	0.060	0.010	0.001	–	0.350	4.400	0.010	–
		D	–	–	1.680	–	1.850	–	0.080	0.110	0.010	–

Table 4.3.9: Results of hydraulic parameters of all study sites(A-D)

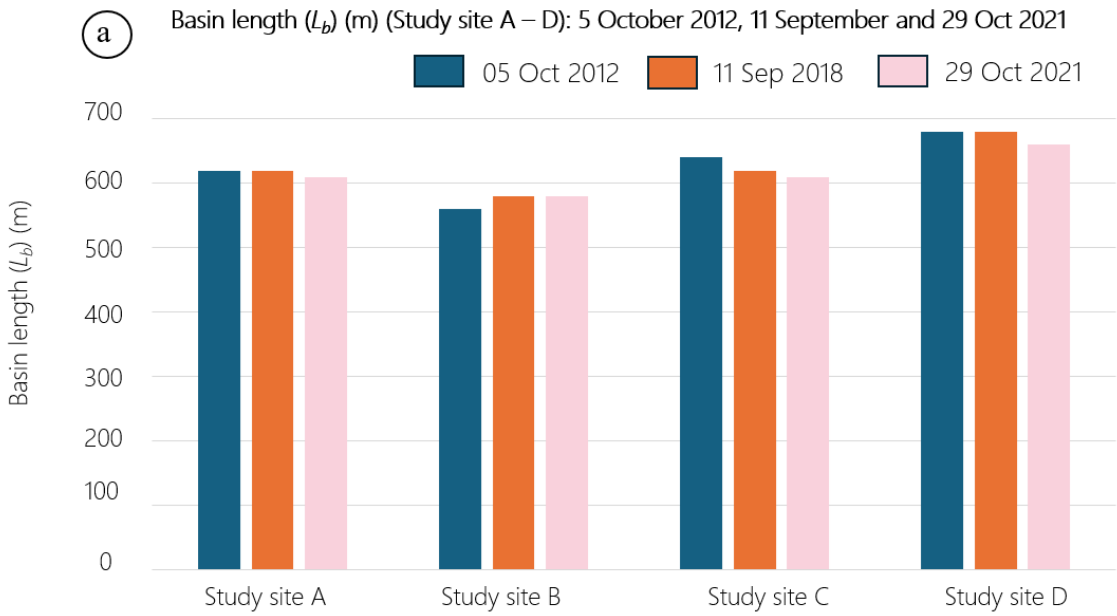
a
Basin length (L_b) (m) (Study site A – D): 5 October 2012, 11 September and 29 Oct 2021
05 Oct 2012
11 Sep 2018
29 Oct 2021
Basin length (L_b) (m)
700
600
500
400
300
200
100
0
Study site A
Study site B
Study site C
Study site D

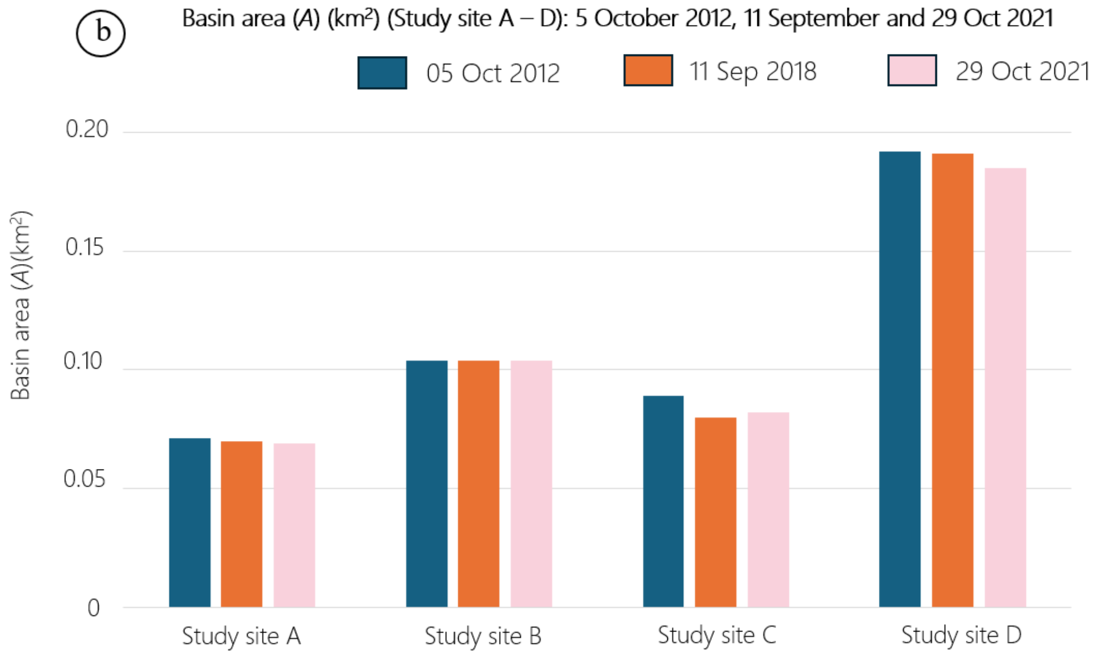
b
Basin area (A) (km²) (Study site A – D): 5 October 2012, 11 September and 29 Oct 2021
05 Oct 2012
11 Sep 2018
29 Oct 2021
Basin area (A)(km²)
0.20
0.15
0.10
0.05
0
Study site A
Study site B
Study site C
Study site D

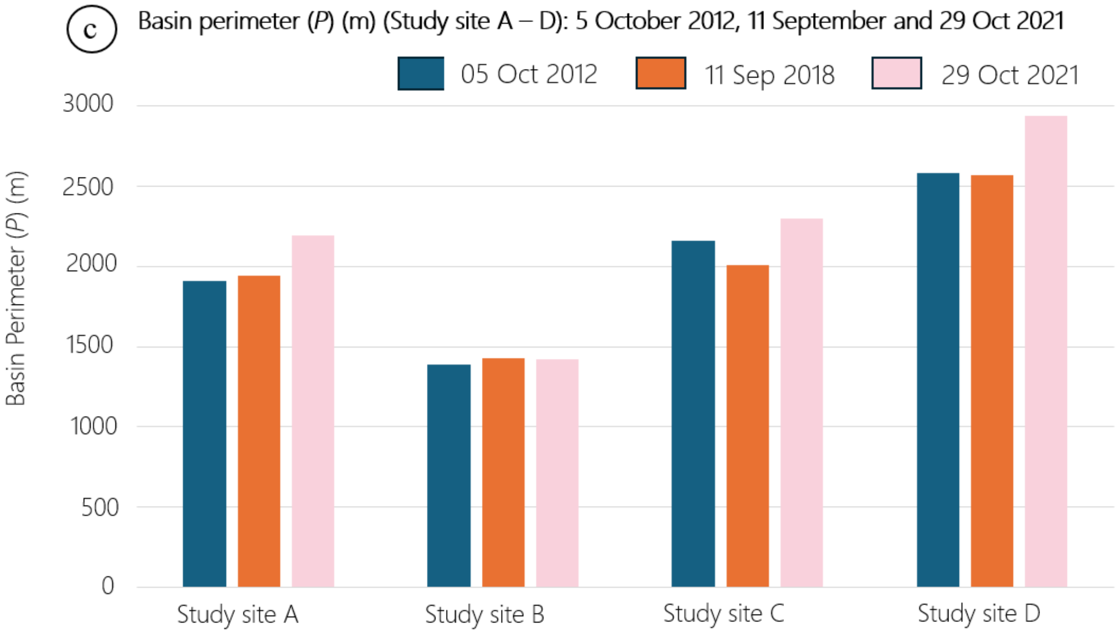
c
Basin perimeter (P) (m) (Study site A – D): 5 October 2012, 11 September and 29 Oct 2021
05 Oct 2012
11 Sep 2018
29 Oct 2021
Basin Perimeter (P) (m)
3000
2500
2000
1500
1000
500
0
Study site A
Study site B
Study site C
Study site D

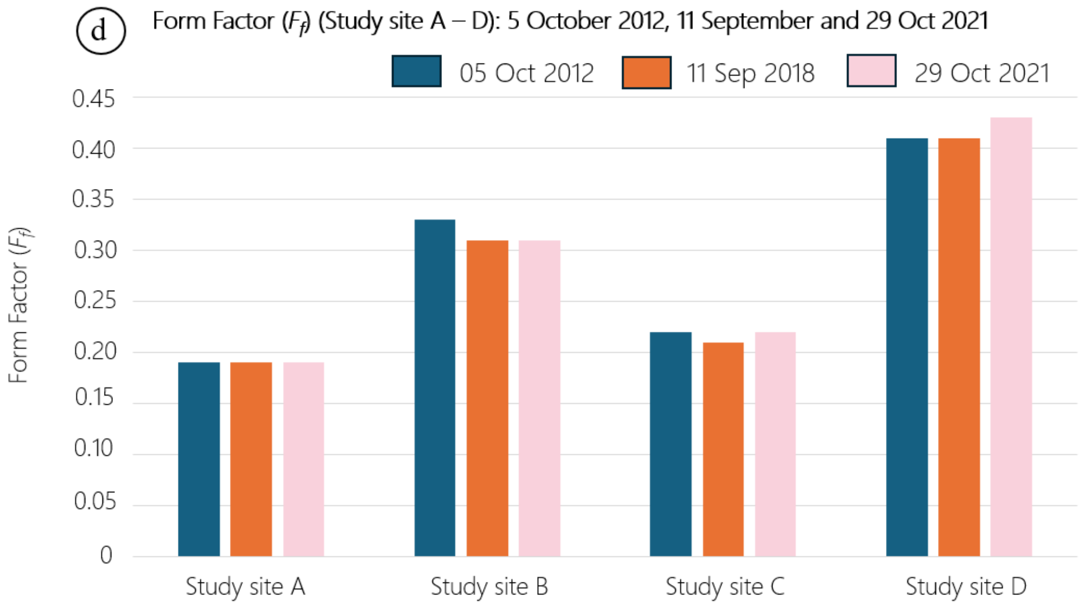
d
Form Factor (F_f) (Study site A – D): 5 October 2012, 11 September and 29 Oct 2021
05 Oct 2012
11 Sep 2018
29 Oct 2021
Form Factor (F_f)
0.45
0.40
0.35
0.30
0.25
0.20
0.15
0.10
0.05
0
Study site A
Study site B
Study site C
Study site D

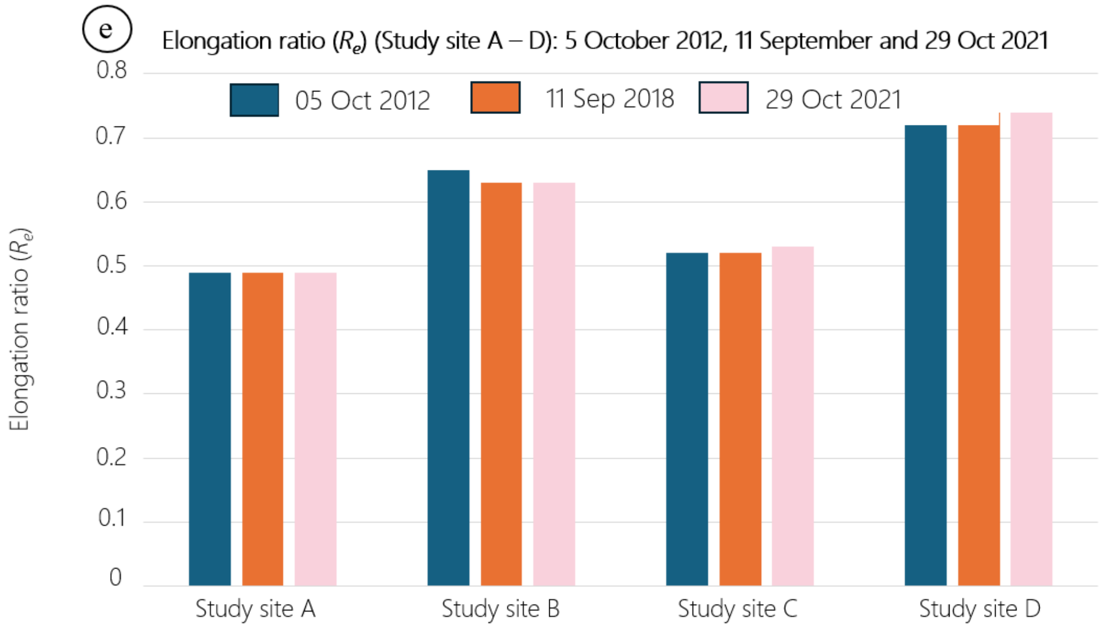
e
Elongation ratio (R_e) (Study site A – D): 5 October 2012, 11 September and 29 Oct 2021
05 Oct 2012
11 Sep 2018
29 Oct 2021
Elongation ratio (R_e)
0.8
0.7
0.6
0.5
0.4
0.3
0.2
0.1
0
Study site A
Study site B
Study site C
Study site D

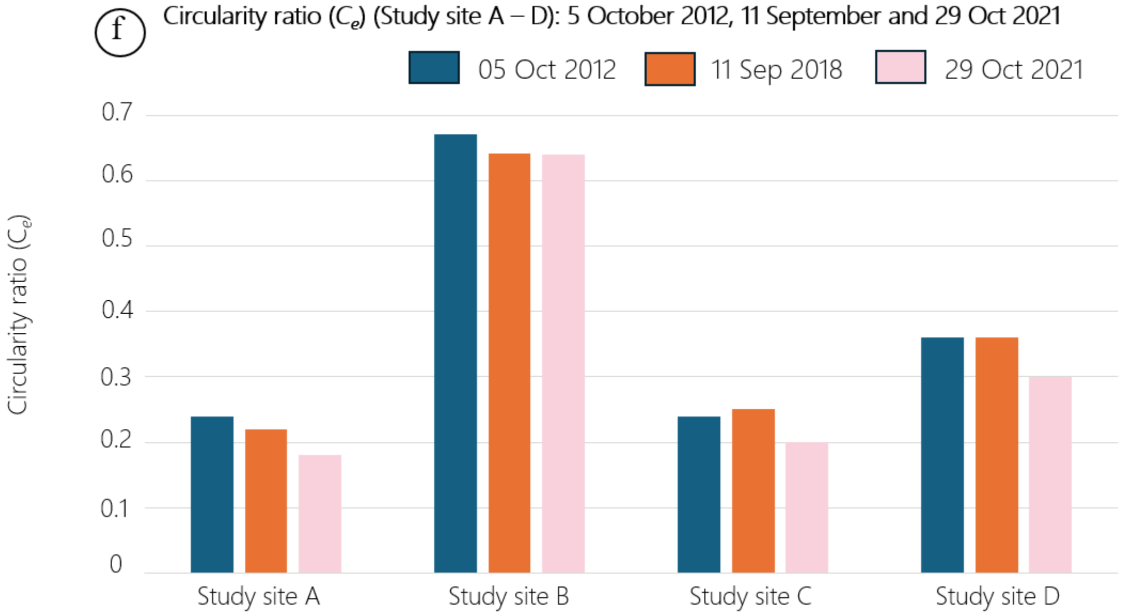
f
Circularity ratio (C_e) (Study site A – D): 5 October 2012, 11 September and 29 Oct 2021
05 Oct 2012
11 Sep 2018
29 Oct 2021
Circularity ratio (C_e)
0.7
0.6
0.5
0.4
0.3
0.2
0.1
0
Study site A
Study site B
Study site C
Study site D

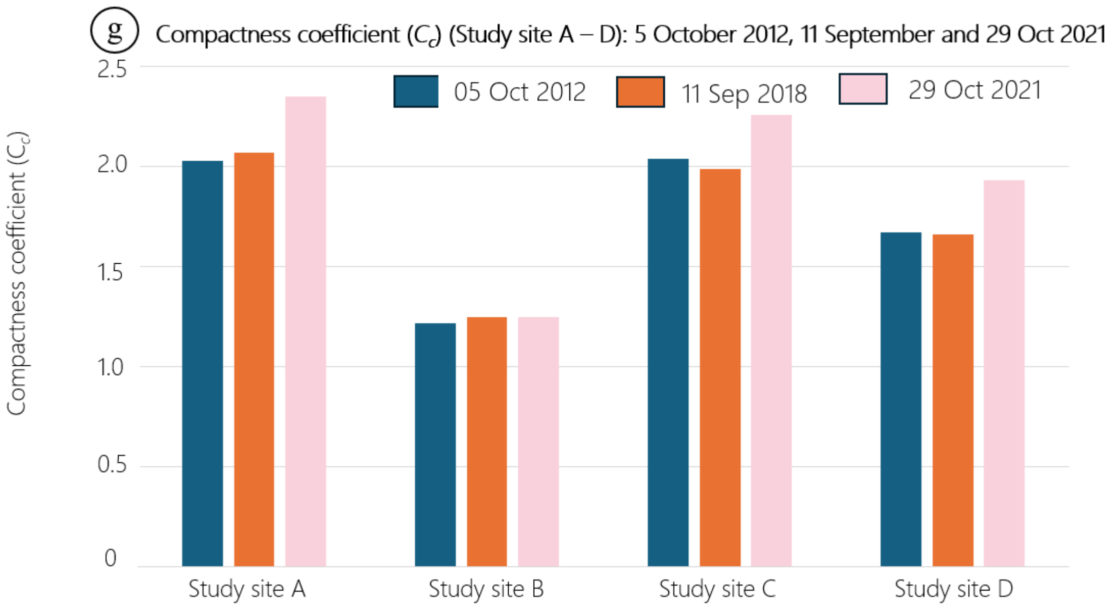

Figure 4.3.1: Results of parameters of watershed geometry (Study sites A-D). (a) Basin length (L_b), (b) Basin area (A), (c) Basin perimeter (P), (d) Form factor (F_f), (e) Elongation ratio (R_e), (f) Circularity ratio (R_c), (g) Compactness coefficient (C_c).

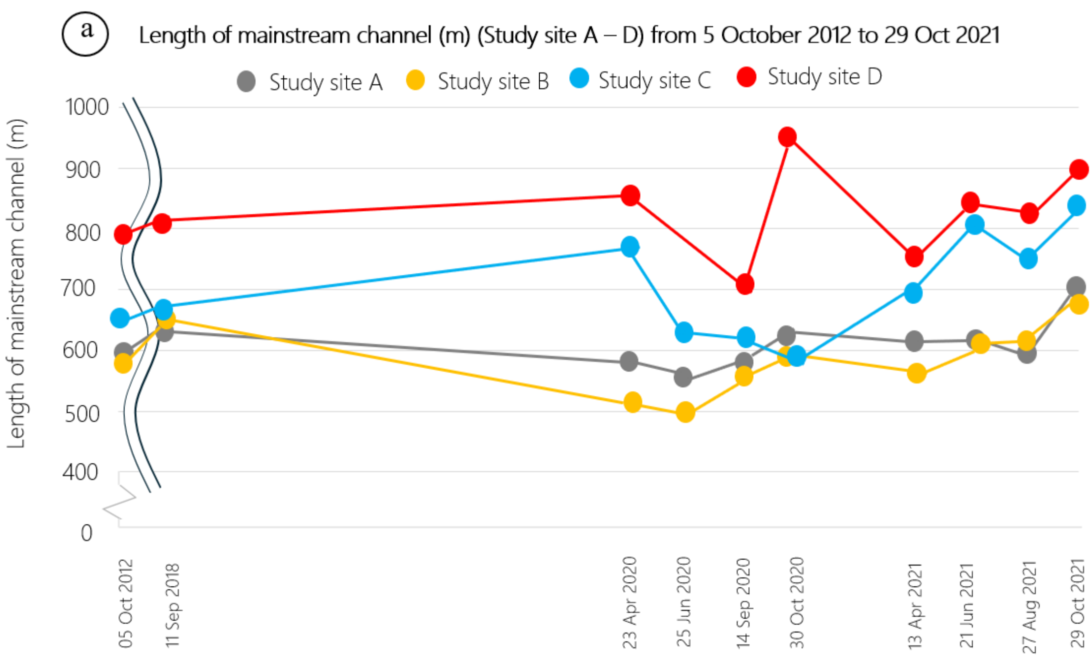

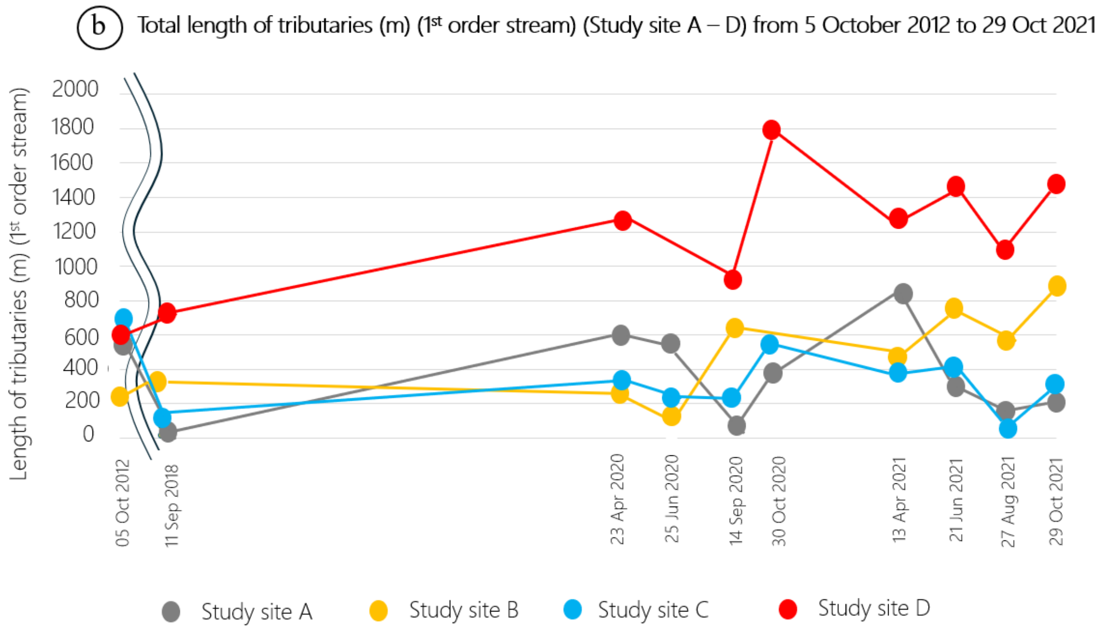
b
Total length of tributaries (m) (1st order stream) (Study site A – D) from 5 October 2012 to 29 Oct 2021
Length of tributaries (m) (1st order stream)
2000
1800
1600
1400
1200
1000
800
600
400
200
0
05 Oct 2012
11 Sep 2018
23 Apr 2020
25 Jun 2020
14 Sep 2020
30 Oct 2020
13 Apr 2021
21 Jun 2021
27 Aug 2021
29 Oct 2021
Study site A
Study site B
Study site C
Study site D

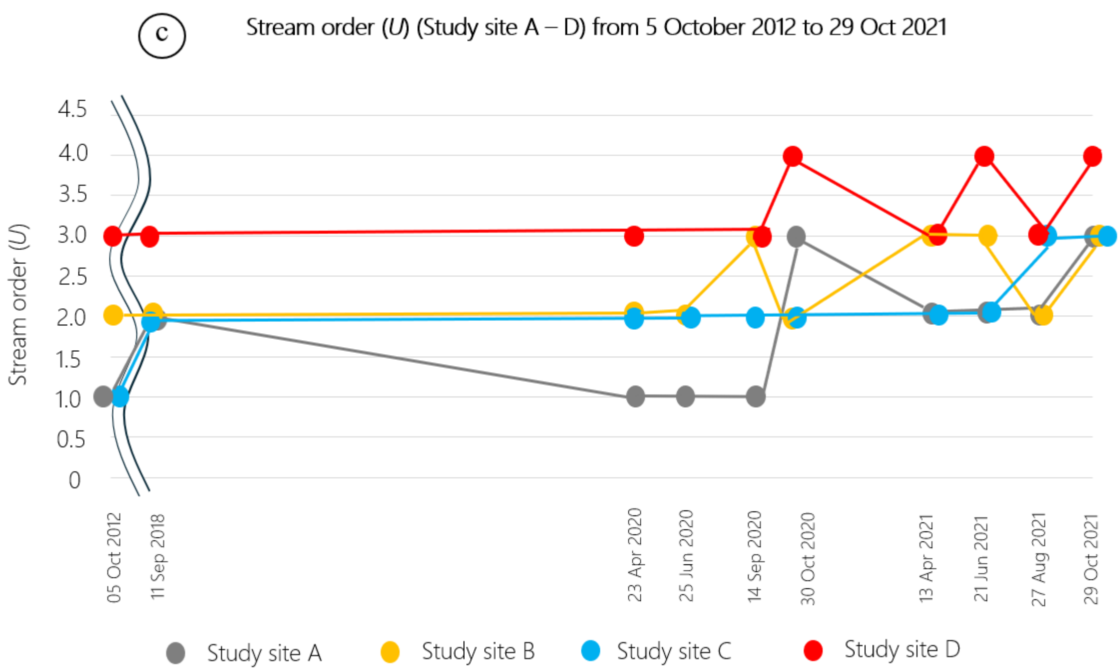
c
Stream order (U) (Study site A – D) from 5 October 2012 to 29 Oct 2021
Stream order (U)
4.5
4.0
3.5
3.0
2.5
2.0
1.5
1.0
0.5
0
05 Oct 2012
11 Sep 2018
23 Apr 2020
25 Jun 2020
14 Sep 2020
30 Oct 2020
13 Apr 2021
21 Jun 2021
27 Aug 2021
29 Oct 2021
Study site A
Study site B
Study site C
Study site D

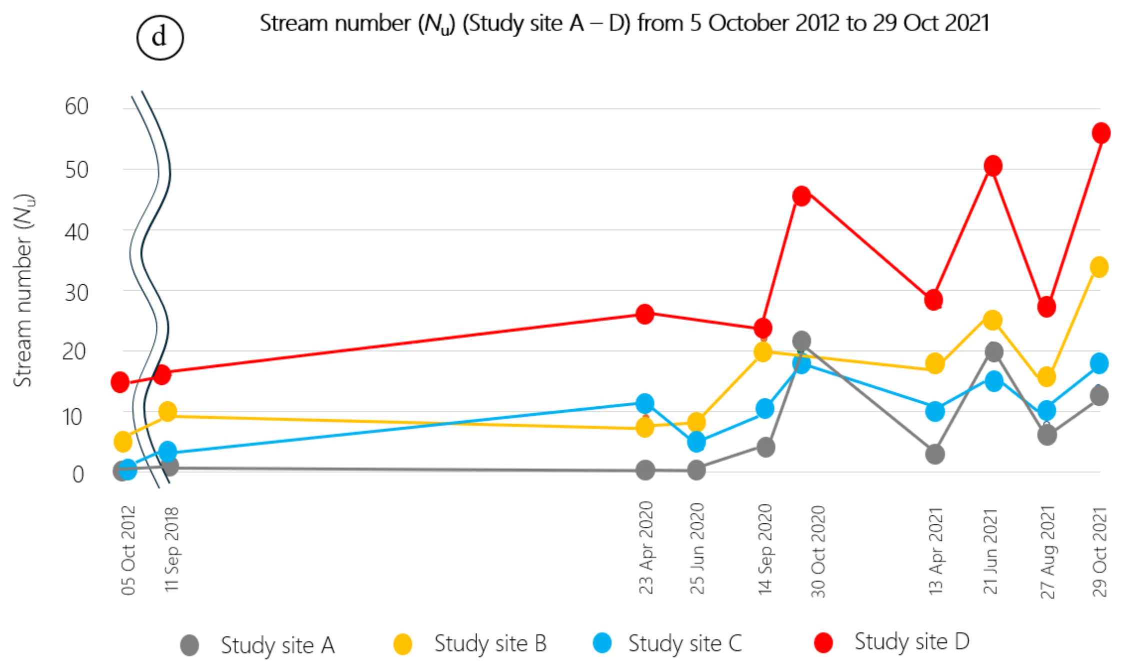
d
Stream number (N_u) (Study site A – D) from 5 October 2012 to 29 Oct 2021
Stream number (N_u)
60
50
40
30
20
10
0
05 Oct 2012
11 Sep 2018
23 Apr 2020
25 Jun 2020
14 Sep 2020
30 Oct 2020
13 Apr 2021
21 Jun 2021
27 Aug 2021
29 Oct 2021
Study site A
Study site B
Study site C
Study site D

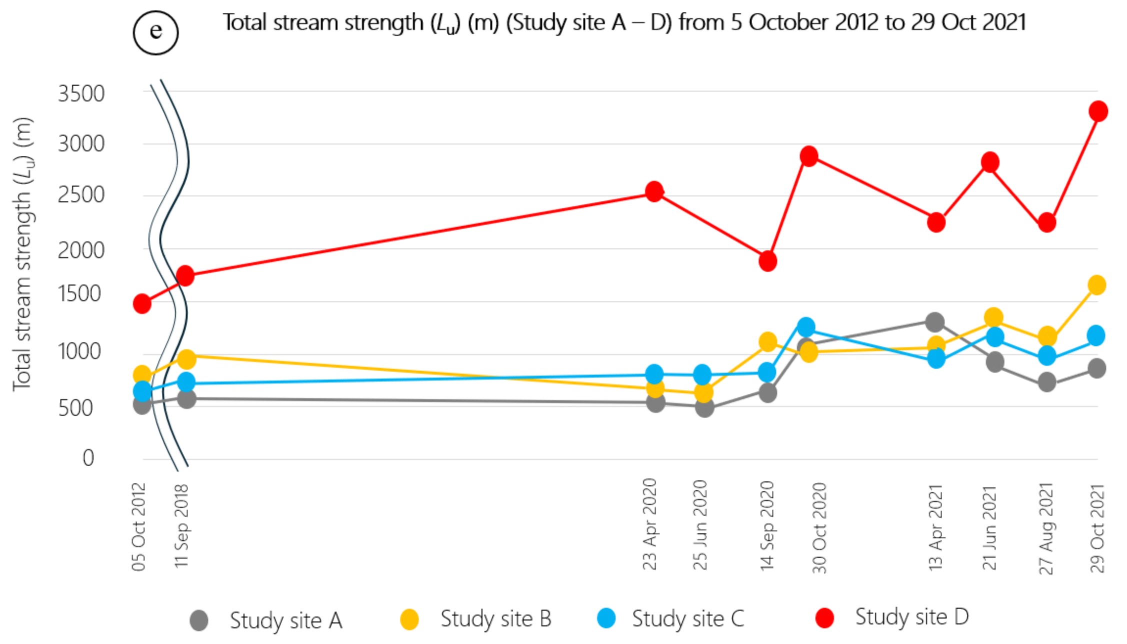
e
Total stream strength (L_u) (m) (Study site A – D) from 5 October 2012 to 29 Oct 2021
Total stream strength (L_u) (m)
3500
3000
2500
2000
1500
1000
500
0
05 Oct 2012
11 Sep 2018
23 Apr 2020
25 Jun 2020
14 Sep 2020
30 Oct 2020
13 Apr 2021
21 Jun 2021
27 Aug 2021
29 Oct 2021
Study site A
Study site B
Study site C
Study site D

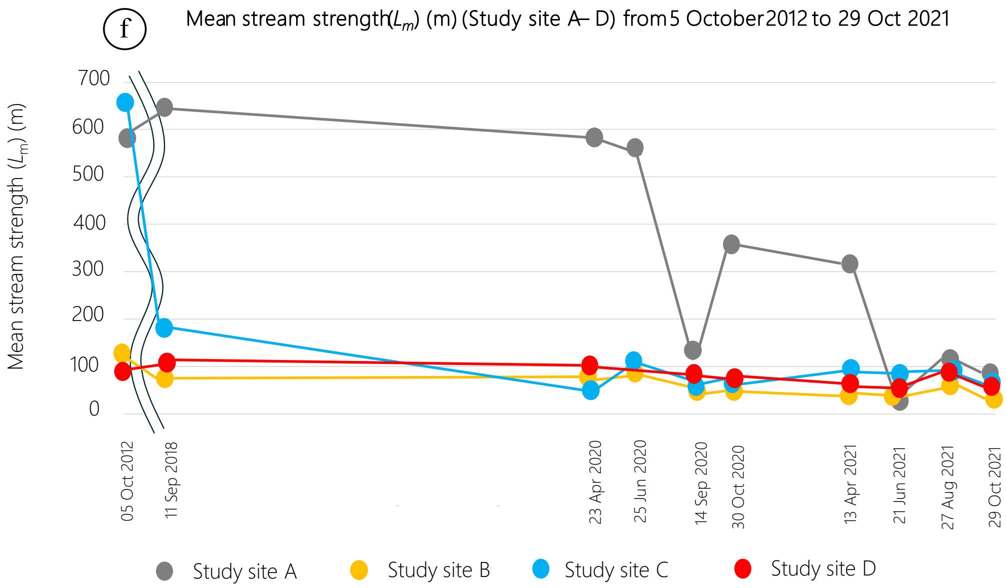

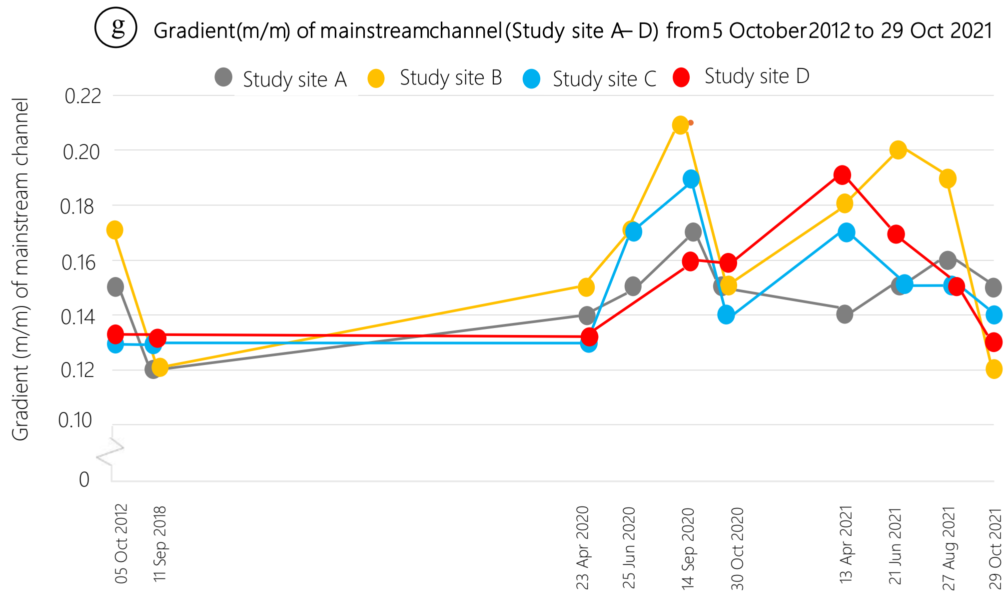

Figure 4.3.2: Results of parameters of drainage network (Study sites A-D). (a) Length of main stream channel , (b) Total length of tributaries, (c) Stream order (U), (d) Stream number (N_u), (e) Total stream length (L_u), (f) Mean stream length (L_m), (g) Gradient of mainstream.

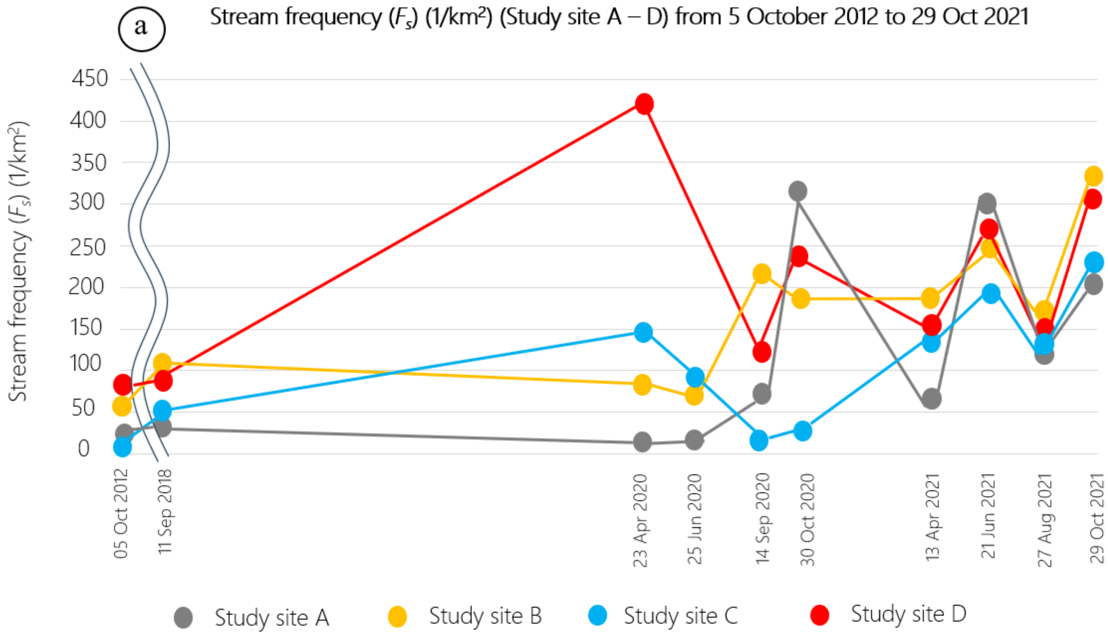

a
Stream frequency (F_s) (1/km²) (Study site A – D) from 5 October 2012 to 29 Oct 2021
Stream frequency (F_s) (1/km²)
450
400
350
300
250
200
150
100
50
0
05 Oct 2012
11 Sep 2018
23 Apr 2020
25 Jun 2020
14 Sep 2020
30 Oct 2020
13 Apr 2021
21 Jun 2021
27 Aug 2021
29 Oct 2021
Study site A
Study site B
Study site C
Study site D

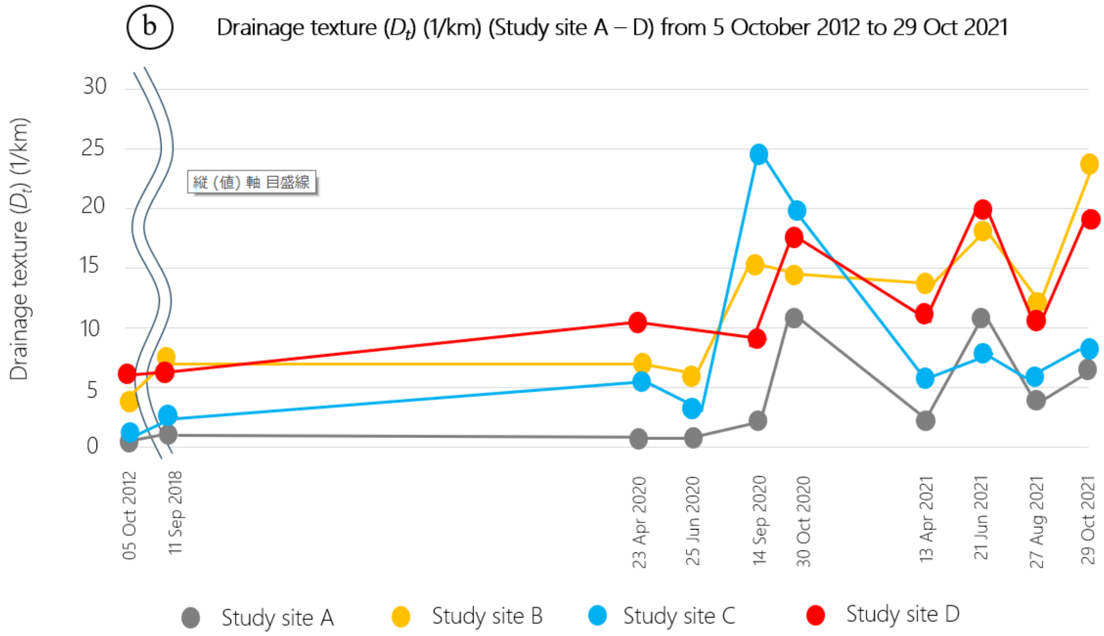

b
Drainage texture (D_t) (1/km) (Study site A – D) from 5 October 2012 to 29 Oct 2021
Drainage texture (D_t) (1/km)
30
25
20
15
10
5
0
縦 (値) 軸 目盛線
05 Oct 2012
11 Sep 2018
23 Apr 2020
25 Jun 2020
14 Sep 2020
30 Oct 2020
13 Apr 2021
21 Jun 2021
27 Aug 2021
29 Oct 2021
Study site A
Study site B
Study site C
Study site D

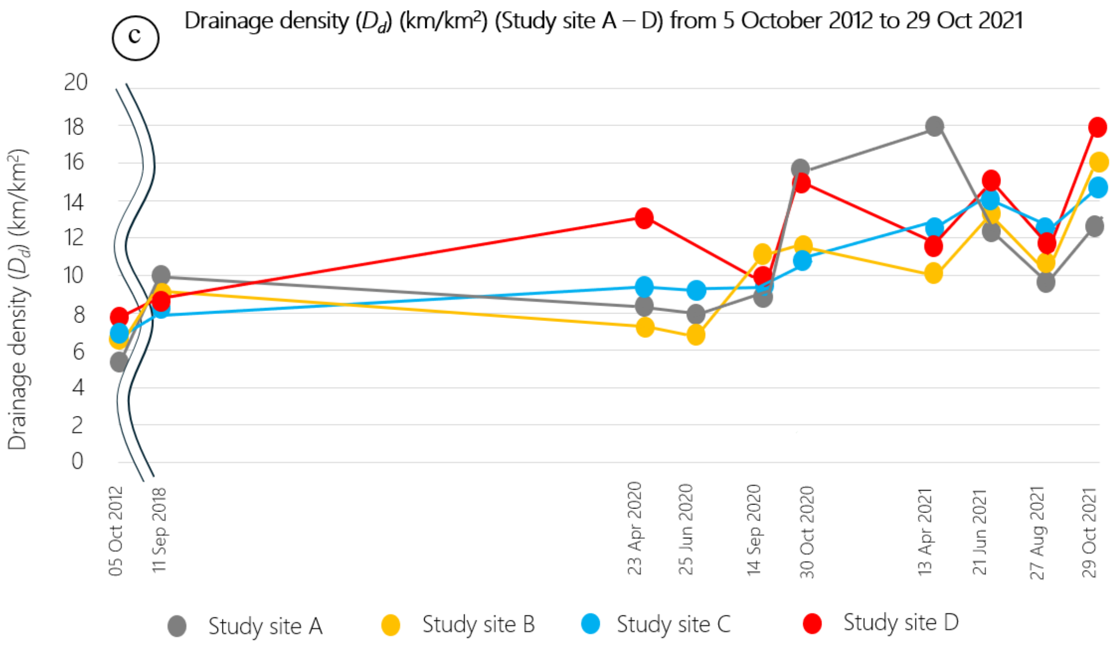
c
Drainage density (D_d) (km/km²) (Study site A – D) from 5 October 2012 to 29 Oct 2021
Drainage density (D_d) (km/km²)
20
18
16
14
12
10
8
6
4
2
0
05 Oct 2012
11 Sep 2018
23 Apr 2020
25 Jun 2020
14 Sep 2020
30 Oct 2020
13 Apr 2021
21 Jun 2021
27 Aug 2021
29 Oct 2021
Study site A
Study site B
Study site C
Study site D

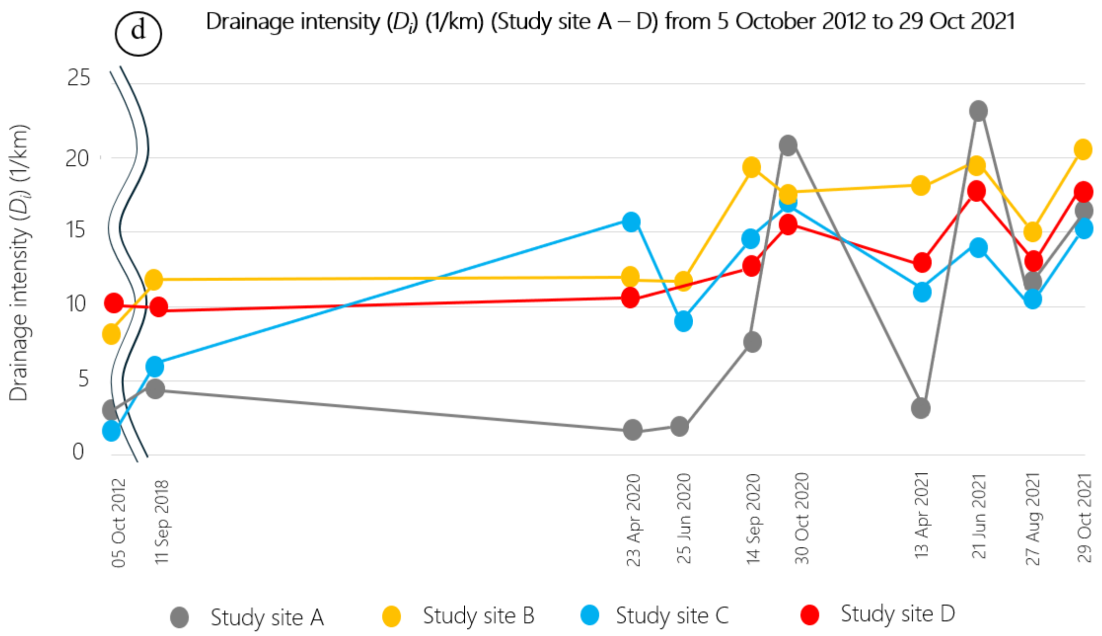
d
Drainage intensity (D_i) (1/km) (Study site A – D) from 5 October 2012 to 29 Oct 2021
Drainage intensity (D_i) (1/km)
25
20
15
10
5
0
05 Oct 2012
11 Sep 2018
23 Apr 2020
25 Jun 2020
14 Sep 2020
30 Oct 2020
13 Apr 2021
21 Jun 2021
27 Aug 2021
29 Oct 2021
Study site A
Study site B
Study site C
Study site D

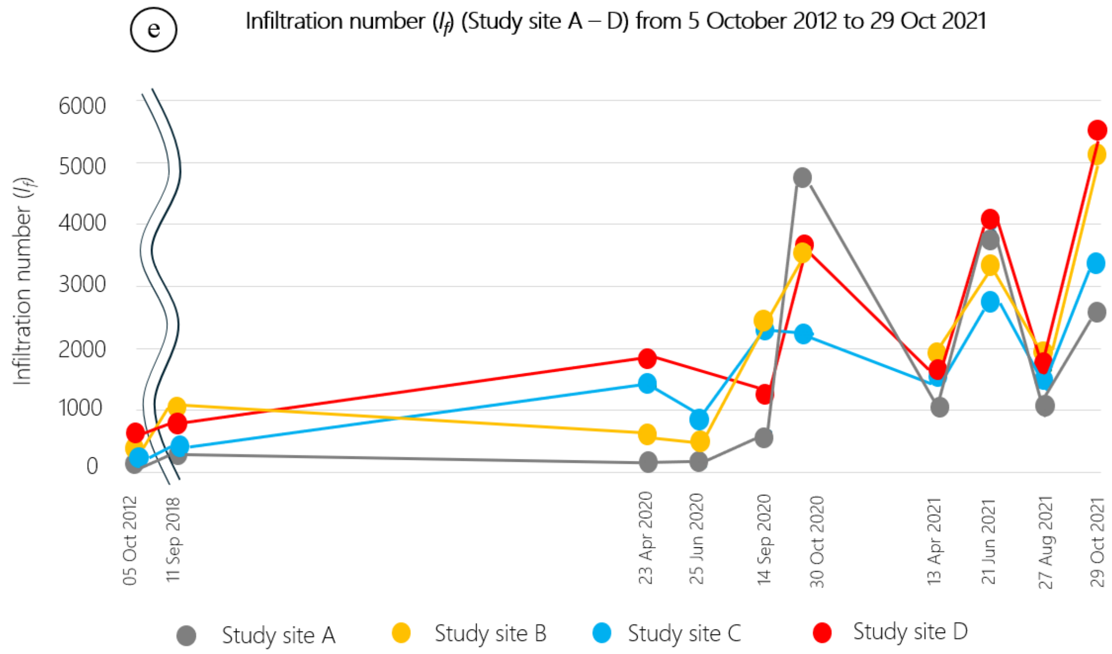
e
Infiltration number (I_f) (Study site A – D) from 5 October 2012 to 29 Oct 2021
Infiltration number (I_f)
6000
5000
4000
3000
2000
1000
0
05 Oct 2012
11 Sep 2018
23 Apr 2020
25 Jun 2020
14 Sep 2020
30 Oct 2020
13 Apr 2021
21 Jun 2021
27 Aug 2021
29 Oct 2021
Study site A
Study site B
Study site C
Study site D

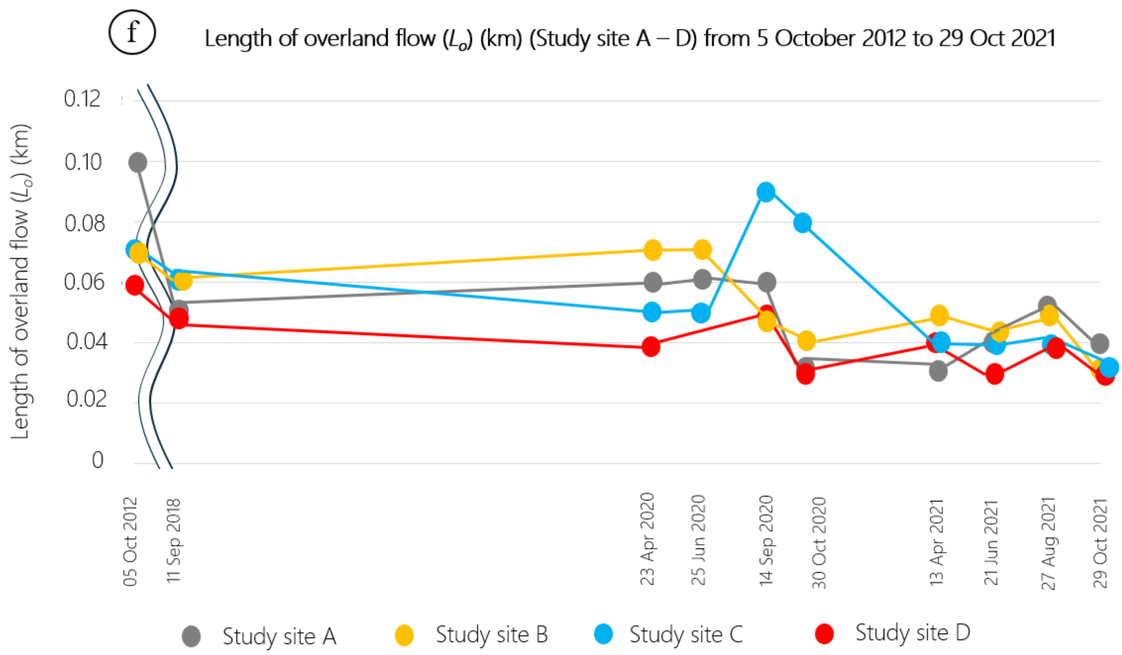
f
Length of overland flow (L_o) (km) (Study site A – D) from 5 October 2012 to 29 Oct 2021
Length of overland flow (L_o) (km)
0.12
0.10
0.08
0.06
0.04
0.02
0
05 Oct 2012
11 Sep 2018
23 Apr 2020
25 Jun 2020
14 Sep 2020
30 Oct 2020
13 Apr 2021
21 Jun 2021
27 Aug 2021
29 Oct 2021
Study site A
Study site B
Study site C
Study site D

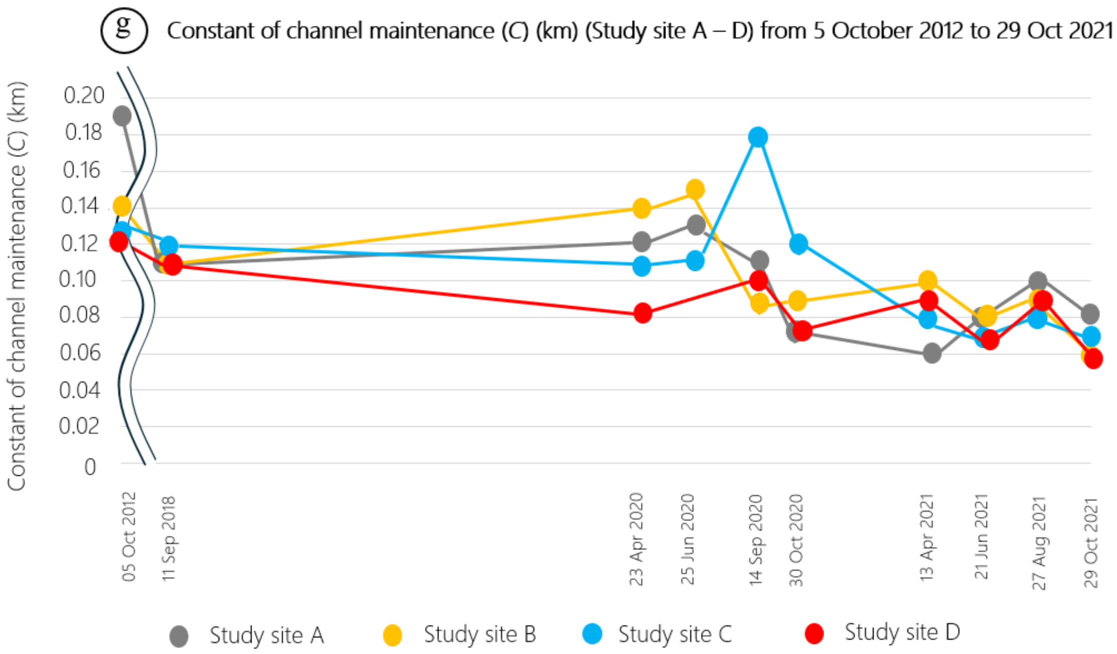

Figure 4.3.3: Results of parameters of drainage texture (Study sites A-D). (a) Stream frequency (F_s), (b) Drainage texture (D_t), (c) Drainage density (Dd), (d) Drainage intensity (D_i), (e) Infiltration number (I_f), (f) Length of overland flow (L_o), (g) Constant of channel maintenance (C).

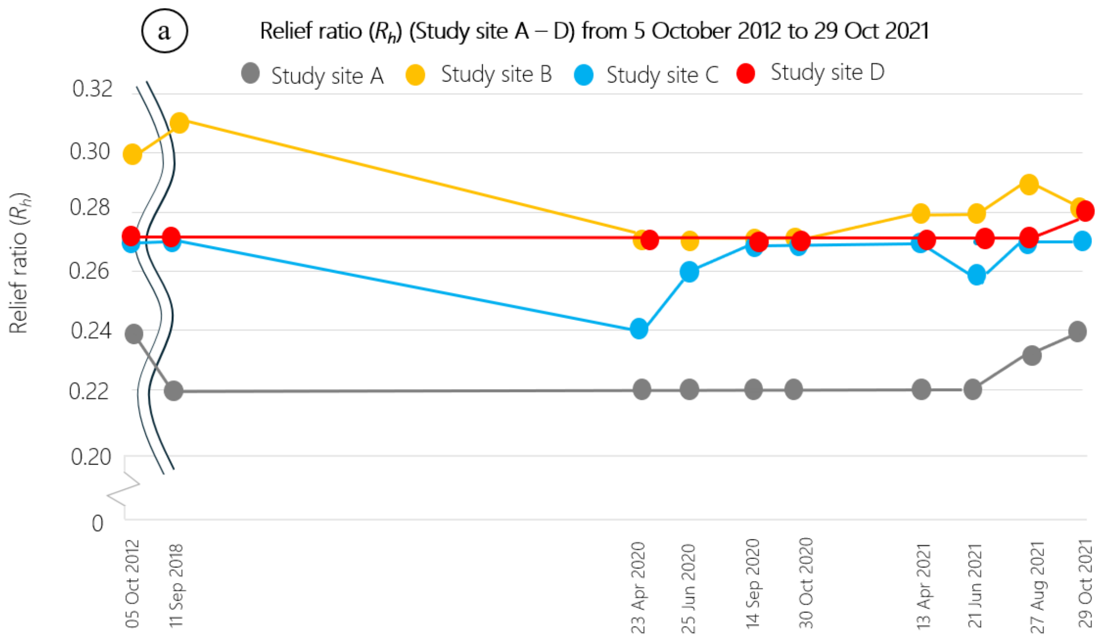

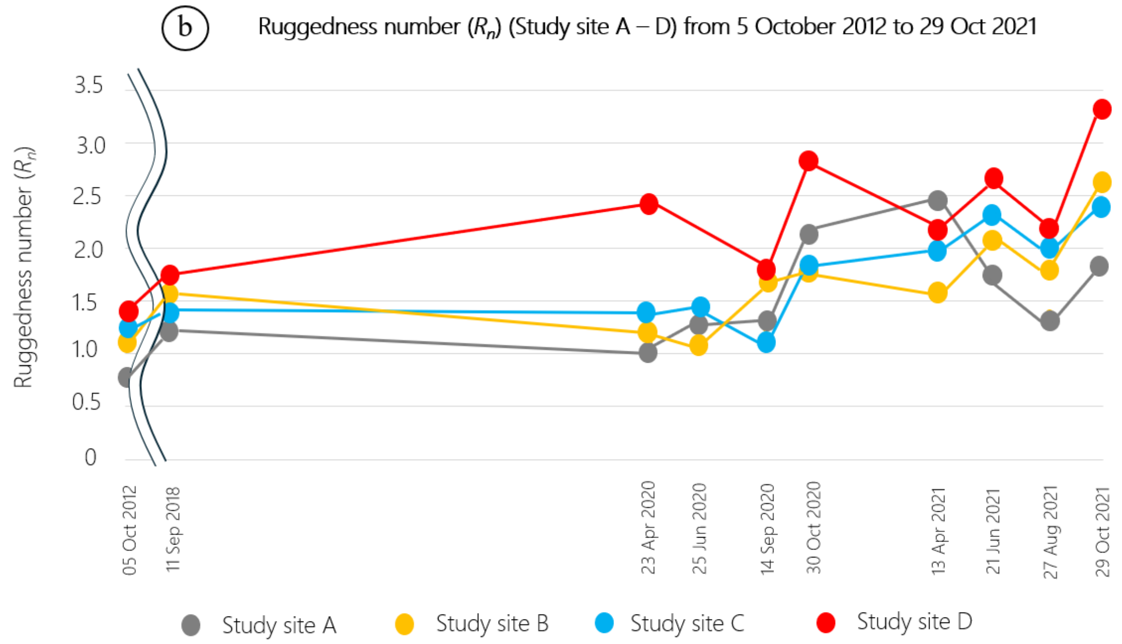

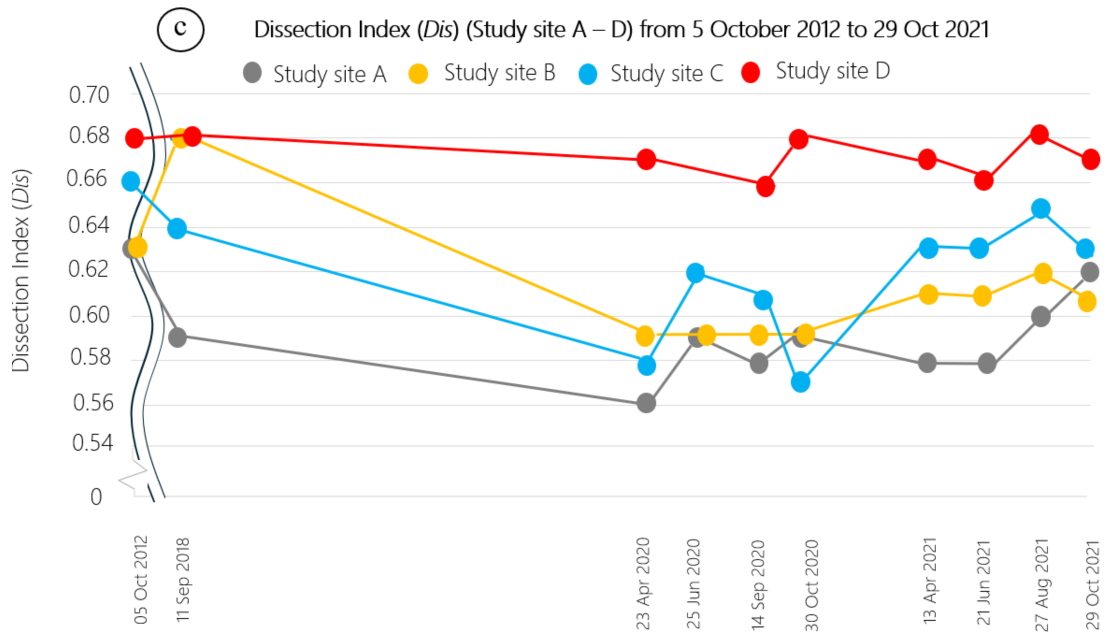

Figure 4.3.4:.Results of parameters of relief characteristics (Study sites A-D). (a) Relief ratio (R_h), (b) Ruggedness number (R_n), (c) Dissection Index (*Dis*).

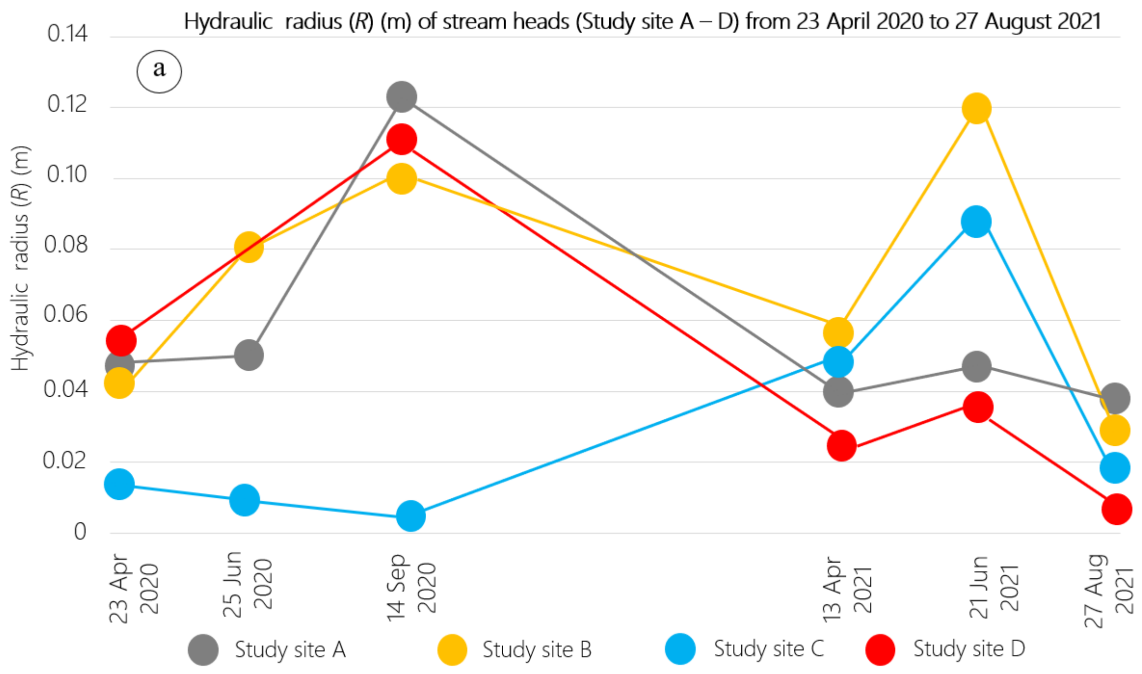
Hydraulic radius (R) (m) of stream heads (Study site A – D) from 23 April 2020 to 27 August 2021
a
Hydraulic radius (R) (m)
0.14
0.12
0.10
0.08
0.06
0.04
0.02
0
23 Apr 2020
25 Jun 2020
14 Sep 2020
13 Apr 2021
21 Jun 2021
27 Aug 2021
Study site A
Study site B
Study site C
Study site D

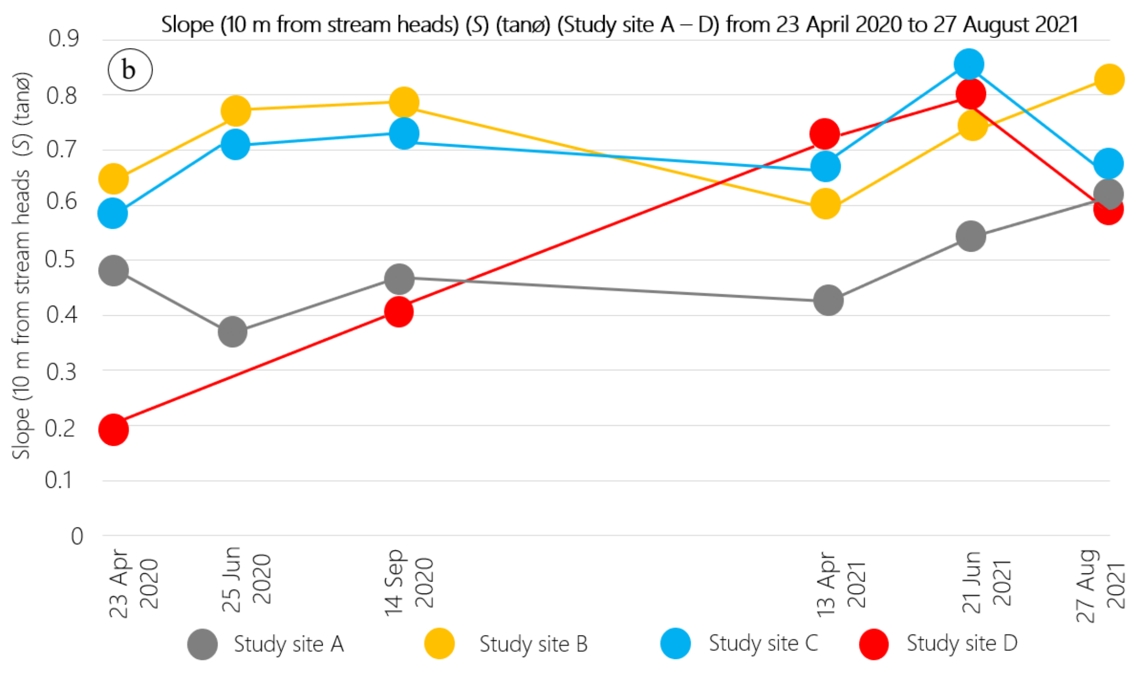
Slope (10 m from stream heads) (S) (tanø) (Study site A – D) from 23 April 2020 to 27 August 2021
b
Slope (10 m from stream heads (S) (tanø)
0.9
0.8
0.7
0.6
0.5
0.4
0.3
0.2
0.1
0
23 Apr 2020
25 Jun 2020
14 Sep 2020
13 Apr 2021
21 Jun 2021
27 Aug 2021
Study site A
Study site B
Study site C
Study site D

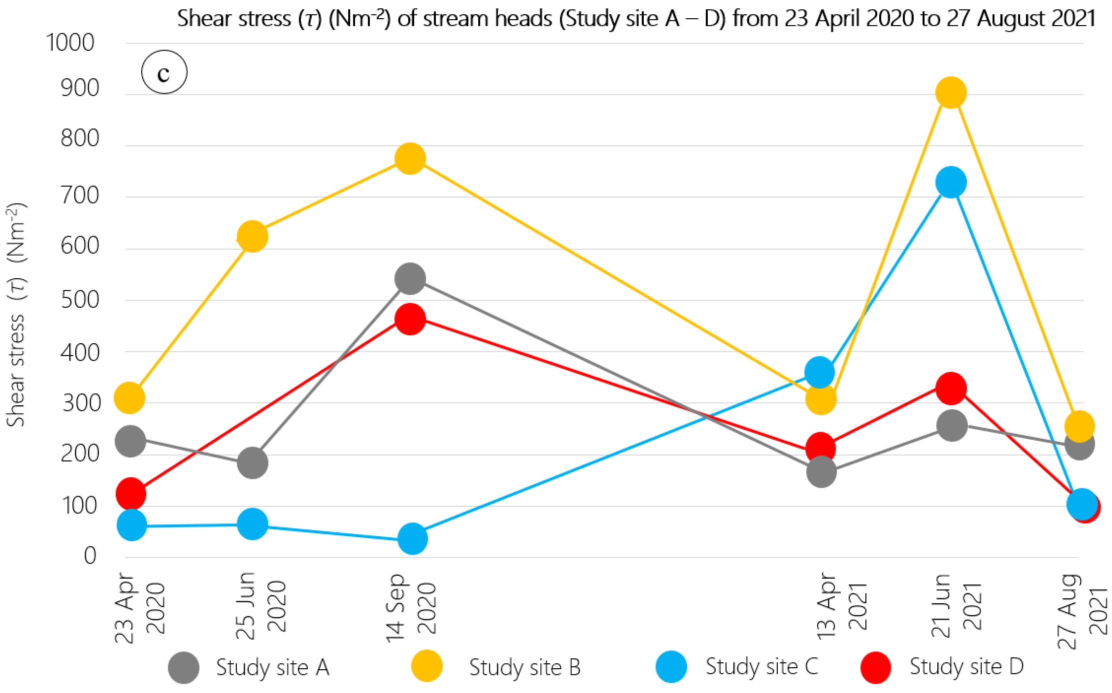
Shear stress (τ) (Nm-2) of stream heads (Study site A – D) from 23 April 2020 to 27 August 2021
c
Shear stress (τ) (Nm-2)
1000
900
800
700
600
500
400
300
200
100
0
23 Apr 2020
25 Jun 2020
14 Sep 2020
13 Apr 2021
21 Jun 2021
27 Aug 2021
Study site A
Study site B
Study site C
Study site D

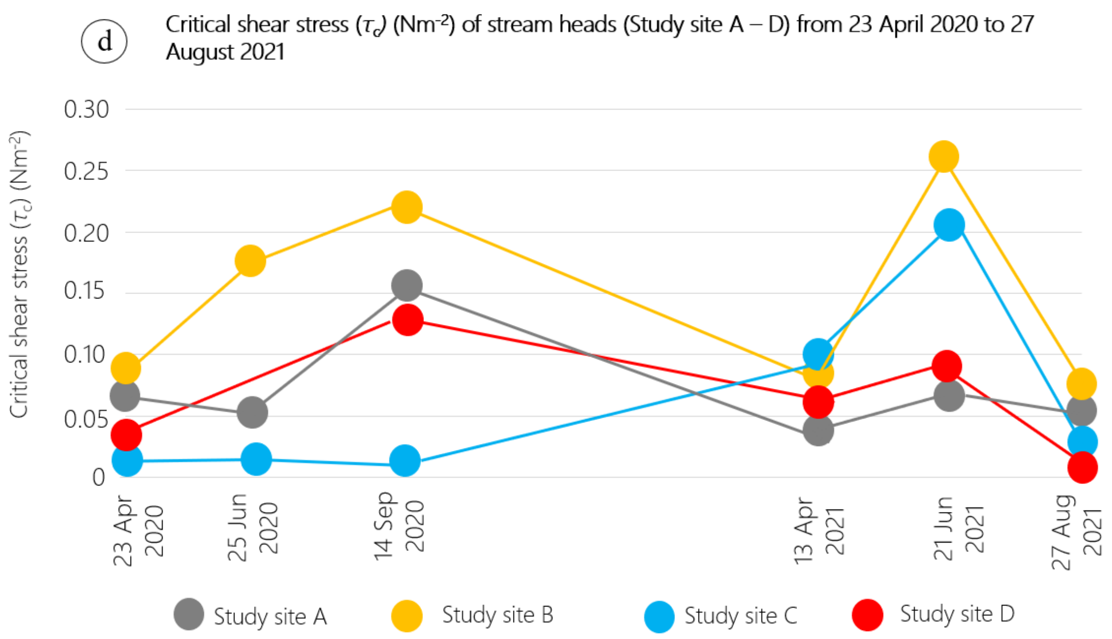
d
Critical shear stress (τc) (Nm-2) of stream heads (Study site A – D) from 23 April 2020 to 27 August 2021
Critical shear stress (τc) (Nm-2)
0.30
0.25
0.20
0.15
0.10
0.05
0
23 Apr 2020
25 Jun 2020
14 Sep 2020
13 Apr 2021
21 Jun 2021
27 Aug 2021
Study site A
Study site B
Study site C
Study site D

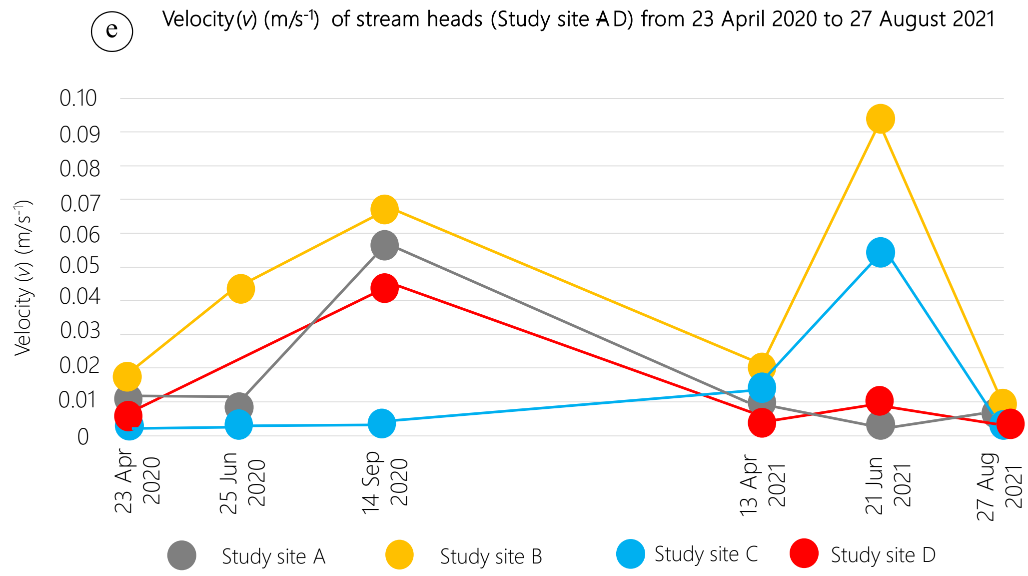

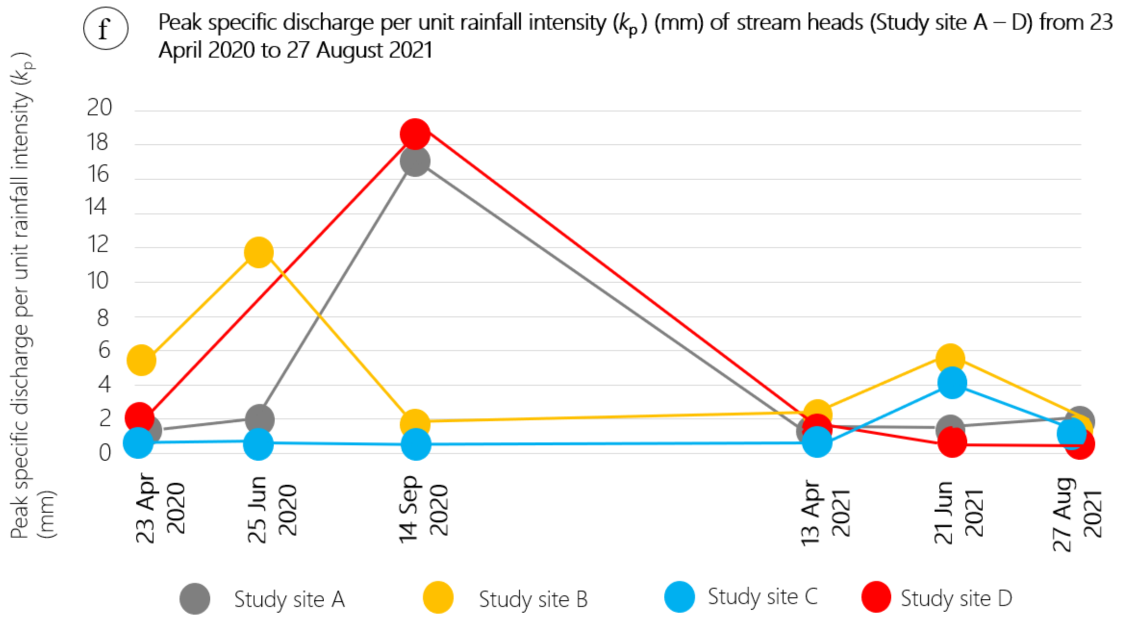

Figure 4.3.5: Results of hydrological parameters (Study sites A-D). (a) Hydraulic radius (R), (b) Slope (10m from stream head) (S), (c) Shear stress (τ), (d) Critical shear stress (τ_c), (e) Velocity (v), (f) Peak specific discharge per unit rainfall intensity (k_p).

Study site A	Date	Oct 05, 2012 - Oct 29, 2021
Geomorphometric parameters	Unit	Average
Watershed geometry		
Basin length (L_b)	m	613.30
Basin area (A)	m^2	69989
Basin Perimeter (P)	m	2014.85
Form factor (F_f)	–	0.19
Elongation ratio (R_e)	–	0.49
Circularity ratio (R_c)	–	0.22
Compactness coefficient (C_c)	–	2.08
Drainage network		
Length of mainstream channel	m	608.93
Total length of tributaries (1st order stream)	m	368.06
Stream order (U)	–	2
Stream number (N_u)	–	8
Total stream length (L_u)	m	780.71
Mean stream length (L_m)	m	335.72
Stream length ratio (R_L)	–	–
Bifurcation ratio (R_b)	–	–
Gradient of mainstream	m/m	0.15
Drainage texture		
Stream frequency (F_s)	$1/km^2$	114.14
Drainage texture (D_t)	1/km	4.03
Drainage density (D_d)	km/km^2	10.83
Drainage intensity (D_i)	1/km	9.31
Infiltration number (I_f)	–	1468.46
Length of overland flow (L_o)	km	0.05
Constant of channel maintenance (C)	km^2/km	0.11
Relief characteristics		
Height of basin outlet (Z_{min})	m	175.23
Maximum height of basin (Z_{max})	m	235.29
Total basin relief (H)	m	139.24
Relief ratio (R_h)	–	0.23
Ruggedness number (R_n)	km/km^2	1.52
Dissection index (D_{is})		0.59
		Apr 23, 2020 - Aug 27, 2021
Hydraulic Parameters		Average
Hydraulic radius (R)	m	0.06
Slope (10 m from stream head) (S)	tanø	0.49
Shear stress (τ)	Nm^{-2}	269.74
Critical shear stress (τ_c)	Nm^{-2}	0.077
Velocity (v)	$m\ s^{-1}$	0.017
Peak specific discharge per unit rainfall intensity (k_p)	mm	1.028

Table 4.3.10. Average value of 35 geomorphometric and hydraulic parameters of drainage basin characteristics in the study site A during investigation periods.

Study site B	Date	Oct 05, 2012 - Oct 29, 2021
Geomorphometric parameters	Unit	Average
Watershed geometry		
Basin length (L_b)	m	573.17
Basin area (A)	m^2	103972
Basin Perimeter (P)	m	1414.37
Form factor (F_f)	–	0.32
Elongation ratio (R_e)	–	0.64
Circularity ratio (R_c)	–	0.65
Compactness coefficient (C_c)	–	1.24
Drainage network		
Length of mainstream channel	m	587.86
Total length of tributaries (1st order stream)	m	486.89
Stream order (U)	–	2
Stream number (N_u)	–	17
Total stream length (L_u)	m	1060.92
Mean stream length (L_m)	m	70.91
Stream length ratio (R_L)	–	–
Bifurcation ratio (R_b)	–	–
Gradient of mainstream	m/m	0.17
Drainage texture		
Stream frequency (F_s)	$1/km^2$	165.39
Drainage texture (D_t)	1/km	12.01
Drainage density (D_d)	km/km^2	10.21
Drainage intensity (D_i)	1/km	15.27
Infiltration number (I_f)	–	1909.32
Length of overland flow (L_o)	km	0.05
Constant of channel maintenance (C)	km^2/km	0.11
Relief characteristics		
Height of basin outlet (Z_{min})	m	103.88
Maximum height of basin (Z_{max})	m	267.30
Total basin relief (H)	m	163.68
Relief ratio (R_h)	–	0.28
Ruggedness number (R_n)	km/km^2	1.67
Dissection index (D_{is})		0.61
		Apr 23, 2020 - Aug 27, 2021
Hydraulic Parameters		Average
Hydraulic radius (R)	m	0.07
Slope (10 m from stream head) (S)	tanø	0.73
Shear stress (τ)	Nm^{-2}	529.00
Critical shear stress (τ_c)	Nm^{-2}	0.15
Velocity (v)	$m\,s^{-1}$	0.040
Peak specific discharge per unit rainfall intensity (k_p)	mm	4.084

Table 4.3.11. Average value of 35 geomorphometric and hydraulic parameters of drainage basin characteristics in the study site B during investigation periods

Study site C	Date	Oct 05, 2012 - Oct 29, 2021
Geomorphometric parameters	Unit	Average
Watershed geometry		
Basin length (L_b)	m	621.13
Basin area (A)	m^2	86297
Basin Perimeter (P)	m	2155.16
Form factor (F_f)	–	0.22
Elongation ratio (R_e)	–	0.52
Circularity ratio (R_c)	–	0.23
Compactness coefficient (C_c)	–	2.10
Drainage network		
Length of mainstream channel	m	703.99
Total length of tributaries (1st order stream)	m	317.84
Stream order (U)	–	2
Stream number (N_u)	–	11
Total stream length (L_u)	m	922.63
Mean stream length (L_m)	m	145.68
Stream length ratio (R_L)	–	–
Bifurcation ratio (R_b)	–	–
Gradient of mainstream	m/m	0.15
Drainage texture		
Stream frequency (F_s)	$1/km^2$	102.74
Drainage texture (D_t)	1/km	8.32
Drainage density (D_d)	km/km^2	9.05
Drainage intensity (D_i)	1/km	11.46
Infiltration number (I_f)	–	1798.93
Length of overland flow (L_o)	km	0.06
Constant of channel maintenance (C)	km^2/km	0.11
Relief characteristics		
Height of basin outlet (Z_{min})	m	97.62
Maximum height of basin (Z_{max})	m	258.45
Total basin relief (H)	m	160.83
Relief ratio (R_h)	–	0.27
Ruggedness number (R_n)	km/km^2	1.63
Dissection index (D_{is})		0.62
		Apr 23, 2020 - Aug 27, 2021
Hydraulic Parameters		Average
Hydraulic radius (R)	m	0.03
Slope (10 m from stream head) (S)	tanø	0.70
Shear stress (τ)	Nm^{-2}	224.37
Critical shear stress (τ_c)	Nm^{-2}	0.064
Velocity (v)	$m\ s^{-1}$	0.013
Peak specific discharge per unit rainfall intensity (k_p)	mm	0.805

Table 4.3.12. Average value of 35 geomorphometric and hydraulic parameters of drainage basin characteristics in the study site C during investigation periods

Study site D	Date	Oct 05, 2012 - Oct 29, 2021
Geomorphometric parameters	Unit	Average
Watershed geometry		
Basin length (L_b)	m	674.85
Basin area (A)	m^2	189598
Basin Perimeter (P)	m	2696.49
Form factor (F_f)	–	0.42
Elongation ratio (R_e)	–	0.73
Circularity ratio (R_c)	–	0.34
Compactness coefficient (C_c)	–	1.75
Drainage network		
Length of mainstream channel	m	743.13
Total length of tributaries (1st order stream)	m	1064.28
Stream order (U)	–	3
Stream number (N_u)	–	29
Total stream length (L_u)	m	2119.21
Mean stream length (L_m)	m	68.77
Stream length ratio (R_L)	–	–
Bifurcation ratio (R_b)	–	–
Gradient of mainstream	m/m	0.14
Drainage texture		
Stream frequency (F_s)	$1/km^2$	182.05
Drainage texture (D_t)	1/km	11.15
Drainage density (D_d)	km/km^2	11.14
Drainage intensity (D_i)	1/km	11.96
Infiltration number (I_f)	–	2115.78
Length of overland flow (L_o)	km	0.04
Constant of channel maintenance (C)	km^2/km	0.08
Relief characteristics		
Height of basin outlet (Z_{min})	m	81.29
Maximum height of basin (Z_{max})	m	247.86
Total basin relief (H)	m	166.58
Relief ratio (R_h)	–	0.24
Ruggedness number (R_n)	km/km^2	2.06
Dissection index (D_{is})		0.61
		Apr 23, 2020 - Aug 27, 2021
Hydraulic Parameters		Average
Hydraulic radius (R)	m	0.05
Slope (10 m from stream head) (S)	tanø	0.37
Shear stress (τ)	Nm^{-2}	205.39
Critical shear stress (τ_c)	Nm^{-2}	0.051
Velocity (v)	$m\,s^{-1}$	0.011
Peak specific discharge per unit rainfall intensity (k_p)	mm	0.622

Table 4.3.13. Average value of 35 geomorphometric and hydraulic parameters of drainage basin characteristics in the study site D during investigation periods

4.4 Quantitative analysis of Landslide (Areas with elevation decrease) mobility and sediment connectivity

Quantitative analysis of Landslide (Areas with elevation decrease) mobility including Landslide (elevation decreased) area (m^2), Sedimentation (elevation increased) area (m^2), Volume (m^3) of landslide (elevation decreased), Volume (m^3) of sedimentation (elevation increased), Total stream length in locations in locations with landslides / elevation decreased Total stream length in locations in locations with sedimentation /elevation increased were indicated in Table 4.4.1 and Table 4.4.2.

Quantitative analysis of sediment connectivity including Landslide (Area with elevation decrease) travel distance (m), Landslide (Area with elevation decrease) height (m), Landslide (Area with elevation decrease) area density (LAD) and Deposit length ratio (DLR) were also indicated in Table 4.4.1 and 4.4.2.

Date	Oct 05, 2012 - Sep 11, 2018 (Period 1)			
Study sites	A	B	C	D
Total Stream length (m)	638.30	923.93	707.93	1758.49
Landslides (Areas with elevation decrease) (- 0.2 m (+/- 20cm) to – 10.0 m (+/- 20cm))				
Area (m^2)	12721	22706	9027	60934
Volume (m^3)	62333	111259	44231	298577
Volume per unit area of catchment (m^3/m^2)	0.886	1.070	0.542	1.563
Total stream length (m) in those locations	266.59 (47.77%)	379.526 (41.08%)	131.708 (18.60%)	292.6 (16.63%)
Sedimentation (Areas with elevation increase) (+ 0.2 m (+/- 20cm) to + 20.0 m (+/- 20cm))				
Area (m^2)	2351	3250	2188	2590
Volume (m^3)	23278	32175	21664	25640
Volume per unit area of catchment (m^3/m^2)	0.331	0.309	0.265	0.134
Total stream length (m) in those locations	272.02 (42.62%)	233.81 (25.31%)	226.7 (32.02%)	528.08 (30.03%)
Landslide area density (LAD) (m^2/m^2)	0.18	0.22	0.11	0.32
Deposit length ratio (DLR) (m/m)	0.42	0.25	0.32	0.30
Landslide mobility index (y)	0.47	0.41	0.51	0.31
Landslide travel distance (m)	223.29	314.11	180.93	539
Landslide height (m)	65.08	83.98	55.32	123.93

Table 4.4.1: Quantitative analysis of Landslide (Elevation decreased) mobility and Sediment connectivity (Study sites A -D): Analysis from the pre-seismic ALS DEM on October 05, 2012 and post-seismic ALS DEM on September 11, 2018 (Period 1).

4.4.1 Analysis from the pre-seismic ALS DEM on October 2012, 05 and post-seismic ALS DEM on September 11, 2018 (Period 1).

Table 4.4.1. indicates the results of quantitative analysis of landslide (elevation decreased) mobility and sediment connectivity (Study sites A -D) by using the pre-seismic ALS DEM in October 05, 2012 and post-seismic ALS DEM in September 11, 2018 (Period 1).

4.4.1.1 Study site A

The total stream length in Study site A was 638.30 m (ALS DEM September 11, 2018) and the total stream length in landslide areas was 266.59 m (47.77 % of total stream length). The areas affected by landslides (locations with elevation decrease) (-0.2 m (+/- 20 cm) to -10 m (+/- 20 cm)) was 12721 m^2, with a volume of 62333 m^3. The volume of landslide (locations with elevation decrease (-0.2 m (+/- 20 cm) to -10 m (+/- 20 cm)) per unit area of catchment was 0.886 m^3/m^2).

The total stream length in Study site A was 638.30 m (ALS DEM September 11, 2018) and the total stream length in sedimentation areas was 272.02 m (42.62 % of total stream length). The areas affected with sedimentation (locations with elevation increase) (+0.2 m (+/- 20 cm) to +10 m (+/- 20 cm)) was 2351 m^2, with a volume of 23278 m^3. The volume of sedimentation (locations with elevation increase (0.2 m (+/- 20 cm) to +10 m (+/- 20 cm)) per unit area of catchment was 0.33 m^3/m^2).

The Landslide area density (LAD) (m^2/m^2) was 0.18 (m^2/m^2), while the Deposit length ratio (DLR) (m/m) was 0.42. Landslide mobility index (y) was 0.47. The Landslide travel distance (m) was 223.29 m and the Landslide height (m) was 65.08 m.

4.4.1.2 Study site B

The total stream length in Study site B was 923.93 m (ALS DEM September 11, 2018) and the total stream length in landslide areas was 379.53 m (41.08 % of total stream length). The areas affected by landslides (locations with elevation decrease) (-0.2 m (+/- 20 cm) to -10 m (+/- 20 cm)) was 22706 m^2, with a volume of 111259 m^3. The volume of landslide (locations with elevation decrease (-0.2 m (+/- 20 cm) to -10 m (+/- 20 cm)) per unit area of catchment was 1.070 m^3/m^2.

The total stream length in Study site B was 923.93 m (ALS DEM September 11, 2018) and the total stream length in sedimentation areas was 233.81 m (25.31 % of total stream length). The areas affected with sedimentation (locations with elevation increase) (+0.2 m (+/- 20 cm) to +10 m (+/- 20 cm)) was 3250 m^2, with a volume of 32175 m^3. The volume of sedimentation (locations with elevation increase (+0.2 m (+/- 20 cm) to +10 m (+/- 20 cm)) per unit area of catchment was 0.309 m^3/m^2).

The Landslide area density (LAD) (m^2/m^2) was 0.22 (m^2/m^2), while the Deposit length ratio (DLR) (m/m) was 0.25. Landslide mobility index (y) was 0.41. The Landslide travel distance (m) was 314.11 m and the Landslide height (m) was 83.98 m.

4.4.1.3 Study site C

The total stream length in Study site C was 707.93 m (ALS DEM September 11, 2018) and the total stream length in landslide areas was 131.71 m (18.60 % of total stream length). The areas affected by landslides (locations with elevation decrease) (-0.2 m (+/- 20 cm) to -10 m (+/- 20 cm)) was 9027 m^2, with a volume of 44231 m^3. The volume of landslide (locations with elevation decrease (-0.2 m (+/- 20 cm) to -10 m (+/- 20 cm)) per unit area of catchment was 0.542 m^3/m^2).

The total stream length in Study site C was 707.93 m (ALS DEM September 11, 2018) and the total stream length in sedimentation areas was 226.70 m (32.02 % of total stream length). The areas affected with sedimentation (locations with elevation increase) (+0.2 m (+/- 20 cm) to +10 m (+/- 20 cm)) was 2188 m^2, with a volume of 21664 m^3. The volume of sedimentation (locations with elevation increase (+0.2 m (+/- 20 cm) to +10 m (+/- 20 cm)) per unit area of catchment was 0.265 m^3/m^2).

The Landslide area density (LAD) (m^2/m^2) was 0.11 (m^2/m^2), while the Deposit length ratio (DLR) (m/m) was 0.32. Landslide mobility index (y) was 0.51. The Landslide travel distance (m) was 180.93 m and the Landslide height (m) was 55.32 m.

4.4.1.4 Study site D

The total stream length in Study site D was 1758.49 m (ALS DEM September 11, 2018) and the total stream length in landslide areas was 292.60 m (16.63 % of total stream length). The areas affected by landslides (locations with elevation decrease) (-0.2 m (+/- 20 cm) to -10 m (+/- 20 cm)) was 60934 m^2, with a volume of 298577 m^3. The volume of landslide (locations with elevation decrease (-0.2 m (+/- 20 cm) to -10 m (+/- 20 cm)) per unit area of catchment was 1.563 m^3/m^2).

The total stream length in Study site D was 1758.49 m (ALS DEM September 11, 2018) and the total stream length in sedimentation areas was 528.08 m (30.03 % of total stream length). The areas affected with sedimentation (locations with elevation increase) (+0.2 m (+/- 20 cm) to +10 m (+/- 20 cm)) was 2590 m^2, with a volume of 25640 m^3. The volume of sedimentation (locations with elevation increase (+0.2 m (+/- 20 cm) to +10 m (+/- 20 cm)) per unit area of catchment was 0.134 m^3/m^2.

The Landslide area density (LAD) (m^2/m^2) was 0.32 (m^2/m^2), while the Deposit length ratio (DLR) (m/m) was 0.30. Landslide mobility index (y) was 0.31. The Landslide travel distance (m) was 539.00 m and the Landslide height (m) was 123.93 m.

4.4.1.5 Comparing the results from the pre-seismic ALS DEM on October 05, 2012 and post-seismic ALS DEM on September 11, 2018 (Period 1).

Comparing the analysed results, Study site D and B had the highest and 2nd highest value of Total stream length (m) (1758.49 m and 923.93 m respectively), Areas and volume affected by landslides (locations with elevation decrease) (-0.2 m (+/- 20 cm) to -10 m (+/- 20 cm)) (60934 m^2 and 298577 m^3; and 22706 m^2 and 111259 m^3 respectively) and Volume of landslide (locations with elevation decrease (-0.2 m (+/- 20 cm) to -10 m (+/- 20 cm)) per unit area of catchment (1.563 m^3/m^2 and 1.070 m^3/m^2 respectively), Landslide area density (LAD) (m^2/m^2) (0.32 and 0.22 respectively), Landslide travel distance (m) (539.00 m and 314.11 m respectively) and Landslide height (m) (123.93 m and 83.98 m respectively); while Study site D and B had the 3rd highest and the lowest value in the percentage of stream length on sedimentation area with total stream length (30.3% and 25.31 % respectively).

Study site A and C had the 3rd highest and the lowest value in the above data except in Total stream length (m) which was vice verse.

Meanwhile, Study site B and D had the highest and 2nd highest value Areas and volume with sedimentation (locations with elevation increase) (-0.2 m (+/- 20 cm) to -10 m (+/- 20 cm)) (3250 m^2 and 32175 m^3; and 2590 m^2 and 25640 m^3 respectively).

Study site C and A had highest and 2nd highest value of Landslide mobility index (y) (0.51 and 0.47 respectively; while Study site B and D had the 3rd highest and the lowest value of Landslide mobility index (y) (0.41 and 0.31respectively). It implies that the landsides happened in Study D and B had higher mobility for moving a longer horizontal distance than those in Study site C and A, which reflected in the value of landslide travel distance that landslide happened in Study site D (539.00 m) and B (314.11 m) were longer than Study site A (223.39 m) and C (180.93 m).

4.4.2 Analysis from the post-seismic ALS DEMs on September 11, 2018 and UAV-Lidar DEM on October 29, 2021 (Period 2-9).

Table 4.4.2 indicates the results of quantitative analysis of Mobility (Area with elevation decrease) and Sediment connectivity (Study sites A -D) by using the pre-seismic ALS DEM of September 11, 2018 and UAV-Lidar DEM of October 29, 2021 (Period 2-9).

Date	Sep 11, 2018 - Oct 29, 2021 (Period 2 - 9)			
Study sites	A	B	C	D
Total Stream length (m)	865.98	1663.27	1207.69	3320.03
Area with elevation decrease (- 0.2 m (+/- 20cm) to – 10.0 m (+/- 20cm))				
Area (m^2)	1829	5164	3167	15373
Volume (m^3)	1646	4647	1267	13836
Volume per unit area of catchment (m^3/m^2)	0.024	0.045	0.015	0.075
Total stream length (m) in those locations	193.85 (22.62%)	203.61 (12.24%)	197.11 (16.32%)	254.05(7.65%)
Sedimentation (Areas with elevation increase) (+ 0.2 m (+/- 20cm) to + 20.0 m (+/- 20cm))				
Area (m^2)	240	373	224	1065
Volume (m^3)	250	149	202	958
Volume per unit area of catchment (m^3/m^2)	0.004	0.001	0.002	0.005
Total stream length (m) in those locations	15.79 (1.82%)	61.52 (3.70%)	25.79 (13.08%)	110.34(3.32%)
Area density (LAD) (m^2/m^2) (area with elevation decrease)	0.03	0.05	0.04	0.08
Deposit length ratio (DLR) (m/m)	0.02	0.04	0.02	0.03
Mobility index (y)(area with elevation decrease)	0.68	0.57	0.62	0.46
Travel distance (m) (area with elevation decrease)	64.38	126.94	92.27	250.14
Height (m) of area with elevation decrease	21.91	41.51	31.36	70.91

Table 4.4.2: Quantitative analysis of Landslide (Elevation decreased area) mobility and Sediment connectivity (Study sites A -D): Analysis from the post-seismic ALS DEM on September 11, 2018 and UAV-Lidar DEM on October 29, 2021 (Period 2-9).

4.4.2.1 Study site A

The total stream length in Study site A was 865.98 m (UAV-Lidar DEM 29th October 2021) and the total stream length in elevation decreased areas was 193.85 m (22.62 % of total stream length). The areas with elevation decrease) (-0.2 m (+/- 20 cm) to -10 m (+/- 20 cm)) was 1829 m^2, with a volume of 1646 m^3. The volume of areas with elevation decrease (-0.2 m (+/- 20 cm) to -10 m (+/- 20 cm)) per unit area of catchment was 0.024 m^3/m^2).

The total stream length in Study site A was 865.98 m (ALS DEM September 11, 2018) and the total stream length in sedimentation areas was 15.79 m (1.82% of total stream length). The areas affected with sedimentation (locations with elevation increase)

(+0.2 m (+/- 20 cm) to +10 m (+/- 20 cm)) was 240 m^2, with a volume of 250 m^3. The volume of sedimentation (locations with elevation increase (0.2 m (+/- 20 cm) to +10 m (+/- 20 cm)) per unit area of catchment was 0.004 m^3/m^2).

The Area density (LAD) (area with elevation decrease) (m^2/m^2) was 0.03 (m^2/m^2), while the Deposit length ratio (DLR) (m/m) was 0.02. Mobility index (y) (area with elevation decrease) was 0.68. Travel distance (m) (area with elevation decrease) was 64.38 m and the Height (m) of area with elevation decrease was 21.91 m.

4.4.2.2 Study site B

The total stream length in Study site B was 1663.27 m (UAV-Lidar DEM 29th October 2021) and the total stream length in elevation decreased areas was 203.61 m (12.24 % of total stream length). The areas with elevation decrease) (-0.2 m (+/- 20 cm) to -10 m (+/- 20 cm)) was 5164 m^2, with a volume of 4647 m^3. The volume of areas with elevation decrease (-0.2 m (+/- 20 cm) to -10 m (+/- 20 cm)) per unit area of catchment was 0.045 m^3/m^2).

The total stream length in Study site B was 1663.27 m (ALS DEM September 11, 2018) and the total stream length in sedimentation areas was 61.25 m (3.70 % of total stream length). The areas affected with sedimentation (locations with elevation increase) (+0.2 m (+/- 20 cm) to +10 m (+/- 20 cm)) was 373 m^2, with a volume of 149 m^3. The volume of sedimentation (locations with elevation increase (0.2 m (+/- 20 cm) to +10 m (+/- 20 cm)) per unit area of catchment was 0.001 m^3/m^2).

The Area density (LAD) (area with elevation decrease) (m^2/m^2) was 0.05 (m^2/m^2), while the Deposit length ratio (DLR) (m/m) was 0.04. Mobility index (y) (area with elevation decrease) was 0.57. Travel distance (m) (area with elevation decrease) was 126.94 m and the Height (m) of area with elevation decrease was 41.51 m.

4.4.2.3 Study site C

The total stream length in Study site C was 1207.69 m (UAV-Lidar DEM 29th October 2021) and the total stream length in elevation decreased areas was 197.11 m (16.32 % of total stream length). The areas with elevation decrease) (-0.2 m (+/- 20 cm) to -10 m (+/- 20 cm)) was 3167 m^2, with a volume of 1267 m^3. The volume of areas with elevation decrease (-0.2 m (+/- 20 cm) to -10 m (+/- 20 cm)) per unit area of catchment was 0.015 m^3/m^2).

The total stream length in Study site C was 1207.69 m (ALS DEM September 11, 2018) and the total stream length in sedimentation areas was 25.79 m (13.08 % of total stream length). The areas affected with sedimentation (locations with elevation increase) (+0.2 m (+/- 20 cm) to +10 m (+/- 20 cm)) was 224 m^2, with a volume of 202 m^3. The volume of sedimentation (locations with elevation increase (0.2 m (+/- 20 cm) to +10 m (+/- 20 cm)) per unit area of catchment was 0.002 m^3/m^2).

The Area density (LAD) (area with elevation decrease) (m^2/m^2) was 0.04 (m^2/m^2), while the Deposit length ratio (DLR) (m/m) was 0.02. Mobility index (y) (area with elevation decrease) was 0.62. Travel distance (m) (area with elevation decrease) was 92.27 m and the Height (m) of area with elevation decrease was 31.36 m.

4.4.2.4 Study site D

The total stream length in Study site D was 3320.03 m (UAV-Lidar DEM 29th October 2021) and the total stream length in elevation decreased areas was 254.05 m (7.65 % of total stream length). The areas with elevation decrease) (-0.2 m (+/- 20 cm) to -10 m (+/- 20 cm)) was 15373 m^2, with a volume of 13836 m^3. The volume of areas with elevation decrease (-0.2 m (+/- 20 cm) to -10 m (+/- 20 cm)) per unit area of catchment was 0.075 m^3/m^2).

The total stream length in Study site D was 3320.03 m (ALS DEM September 11, 2018) and the total stream length in sedimentation areas was 110.34 m (3.32 % of total stream length). The areas affected with sedimentation (locations with elevation increase) (+0.2 m (+/- 20 cm) to +10 m (+/- 20 cm)) was 1065 m^2, with a volume of 958 m^3. The volume of sedimentation (locations with elevation increase (0.2 m (+/- 20 cm) to +10 m (+/- 20 cm)) per unit area of catchment was 0.005 m^3/m^2).

The Area density (LAD) (area with elevation decrease) (m^2/m^2) was 0.08 (m^2/m^2), while the Deposit length ratio (DLR) (m/m) was 0.03 (m/m). Mobility index (y) (area with elevation decrease) was 0.46. Travel distance (m) (area with elevation decrease) was 250.14 m and the Height (m) of area with elevation decrease was 70.91 m.

4.4.2.5 Comparing the results from post-seismic ALS DEMs on September 11, 2018 and UAV-Lidar DEM on October 29, 2021 (Period 2-9).

Comparing the analysed results, Study site D and B had the highest and 2nd highest value of Total stream length (m) (3320.03 m and 1663.27 m respectively), Total stream length on area with elevation decrease and sedimentation (254.05 m and 110.34 m; and 203.61 m and 61.52 m respectively), Areas and with elevation decrease) (-0.2 m (+/- 20 cm) to -10 m (+/- 20 cm)) (1065 m^2 and 373 m^2 respectively). Areas with elevation increase (1065 m^2 and 373 m^2), Area density (LAD) (area with elevation decrease) (m^2/m^2) (0.08 and 0.05 respectively), Landslide travel distance (m) (539.00 m and 314.11 m respectively) and Landslide height (m) (123.93 m and 83.98 m respectively); while Study site D and B had the 3rd highest and the lowest value in the percentage of stream length on sedimentation area with total stream length (30.3% and 25.31 % respectively). Also, Study site B and D had the 3rd highest and the lowest value on the percentage of total stream length on elevation decreased area of the total stream length in drainage basin (12.24 % and 7.65 %), Mobility index (y) (area with elevation decrease).

Study site A and C had the 3rd highest and the lowest value in the Volume of areas with elevation decrease, Volume of elevation decreased area per unit area of catchment, area of sedimentation and total stream length on area with elevation increase, Area density (LAD) (area with elevation decrease) (0.03 (m2/m2) and 0.04 (m^2/m^2)), Mobility index (y) (area with elevation decrease) (0.68 and 0.62), and Height (m) of area with elevation decrease (21.91 m and 31.36 m).

Study site A and C had highest and 2nd highest value of percentage of total stream length in area with elevation decrease to the total stream length in drainage basin (22.62 % and 16.32 % respectively) and Mobility index (area with elevation decrease) (0.68 and 0.62), which implies the mobility for moving a horizontal distance on area with elevation decrease in Study A and C were lower than Study B and D (0.57 and 0.46 respectively), which reflected in the value of Trave distance in Study B and D (126.94 m and 250.14 m respectively)

4.4.3 Pre and post-seismic difference in quantitative analysis of landslide (Elevation decreased area) Mobility and Sediment connectivity (Study sites A -D)

Table 4.4.3 indicates the differences on value of changes of Pre- and Post-seismic Periods by comparing the data during Period 1 (Table 4.4.1) and during Period 2 to 9 (Table 4.4.2), in quantitative analysis of landslide (Elevation decreased area) Mobility and Sediment connectivity in Study sites A, B, C and D) by using the Pre-earthquake ALS DEM in October 05, 2012 and Post-earthquake ALS DEM in September 11, 2018 and UAV-Lidar DEM in October 29, 2021.

	Pre and Post-seismic difference between the results of Period 1 and Period 2-9			
Study sites	A	B	C	D
Total Stream length (m)	227.68	739.34	499.76	1561.54
Landslides /Areas with elevation decrease (- 0.2 m (+/- 20cm) to – 10.0 m (+/- 20cm))				
Area (m^2)	-10892	-17542	-5860	-45561
Volume (m^3)	-60687	-106612	-42964	-284741
Volume per unit area of catchment (m^3/m^2)	-0.863	-1.025	-0.526	-1.488
Total stream length (m) in those locations	-72.74	-175.92	65.41	-38.55
Sedimentation (Areas with elevation increase) (+ 0.2 m (+/- 20cm) to + 20.0 m (+/- 20cm))				
Area (m^2)	-2111	-2877	-1964	-1525
Volume (m^3)	-2111	-32026	-21462	-24682
Volume per unit area of catchment (m^3/m^2)	-0.030	-0.308	-0.263	-0.129
Total stream length (m) in those locations	-256.23	-172.29	-200.91	-417.74
Landslide (Elevation decreased) area density (LAD) (m^2/m^2)	-0.15	-0.17	-0.07	-0.24
Deposit length ratio (DLR) (m/m)	-0.40	-0.21	-0.30	-0.27
Landslide (Elevation decreased area) Mobility index (LAD) (y)	0.21	0.16	0.11	0.15
Landslide (Elevation decrease area) travel distance (m)	-158.91	-187.17	-88.66	-288.86
Landslide (Elevation decreased area) height (m)	-43.17	-42.47	-23.96	-53.02

Table 4.4.3: Pre- and post-seismic difference in quantitative analysis of landslide (Elevation decreased area) Mobility and Sediment connectivity (Study sites A -D): Analysis from the ALS DEMs the pre-earthquake ALS DEMs in October 05, 2012 and post-earthquake DEM in September 11, 2018 and UAV-Lidar DEM in October 29,2021.

Most of the results had negative value of changes, except the differences in Total stream length (m) and Landslide (Elevation decreased area) Mobility index (LAD) which had positive value of changes.

Areas with landslides and elevation decrease (-0.2 m (+/- 20 cm) to -10 m (+/- 20 cm)) (m^2) had negative values of changes of -10892 m^2, -17542m^2, -5860 m^2 and -45561 m^2 in Study site A, B, C and D respectively.

Volume with landslides and elevation decrease (-0.2 m (+/- 20 cm) to -10 m (+/- 20 cm)) (m^3) had negative values of changes of -60687 m^3, -106612 m^3, -42964 m^3 and -284741 m^3 in Study site A, B, C and D respectively.

Volume with landslides and elevation decrease (-0.2 m (+/- 20 cm) to -10 m (+/- 20 cm)) per unit area of catchment (m^3/m^2) had negative values of changes of -0.863 m^3/m^2, -1.025 m^3/m^2, -0.526 m^3/m^2 and -1.488 m^3/m^2 in Study site A, B, C and D respectively.

Total stream length in (m) areas with landslides and elevation decrease (-0.2 m (+/- 20 cm) to -10 m (+/- 20 cm)) had negative and positive values of changes of -72.74 m, -175.92 m, 65.41 m and -38.55 m in Study site A, B, C and D respectively.

Areas with sedimentation and elevation increase (-0.2 m (+/- 20 cm) to -20 m (+/- 20 cm)) (m^2) had negative values of changes of -2111 m^2, -2877 m^2, -1964 m^2 and -1525 m^2 in Study site A, B, C and D respectively.

Volume with sedimentation and elevation increase (-0.2 m (+/- 20 cm) to -20 m (+/- 20 cm)) (m^3) had negative values of changes of -2111 m^3, -32026 m^3, -21462 m^3 and -24682 m^3 in Study site A, B, C and D respectively.

Volume with sedimentation and elevation increase (-0.2 m (+/- 20 cm) to -20 m (+/- 20 cm)) per unit area of catchment (m^3/m^2) had negative values of changes of –0.030 m^3/m^2, -0.308 m^3/m^2, -0.263 m^3/m^2 and -0.129 m^3/m^2 in Study site A, B, C and D respectively.

Total stream length in (m) areas with sedimentation and elevation increase (-0.2 m (+/- 20 cm) to -20 m (+/- 20 cm)) had negative and positive values of changes of -256.23 m, -172.29 m, 200.91 m and -417.74 m in Study site A, B, C and D respectively.

Landslide (Elevation decreased) area density (LAD) (m^2/m^2) had negative values of changes of –0.15 m^2/m^2, -0.17 m^2/m^2, -0.07 m^2/m^2 and -0.24 m^2/m^2 in Study site A, B, C and D respectively.

Deposit length ratio (DLR) (m/m) had negative values of changes of –0.40 m/m, -0.21 m/m, -0.30 m/m and -0.27 m/m in Study site A, B, C and D respectively.

Landslide (Elevation decreased area) travel distance (m) had negative values of changes of -158.91 m, -187.17 m, -88.66 m and -288.86 m in Study site A, B, C and D respectively.

Landslide (Elevation decreased area) height (m) had negative values of changes of -43.17 m, -42.47 m, -23.96 m and -53.02 m in Study site A, B, C and D respectively.

Conversely, Total Stream length (m) had positive values of changes of 227.68 m, 739.34 m, 499.76 m and 1561.54 m in Study site A, B, C and D respectively.

Also, Landslide (Elevation decreased area) Mobility index (LAD) (y) had positive values of changes of 0.21, 0.16, 0.11 and 0.15 in Study site A, B, C and D respectively.

Comparing those differences on value of changes of Pre- and Post-seismic Periods by comparing the data during Period 1 (Table 4.4.1) and during Period 2 to 9 (Table 4.4.2) in quantitative analysis of landslide (Elevation decreased area) Mobility and Sediment connectivity in Study sites A, B, C and D), Study site D and B had the highest and 2nd highest value of changes in Total stream length (m) (1561.54 m and 739.34 m respectively), Areas with landslides and elevation decrease (-0.2 m (+/- 20 cm) to -10 m (+/- 20 cm)) (m^2) (-45561 m^2 and -17542 m^2respectively), Volume with landslides and elevation decrease (-0.2 m (+/- 20 cm) to -10 m (+/- 20 cm)) (m^3) (-284741 m^3 and -106612 m^3 respectively), Volume with landslides and elevation decrease (-0.2 m (+/- 20 cm) to -10 m (+/- 20 cm)) per unit area of catchment (m^3/m^2) (-1.488 m^3/m^2 and -1.025m^3/m^2), Landslide (Elevation decreased) area density (LAD) (m^2/m^2) (-0.24 m^2/m^2 and -0.17 m^2/m^2), and Landslide (Elevation decreased area) travel distance (m) (-288.86 m and -187.17 m).

Meanwhile, Study site B and D had the highest and 2nd highest value of changes in Volume with sedimentation and elevation increase (-0.2 m (+/- 20 cm) to -20 m (+/- 20 cm)) (m3) (-32026 m^3 and -24682 m^3). Also, Study site D and B had the 3rd highest and the lowest value of changes among the 4 Study sites in Deposit length ratio (DLR) (m/m) (-0.27 m/m and -0.21 m/m)

Conversely, Study site A and C had the 3rd highest and the lowest value of changes among the 4 Study sites in Areas with landslides and elevation decrease (-0.2 m (+/- 20 cm) to -10 m (+/- 20 cm)) (m^2) (-10892 m^2 and -5860 m^2 respectively), Volume with landslides and elevation decrease (-0.2 m (+/- 20 cm) to -10 m (+/- 20 cm)) (m^3) (-60687 m^3 and -42964 m^3 respectively), Volume with landslides and elevation decrease (-0.2 m (+/- 20 cm) to -10 m (+/- 20 cm)) per unit area of catchment (m^3/m^2) (-0.863 m^3/m^2 and -0.526 m^3/m^2), Landslide (Elevation decreased) area density (LAD) (m^2/m^2) (-0.15 m^2/m^2 and -0.07 m^2/m^2) and Landslide (Elevation decreased area) travel distance (m) (-158.91 m and -88.86 m).

Study site A and C had the highest and 2nd highest value of changes in Deposit length ratio (DLR) (m/m) (-0.40 m/m and -0.30 m/m)

Study site C and A had the 3rd highest and the lowest value of changes among the 4

Study sites in Volume with sedimentation and elevation increase (-0.2 m (+/- 20 cm) to -20 m (+/- 20 cm)) per unit area of catchment (m^3/m^2) (21462 m^3/m^2 and -2111 m^3/m^2),

4.4.4 Comparing the results Landslide (Areas with elevation decrease) mobility and sediment connectivity of Study site A, B, C and D during October 05, 2012 to September 11, 2018 (Period 1) and September 11, 2018 to October 29, 2021 (Period 2 – 9).

Figures 4.4.1 – 4.4.6 indicate the quantitative analysis of Landslide (Areas with elevation decrease) (m^2) and Sedimentation (Areas with elevation increase) (m^2), Landslide (Areas with elevation decrease) volume (m^3) and Sedimentation (Areas with elevation increase) volume (m^3), Stream length (m) in landslides areas (Areas with elevation decrease) and Sedimentation areas (Areas with elevation increase), Landslide area (Areas with elevation decrease) density (LAD) (m^2/m^2) and Deposit length ratio (DLR) (m/m), Landslide (Areas with elevation decrease) mobility index and Landslide travel distance (m) and height (m) of Study site A, B, C and D during October 05, 2012 to September 11, 2018 (Period 1) and September 11, 2018 to October 29, 2021 (Period 2 – 9).

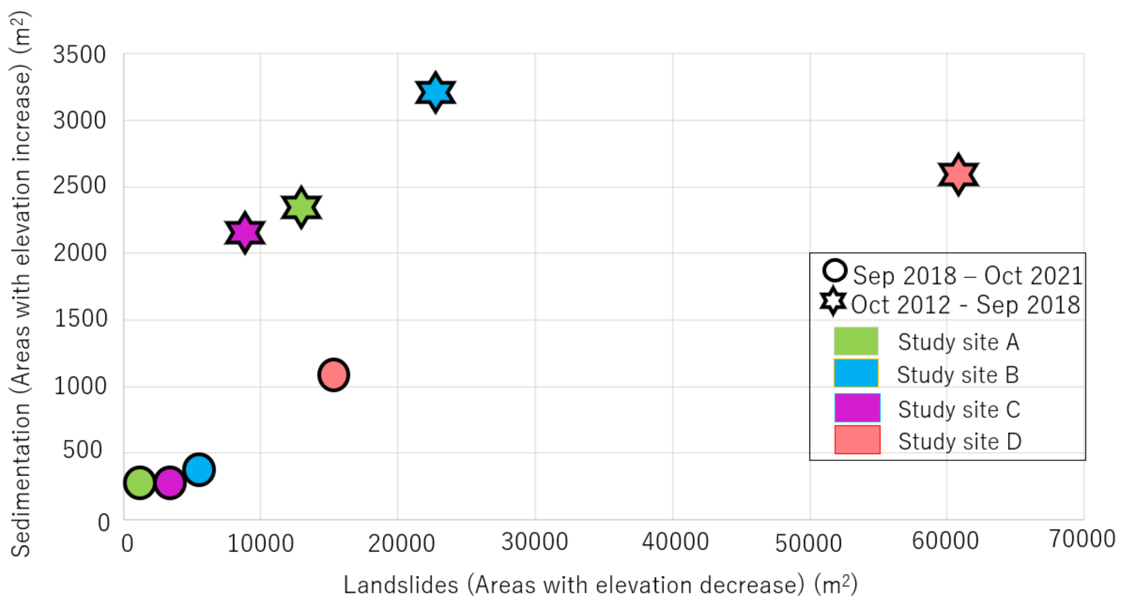

Figure 4.4.1: Landslide (Areas with elevation decrease) (m^2) and Sedimentation (Areas with elevation increase) (m^2) of Study site A – D: October 05, 2012 – September 11, 2018 (Period 1) and September 11, 2018 – October 29, 2021 (Period 2 – 9).

4.4.4.1 Landslide (Areas with elevation decrease) (m^2) and Sedimentation (Areas with elevation increase) (m^2)

Figure 4.4.1 indicates the data of Landslide (Areas with elevation decrease) (m^2) and Sedimentation (Areas with elevation increase) (m^2) of Study site A, B, C and D during October 05, 2012 to September 11, 2018 (Period 1) and September 11, 2018 to October 29, 2021 (Period 2 – 9). In all Study site A, B, C and D, the Landslide (Areas with elevation decrease) areas (m^2) were greater than Sedimentation (Areas with elevation increase) areas (m^2) during October 05, 2012 to September 11, 2018 (Period 1) and September 11, 2018 to October 29, 2021 (Period 2 – 9).

One more special feature is that, both Landslide (Areas with elevation decrease) areas (m^2) were greater than Sedimentation (Areas with elevation increase) areas (m^2) in Study site B and D were greater than Study site A and C. This situation was same as Landslide (Areas with elevation decrease) volume (m^3) and Sedimentation (Areas with elevation increase) (m^3) of Study site A – D: October 05, 2012 – September 11, 2018 (Period 1) and September 11, 2018 – October 29, 2021 (Period 2 – 9). Regression analysis indicated increase of 1 m^2 of landslide (areas of elevation decrease) volume positively corresponding to 0.005 m^2 and 0.064 m^2 increase of sedimentation (areas with elevation increase) volume during Period 1 and Period 2-9 respectively.

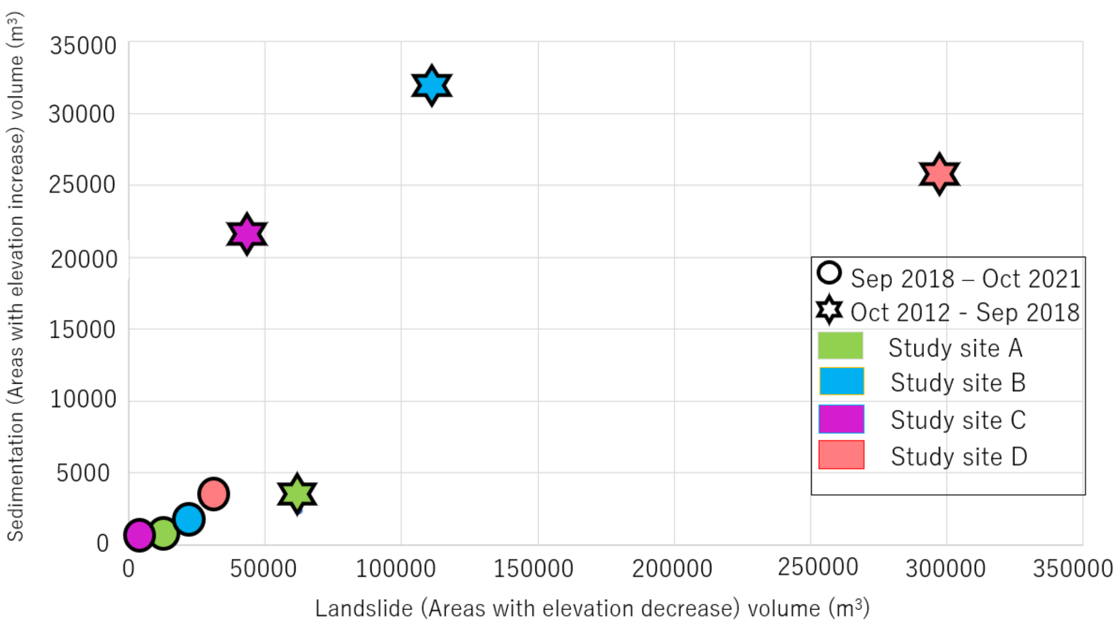

Figure 4.4.2: Landslide (Areas with elevation decrease) volume (m^3) and Sedimentation (Areas with elevation increase) volume (m^3) of Study site A – D: October 05, 2012 –

September 11, 2018 (Period 1) and September 11, 2018 – October 29, 2021 (Period 2 – 9).

4.4.4.2 Landslide (Areas with elevation decrease) volume (m^3) and Sedimentation (Areas with elevation increase) volume (m^3)

Figure 4.4.2 indicates the data of Landslide (Areas with elevation decrease) volume (m^3) and Sedimentation (Areas with elevation increase) volume (m^3) of Study site A, B, C and D during October 05, 2012 to September 11, 2018 (Period 1) and September 11, 2018 to October 29, 2021 (Period 2 – 9).

Landslide (Areas with elevation decrease) volume (m^3) was greater than Sedimentation (Areas with elevation increase) (m^3). Besides, both Landslide (Areas with elevation decrease) volume (m^3) and Sedimentation (Areas with elevation increase) (m^3) in Study site B and D were greater than Study site A and C. Regression analysis indicated increase of 1 m^3 of landslide (areas with elevation decrease) volume positively corresponding to 0.044 m^3 and 0.061 m^3 increase of sedimentation (areas with elevation increase) volume during Period 1 and Period 2-9 respectively.

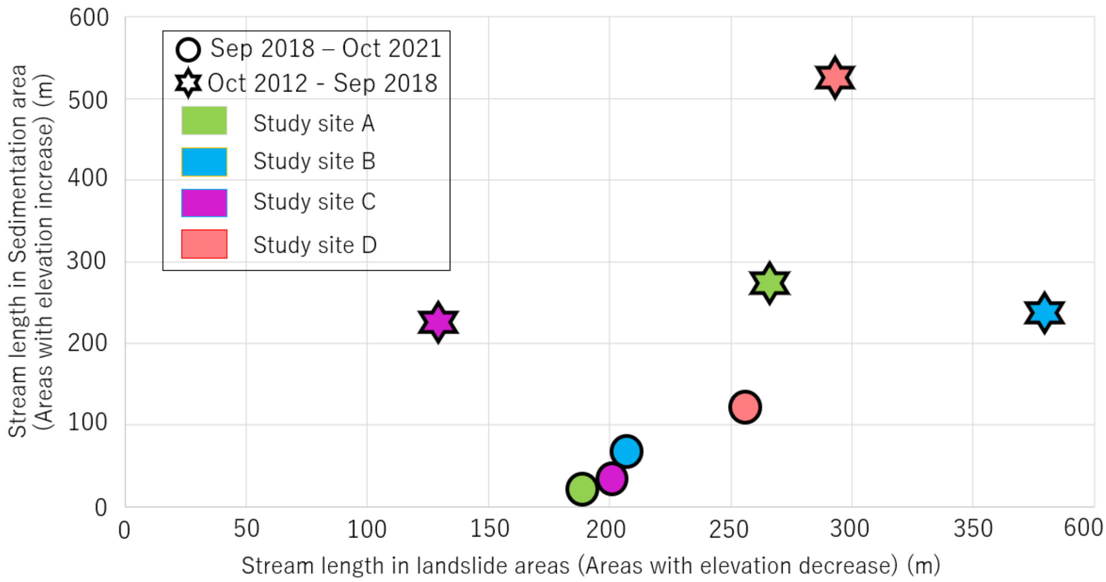

Figure 4.4.3: Stream length (m) in landslides areas (Areas with elevation decrease) and Sedimentation areas (Areas with elevation increase) (Study site A – D): October 05, 2012 – September 11, 2018 (Period 1) and September 11, 2018 – October 29, 2021 (Period 2 – 9)

4.4.4.3 Stream length (m) in landslides areas (Areas with elevation decrease) and

Sedimentation areas (Areas with elevation increase)

Figure 4.4.3 indicates the data of Stream length (m) in landslides areas (Areas with elevation decrease) and Sedimentation areas (Areas with elevation increase) of Study site A, B, C and D during October 05, 2012 to September 11, 2018 (Period 1) and September 11, 2018 to October 29, 2021 (Period 2 – 9).

Only Study site C, Stream length (m) in landslides areas (Areas with elevation decrease) increased. Also, Stream length (m) in Sedimentation areas (Areas with elevation increase) decreased in all Study sites A, B, C and D. Regression analysis indicated increase of 1 m of stream length on landslide areas (areas with elevation decrease) positively corresponding to 0.262 m and 0.43 m increase of stream length on sedimentation areas (areas with elevation increase) during Period 1 and Period 2-9 respectively.

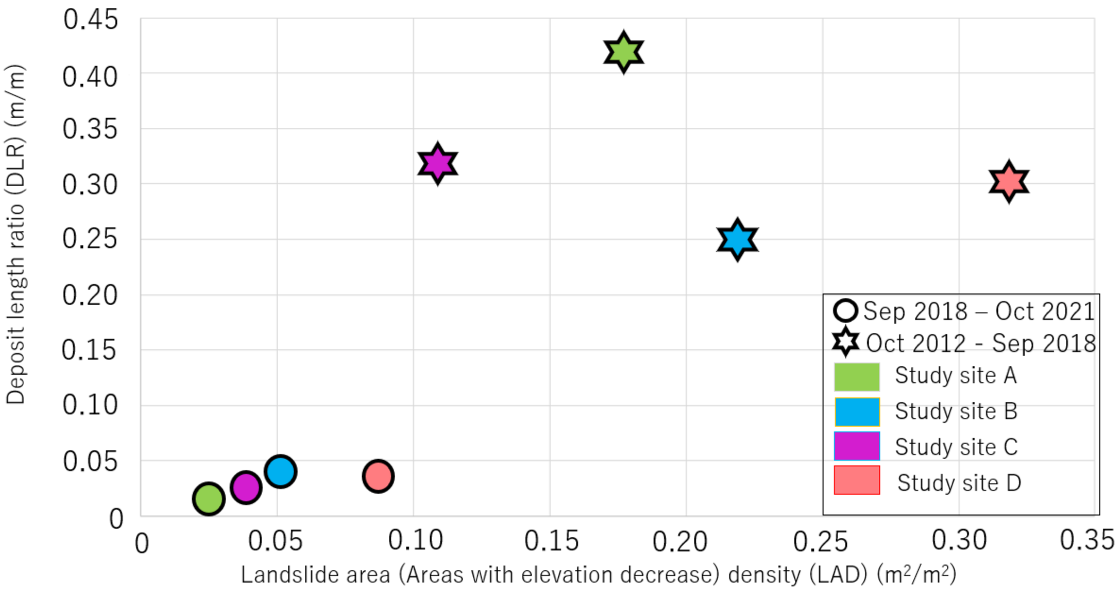

Figure 4.4.4: Landslide area (Areas with elevation decrease) density (LAD) (m^2/m^2) and Deposit length ratio (DLR) (m/m) of Study site A – D: October 05, 2012 – September 11, 2018 (Period 1) and September 11, 2018 – October 29, 2021 (Period 2 – 9).

4.4.4.4 Landslide area (Areas with elevation decrease) density (LAD) (m^2/m^2) and Deposit length ratio (DLR) (m/m)

Figure 4.4.4 indicates the data of Landslide area (Areas with elevation decrease) density (LAD) (m^2/m^2) and Deposit length ratio (DLR) (m/m) of Study site A, B, C and D during October 05, 2012 to September 11, 2018 (Period 1) and September 11, 2018 to

October 29, 2021 (Period 2 – 9).

We found that in all Study site A, B, C and D, both Landslide area (Areas with elevation decrease) density (LAD) (m^2/m^2) and Deposit length ratio (DLR) (m/m) during October 05, 2012 to September 11, 2018 (Period 1) were higher than during September 11, 2018 to October 29, 2021 (Period 2 – 9). Also, Landslide area (Areas with elevation decrease) density (LAD) (m^2/m^2) in Study site B and D were higher than Study site A and C during both October 05, 2012 to September 11, 2018 (Period 1) and September 11, 2018 to October 29, 2021 (Period 2 – 9). Regression analysis indicated increase of 1 (m^2/m^2) Landslide area density (LAD) negatively corresponding to -0.255 (m/m) to decrease and positively corresponding to 0.214 (m/m) increase of Deposit length ratio (DLR) during Period 1 and Period 2-9 respectively.

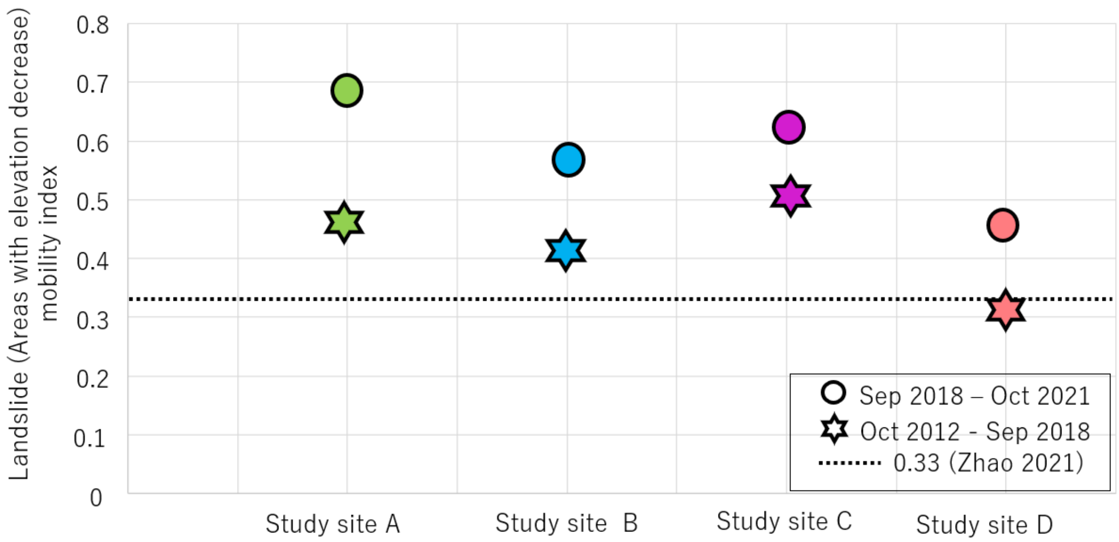

Figure 4.4.5: Landslide (Areas with elevation decrease) mobility index of Study site A – D: October 05, 2012 – September 11, 2018 (Period 1) and September 11, 2018 – October 29, 2021 (Period 2 – 9).

4.4.4.5 Landslide (Areas with elevation decrease) mobility index

Figure 4.14.5 indicates the data of Landslide (Areas with elevation decrease) mobility index of Study site A, B, C and D during October 05, 2012 to September 11, 2018 (Period 1) and September 11, 2018 to October 29, 2021 (Period 2 – 9).

Increasing trend of Landslide (Areas with elevation decrease) mobility index of Study site A, B, C and D during September 11, 2018 – October 29, 2021 (Period 2 – 9).

Also, Landslide (Areas with elevation decrease) mobility index of Study site A and C were higher than Study site B and D during both October 05, 2012 to September 11, 2018 (Period 1) and September 11, 2018 to October 29, 2021 (Period 2 – 9).

Furthermore, most of the Landslide (Areas with elevation decrease) mobility index of Study site A, B, C and D during October 05, 2012 to September 11, 2018 (Period 1) and September 11, 2018 to October 29, 2021 (Period 2 – 9) were higher than the average of 0.33 (Zhao, 2021), except Study site D during October 05, 2012 to September 11, 2018 (Period 1).

The above results were compared with the results of Zhao 2021, by which the average landslide mobility index was 0.33 with the analysis of total 472 coseismic landslides due to the 2018 Hokkaido Eastern Iburi Earthquake. Within them, 58% of the studied coseismic landslides had the range between 0.25 -4.00.

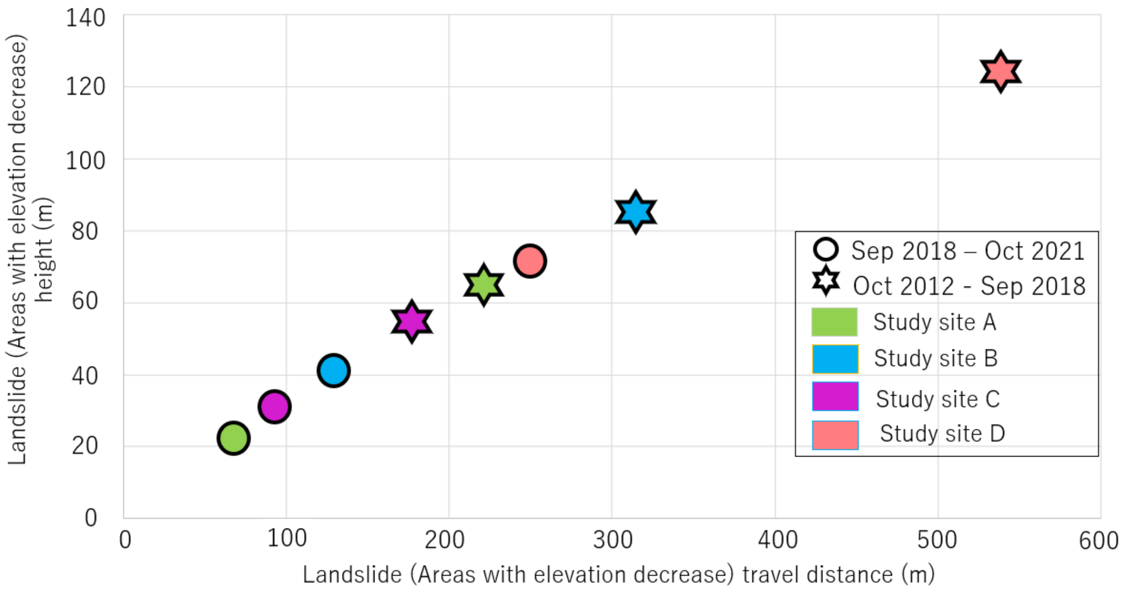

Figure 4.4.6: Landslide (Areas with elevation decrease) travel distance (m) and height (m) of Study site A – D: October 05, 2012 – September 11, 2018 (Period 1) and September 11, 2018 – October 29, 2021 (Period 2 – 9).

4.4.4.6 Landslide (Areas with elevation decrease) travel distance (m) and height (m)

Figure4.14.6 indicates Landslide (Areas with elevation decrease) travel distance (m) and height (m) of Study site A – D: October 05, 2012 – September 11, 2018 (Period 1) and September 11, 2018 – October 29, 2021 (Period 2 – 9).

Landslide (Areas with elevation decrease) travel distance (m) was positively correlated with landslide (Areas with elevation decrease) height (m) of Study sites A, B, C and D during October 05, 2012 – September 11, 2018 (Period 1) and September 11, 2018 – October 29, 2021 (Period 2 – 9).

Also, Landslide (Areas with elevation decrease) travel distance (m) and height (m) of Study site B and D were higher than those in Study site A and C. Regression analysis indicated increase of 1 m of landslide (areas of elevation decrease) height positively corresponding to 5.260 (m) and 3.849 (m) increase of landslide (areas of elevation decrease) travel distance during Period 1 and Period 2-9 respectively.

Chapter 5. Discussion

5.1 Correspondence of changes of geomorphometric and hydraulic parameters with rainfall intensity during the investigation periods.

The changes of the drainage basin characteristics including changes of morphology, hydraulic and geomorphometric parameters, fluvial network development in drainage basin after the earthquake, which might correspond to gradual or periodical erosion by fluvial and/or slope processes associated with the gully and channel networks on the bare surface of the areas with coseismic landslides (Lo et al., 2023).

Fluvial erosion on slid slopes due to increased surface runoff and stream discharge in Study site A – D were expected, which corresponded with rainfall intensity assisted by vegetation removal by coseismic landslides. The volume of erosion was 0.253 m^3/m^2 after the earthquake in Atsuma basin (14.5 times increased) due to the influence of interannual variability of rainfall and deforestation caused by coseismic landslides (Miyazaki et al., 2023). Rainfall runoff is an indicator for measuring soil erosion of a slope. Runoff occurs when rainfall intensity (mm/hr) is greater than infiltration intensity which causes excess water failed to infiltrate (Wu, 2018). The runoff volume increased with increasing rainfall intensity and rainfall kinetic energy is positively correlated with rainfall intensity (Jiang et al., 2014; Mineo et al., 2019). The action of water may decrease shear strength on soil and cause mass movement of soil (Van Westen et al., 2008; Graeff et al., 2012; Petrucci et al., 2013; Kanungo and Sharma, 2014). Soil loss under heavy precipitation caused incision of gullies in many landscapes (Dreibrodt and Wiethold, 2015). Also, accumulated runoff volume that occurred on the soil layer without vegetation cover were typically higher than those with vegetation coverage (Zhang, 2015). The ability of absorption and interception of rainwater by vegetation might be greatly reduced due to collapse of vegetation by coseismic landslides in both study sites. Also, raindrop can directly strike the soil surface with greater kinetic energy (Xu et al., 2010).

5.1.1 Changes of geomorphometric and hydraulic parameters correspond with pattern of rainfall intensity

The amount and pattern of rainfall intensity during post-earthquake periods might play an important role in the changes of drainage basin morphology and stream network development in the study sites (Figure 2.3.1). Some Typhoon-induced rainfalls were present in Period 2 (Typhoon No. 24 in October 2018 and Typhoon No. 18 in October 2019). Relatively high rainfall intensity was also recorded in post-earthquake Period 3 (11.5 mm/hr), Period 4 (16.5 mm/hr), Period 5 (7.5 mm), Period 7 (9.5 mm/hr), Period 8 (22.5 mm/hr) and Period 9 (13.5 mm/hr) (Japan Meteorological Agency, 2023) .

In Study site A – D, increase of Length of mainstream channel (m) in Period 7 and 9, Total length of tributaries (m) (1st order stream) in Period 9, Stream order (U) in Period 9, Stream number (N_u) in Period 7 and 9, Total stream strength (L_u) (m) in Period 9, Gradient (m/m) of mainstream channel in Period 3 and 4, Stream frequency (F_s) (1/km^2) in Period 5, 7 and 9, Drainage texture (D_t) (1/km) in Period 7 and 9, Drainage density (D_d) (km/km^2) in Period 5 and 9, Drainage intensity (Di) (1/km) in Period 4, 7 and 9, Infiltration number (I_f) in Period 4, 5, 7 and 9, Ruggedness number (R_n) in Period 5 and 9, Dissection Index (*Dis*) in Period 8, Average gradient of all tributaries (1st order streams) (m/m) Period 3, 4, 5 and 7, Hydraulic radius (R) (m) in Period 7, Slope (10 m from stream heads) (S) (tanø) in Period 5 and 7, Shear stress (τ) (Nm^{-2}) of stream heads in Period 7, Critical shear stress (τ_c) (Nm^{-2}) of stream heads in Period 5 and 7, Velocity (v) (m/s^{-1}) of stream heads in Period 5, Peak specific discharge per unit rainfall intensity (k_p) (mm) of stream heads in Period 4 are confirmed. In addition, decrease of Length of overland flow (L_o) (km) in Period 5 and 9, and Constant of channel maintenance (C) (km) in Period 5 and 9 are observed.

Moreover, at least 3 study sites have increase of Length of mainstream channel (m) in Period 4 (Study site A, B and C) and Period 5 (Study site A, C and D), Total length of tributaries (m) (1st order stream) in Period 5 (Study sites A, C and D) and Period 7 (B, C and D), Stream number (N_u) in Period 4 (Study site A, B and C) and Period 5 (Study site A, C and D), Total stream strength (L_u) (m) in Period 5 (Study sites A, C and D) and

Period 7 (Study site B, C and D), Gradient (m/m) of mainstream channel in Period 6 (Study site B, C and D), Stream frequency (F_s) (1/km^2) in Period 5 (Study site A, C and D), Drainage texture (D_t) (1/km) in Period 4 (Study site A, B, C), Drainage density (D_d) (km/km^2) in Period 7 (Study site B, C and D), Drainage intensity (Di) (1/km) in Period 5 (Study site A, C and D), Infiltration number (I_f) in Period 4 (Study site A, B, C), Ruggedness number (R_n) in Period 7 (Study site B, C, D), Average gradient of all tributaries (1st order streams) (m/m) Period 8 (Study site B, C, D), Hydraulic radius (R) (m) in Period 4, 5 (Study site A, B, D), Slope (10 m from stream heads) (S) (tanø) in Period 4 (Study site B, C, D), Shear stress (τ) (Nm^{-2}) of stream heads in Period 5 (Study site A, B, D), Critical shear stress (τ_c) (Nm^{-2}) of stream heads in Period 4 (Study site B, C, D), Velocity (v) (m/s^{-1}) of stream heads in Period 7 (Study site B, C, D) and Peak specific discharge per unit rainfall intensity (k_p) (mm) of stream heads in Period 5 (Study site A, C, D) are confirmed. In addition, decrease of Constant of channel maintenance (C) (km) in Period 3 (Study site B, C, D) and Period 5 (Study site A, C, D) and decrease of Length of overland flow (L_o) (km) in Period 7 (Study site B, C, D) are observed.

5.1.2 Changes of geomorphometric and hydraulic parameters correspond with increase of rainfall intensity (1 mm/per hour, daily maximum)

Furthermore, Tabe 5.1 indicates the value of changes of geomorphometric and hydraulic parameters correspond with increase of rainfall intensity (1 mm/per hour, daily maximum) recorded by Atsuma Meteorological Station (Japan Meteorological Agency, 2023) during the investigation periods of this study.

The geomorphometric parameters of Length of mainstream channel (m), Stream order (U), Stream number (N_u), Gradient of mainstream channel (m/m), Stream frequency (Fs) Drainage texture (Dt) (1/km), Drainage intensity (D_i) (1/km), Drainage density (D_d) (km/km^2), Length of overland flow (L_o) (km), Constant of channel maintenance (C) (km,) Dissection Index (D_{is}); and the hydraulic parameters of hydraulic radius (R) (m), Critical shear stress (τ_c) (Nm^{-2}) had positive correlation with increase of rainfall intensity (1 mm/per hour, daily maximum) (Table 5.1).

For the Total length of tributaries (1st order stream) (m,) positive correlation with increase of rainfall intensity (1 mm/per hour, daily maximum) was indicated in Study site B and D (Table 5.1). For the Total stream length (L_u) (m), positive correlation with increase of rainfall intensity (1 mm/per hour, daily maximum) was indicated in Study site B, C and D (Table 5.1). For the Mean stream length (L_m) (m), positive correlation with increase of rainfall intensity (1 mm/per hour, daily maximum) was indicated in Study site C and D (Table 5.1). For the infiltration number (I_f), positive correlation with increase of rainfall intensity (1 mm/per hour, daily maximum) was indicated in Study site B, C and D (Table 5.1). For the Ruggedness number (R_n), positive correlation with increase of rainfall intensity (1 mm/per hour, daily maximum) was indicated in Study site B and D (Table 5.1). For Slope (10 m from stream heads) (S) (tanø), positive correlation with increase of rainfall intensity (1 mm/per hour, daily maximum) was indicated in Study site A, B and D (Table 5.1). For the Shear stress (τ)(Nm-2), positive correlation with increase of rainfall intensity (1 mm/per hour, daily maximum) was indicated in Study site A and D (Table 5.1). For the Velocity (v) (m/s-1) of stream head, positive correlation with increase of rainfall intensity (1 mm/per hour, daily maximum) was indicated in Study site A and D (Table 5.1).

Therefore, for a large extent, most of the geomorphometric and hydraulic parameters had positive correlation with increase of rainfall intensity (1 mm/per hour, daily maximum) in Study site A - D (Table 5.1).

The above results may correspond to the high-intensity rainfall event, which potentially contributed to the fluvial erosion with gully development on the bare slope surfaces by increased runoff. Since coseismic landslides involved areas about 18.01 % of Study site A, 21.84 % of Study site B, 11.06 % of Study site C and 31.89 % of Study site D with collapsed vegetation, large areas of bare soil were exposed to direct rainsplash which might cause surface sheet flow and concentration as runoff for the surficial erosion on slid slope. These situations might cause the increase of surface runoff and discharge, which probably enhanced fluvial erosion and gully stream development on slid slopes in both sites after the earthquake and during the rain seasons in Periods 2 to 9 in Study sites A - D.

In fact, significant gully erosion was observed on landslide-affected slopes in northwestern Atsuma town with similar conditions to our study area during the rainy seasons from June to August in 2019 and from May to October in 2020 (Koshimizu et al., 2021). Those changes may also have occurred during Period 2, but this might be hindered by the longer time period (nearly 2 years) compared to the other periods (2–3 months) due to the infilling processes after erosion (Imaizumi et al., 2010).

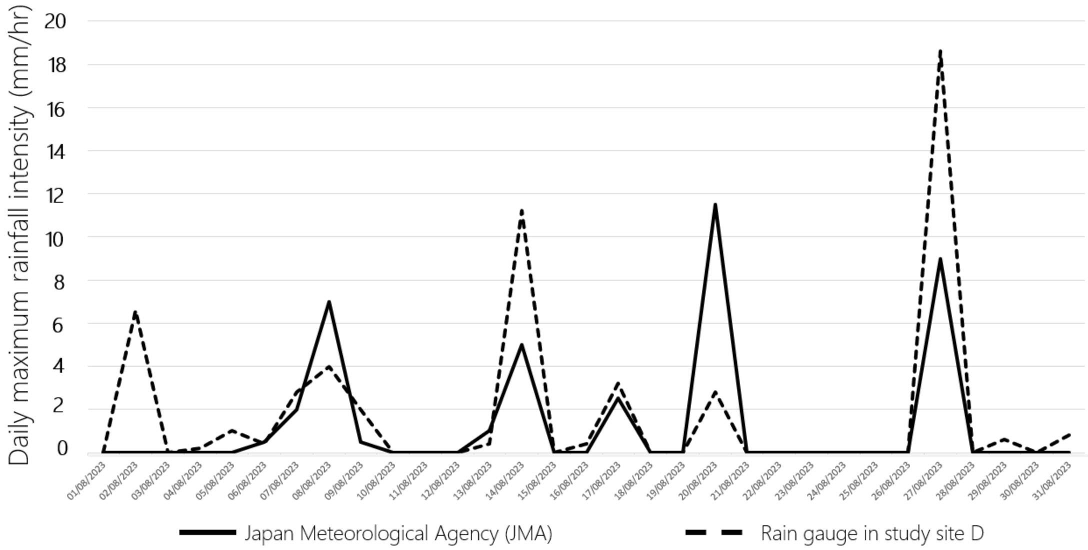

Figure 5.1.1: Daily maximum rainfall intensity (mm/hr) recorded by the rain gauge set in the Study site D (August 2023) and by Japan Meteorological Agency (JMA).

Maximum rainfall intensity (mm/hr) of Study site D from August to October 2023 recorded by the rain gauge set in the site (Figure 5.1.1), were compared with the data from Japan Meteorological Agency (JMA) 2023, which indicated the similar distribution of maximum rainfall intensity (mm/hr) of the two sets of data. Therefore, the data of maximum rainfall intensity of JMA during post-seismic periods may also represent the situation in the study sites during the periods without data from rain gauge.Since there is no data of daily maximum rainfall intensity in the study sites during the investigation periods of this study (Sep 11, 2018 to Oct 29, 2021), the data from Japan Meteorological Agency are applied for analysis in this study. Similar amount and pattern of data of rainfall intensity per hour are confirmed by comparing the data collected by the rain gauge in the study site D with those recorded by Japan Meteorological Agency (Figure 5.1)

Study site A	Date	Sep 11, 2018 - Oct 29, 2021			
Geomorphometric parameters		Changes correspond with increase of rainfall intensity (1 mm/hr, daily maximum)			
	Study sites	A	B	C	D
Drainage network					
Length of mainstream channel	m	1.241	4.578	4.063	22.170
Total length of tributaries (1st order stream)	m	-29.490	19.993	-13.428	20.670
Stream order (U)	–	0.012	0.013	0.050	0.087
Stream number (N_u)	–	0.094	0.520	0.035	0.809
Total stream length (L_u)	m	-8.081	21.057	4.166	58.965
Mean stream length (L_m)	m	-26.833	-0.905	0.878	2.443
Stream length ratio (R_L)	–				
Bifurcation ratio (R_b)	–				
Gradient of mainstream	m/m	0.001	0.002	0.001	0.001
Drainage texture					
Stream frequency (F_s)	1/km^2	1.379	4.98	0.814	1.297
Drainage texture (D_t)	1/km	0.040	0.362	0.282	0.288
Drainage density (D_d)	km/km^2	0.123	0.202	0.047	0.314
Drainage intensity (D_i)	1/km	0.316	0.200	0.007	0.396
Infiltration number (I_f)	–	-14.124	82.147	28.100	51.524
Length of overland flow (L_o)	km	0.001	0.001	0.001	0.001
Constant of channel maintenance (C)	km^2/km	0.001	0.003	0.001	0.003
Relief characteristics					
Ruggedness number (R_n)	km/km^2	-0.019	0.03	-0.009	0.058
Dissection index (D_{is})		0.001	0.001	0.002	0.020
	Date	Apr 23, 2020 - Aug 27, 2021			
Hydraulic Parameters		Changes correspond with increase of rainfall intensity (1 mm/hr, daily maximum)			
Hydraulic radius (R)	m	0.001	0.001	0.001	0.003
Slope (10 m from stream head) (S)	tanø	0.010	0.007	-0.001	0.024
Shear stress (τ)	Nm^{-2}	8.217	-4.876	-7.717	11.700
Critical shear stress (τ_c)	Nm^{-2}	0.002	0.001	0.002	0.001
Velocity (v)	m s^{-1}	0.001	-0.001	-0.005	0.001
Peak specific discharge per unit rainfall intensity (k_p)	mm	-0.047	-0.427	-0.033	0.015

Table 5.1: Changes of geomorphometric and hydraulic parameters correspond with increase of rainfall intensity (1 mm/per hour, daily maximum) recorded by Atsuma Meteorological Station (Japan Meteorological Agency, 2023) during the investigation periods of this study.

5.1.3 Changes of hydraulic parameters correspond with total daily rainfall of 10 days before the dates of investigation

Moreover, Figure 5.2 a – e indicates the correspondence of hydraulic parameters with total daily rainfall of 10 days before the dates of investigation (September 14 2020 to August 27 2021) in Study site A, B, C and D.

Figure 5.1.2 a - e indicate the value of several hydraulic parameters: Hydraulic radius (R) (m), Shear stress (τ) (Nm^{-2}), Critical shear stress (τ_c) (Nm^{-2}), Velocity (v) (ms^{-1}) and

Peak specific discharge per unit rainfall intensity (k_p) (mm) based on the UAV-SfM DEMS September 14, 2020, April 13, 2021, 21st June 2021 and August 27, 2021, with total daily rainfall (mm) of 10 days before the dates of investigation during the post-seismic periods (September 14, 2020 to August 27, 2021)

Total daily rainfall (mm) of 10 days before 14th September 2020, 13th April 2021, 21st June 2021 and 27th August 2021 were 50.5 mm, 27.0 mm 47.0 mm and 27.0 mm. The daily rainfall (mm) of 10 days before 14th September 2020 and 21st June 2021 had highest and 2nd highest values of 50.5 mm and 47.0 mm respectively, while the daily rainfall (mm) of 10 days before April 13, 2021 and August 27, 2021 had the same lowest value of 27 mm. (Figure 5.1.2 a - e)

Hydraulic radius (R) (m) was 0.12 m, 0.10 m, 0.003 m and 0.11 m for Study site A, B, C respectively and based on the UAV-SfM DEM 14th September 2020. Hydraulic radius (R) (m) was 0.04 m, 0.06 m, 0.05 m and 0.04 m for Study site A, B, C and D respectively and based on the UAV-SfM DEM April 13, 2021. Hydraulic radius (R) (m) was 0.05 m, 0.12 m, 0.09 m and 0.05 m for Study site A, B, C and D respectively and based on the UAV-SfM DEM June 21, 2021. Hydraulic radius (R) (m) was 0.04 m, 0.03 m, 0.02 m and 0.04 m for Study site A, B, C and D respectively and based on the UAV-SfM DEM August 27, 2021 (Figure 5.1.2 a and Table 4.3.5 – 4.3.8.)

For Hydraulic radius (R) (m), Study site A, B and D had highest and 2nd highest value of Hydraulic radius (R) (m) based on the UAV-SfM DEM September 14, 2020 and June 21, 2021respectively, while they had 2nd lowest and lowest value of Hydraulic radius (R) (m) based on the UAV-SfM DEMS April 13, 2021 and August 27, 2021 (Figure 5.1.2 a and Table 4.3.5– 4.3.8.)

Shear stress (τ) (Nm^{-2}) was 544.28 Nm^{-2}, 771.49 Nm^{-2}, 22.47 Nm^{-2} and 462.57 (Nm^{-2}) for Study site A, B, C respectively and based on the UAV-SfM DEM September 14, 2020. Shear stress (τ) (Nm^{-2}) was 173.72 Nm^{-2}, 331.43 Nm^{-2}, 342.90 Nm^{-2} and 182.68 (Nm^{-2}) for Study site A, B, C respectively and based on the UAV-SfM DEM April 13, 2021. Shear stress (τ) (Nm^{-2}) was 254.12 Nm^{-2}, 908.66 Nm^{-2}, 725.74 Nm^{-2} and 310.65 (Nm^{-2}) for Study site A, B, C respectively and based on the UAV-SfM DEM June 21, 2021. Shear stress (τ) (Nm^{-2}) was 219.10 Nm^{-2}, 249.85 Nm^{-2}, 107.64 Nm^{-2} and 175.69 (Nm^{-2}) for Study site A, B, C respectively and based on the UAV-SfM DEM August 27, 2021 (Figure 5.1.2 b and Table 4.3.5– 4.3.8.).

For Shear stress (τ) (Nm^{-2}), Study site A, B and D had highest and 2nd highest value of Shear stress (τ) (Nm^{-2}) based on the UAV-SfM DEM September 14, 2020 and June 21, 2021, while they had 2nd lowest and lowest value of Shear stress (τ) (Nm^{-2}) based on the UAV-SfM DEMS April 13, 2021 and August 27, 2021 (Figure 5.1.2 b and Table 4.3.5–4.3.8.)

Critical shear stress (τ_c) (Nm^{-2}) was 0.155 Nm^{-2}, 0.220 Nm^{-2}, 0.006 Nm^{-2} and 0.132 (Nm^{-2}) for Study site A, B, C respectively and based on the UAV-SfM DEM September 14, 2020. Critical shear stress (τ_c) (Nm^{-2}) was 0.050 Nm^{-2}, 0.094 Nm^{-2}, 0.098 Nm^{-2} and 0.052 (Nm^{-2}) for Study site A, B, C respectively and based on the UAV-SfM DEM 13th April 2021. Critical shear stress (τ_c) (Nm^{-2}) was 0.072 Nm^{-2}, 0.259 Nm^{-2}, 0.207 Nm^{-2} and 0.089 (Nm^{-2}) for Study site A, B, C respectively and based on the UAV-SfM DEM June 21, 2021. Critical shear stress (τ_c) (Nm^{-2}) was 0.062 Nm^{-2},0.071 Nm^{-2}, 0.031 Nm^{-2} and 0.001 (Nm^{-2}) for Study site A, B, C respectively and based on the UAV-SfM DEM August 27, 2021 (Figure 5.1.2 c and Table 4.3.5– 4.3.8.).

For Critical shear stress (τ_c) (Nm^{-2}), Study site A, B and D had highest and 2nd highest value of Critical shear stress (τ_c) (Nm^{-2}) based on the UAV-SfM DEM September 14, 2020 and June 21, 2021, while they had 2nd lowest and lowest value of Critical shear stress (τ_c) (Nm^{-2}) based on the UAV-SfM DEMS April 13, 2021 and August 27, 2021 (Figure 5.1.2 c and Table 4.3.5– 4.3.8.)

Velocity (v) (ms^{-1}) was 0.057 ms^{-1}, 0.067 ms^{-1}, 0.001 ms^{-1}, 0.044 ms^{-1} for Study site A, B, C respectively and based on the UAV-SfM DEM September 14, 2020. Velocity (v) was 0.006 ms^{-1}, 0.016 ms^{-1}, 0.015 ms^{-1}, 0.004 ms^{-1} for Study site A, B, C respectively and based on the UAV-SfM DEM April 13, 2021. Velocity (v) was 0.010 ms^{-1}, 0.095 ms^{-1}, 0.055 ms^{-1} and 0.010 ms^{-1} for Study site A, B, C respectively and based on the UAV-SfM DEM June 21, 2021. Velocity (v) was 0.007 ms^{-1}, 0.007 ms^{-1}, 0.002 ms^{-1}, 0.001 ms^{-1} for Study site A, B, C respectively and based on the UAV-SfM DEM August 27, 2021 (Figure 5.1.2 d and Table 4.3.5– 4.3.8)

For Velocity (v) (ms^{-1}), Study site A, B and D had highest and 2nd highest value of Velocity (v) (ms^{-1}) based on the UAV-SfM DEM September 14, 2020 and June 21, 2021, while they had 2nd lowest and lowest value of Velocity (v) (ms^{-1}) based on the UAV-SfM DEMS April 13, 2021 and August 27, 2021 (Figure 5.1.2 d and Table 4.3.5– 4.3.8)

Peak specific discharge per unit rainfall intensity (k_p) (mm) was 1.760 mm, 1.860 mm, 0.001 mm and 1.850 mm for Study site A, B, C and D based on the UAV-SfM DEMS 14th September 2020. Peak specific discharge per unit rainfall intensity (k_p) (mm) was 0.500 mm, 0.940 mm, 0.350 mm and 0.080 mm for Study site A, B, C and D based on the UAV-SfM DEMS 13th April 2021. Peak specific discharge per unit rainfall intensity (k_p) (mm) was 0.590 mm, 4.530 mm, 4.400 mm and 0.110 mm for Study site A, B, C and D based on the UAV-SfM DEMS June 21, 2021. Peak specific discharge per unit rainfall intensity (k_p) (mm) was 0.060 mm, 0.014 mm, 0.010 mm and 0.010 mm for Study site A, B, C and D based on the UAV-SfM DEMS August 27, 2021 (Figure 5.1.2e and Table 4.3.5– 4.3.8).

For Peak specific discharge per unit rainfall intensity (k_p) (mm), Study site A, B and D had highest and 2nd highest value of Peak specific discharge per unit rainfall intensity (k_p) (mm) based on the UAV-SfM DEM September 14, 2020 and June 21, 2021, while they had 2nd lowest and lowest value of Peak specific discharge per unit rainfall intensity (k_p) (mm) based on the UAV-SfM DEMS April 13, 2021 and August 27, 2021 (Figure 5.1.2 e and Table 4.3.5– 4.3.8)

It implies that the changes in the value of several hydraulic parameters: Hydraulic radius (R) (m), Shear stress (τ) (Nm^{-2}), Critical shear stress (τc) (Nm^{-2}), Velocity (v) (ms^{-1}) and Peak specific discharge per unit rainfall intensity (k_p) (mm) in Study site A, B and D, were corresponding with the Total daily rainfall (mm) of 10 days before September 14, 2020, April 13, 2021, June 21, 2021 and August 27, 2021.

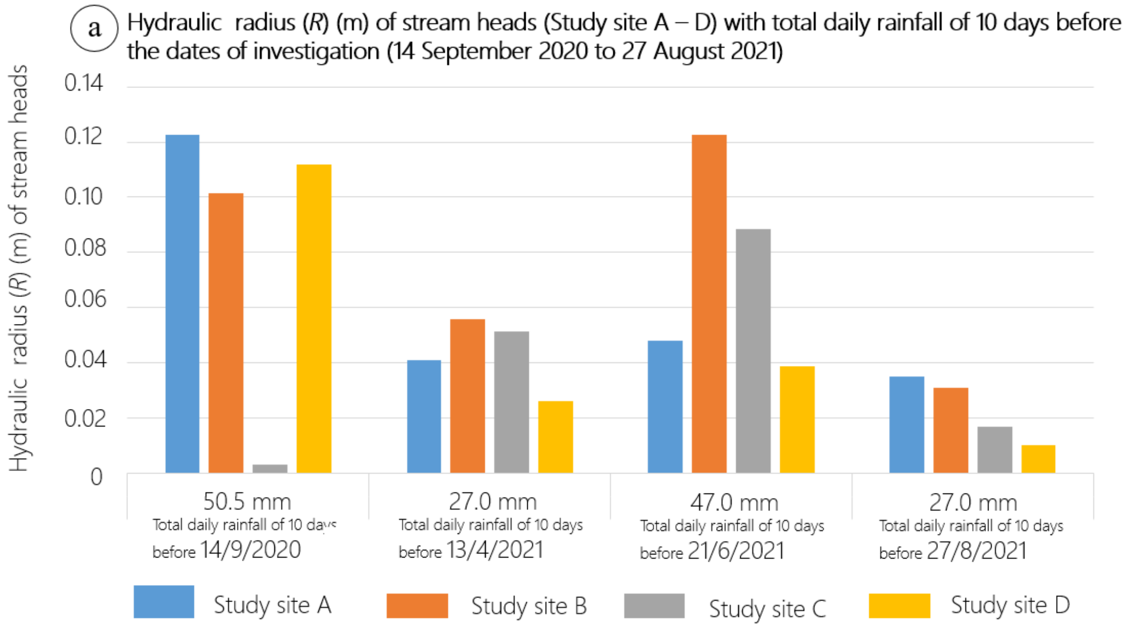
a
Hydraulic radius (R) (m) of stream heads (Study site A – D) with total daily rainfall of 10 days before the dates of investigation (14 September 2020 to 27 August 2021)
Hydraulic radius (R) (m) of stream heads
0.14
0.12
0.10
0.08
0.06
0.04
0.02
0
50.5 mm
Total daily rainfall of 10 days
before 14/9/2020
27.0 mm
Total daily rainfall of 10 days
before 13/4/2021
47.0 mm
Total daily rainfall of 10 days
before 21/6/2021
27.0 mm
Total daily rainfall of 10 days
before 27/8/2021
Study site A
Study site B
Study site C
Study site D

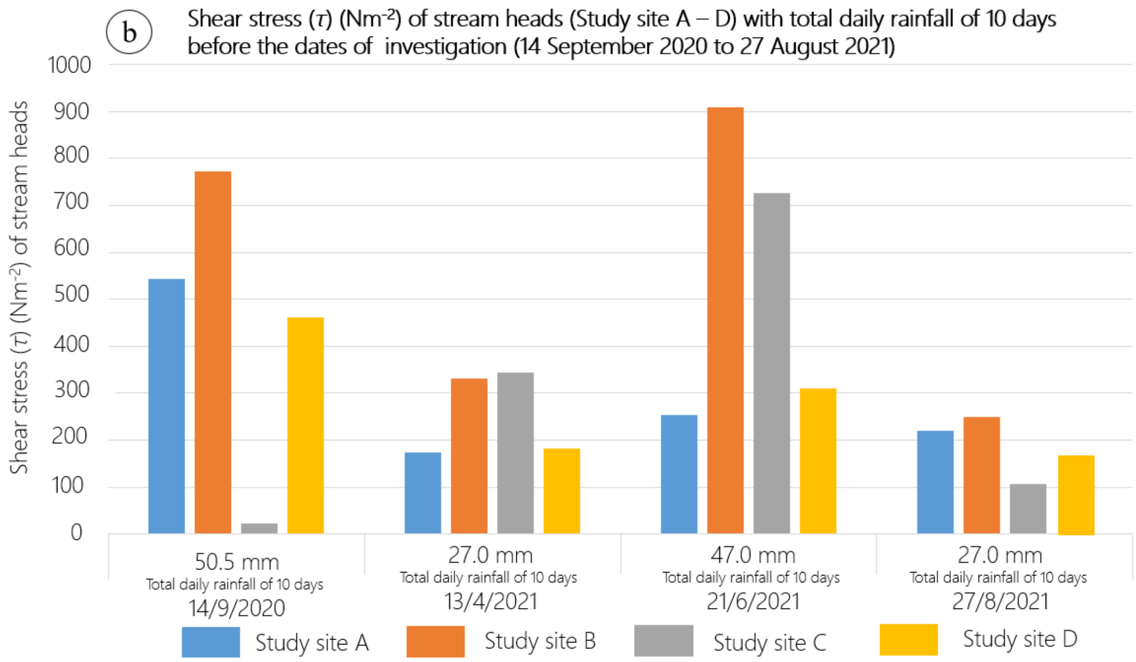
b
Shear stress (τ) (Nm-2) of stream heads (Study site A – D) with total daily rainfall of 10 days before the dates of investigation (14 September 2020 to 27 August 2021)
Shear stress (τ) (Nm-2) of stream heads
1000
900
800
700
600
500
400
300
200
100
0
50.5 mm
Total daily rainfall of 10 days
14/9/2020
27.0 mm
Total daily rainfall of 10 days
13/4/2021
47.0 mm
Total daily rainfall of 10 days
21/6/2021
27.0 mm
Total daily rainfall of 10 days
27/8/2021
Study site A
Study site B
Study site C
Study site D

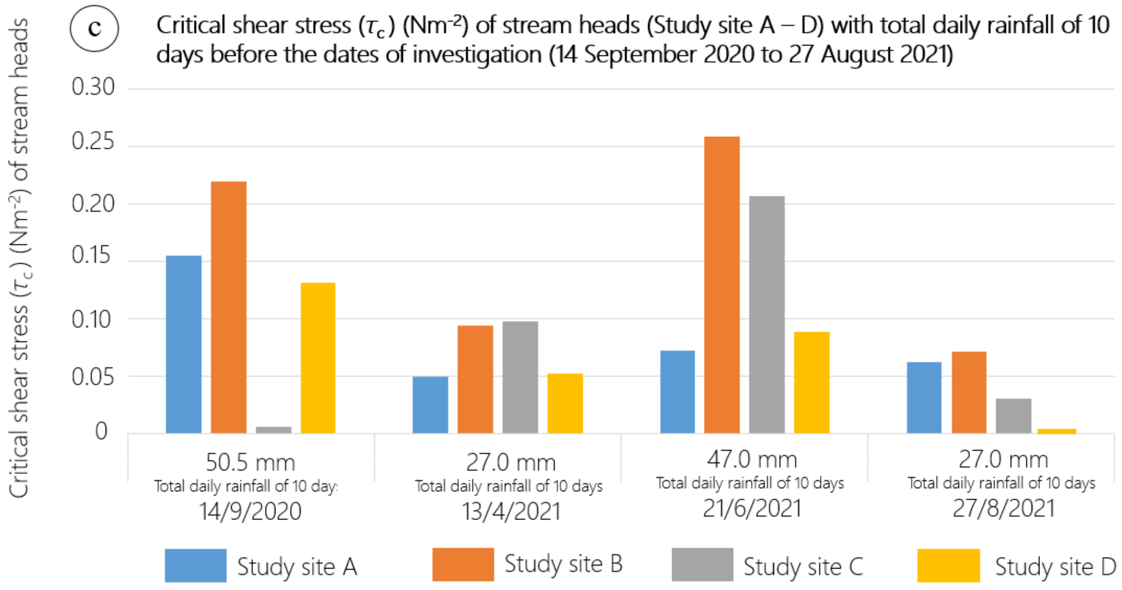
c
Critical shear stress (τ_c) (Nm^{-2}) of stream heads (Study site A – D) with total daily rainfall of 10 days before the dates of investigation (14 September 2020 to 27 August 2021)
Critical shear stress (τ_c) (Nm^{-2}) of stream heads
0.30
0.25
0.20
0.15
0.10
0.05
0
50.5 mm
Total daily rainfall of 10 days
14/9/2020
27.0 mm
Total daily rainfall of 10 days
13/4/2021
47.0 mm
Total daily rainfall of 10 days
21/6/2021
27.0 mm
Total daily rainfall of 10 days
27/8/2021
Study site A
Study site B
Study site C
Study site D

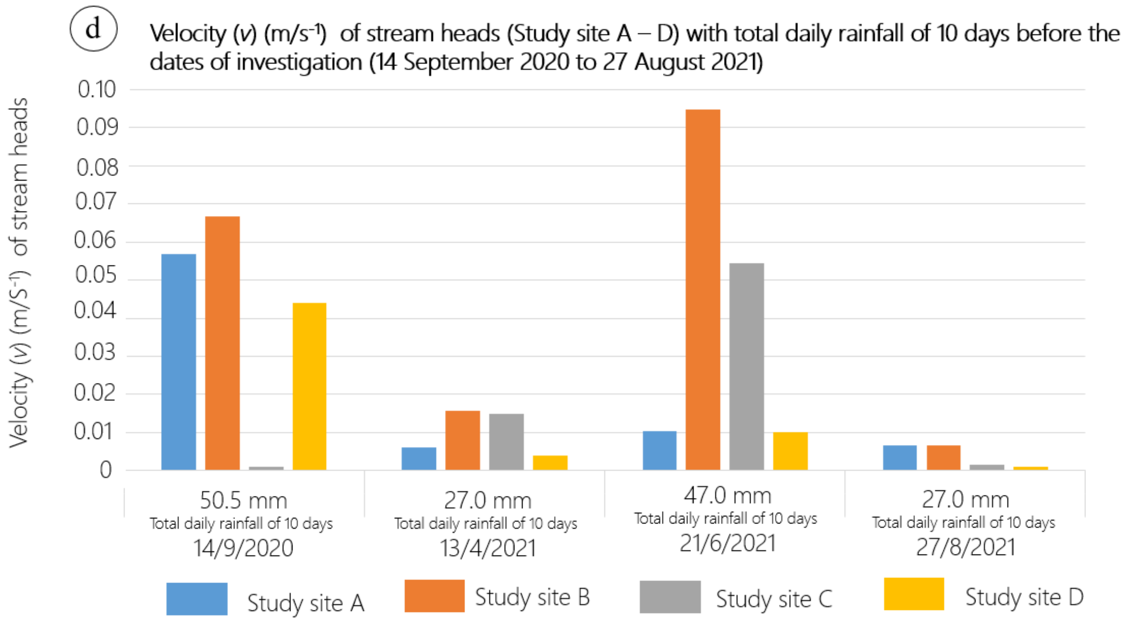
d
Velocity (v) (m/s^{-1}) of stream heads (Study site A – D) with total daily rainfall of 10 days before the dates of investigation (14 September 2020 to 27 August 2021)
Velocity (v) (m/S^{-1}) of stream heads
0.10
0.09
0.08
0.07
0.06
0.05
0.04
0.03
0.02
0.01
0
50.5 mm
Total daily rainfall of 10 days
14/9/2020
27.0 mm
Total daily rainfall of 10 days
13/4/2021
47.0 mm
Total daily rainfall of 10 days
21/6/2021
27.0 mm
Total daily rainfall of 10 days
27/8/2021
Study site A
Study site B
Study site C
Study site D

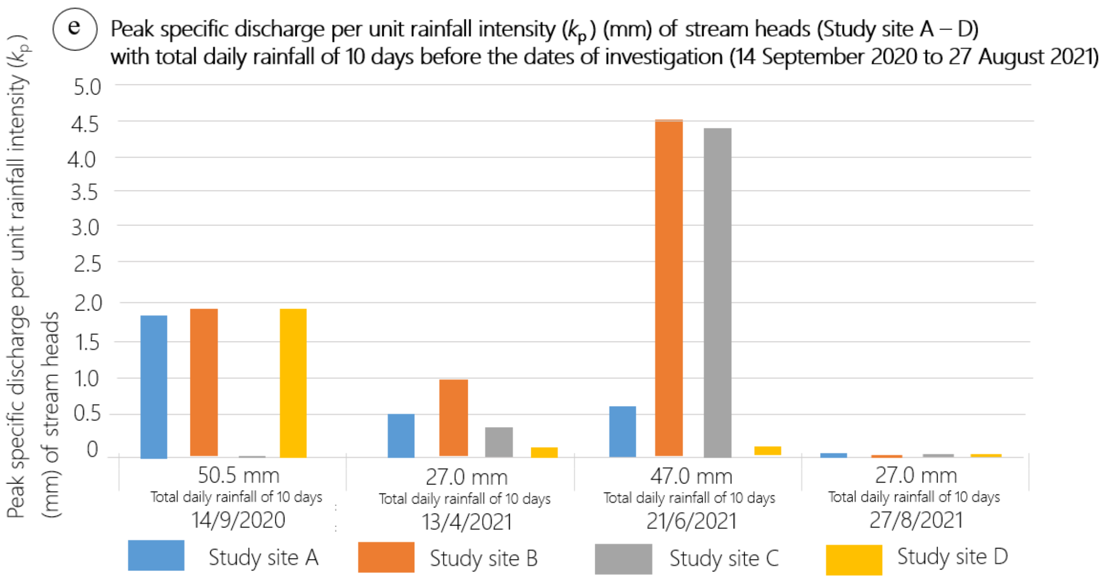

Figure 5.1.2 Correspondence of hydraulic parameters with total daily rainfall of 10 days before the dates of investigation (September 14, 2020 to August 27, 2021): (a) Hydraulic radius (R), (b) Shear stress (τ), (c) Critical shear stress (τ_c), (d) Velocity (v) and (e) Peak specific discharge per unit rainfall intensity (k_p).

5.2 Correspondence of morphological changes and sediment connectivity with soil minerals (Halloysite and Paleosol) on the slid slopes in study sites

5.2.1 Halloysite

The presence of hydrated halloysite, which formed the base layer of soil strata (Ta-d clay rich layer) on the slopes along the edges of slid slopes caused by coseismic landslides and the exposed soil on the sliding slope after the earthquake was paleosol was confirmed by X-ray diffraction (XRD) analysis (Wang and Nam, 2023).

Halloysite is weathered pyroclastic deposits (clay minerals) with rich pumice fall, which is commonly found on slopes of mountainous valleys in Japan, Indonesia and New Zealand (Umeda et al., 2019). It consists mainly alumino-silicate clay mineral with high water retention capacity and high mesopore volumes (Kameda, 2019). With absorbing of water, chemical changes happened with increasing ph value and electrostatic repulsion between the minerals since the ionic and cohesive strength among minerals decreased. This causes destabilization of slope and high mobility of soil materials on the slid slope (liquidity index greater than 1) (Kameda, 2019).

In addition, the grain size analysis indicated that the main content of Tarumae-d tephra layer were clay and silt with sand (Kasai and Yamada, 2019), while paleosol mainly consists of gravel and sand (Wang and Nam, 2023). These situation causes high volumetric moisture and water content in the soil on the slid slopes (Wang and Nam, 2023).

5.2.2 Paleosol

The presence of paleosol, which exposed on sliding surface (Wang and Nam., 2023) caused by coseismic landslides in the study sites, was examined by analysing the mineral composition of the 2 soil samples collected on the slid slopes in study site B (Figure 5.2.1 and 5.2.2) with the X-ray diffusion (XRD) method. X-ray diffusion of 2 soil samples (site B) in this study were done with the assistance of the trained X-ray laboratory specialist to avoid error and avoid inappropriate procedures during the experiment to a large extent, which can increase the reliability and level of confidence of the results of X-ray diffusion as the evidence of existence of Halloysite and Paleosol on the slid slope in the study site of the present study.

Mineral composition was analyzed for both silt (>4 μm) and clay (<4 μm) fractions, as well as potential source materials by using a powder XRD method. A powder sample mounted on a glass holder was scanned from 2° to 40° 2θ by 1° 2θ/min at 40 kV and 20 mA using CuKα radiation, where the diffraction intensity (counts per second: cps) was recorded with a 0.02° 2θ step (Lee et al, 2022). Identification of major and clay minerals was performed according to the position of diagnostic peaks of these minerals on the XRD diffractograms.

The results (Figure 5.2.1 and 5.2.2) were compared with the analysis by Wang and Nam (2023) to confirm the presence of paleosol on the exposed slide slope for examining the correspondence of the soil characteristics with the sediment mobility and connectivity, which facilitated the changes of morphology in drainage basin and development of drainage network in the study site during post-seismic periods.

Besides, the soil in Study sites has a very fine structure (Silt & clay 0.008mm 0.71mm) (Kasai and Yamada, 2019). The soil cohesion of dry sit and clay decreased from 105 to 20 kPa after saturated (Chok, et al, 2015) and chemical changes with electrostatic repulsion and decreased ionic cohesive strength within soil minerals after absorbing water caused theincreasing in liquidity index (>1)(Kameda, 2019), that means the soil on top layer of slope may easily be loosened when it absorbs water and saturated under rainfall and may cause mass wasting process along the slope.

These may be the factors causing the entrainment of sediment and along stream channels, and continuous slope processing on slid slopes in the study sites, which were correspondent to the morphological changes, drainage network development, changes of hydraulic and geomorphometric parameters, and landslide (Areas with elevation decrease) mobility with sediment connectivity during the rain seasons of post-seismic periods in the Study sites A, B, C and D.

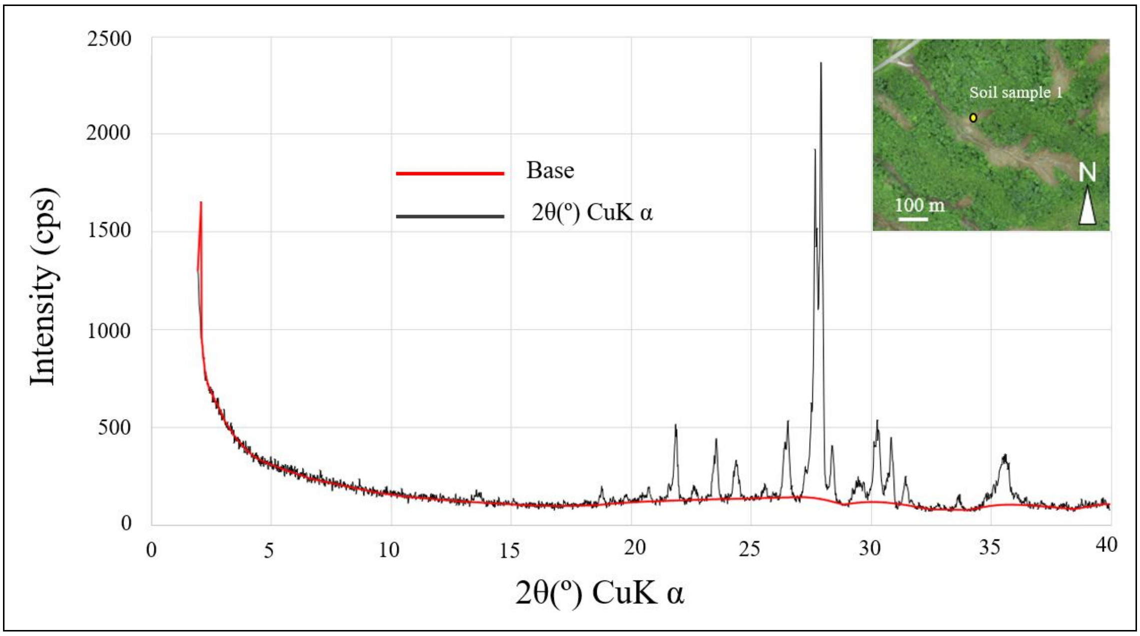

Figure 5.2.1: Schematic cross-section of pyroclastic fall deposits in the study site B based on X-ray diffraction (XRD) patterns for air-dried soil sample 1 (black line). Identification of minerals was performed according to the position of their diagnostic peaks on the XRD diffractogram.

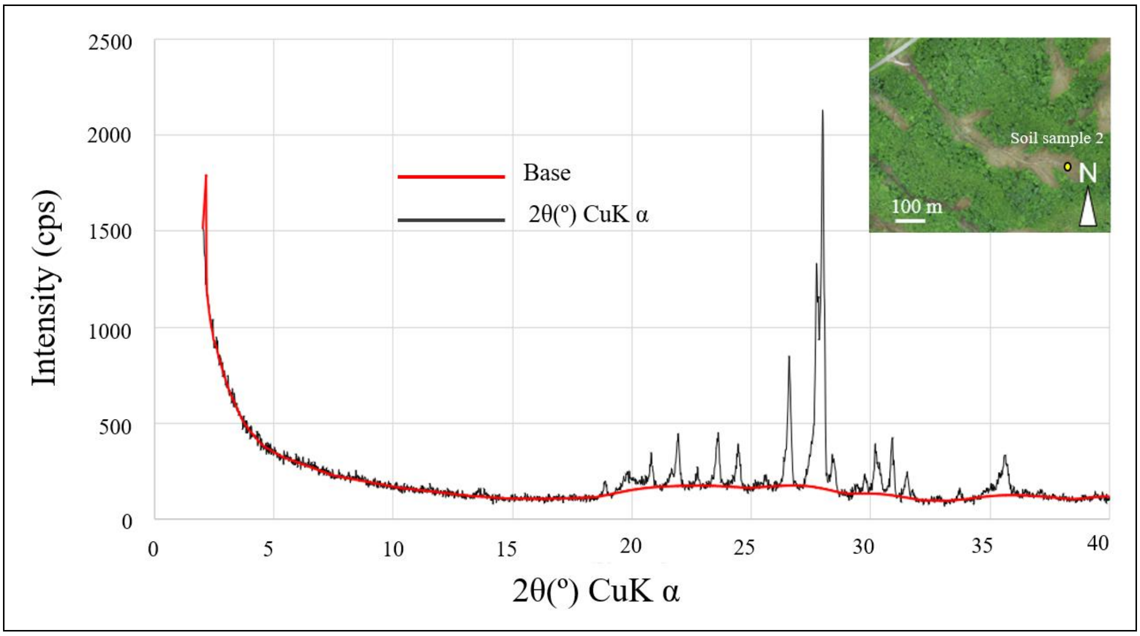

Figure 5.2.2:.Schematic cross-section of pyroclastic fall deposits in the study site B based on X-ray diffraction 2 (XRD) patterns for air-dried soil sample 2 (black line). Identification of minerals was performed according to the position of their diagnostic peaks on the XRD diffractogram.

5.3 Correspondence of post-seismic morphological change, drainage network development, change of drainage basin geomorphological parameters and sediment connectivity with the variability on forms of drainage basins.

The findings of this study clearly showed the post-seismic morphological change, drainage network development and change of drainage basin geomorphological parameters of Study site A, B C and D, which related to the variability on forms of drainage basin. According to the watershed geometry analysis, study site B and D had higher value of Form Factor, Elongation ratio, Circularity ratio and relief ratio than site A and C. Site B and D were classified as catchment with relative circular shape, while site A and C were classified as catchment with relative elongated shape. Volume of fluvial erosion of study A, B, C and D during period 2 – 9 was 1646 m^3, 4647 m^3, 1267 m^3 and 13836 m^3respectivity. The volume of fluvial erosion of study site B and D during period 2 – 9 was higher than study site A and C.

For the results of geomorphometric parameters, study site B and D had higher average value than study site A and C in the Basin area (A), Form factor (F_f), Elongation ratio (R_e), Circularity ratio (C_e), Total length of tributaries (m), Total stream length (m), Gradient of main stream channel (m/m), Stream frequency (F_s)(1/km^2), Drainage texture

(D_t), Drainage intensity (D_i) (1/km), Infiltration number (I_f), Total Dasin (H) and Ruggedness number (R_n) but lower average value in Compactness coefficient (C_c), Mean stream strength (L_m), Length of overland flow (L_o) than site A and C. Average gradient of all tributaries (1st order streams) from 05 Oct, 2012 to 29 Oct, 2021 were calculated as 0.38, 0.51, 0.60 and 0.44 for Study site A, B, C and D respectively. The maximum value of those gradients (m/m) were 0.77, 0.81, 1.06 and 0.67 for Study site A, B, C and D respectively. The minimum value of those gradients (m/m) were 0.09, 0.34, 0.13 and 0.32 for Study site A, B, C and D respectively. Those ranges were 0.68, 0.47, 0.93 and 0.35 for Study site A, B, C and D respectively, which indicated study site B and D have a smaller range and vice versa for site A and C.

For the results of hydraulic parameters, during Period 3 – 8 (April 23, 2020 – August 27, 2021) (Table), Hydraulic radius (R) (m) decreased with -0.01 m and -0.02 m in Study site A and B respectively, while it increased with 0.01 m and decreased with -0.01 m in Study site C and D respectively. Slope (10 m from stream head) (S) (tanø) increased with 0.16 (tanø), 0.19 (tanø), 0.07 (tanø) and 0.45 (tanø) in Study site A, B, C and D respectively. Study site B and D had the highest and 2nd highest value of increase in slope (tanø); while Study site A and C had the 3rd highest and lowest value of increase in slope (tanø). Velocity (v) (ms^{-1}) also had similar changes which decreased with -0.004 (ms^{-1}) and -0.005 (ms^{-1}) in Study site A and B respectively, while it increased with 0.001 (ms^{-1}) and decreased with -0.004 (ms^{-1}) in Study sites C and D respectively. Shear stress (τ) (Nm^{-2}) decreased with -23.96 (Nm^{-2}) and -46.62 (Nm^{-2}) in Study site A and B respectively, while it increased with 25.52 (Nm^{-2}) and 74.96 (Nm^{-2}) in Study sites C and D respectively. Critical shear stress (τ_c) (Nm^{-2}) decreased with -0.007 (Nm^{-2}) and -0.013 (Nm^{-2}) in Study site A and B respectively, while it increased with 0.008 (Nm^{-2}) and decreased with -0.028 (Nm^{-2}) in Study sites C and D respectively. Peak specific discharge per unit rainfall intensity (k_p) (mm) decreased with -1.330 (mm), -5.436 (mm), -0.050 mm and -1.670 mm in Study site A, B, C and D respectively during Period 3 – 8 (April 23, 2020 – August 27, 2021); while Study site B and D had the highest and 2nd highest value of decrease and Study site A and C had the 3rd highest and the lowest value of decrease.

For the post-seismic periods 2 – 9, the average value of landslide area density (LAD)(m/m), was 0.03, 0.05, 0.04 and 0.08 for study site A – D respectively. These values of study site B and D were higher than study site A and C. The value of deposit length ratio (DLR) (m/m) was 0.02, 0.04, 0.02 and 0.03 for study site A – D respectively. These values of study site B and D were also higher than study site A and C. The value of landslide (Areas with elevation decrease) mobility index was 0.68, 0.57, 0.62 and 0.46 for study site A – D respectively. These values of study site B and D were lower than study site A and C. The landslide travel distance (m) was 64.38 m, 126.95 m, 92.27 m and 250.14 m for study site A – D respectively, by which these values of study site B and D were higher than study site A and C.

The stream length in areas with elevation decrease was 193.85 m, 203.61 m, 197.11 m and 254.05 m for study site A, B, C and D respectively, by which these values of study site B and D were higher than study site A and C. The stream length in areas with elevation increase was 15.79 m, 61.52 m, 25.79 m and 110.34 m for study site A, B, C and D respectively, by which these values of study site B and D were also higher than study site A and C. Site B and D had longer length of stream channel on both areas with elevation decrease and areas with elevation increase than site A and C and vice versa on areas with elevation increase.

Excluded those affected by artificial modification at the stream outlet, linear shaped elevation decreased areas (- 0.2 m (+/- 20cm) to – 2.0 m (+/- 20cm)) at middle course of stream in all study sites implies fluvial erosion along stream channels during Period 2-9 (Figure 4.4.1 and Figure 4.4.2) The volume of erosion per unit area of catchment were (m^3/m^2) per year of study site A to D were 0.019, 0.041, 0.012, and 0.067 during post-seismic Period 2 - 9. Study B and D had higher erosional rate than site A and C.

The drainage basins in 4 Study sites (A-D) have different forms of catchment with similar geology, climatic variables and surface covers.

The catchment of site A and C shows a relatively narrow shape with less tributaries, which can be regarded as the “elongated” form (Horton, 1932; Prabhakaran et al., 2018), while the catchment of site B and D shows a relatively wide shape with more tributaries, which can be regarded as the “circular” form (Horton, 1932; Prabhakaran and Jawahar, 2018). Those difference in form may cause variations on movement of water area, shape of hydrograph and duration of stream flow in drainage basins (Mokarram and Sathyamoorthy, 2015), resulting in different changes of geomorphometric parameters and hydrological processes.

Based on analysis of watershed geometry, site A and C were classified as relatively elongated catchment with average value form factor (Ff) of 0.19 and 0.22 respectively, while site B and D were relatively circular catchment with form factor (Ff) of and 0.32 and 0.42. Also, the average value of elongation ratio (Re) of 0.49 and 0.52 of Study site A and C respectively indicated the catchments of site A and C were relatively elongated form with long straight mainstream, less and shorter tributaries which joining at acute angle. Elongated form catchment may indicate a flat hydrograph peak for longer duration (Mokarram and Sathyamoorthy, 2015) with lower runoff peak. Discharge from all sub-catchments takes long time to peak because of low runoff rates with lesser number of streams (Patton and Baker, 1976; Montgomery and Dietrich, 1989; Montgomery and Dietrich, 1992; Ghoneim et al., 2002) and may give less erosional power on slid slopes in Study site A and C, with lower mobility that less sediment can be delivered out of catchment and most of eroded material remain in drainage basins.

Conversely, the average value of elongation ratio (R_e) of 0.64 and 0.73 of Study site B and D respectively catchments of site B and D were in relatively circular form with more and longer tributaries which join main river in shape of a tree at acute angle. Circular form watershed may indicate steeper rising and recession limb of hydrograph with higher peak discharge for shorter duration. Discharge from all the sub-catchments may take short time to peak because of high runoff rates with larger number of tributaries, and give more erosional power on slid slopes in Study site B and D, with higher mobility that more sediment can be delivered out of catchment and most of eroded material was transported out of drainage basins.

Period 1: 5th October, 2012 – 11th September, 2018					
	Landslide Mobility			Sediment Connectivity	
	Landslide mobility index (y(H/L))	Landslide Travel distance (m)	Landslide height (m)	Landslilde area density (LAD)	Deposit length ratio (DLR)
Study sites					
A	0.47 (2nd)	223.29 (3rd)	65.08 (3rd)	0.18 (3rd)	0.42 (1st)
B	0.41 (3rd)	314.11 (2nd)	83.98 (2nd)	0.22 (2nd)	0.25 (4th)
C	0.51 (1st)	180.93 (4th)	55.32 (4th)	0.11 (4th)	0.32 (2nd)
D	0.31 (4th)	539.00 (1st)	123.93 (1st)	0.32 (1st)	0.30 (3rd)

	Form factor (F_f)	Elongation ratio (R_e)	Circularity ratio (R_c)	Relief ratio (R_h)
Study sites				
A	0.19 (4th)	0.49 (4th)	0.22 (4th)	1.28 (4th)
B	0.31 (2nd)	0.63 (2nd)	0.64 (1st)	1.63 (2nd)
C	0.21 (3rd)	0.52 (3rd)	0.25 (3rd)	1.43 (3rd)
D	0.41 (1st)	0.72 (1st)	0.36 (2nd)	1.71 (1st)

Table 5.3.1: Quantitative analysis of Landslide (Elevation decreased area) mobility, Sediment connectivity and 4 geomorphometric parameters (Study sites A -D) with ranking from highest value (1st) to lowest value (4th): Analysis from the pre-seismic ALS DEM on 5th October 2012 and post-seismic ALS DEM on 11th September 2018 (Period 1).

Period 2-9: 11th September 2018 – 29th October 2021					
	Mobility			Sediment Connectivity	
	Landslide (Areas with elevation decrease) mobility index (y(H/L))	Landslide (Areas with elevation decrease) Travel distance (m)	Landslide (Areas with elevation decrease) height (m)	Landslilde (Areas with elevation decrease) area density (LAD)	Deposit length ratio (DLR)
Study sites					
A	0.68 (1st)	64.38 (4th)	21.91 (4th)	0.0.3(4th)	0.02 (4th)
B	0.57 (3rd)	126.94 (2nd)	41.51 (2nd)	0.05 (2nd)	0.04 (1st)
C	0.62 (2nd)	92.27(3rd)	31.36 (3rd)	0.04 (3rd)	0.02 (3rd)
D	0.46 (4th)	250.14 (1st)	70.91 (1st)	0.08 (1st)	0.03 (2nd)
	Form factor (F_f)	Elongation ratio (R_e)	Circularity ratio (R_c)	Relief ratio (R_h)	
Study sites					
A	0.19 (4th)	0.49 (4th)	0.22 (4th)	1.28 (4th)	
B	0.31 (2nd)	0.63 (2nd)	0.64 (1st)	1.63 (2nd)	
C	0.21 (3rd)	0.52 (3rd)	0.25 (3rd)	1.43 (3rd)	
D	0.41 (1st)	0.72 (1st)	0.36 (2nd)	1.71 (1st)	

Table 5.3.2: Quantitative analysis of Landslide (Elevation decreased area) mobility, Sediment connectivity and 4 geomorphometric parameters (Study sites A -D) with ranking from highest value (1st) to lowest value (4th): Analysis from the post-seismic ALS DEM on September 11, 2018 and UAV-Lidar DEM on October 29, 2021 (Period 2-9).

Tables 5.3.1 and 5.3.2 indicate the classification of Study sites A, B, C and D into 2 groups: Study site A with C and Study sites B with D, based on the ranking from highest value (1st) to lowest value (4th) of Landslide (Elevation decreased area) mobility, Sediment connectivity and 4 geomorphometric parameters (Study sites A -D) during pre- and post-seismic period from October 05, 2012 to post-seismic September 11, 2018 (Period 1) and post-seismic periods from September 11, 2018 to October 29, 2021 (Period 2-9).

Study site B and D 1st and 2nd ranking (highest and second highest value) in Landslide (Areas with elevation decrease) travel distance (m), Landslide (Areas with elevation decrease) height, Landslide area (Areas with elevation decrease) density (LAD) (m^2/m^2) and 4 geomorphometric parameters: Form factor (F_f), Elongation ratio (R_e) Circularity ratio (R_c) and Relief ratio (R_h); while Study site B and D also had 3rd and 4th ranking (3rd highest and the lowest value among the 4 Study sites) in Landslide (Areas with elevation decrease) mobility index (y) and Deposit length ratio (DLR) (m/m) during pre- and post-seismic period from October 05, 2012 to post-seismic September 11, 2018 (Period 1).

Study site B and D had 1st and 2nd ranking (highest and second highest value) in Landslide (Areas with elevation decrease) travel distance (m), Landslide (Areas with elevation decrease) height, Landslide area (Areas with elevation decrease) density (LAD) (m^2/m^2) and Deposit length ratio (DLR) (m/m), and 4 geomorphometric parameters: Form factor (F_f), Elongation ratio (R_e) Circularity ratio (R_c) and Relief ratio (R_h); while Study B and D also had 3rd and 4th ranking (3rd highest and the lowest value among the 4 Study sites) in Landslide (Areas with elevation decrease) mobility index (y) during post-seismic periods from September 11, 2018 to October 29, 2021 (Period 2-9).

Conversely, Study site A and C had 3rd and 4th ranking (3rd highest and the lowest value among the 4 Study sites) in Landslide (Areas with elevation decrease) travel distance (m), Landslide (Areas with elevation decrease) height, Landslide area (Areas with elevation decrease) density (LAD) (m^2/m^2) and 4 geomorphometric parameters: Form factor (F_f), Elongation ratio (R_e) Circularity ratio (R_c) and Relief ratio (R_h); while Study site A and C also had 1st and 2nd ranking ((highest and second highest value) in Landslide (Areas with elevation decrease) mobility index (y) and Deposit length ratio (DLR) (m/m) during pre- and post-seismic period from October 05, 2012 to post-seismic September 11, 2018 (Period 1).

Also, Study site A and C had 3rd and 4th (3rd highest and the lowest value) in Landslide (Areas with elevation decrease) travel distance (m), Landslide (Areas with elevation decrease) height, Landslide area (Areas with elevation decrease) density (LAD) (m^2/m^2), Deposit length ratio (DLR) (m/m) and 4 geomorphometric parameters: Form factor (F_f), Elongation ratio (R_e) Circularity ratio (R_c) and Relief ratio (R_h); while Study site A and C also had 1st and 2nd ranking ((highest and second highest value) in Landslide (Areas with elevation decrease) mobility index (y) during post-seismic periods from September11, 2018 to October 29, 2021 (Period 2-9).

The above results indicate the relationship between 4 geomorphometric parameters: Form factor (F_f), Elongation ratio (R_e) Circularity ratio (R_c) and Relief ratio (R_h), Mobility and Sedimentation connectivity.

Study site D and B have the highest and 2nd highest average value of Basin area (A) (m^2), Form factor (F_f) and Elongation ratio (R_e) respectively; while Study site B and D also have highest and 2nd highest average value of Circularity ratio (R_c) respectively; and lowest and 2nd lowest average value of Compactness coefficient (C_c) respectively among 4 study sites.

Meanwhile, Study site A and C have the lowest and 2nd lowest average value of Basin area (A) (m^2), Form factor (F_f), Elongation ratio (R_e) and Circularity ratio (R_c)

respectively; while Study site C and A also have lowest and 2nd lowest average value of of Compactness coefficient (C_c) respectively among 4 study sites.

The drainage basins in 4 Study sites (A-D) have different forms of catchment with similar geology, climatic variables and surface covers.

The catchment of site A and C shows a relatively narrow shape with less tributaries, which can be regarded as the "elongated" form (Horton, 1932; Prabhakaran et al., 2018), while the catchment of site B and D shows a relatively wide shape with more tributaries, which can be regarded as the "circular" form (Horton, 1932; Prabhakaran and Jawahar, 2018). Those difference in form may cause variations on movement of water area, shape of hydrograph and duration of stream flow in drainage basins (Mokarram and Sathyamoorthy, 2015), resulting in different changes of geomorphometric parameters and hydrological processes.

Based on analysis of watershed geometry, site A and C were classified as relatively elongated catchment with average value form factor (F_f) of 0.19 and 0.22 respectively, while site B and D were relatively circular catchment with form factor (F_f) of and 0.32 and 0.42. Also, the average value of elongation ratio (R_e) of 0.49 and 0.52 of Study site A and C respectively indicated the catchments of site A and C were relatively elongated form with long straight mainstream, less and shorter tributaries which joining at acute angle. Elongated form catchment may indicate a flat hydrograph peak for longer duration (Mokarram and Sathyamoorthy, 2015) with lower runoff peak. Discharge from all sub-catchments takes long time to peak because of low runoff rates with lesser number of streams (Patton and Baker, 1976; Montgomery and Dietrich, 1989; Montgomery and Dietrich, 1992; Ghoneim et al., 2002) and may give less erosional power on slid slopes in Study site A and C, with lower mobility that less sediment can be delivered out of catchment and most of eroded material remain in drainage basins.

Conversely, the average value of elongation ratio (R_e) of 0.64 and 0.73 of Study site B and D respectively catchments of site B and D were in relatively circular form with more and longer tributaries which join main river in shape of a tree at acute angle. Circular form watershed may indicate steeper rising and recession limb of hydrograph with higher peak discharge for shorter duration. Discharge from all the sub-catchments may take short time to peak because of high runoff rates with larger number of tributaries, and give more erosional power on slid slopes in Study site B and D, with higher mobility that more sediment can be delivered out of catchment and most of eroded material was transported out of drainage basins.

The differences on the volume of landslide (areas with elevation decrease) and sedimentation (areas with elevation increase) can represent the rate of erosion and sedimentation within drainage basins of Study site A, B, C and D.

The volume of erosion per unit area of catchment were 0.019 m^3/ m^2, 0.041 m^3/ m^2, 0.012 m^3/ m^2 and 0.067 m^3/ m^2 in Study site A, B, C and D respectively (Figure 5.3.1), which were higher than the average value of 0.023 m^3/ m^2 of Yubari Shuparo Dam (Hokkaido Regional Development Bureau (2021), 0.013 m^3/ m^2 of Hoheikyo Dam (Hokkaido Regional Development Bureau (2021), 0.008 m^3/ m^2 of Azuma River basin (Miyazaki et al., 2023), 0.006 m^3/ m^2 of Jozankei Dam (Hokkaido Regional Development Bureau(2021)), 0.0016 m^3/ m^2 of Oyubari Dam (Hasegawa et al., 2005) and 0.0010 m^3/ m^2 of Hokkaido (Hasegawa et al., 2005).

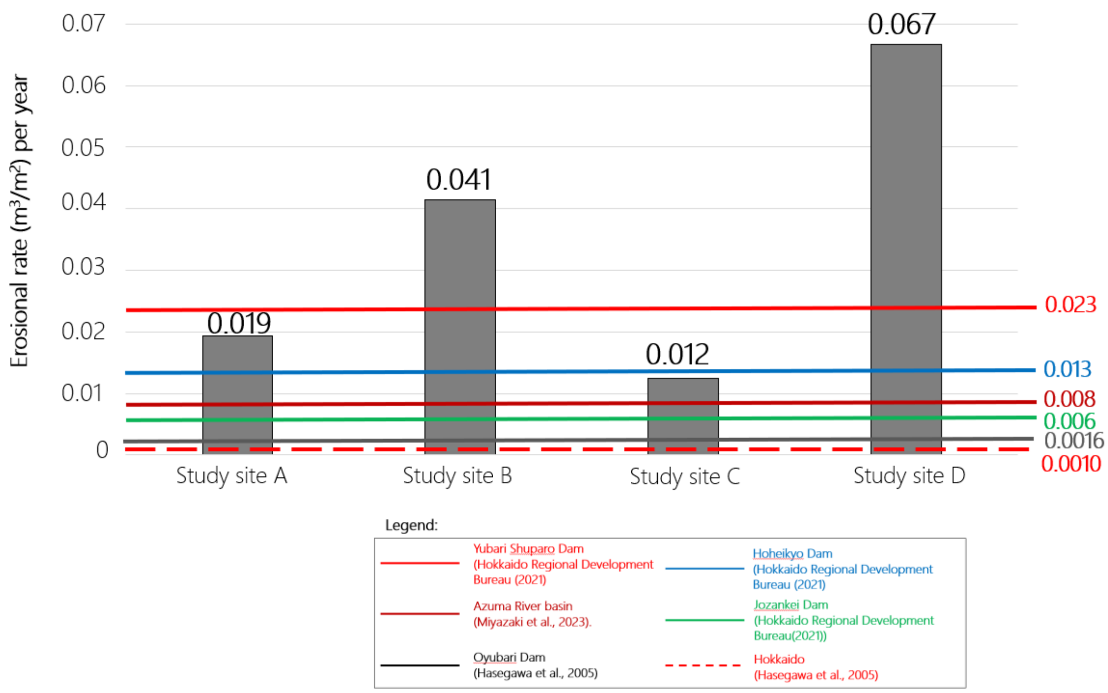

Figure 5.3.1: Erosional rate (m^3/m^2) per year of Study site A, B, C and D during investigation Period 2 – 9 from 11th September, 2018 to 29th October, 2021.

The differences on the volume of landslide (areas with elevation decrease) and sedimentation (areas with elevation increase) with different sediment mobility between the Study sites A, B, C and D with the relative high rate of erosion may indicate the necessity for drainage basin management according to different forms of drainage catchments.

Linkage of landslide (areas with elevation decrease) and sediment accumulation was observed. Larger the landslides (Areas with elevation decrease) area & volume ae positively varies with larger sedimentation area & volume, based on the quantitative analysis of Landslide (Elevation decreased area) mobility, Sediment connectivity and 4 geomorphometric parameters (Study sites A -D) from the pre-seismic ALS DEM in 5th October 2012, post-seismic ALS DEM in September 11, 2018 and UAV-Lidar DEM in October 29, 2021 (Period 2-9).

Also, larger areas of watershed, more landslide (areas with elevation decrease) and sedimentation in terms of both areas & volume in Study sites B and D (Vice versa in Study site A and C).

Those results may also relate with different forms of drainage catchments. Relative Elongated form of catchment in Study site A and C with long straight mainstream, less and shorter tributaries, joining at acute angle and relatively flat hydrograph peak for longer duration (Mokarram and Sathyamoorthy, 2015) and lower runoff peak, caused longer time for discharge from all sub-catchments to reach the peak, because of low runoff rates with lesser number of streams (Patton and Baker, 1976; Montgomery and Dietrich, 1989; Montgomery and Dietrich, 1992; Ghoneim et al., 2002). This may give less erosional power on slid slopes and stream channels in Study site A and C, with lower mobility that less sediment can be delivered out of catchment and most of eroded material remain in drainage basins.

Conversely, relative circular form of catchment in Study site B and D with relative shorter straight mainstream, more and longer tributaries, joining at acute angle, relatively steeper rising and recession limb of hydrograph and reaching the peak for shorter duration (Mokarram and Sathyamoorthy, 2015) and higher runoff peak, caused shorter time for discharge from all sub-catchments to reach the peak , because of high runoff rates with more number of streams (Patton and Baker, 1976; Montgomery and Dietrich, 1989; Montgomery and Dietrich, 1992; Ghoneim et al., 2002). This may give relative higher erosional power on slid slopes and stream channels in Study site B and D, with relative higher mobility that more sediment can be delivered out of catchment and most of eroded material entrained out of drainage basins.

Also, landslide (areas with elevation decrease) area & volume were higher than Sedimentation areas & volume in all Study site A, B, C and D) during Period 1: October 05, 2012 – September 11, 2018, and Period 2 – 9: September 11, 2018 - October 29, 2021. The reason may relate to the rate of fluvial erosion, erosion of sediment due to rainfall and property of sediment (soil) on the slid slope and stream channels, which will discuss on the followings sections.

Besides, the Landslide (areas with elevation decrease) area density (LAD) varies positively with Deposit length ratio (DLR) especially in watersheds with areas less than 0.5 km^2 (Arata 2021).

In all Study site A, B, C and D (basin area: 0.07 km^2, 0.10 km^2, 0.89 km^2 and 0.19 km^2) during Period 2 – 9: September 11, 2018 - October 29, 2021, the Landslide (areas with elevation decrease) area density (LAD) decreased with decreasing Deposit length ratio (DLR) were observed.

The Landslide (areas with elevation decrease) area density (LAD) of Study site B and D were higher than Study site A and C, while the Deposit length ratio (DLR) in Study sites A and C were higher than Study sites B and D during Period 1: October 05, 2012 – September 11, 2018. The coseismic landslides caused by the 2018 Hokkaido Easten Iburi Earthquake were considered as Valley-based landslides (Zhao 2021). Initial sliding direction was perpendicular to the trend of the valleys and deposits accumulated on valley bottom (Zhao 2021). Study sites B and D had relative larger watershed areas and in relative circular form of catchment with more sub-watersheds. The coseismic landslide happened in Study sites B and D were coalescing landslides with mulitple headscarps and one main travel path (Zhao 2021). Conversely, Study sites A and C had relative elongated form of catchment with only one long mainstream and one long valley, so that sedimentation mainly occurred along the main valley and main stream channel, which contributed to longer stream length on sedimentation (areas with elevation increased)

The Landslide (Areas with elevation decrease) mobility index (y(H/L)) was 0.47, 0.41, 0.51 and 0.31 during Period 1: October 05, 2012 – September 11, 2018; 0.68, 0.57, 0.62 and 0.46 during Period 2 to 9: September 11, 2018 - October 29, 2021, of site A, B, C and D respectively. The Landslide (Areas with elevation decrease) mobility index (y(H/L)) of Study sites A and C were lower than Study sites B and D. Also, the volume of erosion was smaller in Study site A and C, which was correspondent with lower Landslide (Areas with elevation decrease) mobility index (y(H/L)) in site A and C.

Catchment of Study site A and C are in elongated form with long straight mainstream, less and shorter tributaries which joining at acute angle. Elongated shaped catchment may indicate a flat hydrograph peak for longer duration (Mokarram and Sathyamoorthy, 2015) with lower runoff peak. Discharge from all sub-catchments takes long time to peak because of low runoff rates with lesser number of streams (Patton and Baker, 1976; Montgomery and Dietrich, 1989; Montgomery and Dietrich, 1992; Ghoneim et al., 2002) and may give lower mobility that less sediment can be delivered out of catchment.

Conversely, catchment of site Band D are in circular form with more and longer tributaries which join main river in shape of a tree at acute angle. Relative circular shaped watershed may indicate steeper rising and recession limb of hydrograph with higher peak discharge for shorter duration. Discharge from all the sub-catchments may take short time to peak because of high runoff rates with larger number of tributaries, which give higher mobility with more delivered sediment out of catchment in site B and D.

The differences in mobility and volume of erosion between 4 study sites may indicate the necessity for drainage basin management according to different forms of drainage basins.

Deposit length ratio (DLR) were 0.42, 0.25, 0.32 and 0.30 in Study sites A , B, C and D during Period 1: 5^{th} October 2012 – 11^{th} September 2018, and 0.02, 0.04, 0.02, 0.03 in Study sites A , B, C and D during Period 2 – 9: September 11, 2018 - October 29, 2021.

Compare with the value of Deposit length ratio (DLR) 0.12 in different sub-watersheds (areas 0.01 to 4.4 km^2) of entire Habiugawa watershed (40 km^2) and sub-watersheds with area from 0.1 to 0.5 km^2 ranged from 0.2 to 0.5 (Arata et al 2021) which located 13 km north of the epicenter and affected by the 2018 Hokkaido Eastern Iburi earthquake, Japan, the Deposit length ratio (DLR) in Study sites A , B, C and D during Period 1: October 05, 2012 – September 11, 2018 were high. Also, Compared to the other earthquake-induced landslides (e.g., Wenchuan earthquake: 0.03) the Deposit length ratio (DLR) in Study sites A, B, C and D during Period 1: October 05, 2012 – September 11, 2018 were high. This implies poorly mobilized sediments that initiate in headwaters rapidly deposit in channels (Arata et al 2021)

The analysis and results (especially the hydro-geomorphometric parameters (indicators)) were the dimensional quantitative methods (which have been proved by various previous researches listed as the references in this thesis, as a fundamental model to indicate the different predominant fluvial processes in drainage system study) and supportive evidence for separating the 4 catchments into 2 groups. Since one of the limitation in this study is lack of long-period continuous record of stream discharge during the investigation period 1-9 (2012-2021) in the study sites, the equations of 35 hydro-geomorphometric parameters were used for making a valuable and convincible prediction on fluvial-geomorphological processes within 4 target drainage basins. For examples: the Form factor, Elongation ratio and Circularity ratio were used to classify Elongated (long and narrow) and Circular (wide) shape of watershed. Then, the values of stream order, stream number, stream length, stream frequency, gradient of main stream, drainage texture, density and intensity, compactness coefficients, total length of tributaries, length of overland flow, infiltration number, landslide areal density, deposit length ratio, mobility index, travel distance, Ruggedness number, Relied ratio, Peak specific discharge also indicated the 2 directional trend of changes between site A and C with B and D. Those results of parameters (indicators) had represented the different predominant fluvial processes and characteristics, such as shorter mainstream and steeper rising and recession limb of hydrograph with higher runoff peak and discharge in site B and D which are correlated to the characteristics of fluvial regime (these were also proved by the results of drainage patterns and drainage networks development during the post-seismic periods in study sites). Therefore, to a large extent, the causal inter-relationship of the results of parameters to explain the occurrence of various natural post-seismic phenomenon in study sites can be defined systematically.

5.4 Correspondence of morphological responses with less root reinforcement by limited vegetation recovery.

Landslide caused damages (Keefer and Larsen, 2007), such as destruction of vegetation cover on hillslope which caused unstable bare land for erosion for many years (Koi et al., 2008; Taukamoto et al., 2001). Natural disturbance agents and vegetation recovery affects biophysical diversity on landslide scars (Geertsema and Pojar, 2007; Restrepo et al., 2009)

For the research about Vegetation Recovery and Landslide Activities in the

Wenchuan Earthquake (2008) Area (Zhong et al, 2021), slid slopes with gradient higher than 1.11 (48º), with surfaces covered by exposed bedrock or a little soil, were not suitable for vegetation growth. Also, the slopes with south and south-west facing had relative higher rate of vegetation recovery. Among 60% slid slopes in coseisimic landslides, vegetation recovery take a period of decade for recovering to higher than 75% of the pre-earthquake level and most vegetation can completely recover to the pre-earthquake level within 20 years. Topographic factors, especially the elevation and slope, have a significant influence on the vegetation recovery rate, and they affect landslide activities ((Zhong et al, 2021). Although the percentage of active landslide from 2009 to 2011 were 100, 99.9 and 99.9 and then decreasing to 75.29 65.70 58.09 38.86 20.15 19.55 and 5.88 in the years of 2012, 2013 .2014, 2015, 2016, 2017 and 2018 respectively, most landslides in Wenchuan Earthquake (2008) Area achieved a relatively stable status, though they did not reach the pre-earthquake level yet. It implies the importance of vegetation recovery on stabilization the slid slopes after the Wenchuan earthquake (2008).

5.4.1 Analysis of Normalized Difference Vegetation Index (NDVI)

The normalized difference vegetation index (NDVI) is an indicator which quantify vegetation by measuring the difference between near-infrared, which vegetation strongly reflects, and red light, which vegetation absorbs by remote sensing measurements for assessing whether the target being observed contains live green vegetation or not. NDVI values varies from -1.0 to 1.0. Negative NDVI values reflect the situation of clouds, water and snow surface. When the NDVI values close to zero (0.1 or less), which indicated rocks, sand or bare soil surface. The positive post-seismic NDVI value on slid slopes in coseismic landslide areas reflects the conversion of fresh landslide surface to vegetation.

Site D	Tributary	16	17	18	19	35	38	39
	Location	M	M	M	M	U	U	U
NDVI Sensor: SGLI (CGOMC)	Aug 29 ~ Sep 05 2018 (Pre-seismic)	0.84	0.84	0.84	0.84	0.84	0.84	0.84
NDVI	Jun 21, 2021 (Post-seismic)	0.18	0.09	0.02	0.02	0.06	0.02	0.03

***NDVI: Normalized Difference Vegetation Index** ***M: Middle part (lower elevation) of valley**
***U: Upper part (higher elevation) of valley**

Table 5.4.1: NDVI (Average between Aug 29 ~ Sep 05, 2018: Sensor: SGLI (CGOMC)) and Jun 21, 2021) of several tributaries in site D.

Based on the data by Sensor: SGLI (CGOMC), the NDVI value of some location in site D were indicated in the following tables for comparing the Pre and Post – earthquake NDVI value. The NDVI value in the location of Tributary 16, 17, 18, 19, 35, 38, 39 were 0.84 from 29 Aug to 5 Sep 2018 (Table 5.4.1). The NDVI value decreased to 0.18, 0.09, 0.02, 0.02, 0.06, 0.02, 0.03 respectively on the date of Jun 21, 2021 which indicated the recovery of vegetation was limited in study sites.

Based on the NDVI map of Study site D on June 21, 2022 (Figure 5.6.1), NDVI was higher (such as 0.86 at stream head of tributary 2) at the sedimentation areas in lower courses of stream with lower elevation and gentle slopes such as along the 4th order stream and 2nd order stream no. 5 (Figure 5.4.1.1). The gradient of the 4th order and 2nd order stream no.5 were 0.07 (4.0^{o}) and 0.24 (13.5^{o}) respectively, which were relatively gentler than other streams such as 0.39 (21.31^{o}) and 0.58 (30.11^{o}) of 2nd order stream no. 4 and no.6 respectively. Also, the lowest elevation of 4th order stream was 93.99 m, while the lowest elevation of 2nd order stream no.5 was 99.21 m. For the 2nd order stream no. 4 and no.6, their lowest elevations were 136.03 m and 142.58 m respectively.

The NDVI (Figure 5.4.1.1) was lower at middle and upper part of valley with steep slopes such as at the stream heads of tributaries 16, 17 and 19 were 0.18, 0.09 and 0.02 respectively, with the gradient of 0.64 (32.62°), 0.57 (29.68°) and 0.63 (32.21°) respectively, and at the stream heads of tributaries 32, 35 and 39 and were 0.18, 0.17, and 0.15 and with the gradient of 0.46 (24.70°), 0,68 (34.22°) and 0.49 (26.10°). The NDVI was lower at locations with higher elevation, such as the lowest elevation of tributaries 16, 17 and 18 were 110.09 m, 112.58 m and 112.02 m respectively. Also, the lowest elevation of tributaries 33, 35 and 39 were 162.96 m, 169.22 m and 187.02 m respectively.

The NDVI (Figure 5.4.1.1) was also lower on the slopes facing south to southwest in middle part of valley such as at the stream heads of tributaries 16, 17 and 19 were 0.18, 0.09 and 0.02 respectively.

The NDVI and amount of vegetation on South-west facing were lower than North-east facing slopes . Vegetation recovery rate decreases as the amount of solar radiation increases. For south-facing slopes with excessive sunlight may cause easier drying progresses and delay vegetation recovery (Nakata et al., 2023). Therefore, amount of soil moisture may also be considered as one of the factors for vegetation recovery in landslide areas (Lin et al., 2005).

Natural vegetation restoration after landslide might be affected by the gradient of slid slopes. Steep slopes typically have a larger actual soil surface cross-sectional area, and thus have a lower average precipitation per unit area. That is, sloping soil has more surface area per km^2 than flat land (Mi. J et al., 2019). The soil moisture may be relative greater in an area with gentle slopes with faster lateral migration and loss of natural precipitation on steep slopes. For the efficiency of soil moisture use, steep slope will also reduce the utilization efficiency of soil moisture by vegetation because the vegetation on a steep slope would have less time to adsorb rainfall because of increased surface runoff (Mi. J et al., 2019). Also, enhanced light intensity and light area varies inversely with slope, that means steeper the slope, the less effective use of solar radiation by vegetation (Mi. J et al., 2019). In gentle slopes, the vertical projection area of light is expected to be greater than steep slopes. Plant attachment ability may be lower on steep slope because seeds of non-native plants will be difficult to establish on steep slopes. Besides, relatively gentle slopes such as the sedimentation areas in the lower course of stream will produce less runoff and less soil erosion with more accumulation of organic matter, nitrogen, and other nutrients in topsoil that enhance the improvement of soil fertility with thicker soil layers which favor the regrowth of vegetation (Mi. J et al., 2019).

By regression tree modeling analysis (Saito H et al., 2022), the NDVI ratio were lower at the aspects of East and Southeast which are sunny slopes in coseismic landslide scarps in Aso (Saito H et al., 2022). Lower vegetation recovery and NDVI on the slopes facing south to southwest in middle part of coseismic landslides in the study site might related to the content of soil moisture. South to southeast facing slopes are the sunny slopes with more direct solar radiation and higher evaporation of soil surface. That means the expected soil moisture content may be less along the south to southwest facing slopes in the middle part of the valley of study sites. Lower soil moisture content may cause less suitable environment for vegetation recovery and biomass development during the post-seismic periods.

Vegetation cover is a parameter used that represent the effect of vegetation in most soil erosion research. Vegetation cover was an effective and acceptable method for reducing runoff and soil loss for soil on slopes and the runoff volume decreased with increasing vegetation coverage and consequently decreased the sediment load under three different rainfall intensities. The vegetation cover reduced the runoff volume about 14.32% to 80.51% and sediment load about 82.89% to 99.11% (Zhao et al., 2019). Also, the vegetation coverage had an important influence on the Darcy–Weisbach friction coefficient and Manning’s roughness coefficient. An increase in vegetation coverage can effectively increase the resistance coefficient, thus reducing runoff and sediment loss. (Zhao et al., 2019).

For the research about the effects of canopy interception and interception capacity of main forest types in Liupan Mountains of China indicated that the ratio of canopy interception to precipitation ranged from 8.59% to 17.94%, throughfall was more than 80%, and stemflow ranged from 0.23% to 3.10%. The canopy interception capacity was 0.78-1.88 mm with leaf interception capacity was 0.62-1.63 mm, and stem interception capacity was 0.13-0.29 mm (Xu et al., 2010). Besides, conifer forest had a higher canopy interception capacity than broad-leaved forest was confirmed (Xu et al., 2010).

The major type of vegetation in the study site is conifer forest plantation. Relatively large areas (40.22% of drainage basin) with conifer forest were collapsed by coseismic landslides and large area of bare soil were exposed. Without the protection of vegetation, the canopy interception to precipitation and canopy interception capacity might be greatly reduced, which caused increasing surface runoff and soil loss on slid slopes. The runoff volume increased with decreasing vegetation coverage and consequently increased the sediment load under rainfall.

Besides, during the post-seismic periods, the vegetation recovery was not obvious in the coseismic landslide areas especially in the middle and upper part of the drainage basin in the study site where the NDVI value were remaining very low. This might imply that the fluvial erosion and mass movement on slid slopes due to increasing runoff will continue which contribute for the extension of stream channels, continuous development of stream network associated with changes in drainage basin morphometric parameters such as increase in stream number, stream order, stream length, drainage density, drainage intensity, infiltration number, length of overland flow and decrease in constant of channel maintenance. Progressive morphological changes within drainage basin may also be expected.

Those areas with elevation decrease between -0.2 m to -0.7 m (Figure 3) which were located at a relatively large slide slopes with tributary 14, 15,16, 17, 19, 26 and left side of 3rd order stream no. 1 and 2 were corresponding with the areas of low NDVI value (Figure 5.4.1.1), which might indicate the effect of lack of vegetation cover with soil erosion on slip slope and elevation decrease in coseismic landslide areas.

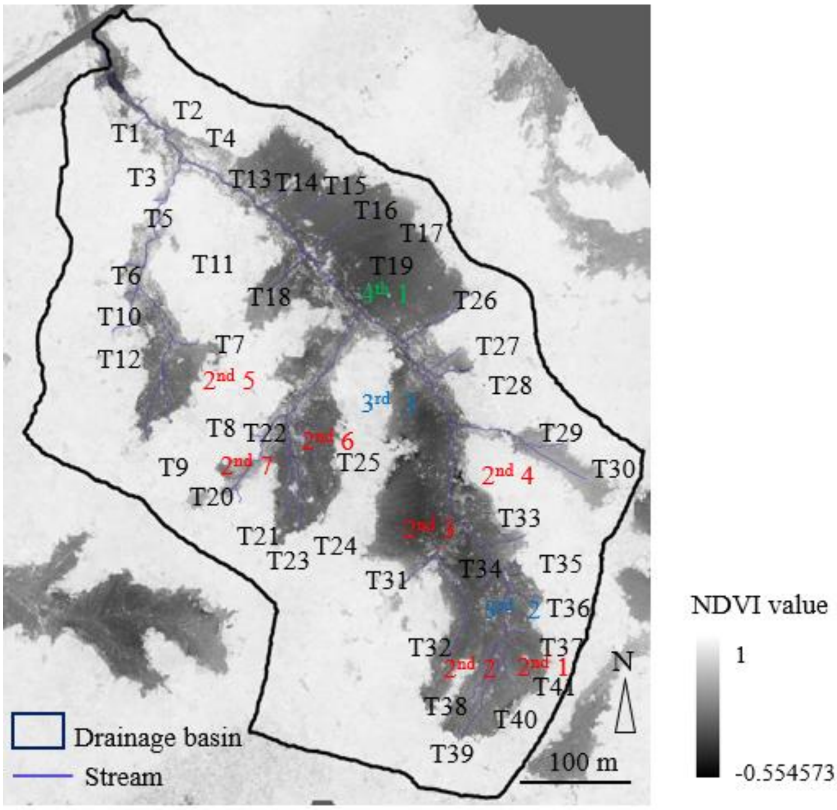

Figure 5.4.1.1. Normalized difference vegetation index (NDVI) of Study site D on June 21, 2022 and all stream channels (with stream orders) in Study site D.

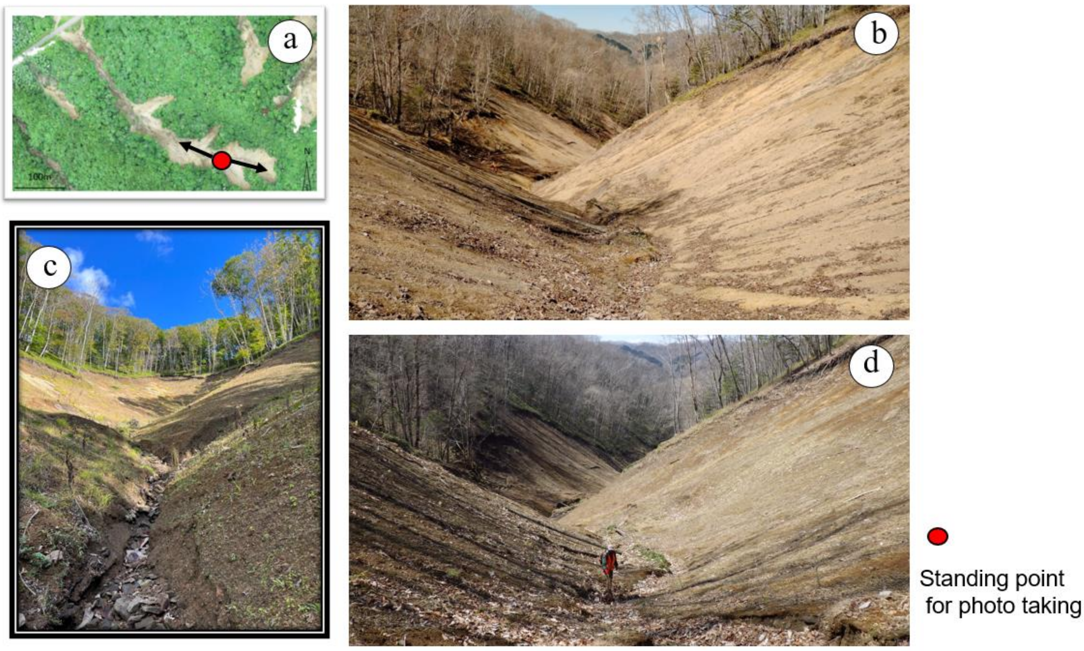

Figure 5.4..1.2: Vegetation recovery (a) Overview of the Study site B (Orthorectified mosaic image), (b) Photo taken on April 25, 2022, (c) Photo taken on September 22, 2022 and (d) Photo taken on April 18, 2023.

5.4.2 Observation of vegetation recovery in field surveys with data of soil temperature (°C), soil moisture (m^3/m^3) and Photosynthetic Active Radiation (PAR) (µmol m^{-2} s^{-1}) in Study site B

During the field surveys in Study site B , the situation of vegetation recovery in Study site B were observed and recorded by photos (Figure 5.4.2 b, c and d) on April 25, 2022, September 22, 2022 and April 18, 2023. The photos indicated no obvious vegetation recovery observed from April 25, 2022 to September 22, 2022 and even almost one year later (April 18, 2023) on the same slopes in Study site B.

The data of soil temperature (°C), soil moisture (m^3/m^3) and Photosynthetic Active Radiation (PAR) (µmol m^{-2} s^{-1}) between 19th April to July 28, 2023 of Data micro station loggers Set A, B, D and E were collected for analyzing the situation and difference in vegetation recovery in the Study site B. (Figure 3.1.4.2).

Set B and E of Data multi station loggers were set on north-east facing slopes in middle course of main stream channel and lower course of main stream channel (near stream outlet) respectively, while Set A and D of Data multi station loggers were set on south-west facing slopes in middle course of main stream channel and lower course of main stream channel (near stream outlet) respectively (Figure3.1.4.2).

		Period: May 19 - July 28 (2023)		Period: May 19 - July 28 (2023)	
Study site B		Set A	Set B	Set D	Set E
Soil temperature (°C)	Maximum	21.20	24.53	22.39	21.68
	Minimum	5.10	3.62	10.20	10.32
	Average	13.46	14.78	16.22	15.89
Soil moisture (m^3/m^3)	Maximum	0.476	0.520	0.311	0.279
	Minimum	0.388	0.257	0.202	0.193
	Average	0.432	0.307	0.230	0.211
Photosyntheic active radiation (PAR) (µmol m^{-2} s^{-1})	Maximum	1641.20	2046.20	1503.70	1,756.20
	Minimum	0.82	2.12	0.78	1.20
	Average	89.24	115.69	85.47	91.84

Table 5.4.2: Soil temperature (°C), soil moisture (m^3/m^3) and PAR Photosynthetic Active Radiation (µmol m^{-2} s^{-1}) of 4 sets of Data micro station loggers in Study site B.

Table 5.4.2 indicate recorded data of soil temperature (°C), soil moisture (m^3/m^3) and PAR Photosynthetic Active Radiation (µmol m^{-2} s^{-1}) of 4 sets Data micro station loggers (from 19th May to 28th July Set A, B, D and E) in Study site B.

Set B and D had the highest and 2nd highest value of maximum soil temperature (°C) of 24.53 °C and 22.39 °C, while Set E and A, had 3rd highest and the lowest (among 4 sets of data) maximum soil temperature of 21.20 °C and 21.68 °C respectively (Table 5.4.2).

Set E and D had the highest and 2nd highest value of minimum soil temperature (°C) of 10.32 °C and 10.20 °C (both located near stream outlet with lower elevation), while Set A and B, had 3rd highest and the lowest (among 4 sets of data) minimum soil temperature of 5.10 °C and 3.62 °C respectively (both located at the middle course of stream with higher elevation) (Table 5.4.2).

Set D and E had the highest and 2nd highest average soil temperature (°C) of 16.22 °C and 15.89 °C (both located near stream outlet with lower elevation), while Set B and A had the same 3rd highest and the lowest (among 4 sets of data) minimum soil temperature of 14.78 °C and 13.46 °C respectively (both located at the middle course of stream with higher elevation) (Table 5.4.2).

Since Set A and B of Data multi station loggers were set on slid slopes in middle course of main stream channel (with higher elevation), while Set D and E were set on slide slopes in lower course of main stream channel (near stream outlet with lower elevation), it implies that slid slopes in middle course of main stream channel (with higher elevation) had lower value of minimum soil temperature (°C) and average soil temperature (°C), while those slid slopes in lower course of main stream channel (near stream outlet with low elevation) had higher value of minimum soil temperature (°C) and average soil temperature (°C)

Set B and A had the highest and 2nd highest maximum soil moisture (m^3/m^3) of 0.520 m^3/m^3 and 0.476 m^3/m^3 (both located at the middle course of stream with higher elevation), while Set D and E, had 3rd highest and the lowest (among 4 sets of data) maximum soil temperature of 0.311 m^3/m^3 and 0.279 m^3/m^3 respectively (both located near stream outlet with lower elevation) (Table 5.4.2).

Set A and B had the highest and 2nd highest value of minimum soil moisture (m^3/m^3) of 0.388 m^3/m^3 and 0.257 m^3/m^3 (both located at the middle course of stream with higher elevation), while Set D and E, had 3rd highest and the lowest value(among 4 sets of data) of minimum soil temperature of 0.202 m^3/m^3 and 0.193 m^3/m^3 respectively (both located near stream outlet with lower elevation) (Table 5.4.2).

Set A and B had the highest and 2nd highest value of average soil moisture (m^3/m^3) of 0.432 m^3/m^3 and 0.307 m^3/m^3 (both located at the middle course of stream with higher elevation), while Set D and E, had 3rd highest and the lowest value (among 4 sets of data) of minimum soil temperature of 0.230 m^3/m^3 and 0.211 m^3/m^3 respectively (both located near stream outlet with lower elevation) (Table 5.4.2).

Since Set A and B of Data multi station loggers were set on slid slopes in middle course of main stream channel (with higher elevation), while Set D and E were set on slide slopes in lower course of main stream channel (near stream outlet with lower elevation), it implies that slid slopes in middle course of main stream channel (with higher elevation) had higher value of maximum soil moisture (m^3/m^3), minimum soil moisture (m^3/m^3) and average soil moisture (m^3/m^3); while slid slopes in lower course of main stream (near stream outlet with lower elevation) had lower value of maximum soil moisture (m^3/m^3), minimum soil moisture (m^3/m^3) and average soil moisture (m^3/m^3)

Set B and E had the highest and 2nd highest value of maximum Photosynthetic Active Radiation (PAR) (μmol m^{-2} s^{-1}) of 2046.20 μmol m^{-2} s^{-1} and 1756.20 μmol m^{-2} s^{-1}, while Set A and D, had 3rd highest and the lowest value (among 4 sets of data) of Photosynthetic Active Radiation (PAR) (μmol m^{-2} s^{-1}) maximum soil temperature of 1641.20 μmol m^{-2} s^{-1} and 1503.70 μmol m^{-2} s^{-1} respectively (Table 5.4.2).

Since Set B and E of Data multi station loggers were set on north-east facing slopes in middle course of main stream channel (with higher elevation) and lower course of main stream channel (near stream outlet with lower elevation) respectively (Figure 3.1.4.2), while Set A and D of Data multi station loggers were set on south-west facing slopes in middle course of main stream channel (with higher elevation and lower course of main stream channel (near stream outlet with lower elevation) respectively.

It implies that slid slopes with north-east facing in both middle course of main stream channel (with higher elevation) and lower course of main stream channel (near stream outlet with lower elevation) (Set B and E) had higher value of maximum Photosynthetic Active Radiation (PAR) (μmol m^{-2} s^{-1}) than the slid slopes with south-west facing in both middle course of main stream channel (with higher elevation) and lower course of main stream channel (near stream outlet with lower elevation) (Set A and D).

The analysed results of soil temperature (°C), soil moisture (m^3/m^3) and Photosynthetic Active Radiation (PAR) (μmol m^{-2} s^{-1}) between19th May April to July 28, 2023 (based on Data micro station loggers Set A, B, D and E) were consistent with the situation observed in field survey on October 09, 2023(Figure 5.4.3).

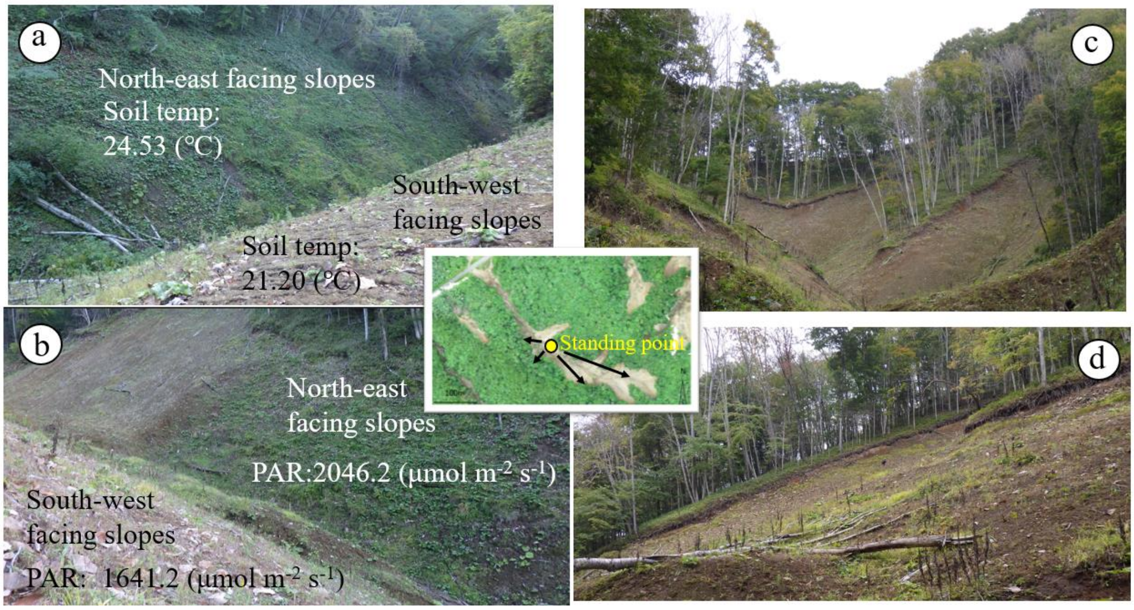

Figure 5.4.2.1 a – d: Difference in vegetation recovery on slid slops in Study site B with difference in soil temperature (°C) and Photosynthetic Active Radiation (PAR) (μmol m^{-2} s^{-1}) by comparing the situation on north-east facing and south-west facing slopes (Photos taken on October 09, 2023 at the standing point indicted in the figure).

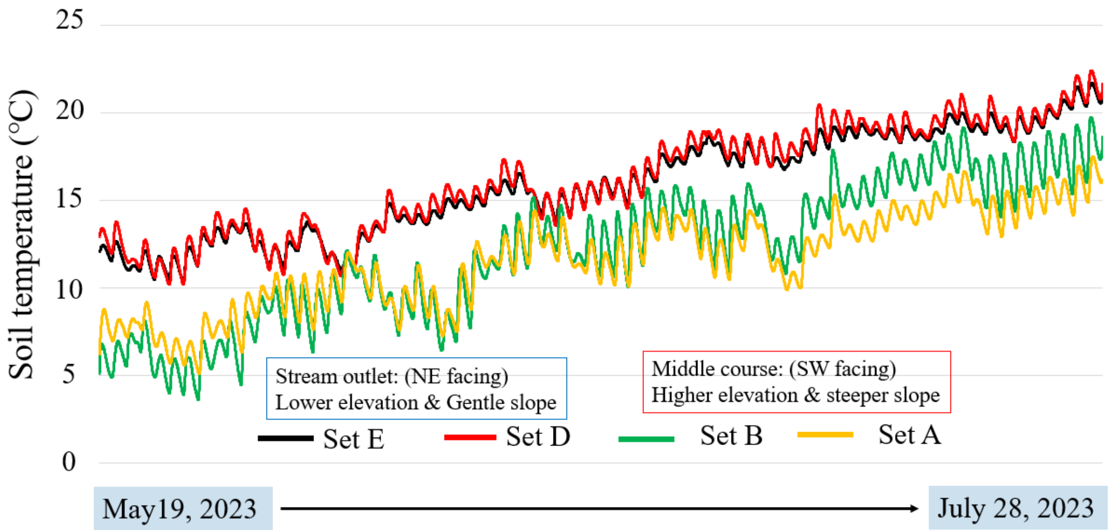

Figure 5.4.2.2: Soil temperature recorded by 4 sets of USB Data micro station loggers (HOBO H21-USB) with soil temperature sensors (S-TMB-M002) in Study site B.

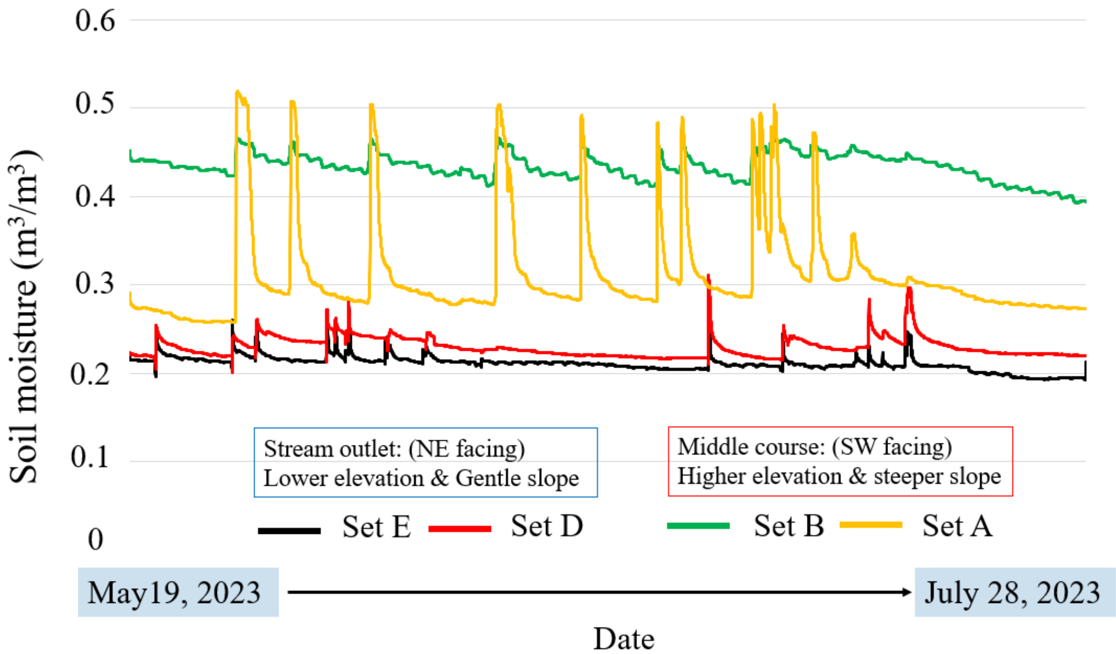

Figure 5.4.2.3: Soil moisture recorded by 4 set of USB Data micro station loggers (HOBO H21-USB) with 5cm fork-shaped soil moisture sensors (S-SMC-M005) in Study site B.

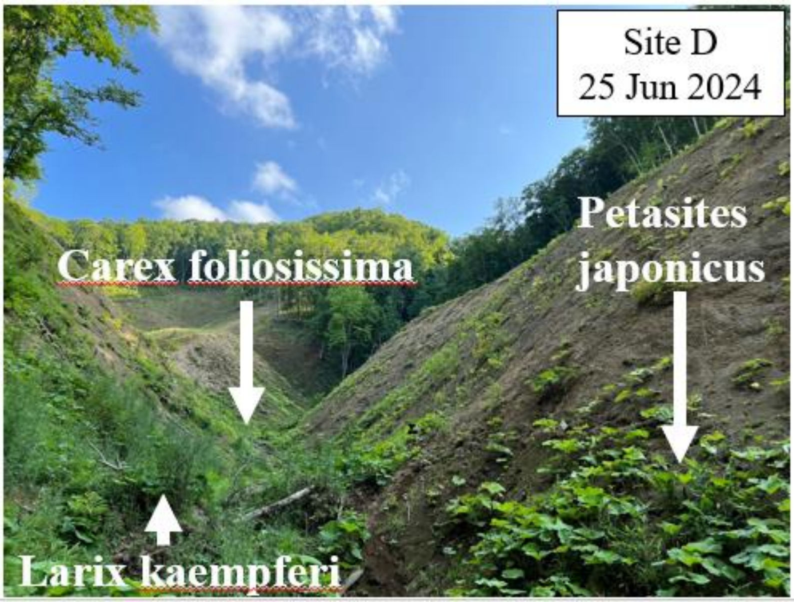

Figure 5.4.2.4: Three species of vegetation observed in Site D (June 25, 2024)

During the field surveys in Study site B on October 09, 2023 (almost the end of vegetation growing season) and in Study site D on June 25, 2024 , Petasites japonicus subsp. giganteus, Larix kaempferi and Carex foliosissima were observed on gentle slopes with normal sunlight and stable areas with little soil erosion, which are the top three species with the highest average cover percentage on adjacent landslide scars (Nakata et al., 2023). Also, Petasites japonicus subsp. giganteus was confirmed having high reproductivity as significant primary recovery during early stages of vegetation succession after the Usu eruption (Tsuyuzaki, 1987). The herbaceous P. japonicus subsp. giganteus (perennial herb that is native to Hokkaido), which reproduces vegetatively by horizontally elongated underground stems after seed establishment, contributed to vegetation recovery (Sakai et al., 2008).

The difference on vegetation recovery on some north-east facing slopes and south-west facing slopes in Study site B were observed and recorded by photos (Figure 5.4.3 a, b, c and d). The photos and observation in the field indicated still no obvious vegetation recovery observed on some slopes even until October 09, 2023 (5 years and one month after the 2018 Hokkaido Eastern Iburi Earthquake in Study site B. Meanwhile, relative higher rate of vegetation growth was observed on north-east facing slopes (rather than south-west facing slopes) (Figure 5.4.3 a and b) and slopes at lower part of valley near the stream outlet (rather upper slopes near the ridge of valley) (Figure 5.4.3 a, c and d)

The observation in Study site B during the field survey on October 09, 2023 was consistent with lower vegetation recovery and lower NDVI on the slopes facing south to southwest in middle part of coseismic landslides scarps in the study site in Aso (Saito H et al., 2022)

Also, the observation in Study site B during the field survey on October 09, 2023 was consistent with lower vegetation recovery and lower NDVI at middle and upper part of valley in Study site D (Figure 5.6.1) with steep slopes and higher elevation such as at tributaries 16, 17, 19, 32, 33, 35 and 39. Meanwhile, the NDVI (Figure 5.4.1) was also lower on the slopes facing south to south-west in middle part of valley in Study site D such as at tributaries 16, 17 and 19.

The observation in Study site B during the field survey on October 09, 2023 was also consistent with the higher NDVI at the sedimentation areas in lower courses of stream with lower elevation and gentle slopes in Study site D, such as at tributary 2, 4th order stream and 2nd order stream no. 5 (Figure 5.4.1). Besides, based on the analysis of morphological changes with the watershed, areas with Elevation decrease (-0.2 m ~ -0.7 m) are correspondent to areas of low NDVI (21 June field survey data). Vegetation growth and plant root reinforcement for stabilizing slope by increasing root cohesion and soil cohesion and the Factor of Safety was confirmed (Chok, et al, 2015). Also, bare slopes of sub catchments with average gradient of 0.50 (26.6º) was prone for mass wasting (Chok, et al, 2015).

The average slope of sub catchments in middle course and upper course of Study site A, B, C and D was between 0.47 to 0.58 (25º to 30º). The vegetation recovery in those slopes was mainly grass to a relatively small extent. It can be considered as bare slope. This means the Factor of Safety was about 1.05 (marginal stable on border line). Just little decrease in soil cohesion or root cohesion, entrainment of soil on slope may happen (Chok, et al, 2015). This might imply that the fluvial erosion and mass movement on slid slopes with increasing runoff will continue on slid slopes affected by earthquake, which contribute for the extension of stream channels, continuous development of stream network associated with changes in drainage basin morphometric parameters such as increase in stream number, stream order, stream length, drainage density, drainage intensity, infiltration number, length of overland flow and decrease in constant of channel maintenance. Progressive morphological changes within drainage basin may also be expected.

Conversely, on the slope along lower course (near the stream outlet with lower elevation) of Study site A, B, C and D, the vegetation recovery with grass was observed on slope surface and toe. The Factor of Safety of this type of slope was 1.20 (Chok, et al, 2015), which indicated relatively stable slope for accumulation of sediment, organic matter, nitrogen, and other nutrients in topsoil that enhance the improvement of soil fertility with thicker soil layers which favor the regrowth of vegetation (Mi. J et al., 2019) which can refrain the soil erosion and stabilizing the slope with increasing plant and soil cohesion. Log-linear relationship between erosion rate and shear stress was observed (Parchure and Mehta, 1985) which indicates that the presence of vegetation increases the critical shear stress with slope stability.

5.5. Correspondence of morphological changes, drainage network development and geomorphometric parameters in drainage basin with and Freeze – thaw action on slid slopes

Snowmelt in daytime and frozen with larger size at night. Such periodical fluctuation of temperature around the freezing point causes deterioration of rocks and other porous geomaterials which is called freeze-thaw (FT) weathering (Deprez, et. al., 2020) (Matsuoka & Murton, 2008). The change of physical status of water in soil between liquid and solid with expansion in the size as ice might initiate uplift and down of soil particle in the top soil layers. If such phenomenon happened on slope, a considerable removal and downward movement of soil particles causing certain type of mass movement along the slope might be expected. This freeze-thaw activity causes gradual processes of a mass moving down a slope is called solifluction. Slope surficial deposits affected by solifluction caused by freeze-thaw cycles actively moved during the last glacial period (~10ka ago) was reported (Ishimaru, et al., 2020). The happening of freeze and thaw action and solifluction which causing the mass movement on slip slope surface within the drainage basin of study site might be expected.

The changes in geomorphometric parameters in stream number (N_u), stream length (L_u), stream frequency (F_s), drainage intensity (D_i), infiltration number (I_f) and ruggedness number (R_n) indicated the increasing trends during the post seismic period 1 to 9. At the same time, the values of length of overland flow (L_o) decreased. One of the possible reasons for those changes may be freeze and thaw action, with formation of frost heave (needle ice) on the upper soil layer, on the collapsed slopes.

The frost heave (needle ice) development which caused downslope sediment movement of upper soil about 1.0 to 1.5 cm through autumn and spring after the deforestation with direct daytime insolation and strong nighttime radiative cooling at clear-cut site in Ikawa University forest was confirmed (Ueno, 2015). During the field survey in study site B on 28th January, 1 cm uplift of soil material by frost heaving was recorded. The formation of frost heave (needle ice) might due to the large range of daily temperature of soil above and below the freezing point.

Daily ground surface changes due to freeze-thaw action by comparing the Digital Elevation Difference at night time and day time on 2 targeted slid slopes in Atsuma were identified (Nakata et al. 2021). The elevation increase was about 0.05 m to 0.3 m at nighttime in slope failure site and the elevation decrease was about -0.05 m to -0.30 m at daytime. Although the actual soil surface temperature in the study site is unknown, such a condition might indicate the occurrence of freeze-thaw actions and associated with the rapid infilling of gullies. Freeze and thaw action with solifluction which might generate slope sliding which buried the channel heads and stream channels during the post-seismic periods associated with parametric changes in quantitative analysis of drainage basin characteristics, such as the shortening of steam length (L_u) and downstream migration of channel heads in certain post-seismic periods might cause the variations on stream frequency, drainage intensity, infiltration number, length of overland flow and ruggedness number.

Locations of frost heave in the study site B and D were identified by observations during field surveys on November 8 and 30, 2022, (Figure 5.5.3), April 2, 10 and 18, 2023 and November 30, 2023 (Figure 5.5.3). The temperature of frost heave was measured by Flir Infra-red camera attached with the i-Phone13 Pro Max. The observed frost heave located along sides of middle and upper course of main stream channel in Study site B and D. Some clusters of frost heave were observed at lower part of those adjacent slopes. Height of frost heave (needle ice) were measured during the surveys on April 2 and November 30,2023 for further analysis.

Temperature of air, soil surface temperature and frost heave (needle ice) were measured in field surveys. During the field survey on April 2, 2023 in Study site B and on November 30, 2023 in both Study site B and D, the air temperature at the location where frost heave (needle ice) observed was 10℃ (middle course of stream channel) on April 2, 2023 in Study site B; while it was 9℃ (upper course of stream channel) in Study site B and 8℃ (upper course of stream channel) in Study site D on November 30, 2023.

Also, according to an infra-camera measurement, the soil surface temperature was 2.3℃, 1.7℃ (middle course of stream) (Figure 5.5.1) in Study site B on April 2, 2023 and 2.8℃ (upper course of stream channel) in Study site B on November 30, 2023. In Study site D, according to the Soil temperature sensors (S-TMB-M002), the average soil temperature was 3.62 ℃ on November 30, 2023 in study site D.

For the temperature of frost heave (needle ice), according to an infra-camera measurement, it was -2.3 ℃ and -3.0 ℃ on April 2, 2023 in Study site B (Figure 5.5.1), while it was -13.3℃ and -13.6℃ in Study site B on November 30, 2023 (Figure 5.5.2). In Study site D, the temperature of frost heave (needle ice) was -14.2 ℃and -14.7℃ on November 30, 2023 (Figure 5.5.3).

Therefore, even the air temperature was above 0℃, lower soil temperature and probability for the formation of frost heave were expected in the Study sites. Also, lower air temperature may co-exist with lower soil temperature and higher probability for the formation of frost heave (needle ice) in the Study sites.

According to Atsuma Meteorological Station (42°43.8’N, 141°53.3’E, ca. 11 km west away from the study sites), the number of days with maximum daily temperature above 0°C (above freezing point) and minimum daily temperature below 0°C (below freezing point) in each month from September, 2018 to October, 2021 (Investigation Period 1 to 9) was shown in Figure 2.3.2. Totally 16 months between September 2018 and October 2021 had 10 or more than 10 days with maximum daily temperature above 0°C and minimum daily temperature below 0°C. Between October 2020 (Autumn) and April 2021 (Spring) (Investigation Period 6), 5 months had 10 or more than 10 days with maximum daily temperature above freezing point and minimum daily temperature below freezing point. Also, in November 2020 (Autumn) and April 2021(Spring) (within Investigation Period 6) had 19 days per month with maximum daily temperature above freezing point and minimum daily temperature below freezing point (Figure 2.3.2). Also, more than 20 days in the Month of March 2019, November 2019 and March 2020 (Investigation Period 2), having the daily maximum and minimum temperature were above and below freezing point (0°C).

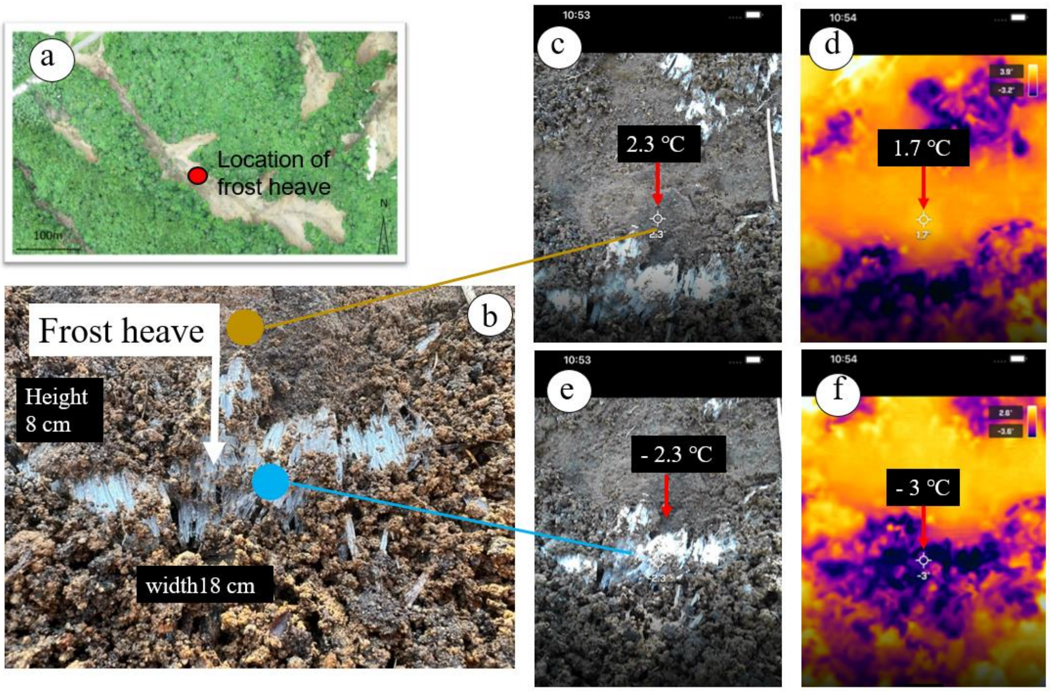

Figure 5.5.1: Frost heave (field survey on April 2, 2023 in Study site B): (a) Study site B and location of frost heave (middle course of stream channel), (b) Frost heave with width (cm) and height (cm), (c) Temperature (°C) of surrounding soil surface, (d) Temperature (°C) of surrounding soil surface (Infra-red camera image). (e) Temperature (°C) of frost heave and (f) Temperature (°C) of frost heave (Infra-red camera image).

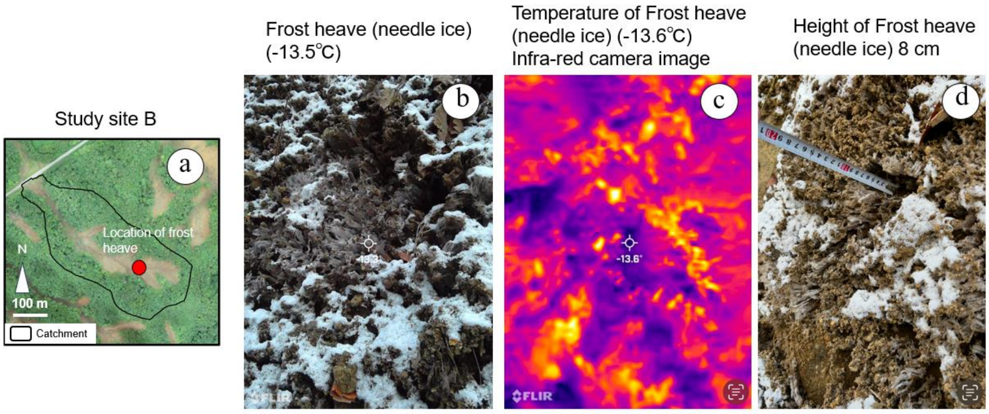

Figure 5.5.2: Frost heave (field survey on November 30, 2023 in Study site B): (a) Study site B and location of frost heave (upper course of stream channel), (b) Temperature (°C) of frost heave (-13.3 °C), (c) Temperature (°C) of frost heave (Infra-red camera image) (-13.6 °C), (d) Height of frost heave (8 cm).

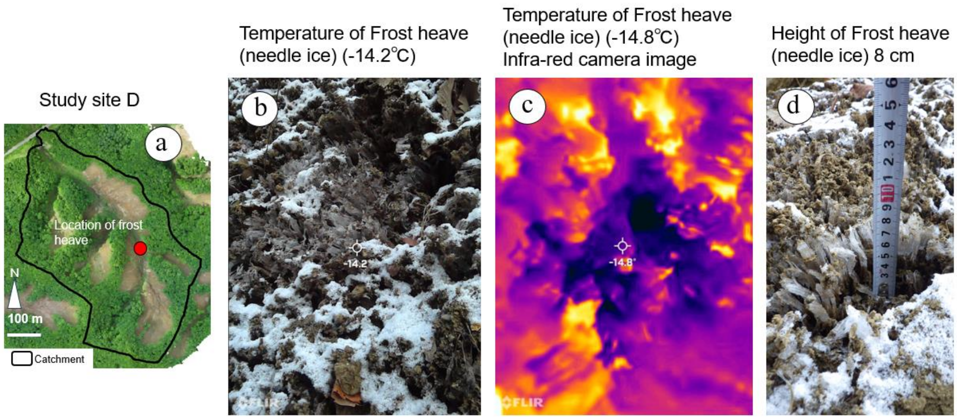

Figure 5.5.3: Frost heave (field survey on November 30, 2023 in Study site D): (a) Study site D and location of frost heave, (b) Temperature (°C) of frost heave (-14.2 °C), (c) Temperature (°C) of frost heave (Infra-red camera image) (-14.8 °C), (d)Height of frost heave (8 cm).

In addition, coseismic landslides involved about 18.01 %, 21.84 %, 11.06 % and 31.89 % of drainage basin areas in the study site A, B, C and D respectively with large areas with vegetation cover removal were expected. The top soil layer in these areas might also be exposed to direct daytime insolation with strong nighttime radiation cooling and caused the occurrence of freeze and thaw action with formation of frost heave (needle ice) on the upper soil layer which directly affected the mass movement on the slid slopes in the study site during the post-earthquake periods. The occurrence of freeze and thaw action on the upper soil layer might directly affect the mass movement on the slid slopes in the study areas in winter and early spring during the post-seismic periods. Also, the channel heads and stream channels initiated by landsliding (mass movement) might be easily buried by infilling processes along the slid slopes after original failure (Imaizumi, 2010).Therefore, I expect that freeze-thaw action, with formation of frost heave (needle ice) on the upper soil layer, caused mass movement, and mixture of unstable surface sediment on the slid slops with morphological changes during post-seismic periods. Such situation also caused some stream channels were easily buried like the photo taken during the field survey on April 25,2022) (Figure 5.5.4) and downstream migration of channel heads. And these may be the one of the reasons for the changes in the quantitative parameters during the post seismic investigation periods.

Such prediction on the slope processing during post-seismic periods may be very useful and important for the prevention of natural disasters by providing more precise hazard maps and contribute for the prediction of re-activate, re-mobilized and new landslides in the near-future. It may also contribute for future researches with data interpretation and analysis.

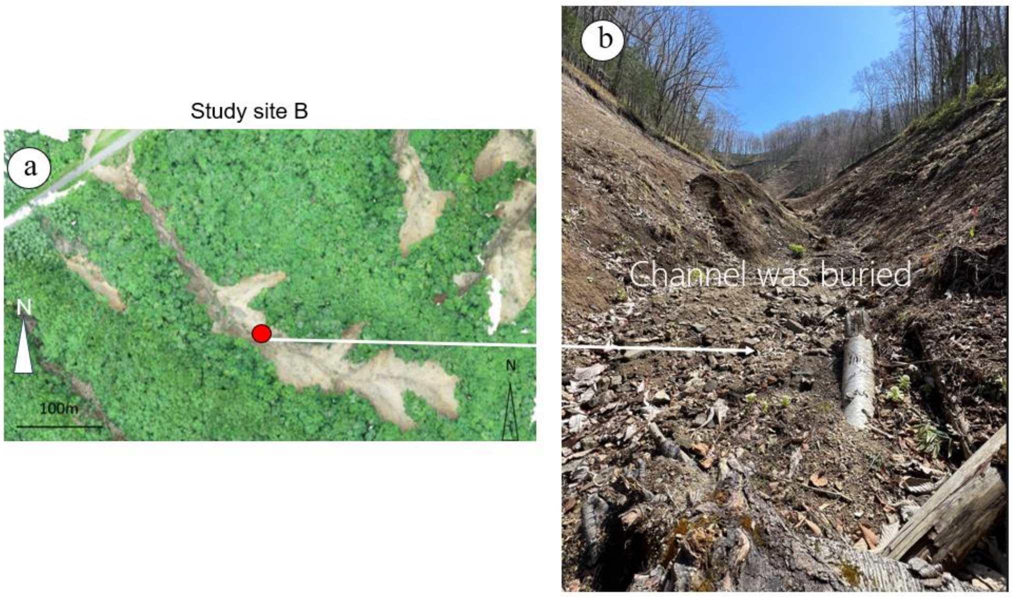

Figure 5.5.4: (a) Location of buried stream channel in Study site B, (b) Photo of buried stream channel (taken on April 25, 2022)

However, it is necessary to have more details and progressive records on the changes on top soil temperature, soil moisture as the evidence of freeze and thaw action especially during early spring and late Autumn in the Study sites. Because the consistence of those data of daily and seasonal changes of soil temperature, moisture with changes in daily maximum temperature above 0 ℃ and minimum temperature below 0 ℃ by Japan Meteorological Agency (JMA) might be a strong support the above prediction of slope sliding by freeze-thaw action and solifluction (frost heave). Also, it may contribute to the interdisciplinary analysis with board-range learning for discovering a comprehensive understanding of those natural phenomenon in the Study sites.

It is expected to be a challenge for recording and applying those data on the morphological changes due to freeze and thaw action. Those data may be applied in both coseismic landslide areas and other slopes for estimating the morphological changes which may have implication and prediction the rate of soil erosion, slope processing and reactivated mass movement.

Chapter 6 Conclusion

This study examined coseismic and post-seismic morphological responses of drainage basin in 4 adjacent catchments with similar geological structure and climatic conditions along the Atsuma River with less artificial modifications following the coseismic landslides caused by the 2018 Hokkaido Eastern Iburi Earthquake (Magnitude 6.7), with particular focuses on coseismicand post-seismic morphological responses particular with elevation changes, development of fluvial channels, continuous fluvial erosion and stream heads migration in catchments by mapping of areas with substantial elevation changes, extraction of stream networks, quantitative analysis of geomorphometric and hydraulic parameters and sediment connectivity, using multi-temporal Digital Elevation Models (DEMs) and Geographical Information System (GIS) associated with field survey observations. GIS software QGIS 3.22.7 was used for geospatial analysis of topographic data and mapping of stream channels, which performed to characterize the drainage network development. Morphological changes were also examined by subtracting the ALS, UAV-SfM and UAV-LiDAR DEMs with different time of acquisitions. Quantitative analysis of post-seismic elevation changes, geomorphometric and hydraulic parameters and landslide mobility and sediment connectivity were also examined. The analysis is divided into to two sections for comparison, that is pre- and post-earthquake (Period 1) and post-seismic periods (Period 2 – 9).

Morphological changes such as stream-bed deposition, rills and gully erosion, slid slopes, collapsed vegetation and stream network development were confirmed during the field surveys in study site B and D. Post-seismic stream network development were also identified by channel features formed by the ephemeral streams in orthorectified images of Study sites A-D. Gully stream channels could be found along the middle and upper course of stream which could indicate the continuous gully erosion especially during the rainy season in Study site A, B, C and D.

By subtracting ALs DEMs 2012 and 2018 (Period 1), morphological changes in drainage basins of all study sites A - D were confirmed, Most of the coseismic landslides could be identified in the upper part of the drainage basins extending to the main valleys, where new tributaries were observed. Some small separated elongated coseismic landslides area were observed in the middle and lower part of drainage basins. Linear sediment deposition area could be identified mainly along the lower course of stream which extended gradually to the outlet of stream. Areas with elevation difference from -0.2 m to - 10 m in study sites A -D were located at the upper part of valleysI, where elongated extension of mainstream and tributaries were observed. Areas with elevation increase from + 0.2 m to +20 m located at the lower part of valleys and near the outlet of streams of Study sites A -D, which were identified as sedimentation

By subtracting Post-seismic ALS DEM in September 2018 and Light Detection and Ranging (Lidar) DEMs in October 2021, areas with elevation decreased in all study sites A -D were located at the stream mouth due to artificial modification. Other areas of elevation decreased were mainly located at middle course of stream in linear shape, which imply fluvial erosion along gully stream channel. Elongated extension of mainstream and tributaries were observed. Linear shape of areas with elevation increased from + 0.2 m to + 2 m implies the sediment deposition along the lower course of streams in study sites A - D. Small and individual areas with elevation increased implies the accumulation of collapsed vegetation and sediment from adjacent slip slopes by small scale landslides in study sites A -D during the post-seismic periods.

Post-seismic drainage network development was confirmed in longitudinal profiles of the mainstream in Study sites A - D. based on the DEM of October 05 2012, September 11, 2018, and October 29, 2021. The extension of mainstream in length with the channel head incision in all Study sites A-D was observed. Increase on length of mainstream in Study site A to D indicate continuous gully erosion and channel development on slid slopes affected by the earthquake.

For quantitative analysis, totally 35 parameters including 29 geomorphometric parameters 6 hydraulic parameters and were used to analyze changes in drainage basin characteristics. The analysis of 29 geomorphometric parameters was divided into to two sections for comparison, that is pre- and post-earthquake (Period 1: October 05, 2012 – September 11, 2018) and post-seismic periods (Period 2 – 9: September 11, 2018 – October 29, 2021). The analysis of 6 hydraulic parameters was examined during the post-seismic periods (Period 2 - 8: September 11, 2018 to April 27, 2021. All results of geomorphometric and hydraulic parameters were derived from the UAV-SfM DEMS with different time of acquisitions for analyzing temporal changes in drainage basin characteristics, which contribute for fluvial landscape evolutionary studies such as fluvial erosion, channel initiation and headward extension.

The analyzed results of Mobility and Sediment connectivity can contribute for understanding the characteristics of coseismic landslides, spatial variability, in-channel sediment accumulations within watersheds and linkage of coseismic landslides with sediment accumulation. It also be an important indicator for landslide hazard and risk assessments, which has potential direct societal impacts because with increasing areas and volume of landslide (Areas with elevation decrease) volume (m^3) and Sedimentation (Areas with elevation increase) (m^3), Landslide (Areas with elevation decrease) mobility index, Landslide area (Areas with elevation decrease) density (LAD) (m^2/m^2) and Deposit length ratio (DLR) (m/m), travel distance and height of landslide. The levels of those influence may be different due to the different forms of catchments of Study sites A, B, C and D. Catchments with relatively circular form (Study site s B and D) will have greater changes in those parameters and more obvious effects on soil erosion and sedimentation than catchments with relative elongated form (Study sites A and C).

Those hydro-geomorphometric and sediment connectivity parameters (indicators)) were the dimensional quantitative method and fundamental model to indicate the different predominant fluvial processes in drainage system study which will contribute to indicate the post-seismic morphological responses on elevation changes and drainage network development in fluvial evolutionary process as the evidence for those co-occurrence of natural post-seismic phenomenon in the study sites even without continuous measurement of hydrological elements, such as stream discharge and stream flow velocity at every locations

The morphological responses of drainage basin including changes of morphology, geomorphometric and hydraulic parameters, fluvial network development in drainage basin after the earthquake, which might correspond to gradual or periodical erosion by fluvial and/or slope processes associated with the gully and channel networks on the bare surface of the areas with coseismic landslides, which are corresponding with rainfall intensity, soil minerals (Halloysite and Paleosol) on the slid slopes, the variability on forms of drainage basins, weak root reinforcement by limited vegetation recovery and Freeze – thaw action on slid slopes in study sites during the investigation periods.

Relatively high rainfall intensity was also recorded in post-seismic Period 3 (11.5 mm/hr), Period 4 (16.5 mm/hr), Period 5 (7.5 mm), Period 7 (9.5 mm/hr), Period 8 (22.5 mm/hr) and Period 9 (13.5 mm/hr) (Japan Meteorological Agency, 2023). High-intensity rainfall event potentially contributed to the fluvial erosion with gully development on the bare slope surfaces by increased runoff. Large areas of bare soil were exposed to direct rainsplash after the earthquake which might cause surface sheet flow and concentration as runoff for the surficial erosion on slid slope. These situations might also cause the increase of discharge, which probably enhanced fluvial erosion and gully stream development on slid slopes during the rain seasons in post seismic Periods 2 to 9 in Study sites A - D.

The presence of hydrated halloysite was confirmed by X-ray diffraction in a research. Halloysite consists of mainly alumino-silicate clay mineral with high water retention capacity and high mesopore volumes. With absorbing of water, chemical changes happened with increasing ph value and electrostatic repulsion between the minerals since the ionic and cohesive strength among minerals decreased, which causes destabilization of slope and high mobility of soil materials on the slid slopes, which facilitated the changes of morphology in drainage basin and development of drainage network in the study site during post-seismic periods. The existence of Paleosol in 2 soil samples on slid slopes in study site B was confirmed by X-ray diffusion (XRD) method. It indicates the soil on top layer of slope may easily be loosened when it absorbs water and saturated under rainfall, which may cause mass wasting process along the slid slopes, entrainment of sediment along stream channels, which were correspondent to the morphological changes, drainage network development, changes of geomorphometric and hydraulic parameters, and landslide (Areas with elevation decrease) mobility with sediment connectivity during the rain seasons of post-seismic periods.

The findings of this study clearly indicated the post-seismic morphological responses of drainage basin are related to the variability on forms of drainage basin. Study sites A and C were classified as relatively elongated catchment with average value form factor (F_f) of 0.19 and 0.22, elongation ratio (R_e) of 0.49 and 0.52 respectively with long straight mainstream, less and shorter tributaries, flat hydrograph peak for longer duration with lower runoff peak. Discharge from all sub-catchments takes long time to peak because of low runoff rates with lesser number of streams and may give less erosional power on slid slopes in Study site A and C. Therefore, less sediment can be delivered out of catchment and most of eroded material remain in drainage basins. Study sites B and D were relatively circular catchment with average value of form factor (F_f) of and 0.32 and 0.42; elongation ratio (R_e) of 0.64 and 0.73 respectively, with more and longer tributaries Circular form watershed may indicate steeper rising and recession limb of hydrograph with higher peak discharge for shorter duration. Discharge from all the sub- catchments may take short time to peak because of high runoff rates with larger number of tributaries, more erosional power on slid slopes in Study site B and D. Thus, more sediment can be delivered out of catchment and most of eroded material was transported out of drainage basins n study sites B and D.

During the field surveys, no obvious vegetation recovery observed. Relative higher rate of vegetation growth was only observed on north-east facing slopes (rather than south-west facing slopes) and slopes at lower part of valley near the stream outlet. Meanwhile, the NDVI was also lower on the slopes facing south to south-west in middle part of valley in Study site D. The observation in Study site B was also consistent with the higher NDVI at the sedimentation areas in lower courses of stream with lower elevation and gentle slopes in Study site D. Besides, based on the analysis of morphological changes with the watershed, areas with Elevation decrease (-0.2 m ~ -0.7m) are correspondent to areas of low NDVI (June 21 field survey data). The bare soil layer on slid slopes with low Factor of Safety and low soil cohesion or root cohesion, caused possible entrainment of soil on slopes. This might imply that the fluvial erosion and mass movement on slid slopes with increasing runoff and decreasing critical shear stress will continue on slid slopes affected by earthquake, which contribute for lower slope stability, extension of stream channels, continuous development of stream network associated with changes in drainage basin geomorphometric parameters such as increase in stream number, stream order, stream length, drainage density, drainage intensity, infiltration number, length of overland flow and decrease in constant of channel maintenance. Progressive morphological changes within drainage basin may also be expected.

The changes in geomorphometric parameters in stream number (N_u), stream length (L_u), stream frequency (F_s), drainage intensity (D_i), infiltration number (I_f) and ruggedness number (R_n) indicated the increasing trends during the post seismic period 1 to 9. At the same time, the values of length of overland flow (L_o) decreased. One of the possible reasons for those changes may be freeze and thaw action, with formation of frost heave (needle ice) on the upper soil layer, on the collapsed slopes. Locations of frost heave in the study site B and D were identified by observations during field surveys and height of frost heave (needle ice) and temperature of top soil were measured. Also, the top soil layer on slid slopes in study sites might also be exposed to direct daytime insolation with strong nighttime radiation cooling and caused the occurrence of freeze and thaw action with formation of frost heave (needle ice) on the upper soil layer. Even the air temperature was above 0°C, relatively lower soil temperature were recorded and probability for the formation of frost heave with occurrence of freeze-thaw actions were expected in the Study sites. According to Atsuma Meteorological Station (42°43.8'N, 141°53.3'E, ca. 11 km west away from the study sites), Totally 16 months between September 2018 and October 2021 had 10 or more than 10 days with maximum daily temperature above 0°C and minimum daily temperature below 0°C. Freeze and thaw action with solifluction which might generate mixture of unstable surface sediment on slid slopes causing slope sliding and downslope sediment movement of upper soil associated with the rapid infilling of gullies and buries of the channel heads and stream channels (confirmed by field survey) during the post-seismic periods associated with parametric changes in quantitative analysis of drainage basin characteristics. Such prediction on the slope processing during post-seismic periods may be very useful and important for the prediction of re-activate, re-mobilized and new landslides in the near-future. It may also contribute for future researches with data interpretation and analysis.

By the observed elevation differences, continuous gully erosion, channel development on slid slopes and results of quantitative analysis in the multi-temporal DEMs, morphological changes with progressive drainage network development and changes of geomorphometric and hydraulic parameters have been confirmed. Coseismic landslides were mainly located at upper part of catchments while sedimentation was mainly accumulated near stream outlet in all study sites. Linear shape of areas with elevation decrease and increase along stream channels were identified during post-seismic periods 2 to 9, which are regarded as fluvial erosion and sedimentation. More tributaries developed on the slid slopes caused by coseismic landslides in all study sites. Stream network development influenced by bare soil exposure on landslide-affected slopes, where intense rainfall events have driven gully formation and gully-head migration. Increasing in stream number, stream length, drainage density, drainage intensity, stream frequency, infiltration number, ruggedness number and decreasing length of overland flow, with increasing in hydraulic radius, shear stress and velocity at stream heads during rain seasons in all study sites, reflected progressive fluvial erosion on stream channels and slid slopes.

Study site A and C showed fluctuating morphometric trends in certain post-seismic periods, in contrast to the more stable trends in Study site B and A, likely due to the elongated, narrow shape of site A, which limits surface runoff and gully erosion in small tributaries. In contrast, steeper slopes and wider terrain in site B allow for concentration of surface runoff and greater opportunities of tributary formation, and more consistent gully development, making it more prone to erosion. Volume of fluvial erosion was greater than sedimentation in both sites, which indicated more sediment were mobilized and delivered out of catchment during the post-seismic periods in all study sites.. Relatively higher rate of erosion in all study sites during the post-seismic periods are observed, by comparing with the average value of Azuma River basin, Jozankei Dam, Oyubari Dam and Hokkaido. Volume of fluvial erosion in site B and D were higher than stie A and C and vice versa on the volume of sedimentation during Period 2 to 9. Stronger fluvial erosion was observed in site B and D which has relatively circular form of watershed, while site A and C has relatively elongated form. The possible higher sediment mobility and delivery in circular form catchment, steeper basin slope and higher value of ruggedness number may be the reasons for more active soil erosion on slid surfaces, with more tributaries and longer streams in site B and D during the post-seismic periods. It indicates the necessity for drainage basin management according to different forms of drainage catchments. Correspondence of those changes in study sites with differences in form of catchment, increase of rainfall intensity as well as assists by lack of vegetation cover on slid slopes, and freeze-thaw action with the interactions between slope and fluvial processes, potentially higher surface runoff with fluvial erosion and stream channel development on bare slopes with further slope deformations were expected.

This study contributes to provide evidence for developing an inventory about the effects of the 2018 Hokkaido Eastern Iburi Earthquake on the changes of drainage basin characteristics in the aspects of morphological changes and drainage network development. The present research also provide an alternative analytical method on stream network extraction and stream head location by using the threshold area assisted with threshold of flow accumulation and flow direction with field verification may be applicable on fluvial system analysis of large-scale watersheds. Moreover, this study highlight the interactions between fluvial erosion and deposition in mountainous basins which enhances understanding of post-seismic hydro-geomorphometric evolution in landslide-affected slopes and the interrelationships between those corresponding factors in multi-aspects. The analyzed results of progressive drainage network development and changes in drainage basin fluvial-geomorphological parameters might be valuable for long-term effects investigation, continuous monitoring for landslide with risk reduction and long-term fluvial landscape evolutionary studies, such as the role of landslides on slope-fluvial channel initiation and drainage headward erosion, which would be beneficial for progressive fluvial-evolutionary study, watershed management and investigation of sediment connectivity in catchments affected by earthquake, such as necessity for effective soil protection measures on slopes affected by coseismic landslides based on the difference in form of catchments. Further assessments and monitoring on morphological changes and drainage network development, impact of other factors and detailed processes over years or decades are recommended.

The present research emphasised the validity and interactions of those corresponding factors affecting the various post-seismic phenomenon confirmed, and enhancement of importance by using inter-related multi aspects/functions analysis for understanding the formation and processes of natural phenomenon in environmental scientific study. Relatively detail discussions on each corresponding factors were provided with relatively sufficient supportive materials (analysed results). Those discussions have explained, to a certain extent, the changes in hydro-geomorphometric parameters, sediment connectivity, rate of erosion and drainage network development were the combined effects of rainfall intensity, property of soil mineral, lack of vegetation recovery and the infilling process due to freeze and thaw action. The various co-existed phenomenon confirmed in the study sites. (Figure 6.1).In case of other researches on fluvial system in Tropical and Subtropical regions, "Rainfall Intensity" may be identified as core factor for fluvial erosion and evolution within the drainage system, because the stream discharge and runoff (which contributes to sediment entrainment along the gully streams and stream channels) are positively correlated to rainfall intensity with high stability of other physical environmental factors, such as pre-existed vegetation cover, gradient, pre-existed structure of soil layer, small variation in soil minerals, temperature and moisture, etc). Conversely, in the study sites of the present research, various natural phenomenon co-currently happened due to the HEIE earthquake, such as sudden elevation changes due to coseismic landslides, sediment accumulation, collapse of top soil and vegetation forming the exposed slid slopes, the location and pattern of tributaries, etc, in addition with the special climatic environment in the study sites, such as soil temperature in Autumn and early Spring, variation in rainfall intensity with sudden intensive high value, the exposure of extensive slid slopes with obvious collapse of vegetation cover due to the earthquake, which minimized the influence of single and individual correspondent factor causing the occurrence of various natural phenomenon mentioned previously. The present study highlights the importance of multi-aspects inter-related/functional analysis (which are always under-estimated in scientific study) in explanation of various co-existed natural phenomenon is one of the objectives and functions (Figure 6.1)

The findings in the present study may contribute to continuous and progressive scientific research on fluvial evolutionary study in catchments affected by coseismic landslides. Therefore, to a large extent, the present study provided significance in the study on fluvial-morphology, fluvial evolution and environmental science.(Figure 6.2). Following this study, further assessments and monitoring of morphological changes and drainage network development over years or decades are recommended to clarify post-seismic slope processes, fluvial erosion rates, sedimentation, and vegetation recovery. Efficient management of drainage basins with varying catchment forms will then be provided. Additionally, future research needs to include the impact of other factors and detailed processes, such as slope aspect and frost heaving, on morphological changes.

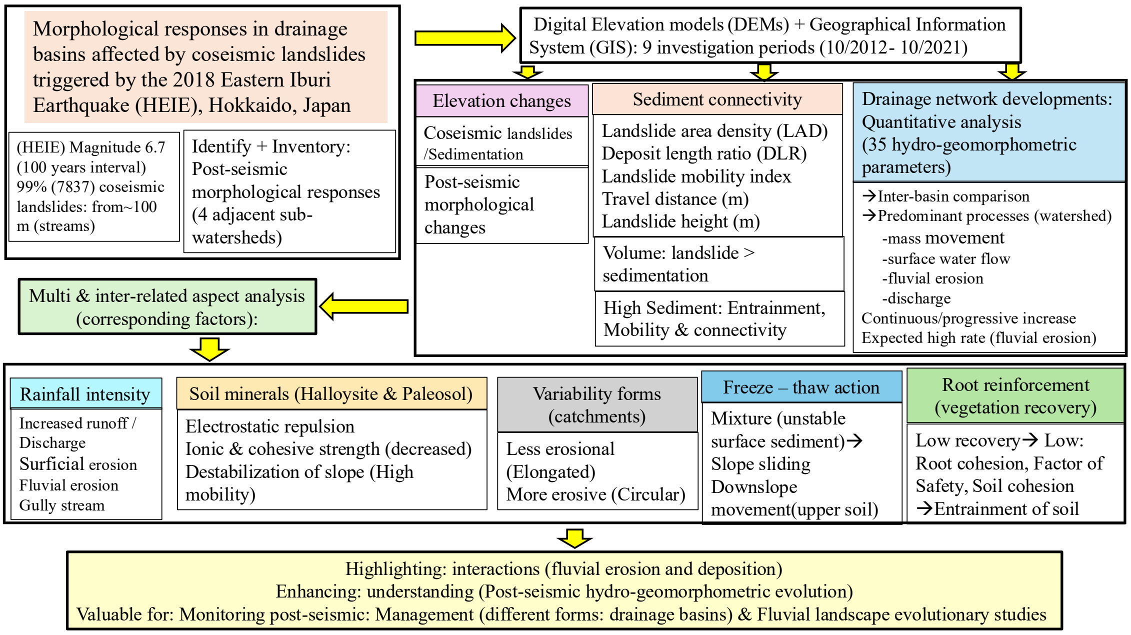

Figure 6.1: Summary of the approach of present study.

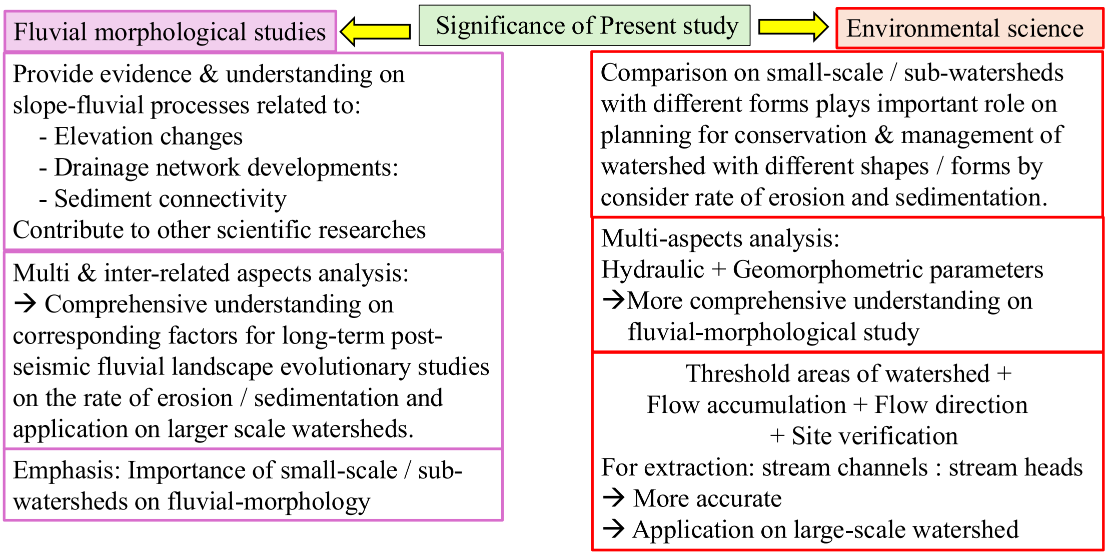

Figure 6.2: The Significance of present study in fluvial morphological studies and environmental science.

Acknowledgments

I would like to express my sincere thanks to Dr. Yuichi Hayakawa for generous supports and guidance in this study. I would also like to thank Dr. Yasutaka Nakata, Dr. Masato Hayamizu, Dr. Takuro Ogura, Dr. Mio Kasai, Dr. Takayuki Shiraiwa, Dr. Maiku Abe, and Dr. Teiji Watanabe for their generous supports on field surveys, data analysis, and constructive discussion. This study is partly supported by Hokkaido University DX fellowship Grant, Hokkaido University Support System for the Joint Research of Next-Generation Researchers, and JSPS KAKENHI Grant Numbers JP16KK0012, JP17H02031, JP21H00625, JP18H03957, JP18H02235, JP19K01156, JP21H00627, and JP22H02374.

References

Aicardi. I., Chiabrando. F., Grasso. N., Lingua. A. M., Noardo. F. and Spanò. A. T. (2016) UAV photogrammetry with oblique images: First analysis on data acquisition and processing: *The International Archives of Photogrammetry, RemoteSensing and Spatial Information Sciences*, 41-B1, 835–842. https://doi.org/10.5194/isprsarchives-XLI-B1-835-2016

Ajioka. O. and Hori. Y. (2014) Application of SFM and laser scanning technology to the description of mosaics piece by piece, International Archives of the Photogrammetry: *Remote Sensing and Spatial Information Sciences*, 40, 23-28. https://doi.org/10.5194/isprsarchives-XL-5-23-2014

Al Sawaf, M.B., Kawanisi, K., Gusti, G.N.N.,Khadami, F.,Xiao, C. and Bahreinimotlagh, M. (2023) Continuous Measurement of Flow Direction and Streamflow Based on Travel Time Principles Using a Triangular Distribution of Acoustic Tomography Systems: Hydrology, 617, 128917.

Alsaihani, M. and Alharbi, R. (2024) Mapping of Soil Erosion Vulnerability in Wadi Bin Abdullah, Saudi Arabia through RUSLE and Remote Sensing: Water, 16(18), 2663. https://doi.org/10.3390/w16182663

Amiri. M., Pourghasemi. H.R., Arabameri. A., Vazirzadeh. A., Yousefi. H and Kafaei. S. (2019)16 – Prioritization of Flood Inundation of Maharloo Watershed in Iran Using Morphometric Parameters Analysis and TOPSIS MCDM Model: *Spatial Modeling in GIS and R for Earth and Environmental Sciences,* 371−390. https://doi.org/10.1016/B978-0-12-815226-3.000168

Asano, Y., Kawasaki, M., Saito, T., Haraguchi, R., Takatoku, K., Saiki, M and Kimura, K. (2020) An Increase in Specific Discharge With Catchment Area Implies That Bedrock Infiltration Feeds Large Rather Than Small Mountain Headwater Streams: *Advancing Earth and Space Sciences AGU*, 56, (9). https://doi.org/10.1029/2019WR025658

Arata. Y., Gomi. T., Ritonga. R.P. and Sidle. R. C. (2023) The spatial variability of landslide occurrences and transported sediments induced by the 2018 Hokkaido Eastern Iburi earthquake, Japan: *European Geosciences Union (EGU) Assembly*

2021, EGU21-16062. https://doi.org/10.5194/egusphere-egu21-16062.

Ayalew, L., Kasahara, M. and Yamagishi, H. (2011) The spatial correlation between earthquakes and landslides in Hokkaido (Japan), a GIS-based analysis of the past and the future: *Landslides*, 8 (4), 433–448. https://doi.org/10.1007/s10346-011-0262-z

Ayele, A. F., Yasuda, H. and Shimizu, K. (2017) Spatial distribution and temporal trends of rainfall and erosivity in the Eastern Africa region: *Hydrological Processes*, 31(25), 4555-4567. https://doi.org/10.1002/hyp.11378

Azmayeen, R. S., Alejandra C. O., Brina M. M and Mohammed A. G. (2021) Bridge Pier Scour: An overview of factors affecting the phenomenon and comparative evaluation of selected models: *Transportation Geotechnics*, 28(2021):100549. https://doi.org/10.1016/j.trgeo.2021.100549

Benassai. G., Aucelli. P.,, Budillon. G., Stefano. M. D., Luccio. D. D., Paola. G. D., Montella. R., Mucerino. L., Sica. M. and Pennetta. M. (2017) Rip current evidence by hydrodynamic simulations, bathymetric surveys and UAV observation: *Natural Hazards Earth System Science*, 17, 1493-1503. https://doi.org/10.5194/nhess-17-1493-2017

Bischetti, G., Gandolfi, C. and Whelan, M.(2018) The Definition of Stream Channel Head Location Using Digital Elevation Data: IAHS-AISH, 248, 545–552.

Bolognesi. M., Farina. G., Alvisi. S., Franchini. M., Pellegrinelli. A. and Russo. P. (2016) Measurement of surface velocity in open channels using a lightweight remotely piloted aircraft system: *Geomatics, Natural Hazard and Risk*, 14. http://doi.org/10.1080/19475705.2016.1184717

Chen, Y., Shi, P., Ji, X., Qu, S., Zhao, L and Dong, F. (2019) New method to calculate the dynamic factor–flow velocity in Geomorphologic instantaneous unit hydrograph: *Scientific Reports*, 9, (1420). https://www.nature.com/articles/s41598-019-50723-x

Chow, V. T. (1964) Handbook of Applied Hydrology: *McGraw-Hill Book Company, New York.*

Chok Y. H., Jaksa, M. B., Kaggwa, W. S. and Griffiths, D. V. (2015) Assessing the influence of root reinforcement on slope stability by finite elements: *International Journal of Geo-Engineering*, 6, (1). https://doi.org/10.1186/s40703-015-0012-5

Chorley, R.J. and Morgan, M.A. (1962) Comparison of morphometric features, Unaka Mountains, Tennessee and North Carolina, and Dartmoor, England: *Geological Society of America Bulletin*, 73, 17–34

Corominas, J. (1996) The angle of reach as a mobility index for small and large landslides: *Canadian Geotechnical Journal (CGJ),* 33, 260-271.

Dadson, S. J., Hovius, N and Chen, H (2004) Earthquake-driven increase in sediment delivery from an active mountain belt: *Geology*, 32(8). https://doi: 10.1130/g20639.1

Das, A.K. and Mukherjee, S. (2005) Drainage Morphometry Using Satellite Data and GIS in Raigad District, Maharashtra: *Engineering, Environmental Science Journal of Geological Society of India*, 65, 577-586.

Deprez, M., Kock, T. D., Schutter, G. D and Cnudde. V. (2020): The role of ink-bottle pores in freeze-thaw damage of oolithic limestone: *Construction and Building Materials*, 246 (118515), 1–12. https://doi.org/10.1016/j.conbuildmat.2020.118515

Dietrich, W.E., Wilson, C.J., and Reneau, S.L. (1986) Hollows, colluvium, and landslides in soil-mantled landscapes: *Hillslope Processes,* 437, 361-388. https://doi.org/10.4324/9781003028840-17

Dreibrodt, S. and Wiethold. J. (2015) Lake Belau and its catchment (northern Germany) A key archive of environmental history in northern central Europe since the onset of agriculture: *Holocene*, 25, 296-322. https://doi.org/10.1177/0959683614558648

Egusa, T., Ohte, N., Oda, T., & Suzuki, M. (2016) Quantifying aggregation and change in runoff source in accordance with catchment area increase in a forested headwater catchment: *Hydrological Processes*, 30(22), 4125–4138. https://doi.org/10.1002/hyp.10916

Elewa, H.H., Ramadan, E.M. and Nosair, A.M. (2016) Spatial-based hydro-morphometric watershed modeling for the assessment of flooding potentialities: *Environmental Earth Science*, 75, 906–927. https://doi.org/10.1007/s12665-016-5692- 4

Ellenberger, J. (2014) Piping and Pipeline Sizing, Friction Losses, and Flow Calculations Piping and Pipeline Calculations Manual (Second Edition), 33-54 https://doi.org/10.1016/B978-0-12-416747-6.00004-8

Faniran, A. (1968) The index of drainage intensity—a provisional new drainage factor: *Australian journal of science*, 31, 328–330.

Feurer, D., and Vinatier, F. (2018). Joining multi-epoch archival aerial images in a single SfM block allows 3-D change detection with almost exclusively image information: *The International Society for Photogrammetry and Remote Sensing*, 146, 495–506. https://doi.org/10.1016/j.isprsjprs.2018.10.016

Fonstad. M. A., Dietrich. J. T., Courville. B. C., Jensen. J. L. and Carbonneau. P. E. (2013) Topographic structure from motion: a new development in photogrammetric measurement: *Earth Surface Processes and Landforms*, 38 (4), 421-430. https://doi.org/10.1002/esp.3366

Frankl. A., Poesen. J., Mitiku. H., Deckers. J. and Nyssen. J. (2013) Quantifying long-term changes in gully networks and volumes: *Geomorphology*, 201, 254–263. https://doi.org/10.1016/j.geomorph.2013.06.025

Furey, P. R., & Gupta, V. K. (2005) Effects of excess rainfall on the temporal variability of observed peak-discharge power laws: *Advances in Water Resources*, 28(11), 1240–1253. https://doi.org/10.1016/j.advwatres.2005.03.014

Gandolfi, C. and Bischetti, G. B. (1997) Influence of the drainage network identification method on geomorphological properties and hydrological response: Hydrological Processes, 11(4), 353–375. https://doi.org/10.1002/(sici)1099-1085(19970330)11:4<353::aid-hyp436>3.0.co;2-l

Ghoneim, E., Arnell, N. and Foody, G. (2002) Characterizing the flash flood hazards potential along the Red Sea coast of Egypt: *The Extremes of the Extremes: Extraordinary Floods. IAHS Publications*, 271, 211–216. http://eprints.soton.ac.uk/id/eprint/15242

Geospatial Information Authority of Japan, GSI (2018) The 2018 Hokkaido eastern Iburi earthquake: fault model (preliminary). http://www.gsi.go.jp/cais/topic180912-index-e.html [Last accessed: 2024.4.18]

Geological Survey of Japan, GSJ (2025) Active Fault Database of Japan. https://gbank.gsj.jp/activefault/search

Gomez. C. and Purdie. H. (2016). UAV- based Photogrammetry and Geocomputing for Hazards and Disaster Risk Monitoring – A Review: *Geoenvironmental Disasters*, 3, 23. https://doi.org/10.1186/s40677-016-0060-y

Graeff, O., Guerra. A. J. T. and Jorge, M. C. O. (2012) Catastrophic floods and landslides in Brazil:*Geographical Review*, 26, 38-41.

Gravelius, H. (1914) Morphometry of Drainage Basins. Elsevier, Amsterdam.

Guerra, A. J.T., Fullen, M. A., Jorge, M. C. O., Bezerra, J. F. R. and Shokr, M. S. (2017) Slope Processes, Mass Movement and Soil Erosion: A Review: *Pedosphere*. 27(1), 27-41. https://doi.org/10.1016/S1002-0160(17)60294-7

Hanson, G. J and Simon, A. (2001) Erodibility of cohesive streambeds in the loess area of the Midwestern USA: *Hydrologic Process*, 15 (1), 23-38. https://doi.org/10.1002/hyp.149

Hasegawa, K., Wakamatsu, K., Matsuoka, M. (2005) Mapping of Potential Erosion-Rate Evaluated from Reservoir Sedimentation in Japan: *Journal Japan Society for Natural Disaster Science*, 24 (3), 287-301. https://jsnds.org/ssk/ssk_24_3_287.pdf

Hattanji, T., Onda, Y and Matsukura, Y. (2006) Thresholds for bed load transport and channel initiation in a chert area in Ashio Mountains, Japan: an empirical approach from hydrogeomorphic observations: Geophysical Research Earth Surface, 111, F2.

https://doi.org/10.1029/2004JF000206

Hayakawa. Y. S., Obanawa. H., Saito. H. and Uchiyama, S. (2016) Geomorphological Applications of Structure-from-Motion Multi-View Stereo Photogrammetry: A Review: Transactions: Japanese Geomorphological Union, 37-3, 321–343. [in Japanese with English abstract]

Hayakawa. Y. S. and Oguchi. T. (2016) Spatial correspondence of knickzones and stream confluences along bedrock rivers in japan: implications for hydraulic formation of knickzones: Geografiska Annaler: Series A, Physical Geography, 96, (1), 9-19. https://doi.org/10.1111/geoa.12024

Hayakawa. Y. S., Kusumoto. S. and Matta. N. (2017) Seismic and inter-seismic ground surface deformations of the Murono mud volcano (central Japan): a laser scanning approach. Progress in Earth and Planetary Science, 4 (3). https://doi.org/10.1186/s40645-016-0116-3

Hayakawa, Y. S. and Oguchi, T. (2006) DEM-based identification of fluvial knickzones and its application to Japanese mountain rivers. *Geomorphology*, 78, 90-106.

Hirose, W., Kawakami, G., Kase, Y., Ishimaru, S., Koshimizu, K., Koyasu, H. and Takahashi, R. (2018) Preliminary report of slope movements at Atsuma Town and its surrounding areas caused by the 2018 Hokkaido eastern Iburi earthquake: Reports of the Geological Survey of Hokkaido, 90, 33–44. [in Japanese]

Hokkaido Prefecture (2020a) Hokkaido airborne laser scanning data: 2018 Atsuma. https://www.harp.lg.jp/opendata/dataset/1845/resource/4667/ source-url [in Japanese] [Last accessed: 2024.04.10]

Hokkaido Prefecture (2020b) Hokkaido airborne laser scanning data: 2012 Apporo Reservoir. https://www.harp.lg.jp/opendata/dataset/1845/resource/4648/ source-url [in Japanese] [Last accessed: 2024.04.10]

Horton, R.E. (1932) Drainage basin characteristics: *Transactions American Geophysical Union*, 13, 350–361. https://doi.org/10.1029/TR013i001p00350

Horton, R. E. (1945) Erosional development of stream and their drainage basins; hydrophysical approach to quantitative morphology: *GSA Bulletin*, 56 (3): 275–370. https://doi. org/10.1130/0016-7606(1945)56[275:EDOSAT]2.0.CO;2

Huang, Y., Chen, X., Li, F., Zhang, J., Lei, T., Li, J., Chen, P and Wang, X (2018) Velocity of water flow along saturated loess slopes under erosion effects: Journal of Hydrology, 561, 304-311. https://doi.org/10.1016/j.jhydrol.2018.03.070

Imaizumi. F and Sidle. R. C. (2007) Linkage of sediment supply and transport processes in Miyagawa Dam catchment, Japan: Journal of Geophysical Research, Earth Surface, 112 (F3), F03012.

Imaizumi. F., Hattanji. T. and Hayakawa. Y. S. (2010) Channel initiation by surface and subsurface flows in a steep catchment of the Akaishi Mountains, Japan: *Geomorphology*, 115, 32–42. https://doi.org/10.1016/j.geomorph.2009.09.026

Ishimaru, S., Hirose, W., Kawakami, G., Takahashi, R., Kase, Z., Koshimizu, K., Koyasu, H., Chigira, M. and Tajika, J. (2019) The sources of landslides occurred by the 2018 Hokkaido Eastern Iburi Earthquake: *Abstracts, Japan Geoscience Union Meeting 2019*, HDS14-01.

Ishimaru, S., Hirose, W., Kawakami, G., Koshimizu, K., Koyasu, H., Kase, Y., Takahashi, R., Chigira, M. and Tajika, J. (2020) Multiple landslides Caused by the 2018 Hokkaido Eastern lburi Earthquake: Topographic Features of Tephra landslides from the Viewpoint of Geomorphic Development: *Transactions, Japanese Geomorphological Union*, 41 (2), 147–167. [in Japanese with English abstract]

Ito, Y., Yamazaki, S. and Kurahashi, T. (2020) Geological features of landslides caused by the 2018 Hokkaido Eastern Iburi Earthquake in Japan: *Geological Society, London, Special Publications*.
https://doi.org/10.1144/SP501-2019-122

Japan Meteorological Agency (2023) *Historical Weather Data Search*.
http://www.data.jma.go.jp/stats/etrn/index.php [in Japanese] [Last accessed: 2023.01.18]

Jiang, F. S., Huang, Y. H., Wang, M. K., Lin. J. S., Zhao. G. and Ge, H. L. (2014) Effects of Rainfall Intensity and Slope Gradient on Steep Colluvial Deposit Erosion in Southeast China: *Soil & Water Management & Conservation*, 78 (5), 1741-1752. https://doi.org/10.2136/sssaj2014.04.0132

Joji V.S., Nair, A.S.K. and Baiju, K.V. (2013) Drainage basin delineation and quantitative analysis of Panamaram watershed of Kabani River Basin, Kerala using remote sensing and GIS: *Journal Geological Society of India, 82*, 368–378. https://doi.org/10.1007/s12594-013-0164-x

Julian, J. P. and Torres, R. (2006) Hydraulic erosion of cohesive riverbanks: *Geomorphology*, 76, (1–2),193-206. https://doi.org/10.1016/j.geomorph.2005.11.003

Kanungo, D. P. and Sharma, S. (2014) Rainfall thresholds for prediction of shallow landslides around Chamoli-Joshimath Region, Garhwal Himalayas, India: *Landslides*, 11, 629-638. https://doi.org/10.1007/s10346-013-0438-9

Kasai, M. and Yamada, T. (2019) Topographic effects on frequency-size distribution of landslides triggered by the Hokkaido Eastern Iburi Earthquake in 2018: *Earth Planets Space*, 71, 89. https://doi.org/10.1186/s40623-019-1069-8

Keefer, D. K. (1984): Landslides caused by earthquakes. Geological Society of America Bulletin, 95 (4), 406–421. https://doi.org/10.1130/0016-7606(1984)95<406:LCBE>2.0.CO;2

Keefer, D. K. (1994): The importance of earthquake-induced landslides to long-term slope erosion and slope-failure hazards in seismically active regions. Geomorphology, 10 (1994), 265–284. https://doi.org/10.1016/0169-555X(94)90021-3

Kimiaghalam, N., Clark, S.P and Ahmari, H. (2016) An experimental study on the effects of physical, mechanical, and electrochemical properties of natural cohesive soils on critical shear stress and erosion rate: *International Journal of Sediment Research*, (31), Issue (1), 1-15. https://doi.org/10.1016/j.ijsrc.2015.01.001

Koi, T., Hotta, N, Ishigaki, I., Matuzaki, N., Uchiyama, Y. and Suzuki, M. (2008): Prolonged impact of earthquake-induced landslides on sediment yield in a mountain watershed: The Tanzawa region, Japan. Geomorphology, 101 (4), 692–702. https://doi.org/10.1016/j.geomorph.2008.03.007

Korup, O. (2005). Geomorphic imprint of landslides on alpine river systems, southwest New Zealand: *Earth Surface Process Landform*,30, 783–800. https://doi.org/10.1002/esp.1171

Lane, S., Westaway, R. and Murray hicks, D. (2003) Estimation of erosion and deposition volumes in a large, gravel-bed, braided river using synoptic remote sensing: *Earth Surface Processes and Landforms*, 28, 249–271.

Lee. M. F. A., Airi Maruyama. A., Lu.S. and Irino, T. (2022) Quantification of Asian Dust Source Variabilities in Silt and Clay Fractions since 10 Ma by Parallel Factor (PARAFAC) Endmember Modeling at IODP Site U1425 in the Japan Sea: Lithosphere, 9. https://doi.org/10.2113/2022/6818103

Lei, T.W., Xia, W.S., Zhao, J., Liu, Z and Zhang, Q.W. (2005) Method for measuring velocity of shallow water flow for soil erosion with an electrolyte tracer: *Journal of Hydrology*, 301, 139–145. https://doi.org/10.1016/j.jhydrol.2004.06.025

Li, G., Joshua West, A., Densmore A, L., Jin Z. D., Parker, R, N and Hiton, R. G. (2014) Coseismic mountain building: Landslides associated with the 2008 Wenchuan earthquake in the context of a generalized model for earthquake volume balance, 15 (4), 833-844.
https://doi.org/10.1002/2013GC005067

Li, G., West, Densmore, A. L., Hammond, D. E., Jin, Z., Zhang, F., Wang, J., Robert G. and Hilton, R. G. (2015) Connectivity of earthquake-triggered landslides with the fluvial network: Implications for landslide sediment transport after the 2008 Wenchuan earthquake: *Journal of Geophysical Research: Earth Surface*, 121 (4), 703–724. https://doi. org/10.1002/2015JF003718

Li, X., Gao, J., Guo, Z., Yin, Y., Zhang, X., Sun, P and Gao, Z (2020) A Study of Rainfall-Runoff Movement Process on High and Steep Slopes Affected by Double Turbulence Sources: *Scientific Reports*, 10, (9001). https://www.nature.com/articles/s41598-020-66060-3

Lin, W.T., Chou, W.H., Lin, C.Y., Huang, P.H., Tsai, J.S (2005) Vegetation recovery monitoring and assessment at landslides caused by earthquake in Central Taiwan: *Forest Ecology and Management*. 210, 55–66. https://doi.org/10.1016/j.foreco.2005.02.026

Lin, Z. and Oguchi, T. (2004) Drainage density, slope angle, and relative basin position in Japanese bare lands from high-resolution DEMs: *Geomorphology*, 63 (3–4), 159-173. https://doi.org/10.1016/j.geomorph.2004.03.012

Lin, Z., & Oguchi, T. (2009) Longitudinal and transverse profiles of hilly and mountainous watersheds in Japan. *Geomorphology*, 111, 17–26.

Lo. T. L. W., Hayakawa, Y. S., Nakata, Y., Hayamizu, M and Ogura, T (2023) Changes in morphological characteristics of drainage basins following coseismic landslides by the 2018 Hokkaido Eastern Iburi Earthquake: *Geographical Studies*, 98(1), 9–20. https://doi.org/10.7886/hgs.98.9

Lo. T. L.W. (2025) Post-seismic morphometric changes in landslide-affected drainage basins following the 2018 Hokkaido Eastern Iburi Earthquake: *Transactions, Japanese Geomorphological Union*, 46(2), 139–153.

Lucieer. A., Jong. S.M.d. and Turner, D. (2013) Mapping Landslide Displacements Using Structure from Motion (SfM) and Image Correlation of Multi-Temporal UAV Photography: *Progress in Physical Geography: Earth and Environment*, 38, 97-116. https://doi.org/10.1177/0309133313515293

Machida, H. and Arai, F. (2003) *Atlas of Tephra in and around Japan: revised edition.* University of Tokyo Press. [in Japanese].

Matsuoka, N. and Murton, J. (2008): Frost weathering: recent advances and future directions: *Permafrost and Periglacial Processes*. 19, 195–210. https://doi.org/10.1002/ppp.620

Matsuno, K. and Ishida, M. (1960) Explanatory Text of the Geological Map of Japan Scale 1: 50,000, Hayakita, *Hokkaido Development Agency*. Sapporo, 43. [in Japanese]

Mineo, C., Ridolfi, E., Bertini, C and Napolitano, F. (2019) Kinetic energy and rainfall intensity relationships: A review. *AIP Conference Proceedings*, 2116 (210005). https://doi.org/10.1063/1.5114216

Mizugaki, S., Murakami, Y. and Fujinami, T. (2019) Suspended sediment discharge from the Atsuma River after the Hokkaido Eastern Ibri Earthquake. Proceedings of the 63rd Hokkaido Development Technology Conference (FY 2019). 436-441. [in Japanese]

Mokarram, K. and Sathyamoorthy, D. (2015) Morphometric analysis of hydrological behavior of North Fars watershed, Iran: *European Journal of Geography*, 6 (4), 88 – 106. https://eurogeojournal.eu/index.php/egj/article/view/403.

Montgomery, D.R., and Dietrich, W.E. (1989) Source areas, drainage density, and channel initiation: *Water Resources Research*, 25, (8), 1907–1918. https://doi.org/10.1029/WR025i008p01907

Montgomery, D.R. and Dietrich, W.E. (1992) Channel initiation and the problem of landscape scale: *Science*, 255 (5046), 826–830. https://doi.org/10.1126/science.255.5046.826

Morisawa, M. E. (1962): Quantitative geomorphology of some watersheds in the Appalachian Plateau: *Geological Society of America Bulletin*, 73, 1025–1046. https://doi.org/10.1130/0016 7606(1962)73[1025:QGOSWI]2.0.CO;2

Mi, J. X., Liu, R., Zhang, S. L., Hou, H. P., Yang, Y. G., Chen, F. Y and Zhang, L. M. (2019) Vegetation patterns on a landslide after five years of natural restoration in the Loess Plateau mining area in China: *Ecological Engineering,* 136, 46-54.

Miyazaki, K., Hoshino, T., Shimizu, K., Shrivastava, S. and Yamada, T. J. (2023) Changes in sediment erosion rate in the Azuma River basin after the Hokkaido eastern Iburi earthquake in 2018. IOP Conference Series: *Earth and Environmental Science*, 1136, 012027.
https://doi.org/10.1088/1755-1315/1136/1/012027

Mizugaki, S., Murakami, Y. and Fujinami, T. (2019): Suspended sediment discharge from the Atsuma River after the Hokkaido Eastern Ibri Earthquake. Proceedings of the 63rd Hokkaido Development Technology Conference (FY 2019). 436-441. [in Japanese]

Morbidelli, R., Saltalippi, C., Flammini, A. and Govindaraju., R. S. (2018) Role of slope on infiltration: A review: Journal of Hydrology, 557, 878-886. htttps://www.sciencedirect.com/science/article/pii/S0022169418300192#:~:text=Partitioning%20of%20rainfall%20at%20the%20soil-atmosphere%20interface%20is https://doi.org/10.1016/j.jhydrol.2018.01.019

Muthukrishnan. K., Manoj. S. and Banu. K. K. (2013) Drainage morphometry evaluation for Kodavanar sub basin to understand the interrelationships in morphological systems and in process-response systems: *The International Society for Photogrammetry and Remote Sensing,* 3 (4), 692–707.

Nakagawa, M., Miyasaka, A. M., Tomijima, C., Matsumoto, A., and Hase, R. (2018) Eruption sequence of the 46 ka caldera-forming eruption of Shikotsu Volcano, inferred from stratigraphy of proximal deposits at South of Lake Shikotsu, Japan: Journal of Geography, 127(2):247–271. https://doi.org/10.5026/jgeography.127.247 (in Japanese with English abstract)

Nakata, Y., Hayamizu, M., Ishiyama, N. and Torita, H. (2021) Observation of Diurnal Ground Surface Changes Due to Freeze- Thaw Action by Real-Time Kinematic Unmanned Aerial Vehicle. Remote Sensing. 13 (11), 2167. https://doi.org/10.3390/rs1311216

Nakata, Y., Hayam Izu, M., & Ishiyama, N. (2023). Assessing primary vegetation recovery from earthquake-induced landslide scars: A real-time kinematic unmanned aerial vehicle approach. *Ecological Engineering*, 193, 107019. https://doi.org/10.1016/j.ecoleng.2023.107019

National Agriculture and Food Research Organization, NARO, Hokkaido (2025) Soil temperature data. https://soil-inventory.rad.naro.go.jp/point.html

Nyimbili, P. H., Demirel, H., Şeker, D.Z. and Erden, T (2016) Structure from motion (sfm) – approaches & applications: *International scientific conference on applied sciences*, 2, 260-267.

Ogden, F., & Dawdy, D. (2003) Peak discharge scaling in small Hortonian watershed. *Journal of Hydrologic Engineering*: 8(2), 64–73. https://doi.org/10.1061/(ASCE)1084-0699(2003)8:2(64)

Ouchi S., 1985. Response of alluvial rivers to slow active tectonic movement. *GSA Bulletin*, 96 (4), 504-515.

Parker, R. N., Densmore, A. L., Rosser, N. J., de Michele, M., Li, Y. and Huang, R. (2011) Mass wasting triggered by the 2008 Wenchuan earthquake is greater than orogenic growth: *Nature Geoscience*, 4(7), 449–452. https://doi.org/10.1038/ngeo1154

Parchure, T. M and Mehta, A. J. M (1985) Erosion of Soft Cohesive Sediment Deposits: *Journal of Hydraulic Engineering*, 111, (10) https://doi.org/10.1061/(ASCE)0733-9429(1985)111:10(1308)

Pareta, K. and Pareta, U. (2011) Quantitative Morphometric Analysis of a Watershed of Yamuna Basin, India using ASTER (DEM) Data and GIS: *International Journal of Geomatics and Geosciences,* 1(2):1-14. http://www.ipublishing.co.in/jggsvol1no12010/voltwo/EIJGGS3022.pdf

Patton, P.C. and Baker, V. R. (1976) Morphometry and floods in small drainage basins subject to diverse hydrogeomorphic controls: *Water Resources Research*, 12 (5), 941–952. https://doi.org/10.1029/WR012i005p00941

Patton, P., Baker, V. and Kochel, R. (1988) Drainage Basin Morphometry and Floods: *Flood Geomorphology*, Wiley, New York, 51-65.

Petrucci, O., Pasqua. A. A. and Polemio, M. (2013) Impact of damaging geo-hydrological events and population development in Calabria, Southern Italy: *Water*, 5, 1780-1796. https://doi.org/10.3390/w5041780

Piras, M., Taddia, G., Forno, M. G., Gattiglio, M., Aicardi, I., Dabove, P., Lo Russo, S., and Lingua, A. (2017). Detailed geological mapping in mountain areas using an unmanned aerial vehicle: Application to the Rodoretto Valley. NW Italian Alps, Geomatics: *Natural Hazards and Risk*, 8(1), 137–149. https://doi.org/10.1080/19475705.2016.1225228

Prabhakaran, A. and Jawahar Raj, N. (2018) Drainage morphometric analysis for assessing form and processes of the watersheds of Pachamalai hills and its adjoinings, Central Tamil Nadu, India: *Applied Water Science*, 8, 31. https://doi.org/10.1007/s13201-018-0646-5

Roback, K., Clark,M. K., Western, A. J., Zekkos, D., Li, G., Gallen, S.f., Chamlagain, D. and Godt, J. W. (2018) The size, distribution, and mobility of landslides caused by the 2015 Mw7.8 Gorkha earthquake, Nepal. *Geomorphology*, 301, 131-138.

Sakai, S., Suzuki, Y., Itagaki, T., Tsujisawa, H., Makino, T.T., 2008. On the function of hermaphrodite florets in female inflorescences of Petasites japonicus (Asteraceae). Botany. 86, 179–184.

Sato. H., Shimamoto. T., Tsutsumi. A. and Kawamoto. E. (1995) Onshore tsunami deposits caused by the 1993 southwest Hokkaido and 1983 Japan Sea earthquake: Pure and applied geophysics, 144, 693-717. https://link.springer.com/article/10.1007/BF00874390

Schumm, S.A. (1956) Evolution of drainage systems and slopes in badlands at Perth Amboy, New Jersey: *Geological Society of America Bulletin*, 67, 597–646. https://doi.org/10.1130/0016- 7606(1956)67[597:EODSAS]2.0.CO;2

Scaioni, M., Crippa, J., Corti, M., Barazzetti., L., Fugazza, D,., Azzoni, R., Cernuschi, M. and Diolaiuti, G. A. (2018) Technical aspects related to the application of SfM photogrammetry in high mountain, The International Archives of the Photogrammetry: *Remote Sensing and Spatial Information Sciences*, XLII (2), 1029–1036.

Shaman, J., Stieglitz, M., and Burns, D. (2004) Are big basins just the sum of small catchments? *Hydrological Processes*: 18(16), 3195–3206. https://doi.org/10.1002/hyp.5739

Singh, S. and Dubey, A. (1994) Geoenvironmental Planning of Watersheds in Indian.

Chugh Publications, Allahabad, 28-69.

Singh, S. and Singh, M.C. (1997) Morphometric Analysis of Kanhar River Basin: *National Geographical Journal of India,* 43, 31-43. https://www.scirp.org/reference/referencespapers?referenceid=1775374

Smith, K.G. (1950) Standards for grading texture of erosional topography. *American Journal of Science*, 248(9), 655–668. https:/ / doi.org/ 10.2475/ ajs.248.9.655

Smerdon, E.T. and Beasley, R. P. (1961) Critical tractive forces in cohesive soils: *Agricultural Engineering*, 42 (1) pp. 26-29.

Strahler, AN. (1964) Part II. Quantitative geomorphology of drainage basins and channel networks: *Handbook of Applied Hydrology: McGraw-Hill*, New York, 39, 4, 4–7.

Takahashi, K., Fukusawa, H., Wada, N., Hoyanagi, K. and Oka, T. (1984) Neogene stratigraphy and Paleogeography in the Area along the Sea of Japan of northern Hokkaido: *Earth Science (Chikyu Kagaku)*, 38, 299–312. https://doi.org/10.15080/agcjchikyukagaku.38.5_299 [in Japanese with English abstract]

Tsuyuzaki, S. (1987) Origin of plants recovering on the volcano Usu, northern Japan, since the eruptions of 1977 and 1978: *Vegetation*, 73, 53–58. https://doi.org/ 10.1007/BF00031851.

Twidale, C. R. (2004) River patterns and their meaning: *Earth-Science Reviews*, 67, 3–4, 159-218. https://doi.org/10.1016/j.earscirev.2004.03.001

Uda, T., Kimura, G., Aida, Y. and Tonosaki, T. (1979) Active fault crosscut pumice layer of Tarumae pumice fall deposit: *Earth Science*, 33, 304–307, https://doi.org/10.15080/agcjchikyukagaku.33.5_304 [in Japanese].

Ueno, K., Kurobe, K., Imaizumi, F. and Nishii, R. (2015) Effects of deforestation and weather on diurnal frost heave processes on the steep mountain slopes in south central Japan: *Earth Surface Processes and Landforms*, 40, 2013–2025.

Van Western, C. J., Castellanos, E. and Kuriakose, S. L. (2008) Spatial data for landslide susceptibility, hazards, and vulnerability assessment: An overview: *Engineering Geology*, 102, 112-131. https://doi.org/10.1016/j.enggeo.2008.03.010

Vente. D., Poesen. J., Verstraeten. G., Govers. Gerard., Vanmaercke. M., Rompaey. A. V., Arbkhedri. M and Boix-Fayos. C. (2013) Predicting soil erosion and sediment yield at regional scales: Where do we stand?: *Earth-Science Reviews*. 127, 16-29. https://doi.org/10.1016/j.earscirev.2013.08.014

Wang, J., Jin, Z., Hilton, R. G., Zhang, F., Densmore, A. L., Li, G. and West, A. J. (2015): Controls on fluvial evacuation of sediment from earthquake-triggered landslides. Geology, 43 (2), 115–118. https://doi.org/10.1130/G36157.1

Wang, F., Fan, X., Yunus, A. P., Subramanian, S. S., AlonsoRodriguez, A., Dai, L., Xu, Q. and Huang, R. (2019) Coseismic landslides triggered by the 2018 Hokkaido, Japan (Mw 6.6), earthquake: spatial distribution, controlling factors, and possible failure mechanism: *Landslides*, 16 (8), 1551–1566. https://doi. org/10.1007/s10346-019-01187-7

Wang, F. and Nam, K. (2023) Landslide Disasters Caused by the 2018 Eastern Iburi Earthquake in Hokkaido Japan and the Countermeasures to Completely Prevent the Similar Disasters in the Future: *Progress in Landslide Research and Technology*, 1, 1, 305–313. https.//doi.org/10.1007/978-3-031-16898-7_23

Wei, M., Cheng, N. S and Lu, Y. (2023) Revisiting the concept of hydraulic radius: *Journal of Hydrology*, 625, B. https://doi.org/10.1016/j.jhydrol.2023.130134

Wu, S., Chen, L., Wang, N. (2018) Modeling Rainfall-Runoff and Soil Erosion Processes on Hillslopes With Complex Rill Network Planform: *Water Resources Research*, 54 (12) https://doi.org/10.1029/2018WR023837

Xu, L. H., Shi, Z., Wang, Y., Xiang, W. (2010) Canopy interception characteristics of main vegetation types in Liupan Mountains of China: *The journal of applied ecology*, 21(10): 2487-93

Yamagishi, H. and Yamazaki, F. (2018) Landslides by the 2018 Hokkaido Iburi-Tobu Earthquake on September 6: *Landslides*, 15, 2521–2524. https://doi.org/10.1007/s10346-018-1092-z

Zhang, F.B., Yang, M.Y., Li, B.B., Li, Z.B. and Shi, W.Y. (2017) Effects of slope gradient on hydro-erosional processes on an aeolian sand-covered loess slope under simulated rainfall: *Journal of Hydrology*, 553, 447-456. https://doi.org/10.1016/j.jhydrol.2017.08.019

Zhang, G.H., Shen, R.C., Luo, R.T., Cao, Y., Zhang, X.C. (2010). Effects of sediment load on hydraulics of overland flow on steep slopes: *Earth Surface Processes and Landforms*, 35, (15), 1811-1819. https://doi.org/10.1002/esp.2019

Zhang, L. and Guilbert, E. (2012) A study of variables characterizing drainage patterns in river networks: *Remote Sensing and Spatial Information Science*, XXXIX, B2. https://doi.org/10.5194/isprsarchives-XXXIX-B2-29-2012

Zhang, L., Wang, J., Bai, Z. K. and Lv, C. J. (2015) Effects of vegetation on runoff and soil erosion on reclaimed land in an opencast coal-mine dump in a loess area: *Catena*, 128, 44-53. https://doi.org/10.1016/j.catena.2015.01

Zhao, B., Zhang, L., Xia, Z., Xu, W., Xia, L., Liang, Y. and Xia, D.,(2019) Rainfall Intensity and Vegetation Cover on Erosion Characteristics of a Soil Containing Rock Fragments Slope: A*dvances in Civil Engineering*, 4, 1-14.

Zhao, B., Su., L.J., Wang, Y.S., Ji, F., Li, W.L. and Tang, C.X. (2021) Insights into the mobility characteristics of seismic earthflows related to the Palu and Eastern Iburi earthquakes: *Geomorphology*, 391, 107886. https://doi.org/10.1016/j.geomorph.2021.107886

Zhong. C., Li. C., Gao. P. and Li. H. (2021) Discovering Vegetation Recovery and Landslide Activities in the Wenchuan Earthquake Area with Landsat Imager: *Sensors*, 21(15), 5243. https://doi.org/10.3390/s21155243